

DESIGN AND REALIZATION OF BROADBAND INSTANTANEOUS
FREQUENCY DISCRIMINATOR

A THESIS SUBMITTED TO
THE GRADUATE SCHOOL OF NATURAL AND APPLIED SCIENCES
OF
MIDDLE EAST TECHNICAL UNIVERSITY

BY

GÖKHAN PAMUK

IN PARTIAL FULFILLMENT OF THE REQUIREMENTS
FOR
THE DEGREE OF MASTER OF SCIENCE
IN
ELECTRICAL AND ELECTRONICS ENGINEERING

JUNE 2010

Approval of the thesis:

**DESIGN AND REALIZATION OF BROADBAND INSTANTANEOUS
FREQUENCY DISCRIMINATOR**

submitted by **GÖKHAN PAMUK** in partial fulfillment of the requirements for the degree of **Master of Science in Electrical and Electronics Engineering Department, Middle East Technical University** by,

Prof. Dr. Canan Özgen _____
Dean, Graduate School of **Natural and Applied Sciences**

Prof. Dr. İsmet Erkmen _____
Head of Department, **Electrical and Electronics Engineering**

Prof. Dr. Nevzat Yıldırım _____
Supervisor, **Electrical and Electronics Engineering Dept., METU**

Examining Committee Members:

Prof. Dr. Canan Toker _____
Electrical and Electronics Engineering Dept., METU

Prof. Dr. Nevzat Yıldırım _____
Electrical and Electronics Engineering Dept., METU

Assoc. Prof. Dr. Sencer Koç _____
Electrical and Electronics Engineering Dept., METU

Assoc. Prof. Dr. Şimşek Demir _____
Electrical and Electronics Engineering Dept., METU

Senior Engineer Tuncay Erdöl _____
Aselsan

Date:

I hereby declare that all information in this document has been obtained and presented in accordance with academic rules and ethical conduct. I also declare that, as required by these rules and conduct, I have fully cited and referenced all material and results that are not original to this work.

Name, Last name :Gökhan PAMUK

Signature :

ABSTRACT

DESIGN AND REALIZATION OF BROADBAND INSTANTANEOUS FREQUENCY DISCRIMINATOR

Pamuk, Gökhan

M. Sc., Department of Electrical and Electronics Engineering

Supervisor: Prof. Dr. Nevzat Yıldırım

June 2010, 190 pages

In this thesis, RF sections of a multi tier instantaneous frequency measurement (IFM) receiver which can operate in 2 – 18 GHz frequency band is designed, simulated and partially realized. The designed structure uses one coarse tier, three medium tiers and one fine tier for frequency discrimination. A novel reflective phase shifting technique is developed which enables the design of very wideband phase shifters using stepped cascaded transmission lines. Compared to the classical phase shifters using coupled transmission lines, the new approach came out to be much easier to design and fabricate with much better responses. This phase shifting technique is used in coarse and medium tiers. In fine frequency measurement tier, I/Q discriminator approach is used because reflective phase shifters would necessitate unacceptably long delay lines. Two I/Q discriminators are designed and fabricated using Lange directional couplers that operate in 2-6 GHz and 6-18 GHz, resulting in satisfactory response. Additionally, 6 GHz HP and 6 GHz LP distributed filters are designed and fabricated to be used for these I/Q discriminators in fine tier. In order to eliminate possible ambiguities in coarse tier, a distributed element LP-HP diplexer with 10 GHz cross-over frequency is designed and fabricated successfully to be used for splitting the frequency spectrum into 2-10 GHz and 10-18 GHz to ease the design and realization problems. Three power dividers operating in the ranges 2-18 GHz, 2-6 GHz and 6-18 GHz are designed for splitting incoming signals into different branches. All of these

dividers are also fabricated with satisfactory response. The fabricated components are all compact and highly reproducible. The designed IFM can tolerate 48 degrees phase margin for resolving ambiguity in the tiers while special precautions are taken in fine tier to help ambiguity resolving process also. The resulting IFM provides a frequency resolution below 1 MHz in case of using an 8-bit sampler with a frequency accuracy of 0.28 MHz rms for 0 dB input SNR and 20 MHz video bandwidth.

Keywords: Instantaneous Frequency Measurement Receiver, Frequency discriminator, Reflective phase shifter, Wideband phase shifter.

ÖZ

GENİŞ BANTLI ANLIK FREKANS AYRIŞTIRICI TASARIMI VE GERÇEKLENMESİ

Pamuk, Gökhan

Yüksek Lisans, Elektrik ve Elektronik Mühendisliği Bölümü

Tez Yöneticisi: Prof. Dr. Nevzat Yıldırım

Haziran 2010, 190 sayfa

Bu tezde 2-18 GHz frekans bandında çalışabilen anlık frekans ölçen çok kollu bir almacın RF bölümü tasarlanmış, benzetimi yapılmış ve kısmen gerçekleştirilmiştir. Tasarlanan yapı bir adet düşük, üç adet orta ve bir adet yüksek çözünürlükte frekans ölçümü yapan kollara sahiptir. Düşük ve orta seviye çözünürlükte frekans ölçümü yapılan kollarda, bu tezde geliştirilen kademeli sıralı iletim hatlarından oluşan geniş bantlı yansıtıcı faz kaydırıcılar kullanılmıştır. Bağlı iletim hatlarından oluşan klasik faz kaydırıcılarla karşılaştırıldığında, tez sunulan faz kaydırma yaklaşımının daha iyi sonuçlar verdiği ve tasarımının ve üretiminin daha kolay olduğu görülmüştür. Yüksek çözünürlüklü frekans ölçümünün yapıldığı kolda, yansıtıcı faz kaydırıcıların çok uzun geciktirme hatlarına ihtiyaç duyması sebebiyle I/Q ayırıştırma yöntemi uygulanmıştır. Bu amaçla Lange bağlayıcılarının kullanıldığı biri 2-18 GHz diğeri ise 6-18 GHz frekans bandında çalışan iki adet I/Q ayırıştırıcı tasarlanmış ve üretilmiştir. Bu ayırıştırıcıların ölçüm sonuçları oldukça iyi çıkmıştır. Ayrıca, bu ayırıştırıcıların girişlerinde kullanılmak üzere dağıtılmış elemanlı 6 GHz yüksek ve alçak geçiren filtreler tasarlanmış ve üretilmiştir. 2-10 GHz ve 10-12 GHz frekans bantlarını ayırarak düşük çözünürlüklü frekans ölçümü yapılan koldan kaynaklanabilecek olası belirsizlikleri bertaraf etmek amacıyla, 10 GHz geçiş frekansına sahip alçak-yüksek

geçirgen filtre tipi dağıtılmış elemanlı bir düpleksör tasarımı ve gerçekleştirilmesi yapılmıştır. Ayrıca 2-18 GHz, 2-6GHz ve 6-18 GHz frekans bantlarında çalışan güç bölücüler tasarlanmış ve üretilmiştir. Üretilen bu güç bölücülerden de oldukça iyi sonuçlar elde edilmiştir. Üretilen parçaların hepsi kompakt ve tekrar üretilebilir yapıdadır. Tasarlanan almaç 48 dereceye kadar olan faz hatalarını tolere edebilecek durumdadır. Ayrıca yüksek çözünürlüklü frekans ölçümlü yapılan kolda olası belirsizlikleri çözmek amacıyla tasarımda önlemler alınmıştır. Tezde sunulan almaç yapısı, 0dB giriş SNR'ı altında, 8 bitlik bir örnekleme kullanılması halinde 1 MHz'den daha küçük bir frekans ölçüm çözünürlüğünü 20 MHz'lik video bant genişliği için 0.28 MHz'lik (rms) ölçüm doğruluğu ile sağlayabilmektedir.

Anahtar Kelimeler: Anlık Frekans Ölçen Almaç, Frekans Ayırıştırıcı, Yansıtıcı Faz Kaydırıcı, Geniş Bantlı Faz Kaydırıcı

*To My Mother and
My Father*

ACKNOWLEDGEMENTS

I would like to thank to Prof. Dr. Nevzat Yıldırım for his valuable supervision and support throughout the development and improvement of this thesis.

I am grateful to Dr. Mustafa Akkul and Tuncay Erdöl for their precious comments and support throughout the development of this thesis.

Also, I would like to express my gratitude to İpek İstanbulluoğlu Turhan for being supportive about everything in my life. She has been an elder sister for me during these three years.

Lastly but mostly, I would like to thank my mother and father for giving me a great and special family. Without their support, I would not be able to overcome the difficulties throughout my life.

TABLE OF CONTENTS

ABSTRACT	iv
ÖZ	vi
DEDICATION	viii
ACKNOWLEDGEMENTS	ix
TABLE OF CONTENTS	x
LIST OF TABLES	xiii
LIST OF FIGURES	xiv
LIST OF ABBREVIATIONS	xxiii
CHAPTERS	
1. INTRODUCTION	1
1.1 Frequency Discrimination Overview	1
1.2 A Short History of IFM.....	3
1.3 IFM Structures	4
1.3.1 Time Domain Frequency Measurement.....	4
1.3.2 Frequency Domain Discriminators	5
1.3.2.1 High-Pass / Low-Pass Discriminator	5
1.3.2.2 Delay Line Discriminator.....	7
1.3.2.3 Three-Phase Discriminator.....	8
1.4 Scope of the Thesis	14
1.5 Outline of the Thesis	15
2. BASIC CONCEPTS	17
2.1 Signal Spectra and Instantaneous Frequency.....	17
2.2 Principle of Operation.....	18
2.3 Phase Discriminators.....	26
2.4 Frequency Resolution	29
2.5 Frequency Accuracy and SNR.....	31
2.6 Number of Tiers, Inter Tier Ratio and Phase Margin	34
3. DIFFERENTIAL PHASE SHIFTER DESIGN.....	36

3.1	Schiffman Phase Shifter.....	37
3.2	Schiffman-Type Phase Shifter Alternatives.....	39
3.2.1	Three Section Schiffman Phase Shifter.....	39
3.2.2	Four Section Schiffman Phase Shifter	43
3.2.3	Five Section Schiffman Phase Shifter.....	45
3.2.4	Six Section Schiffman Phase Shifter	47
3.2.5	Schiffman Class II Phase Shifter.....	50
3.2.6	Tandem Connected Schiffman Phase Shifter.....	53
3.3	Reflective Phase Shifters	57
3.3.1	Phase Shifters Using 0°-180° Hybrids and Uncoupled OC and SC Stepped Lines.....	57
3.3.2	Phase Shifters Using Reflections from Stepped SC and OC Line Sections	60
3.3.2.1	Reflective Uniform Phase Shifters.....	60
3.3.2.2	Simple Reflective Phase Shifters in Stepped Form	68
3.3.2.3	Multi-Step Reflection Phase Shifters.....	71
4.	FREQUENCY DISCRIMINATOR DESIGN	86
4.1	Frequency Resolution and Accuracy	87
4.2	Number of Tiers	89
4.3	Choosing the Appropriate Physical Structure and Substrate	91
4.4	Amplifier.....	92
4.5	2-18 GHz Power Divider	93
4.6	Schottky Diode.....	95
4.7	Tier Designs	98
4.7.1	Coarse Tier.....	98
4.7.1.1	Power Divider	100
4.7.1.2	Diplexer.....	102
4.7.1.3	Phase Shifter Network.....	109
4.7.1.4	Final Circuit	118
4.7.1.5	Measurement Results	122
4.7.2	Medium Tiers.....	125
4.7.2.1	Medium Tier 1	128
4.7.2.2	Medium Tier 2	140

4.7.2.3	Medium Tier 3	141
4.7.3	Fine Tier	142
4.7.3.1	Filters	145
4.7.3.2	Delay Line	150
4.7.3.3	I/Q Discriminators	151
4.7.3.4	Measurement Results	166
4.8	Final Structure	173
5.	SUMMARY AND DISCUSSIONS	179
5.1	Deciding the Phase Shifter Network	179
5.2	Deciding the Parameters	181
5.3	Designing the Frequency Discriminator Structure	182
6.	CONCLUSIONS AND FUTURE WORK	185
	REFERENCES	187

LIST OF TABLES

TABLES

Table 1 Number of tiers vs. phase margin relationship.	90
---	----

LIST OF FIGURES

FIGURES

Figure 1.1 Basic block diagram of an IFM.	2
Figure 1.2 Simplified Frequency Counter.....	5
Figure 1.3 Low-pass discriminator.	6
Figure 1.4 Ratio discriminator.	6
Figure 1.5 Delay line discriminator using 90 degree hybrid couplers.	7
Figure 1.6 Three-Phase Discriminator Output.....	8
Figure 1.7 Reflection-mode Discriminator	9
Figure 1.8 Reflection Discriminator with Phase Shifter	11
Figure 1.9 Three-phase discriminator.	11
Figure 1.10 Reflection discriminator signal paths.	12
Figure 1.11 Basic block diagram of the discriminator.....	14
Figure 2.1 Spectrum of an RF Pulse	17
Figure 2.2 Phase relation of sinusoidal waves with constant time delay.....	19
Figure 2.3 Basic frequency measurement circuit of an IFM receiver [11].	20
Figure 2.4 An example of a frequency discriminator [11].	26
Figure 2.5 IFM receiver with multiple delay lines.....	30
Figure 3.1 Schiffman’s single-section phase shifter.....	37
Figure 3.2 Schiffman’s four-section phase shifter.	37
Figure 3.3 3 section Schiffman phase shifter.....	41
Figure 3.4 Phase difference between phase shifter branch 1 and reference line.....	42
Figure 3.5 Phase difference between reference line and phase shifter branch 2.....	42
Figure 3.6 4 section Schiffman phase shifter.	43
Figure 3.7 Phase difference between phase shifter branch 1 and reference line.....	44
Figure 3.8 Phase difference between reference line and phase shifter branch 2.....	44
Figure 3.9 5 section Schiffman phase shifter.	45
Figure 3.10 Phase difference between phase shifter branch 1 and reference line.....	46
Figure 3.11 Phase difference between reference line and phase shifter branch 2.....	47

Figure 3.12 6 section Schiffman phase shifter	48
Figure 3.13 Phase difference between phase shifter branch 1 and reference line.....	49
Figure 3.14 Phase difference between reference line and phase shifter branch 2.....	49
Figure 3.15 Five-section phase shifter of Class II.	50
Figure 3.16 Five-section phase shifter of Class II, ADS Design.	51
Figure 3.17 Phase difference between phase shifter branch 1 and reference line.....	52
Figure 3.18 Phase difference between reference line and phase shifter branch 2.....	52
Figure 3.19 Four element tandem connected phase shifter.....	53
Figure 3.20 Tandem connection of different two ports to reduce of maximum coupling coefficient.....	53
Figure 3.21 Phase shifter networks in tandem connection.....	55
Figure 3.22 Phase difference between phase shifter branch 1 and reference line.....	56
Figure 3.23 Phase difference between reference line and phase shifter branch 2.....	56
Figure 3.24 Operation and use of 0° - 180° hybrid.	58
Figure 3.25 (a) Even-Odd mode decomposition of a Schiffman phase shifter. (b) Multiple section phase shifter with 180 degree hybrid coupler and uncoupled stepped transmission lines.	59
Figure 3.26 The concept for differential phase shifter design using reflected signals.	61
Figure 3.27 Transmission type phase shifter structure.	62
Figure 3.28 Phase difference between phase shifter branch 1 and reference line in transmission type phase shifter.	63
Figure 3.29 Phase difference between phase shifter branch 2 and reference line in transmission type phase shifter.	63
Figure 3.30 OC ended reflection type phase shifter structure.....	64
Figure 3.31 Phase difference between phase shifter branch 1 and reference line in OC ended reflection type phase shifter.....	65
Figure 3.32 Phase difference between phase shifter branch 2 and reference line in OC ended reflection type phase shifter.....	65
Figure 3.33 First alternative of phase shifter branch 2 in the reflection type phase shifter.	66
Figure 3.34 Second alternative of phase shifter branch 2 in the reflection type phase shifter.	67

Figure 3.35 Simple reflective phase shifter structure.....	69
Figure 3.36 Differential phase response of one step reflective phase shifter.....	69
Figure 3.37 Two-step reflective phase shifter structure.....	70
Figure 3.38 Differential phase response of the two-step reflective phase shifter.....	70
Figure 3.39 Phase shifting branches in alternative forms.....	71
Figure 3.40 Transmission line equivalent model.....	72
Figure 3.41 Phase shifting structure given in section 3.2.4.....	74
Figure 3.42 Decomposed version of the phase shifter branch 1.....	75
Figure 3.43 The phase difference between the decomposed lines of phase shifter branch 1.....	75
Figure 3.44 Original and new versions of the reference line given in section 3.2.4..	76
Figure 3.45 Phase difference between the original and new versions of the reference lines.....	76
Figure 3.46 Decomposed version of 6 section phase shifter.....	77
Figure 3.47 Differential phase response of new structure.....	77
Figure 3.48 Phase of reflection coefficient between TL 29 and TL 30 in phase shifter branch 1.....	78
Figure 3.49 Decomposed version of 6 section phase shifter branch 1, with TL30 omitted and structure is short circuited.....	79
Figure 3.50 Differential phase response of the short circuited phase shifter branch 1.....	79
Figure 3.51 Decomposed, shortened and optimized version of the original phase shifter branch 1.....	80
Figure 3.52 Differential phase response of final phase shifter structure for phase shifter branch 1.....	80
Figure 3.53 Phase shifter branch 2.....	81
Figure 3.54 Phase difference between reference line and phase shifter branch 2.....	81
Figure 3.55 Odd mode impedance branch of decomposed phase shifter branch 2....	82
Figure 3.56 Differential phase response of odd mode impedance branch.....	82
Figure 3.57 Decomposed version of 6 section phase shifter branch 2, TL36 is omitted and structure is open circuited.....	83
Figure 3.58 Differential phase response of the open circuited phase shifter branch 2.....	83

Figure 3.59 Decomposed, shortened and optimized version of the original phase shifter branch 2.....	84
Figure 3.60 Differential phase response of final phase shifter structure for phase shifter branch 1.....	84
Figure 3.61 Final phase shifting network.....	85
Figure 4.1 IFM discriminator, basic block diagram.....	91
Figure 4.2 Cross-sections of common microwave circuit structures.....	92
Figure 4.3 1 dB compression point of the amplifier.....	92
Figure 4.4 5 section Wilkinson power divider layout.....	93
Figure 4.5 Power divider S21, momentum simulation result.....	94
Figure 4.6 Power divider S11 and S23, momentum simulation result.....	94
Figure 4.7 Diode equivalent model in ADS.....	95
Figure 4.8 Diode model with 150 ohm printed resistor.....	96
Figure 4.9 Diode impedance vs. frequency.....	96
Figure 4.10 Simulated circuit at harmonic balance.....	97
Figure 4.11 Circuit matching.....	97
Figure 4.12 Theoretical output of the coarse tier.....	99
Figure 4.13 Example of actual output of coarse tier.....	99
Figure 4.14 General block diagram of coarse tier.....	100
Figure 4.15 4 section Wilkinson power divider layout.....	101
Figure 4.16 Power divider S21, momentum simulation result.....	101
Figure 4.17 Power divider return loss and isolation, momentum simulation result.....	102
Figure 4.18 Low-pass prototype filters for elliptic function filters with (a) series parallel-resonant branches, (b) its dual with shunt series-resonant branches.....	103
Figure 4.19 Low-pass to high-pass prototype conversion.....	103
Figure 4.20 10 GHz diplexer, high-pass section.....	104
Figure 4.21 10 GHz diplexer, high-pass section with unit elements.....	104
Figure 4.22 10 GHz diplexer, high-pass section, capacitances will be split.....	104
Figure 4.23 10 GHz diplexer, high-pass section, capacitances are decomposed.....	105
Figure 4.24 Changing capacitance position according to the related Kuroda identity.....	105
Figure 4.25 The circuit after transformation.....	105
Figure 4.26 Kuroda transformation.....	106

Figure 4.27 10 GHz diplexer, high-pass section.....	106
Figure 4.28 High-pass section layout.....	106
Figure 4.29 10 GHz diplexer, low-pass section.....	107
Figure 4.30 Low-pass section layout.....	107
Figure 4.31 Diplexer layout.....	108
Figure 4.32 Diplexer s-parameters, momentum simulation.....	108
Figure 4.33 Coarse tier with ideal transmission lines.....	109
Figure 4.34 Phase difference between phase shifter branch 1 and reference line (with ideal transmission lines).....	110
Figure 4.35 Phase difference between reference line and phase shifter branch 2 (with ideal transmission lines).....	110
Figure 4.36 Coarse tier with lossy transmission lines.....	111
Figure 4.37 Phase difference between phase shifter branch 1 and reference line (with lossy transmission lines).....	111
Figure 4.38 Phase difference between reference line and phase shifter branch 2 (with lossy transmission lines).....	112
Figure 4.39 Coarse tier phase shifting branches.....	112
Figure 4.40 Phase difference between phase shifter branch 1 and reference line (new version).....	113
Figure 4.41 Phase difference between reference line and phase shifter branch 2 (new version).....	113
Figure 4.42 Re-optimized version phase shifter network.....	114
Figure 4.43 Phase difference between phase shifter branch 1 and reference line (re-optimized version).....	115
Figure 4.44 Phase difference between reference line and phase shifter branch 2 (re-optimized version).....	115
Figure 4.45 Phase shifter part of coarse tier.....	11616
Figure 4.46 Detector outputs.....	117
Figure 4.47 S11 of phase shifter part of coarse tier.....	118
Figure 4.48 Coarse tier with momentum components.....	11919
Figure 4.49 Detector outputs of the final circuit.....	120
Figure 4.50 Non-inverting amplifier.....	120
Figure 4.51 Detector outputs with op-amps.....	121

Figure 4.52 S11 of the coarse tier.	122
Figure 4.53 Detector outputs at the diplexer.	122
Figure 4.54 Fabricated coarse tier.	123
Figure 4.55 Detector outputs of fabricated coarse tier.	123
Figure 4.56 Detector outputs of coarse tier in ADS.	124
Figure 4.57 Diplexer outputs of fabricated coarse tier.	124
Figure 4.58 Coarse tier detector outputs as an example.	125
Figure 4.59 Nesting the outputs of medium tier 1 into coarse tier.	126
Figure 4.60 Medium tier 1 detector outputs as an example.	126
Figure 4.61 Coarse and medium tier outputs in nested form.	127
Figure 4.62 Medium tier phase shifting branches with ideal transmission lines.	128
Figure 4.63 Phase difference between phase shifter branch 1 and reference line (with ideal transmission lines).	129
Figure 4.64 Phase difference between reference line and phase shifter branch 2 (with ideal transmission lines).	129
Figure 4.65 Medium tier phase shifting branches with lossy elements.	130
Figure 4.66 Phase difference between phase shifter branch 1 and reference line (with lossy elements).	130
Figure 4.67 Phase difference between reference line and phase shifter branch 2 (with lossy elements).	131
Figure 4.68 New version of the phase shifter structure.	132
Figure 4.69 Phase difference between phase shifter branch 1 and reference line (modified version).	132
Figure 4.70 Phase difference between reference line and phase shifter branch 2 (modified version).	133
Figure 4.71 Reference line in HFSS.	133
Figure 4.72 Phase shifter 1 in HFSS.	134
Figure 4.73 Phase Shifter 2 in HFSS from two different angles.	134
Figure 4.74 Phase difference between phase shifter branch 1 and reference line (HFSS version).	135
Figure 4.75 Phase difference between reference line and phase shifter branch 2 (HFSS version).	135
Figure 4.76 Schematic version of medium tier 1.	136

Figure 4.77 Output of medium tier 1 (schematic version) and coarse tier (actual version) in nested form.	137
Figure 4.78 Medium tier 1 with HFSS s-parameters and momentum components.	138
Figure 4.79 Output of medium tier 1 and coarse tier in nested form.	139
Figure 4.80 S11 of medium tier 1.	139
Figure 4.81 Output of medium tier 2 and medium tier 1 in nested form.	140
Figure 4.82 Output of medium tier 2 and medium tier 1 in nested form (zoomed around 8.8 GHz).	140
Figure 4.83 Detector outputs of medium tier 3.	141
Figure 4.84 Detector outputs of medium tier 3 (zoomed around 13 GHz).	141
Figure 4.85 Output of medium tier 3 and medium tier 2 in nested form (zoomed around 10 GHz).	142
Figure 4.86 General block diagram of fine tier.	143
Figure 4.87 Basic block diagram representation of an I/Q discriminator.	144
Figure 4.88 Schematic version of low pass filter.	146
Figure 4.89 Momentum version of low pass filter.	146
Figure 4.90 Measured response of low pass filter.	147
Figure 4.91 6 GHz high pass filter in stub form.	147
Figure 4.92 Kuroda transformation.	147
Figure 4.93 Schematic design of 6 GHz high pass filter.	148
Figure 4.94 Momentum lay out of 6 GHz high pass filter.	148
Figure 4.95 Measured response of low pass filter.	149
Figure 4.96. Fabricated 6 GHz high pass and low pass filters.	149
Figure 4.97 2-6 GHz power divider.	151
Figure 4.98 S21 and S31 of 2-6GHz power divider.	152
Figure 4.99 S11 of 2-6 GHz power divider.	152
Figure 4.100 Isolation between output ports of 2-6 GHz power divider.	153
Figure 4.101 Through and coupled ports of 2-6 GHz Lange coupler.	153
Figure 4.102 Phase difference between through and coupled ports.	154
Figure 4.103 Difference amplifier.	155
Figure 4.104 2-6 GHz I/Q discriminator.	156
Figure 4.105 Output of 2-6 GHz I/Q Discriminator.	157
Figure 4.106 Output of 2-6 GHz I/Q Discriminator (zoomed around 4 GHz).	157

Figure 4.107 Outputs of medium tier 3 and 2-6 GHz I/Q discriminator zoomed around 5 GHz in nested form.	158
Figure 4.108 Differences of output pairs in 2-6 I/Q discriminator in nested form with medium tier 3.	158
Figure 4.109 Layout of 6-18 GHz power divider.	159
Figure 4.110 S21 and S31 of 6-18 GHz power divider.	159
Figure 4.111 S11 of 6-18 GHz power divider.	160
Figure 4.112 Isolation between output ports of 6-18 GHz power divider.	160
Figure 4.113 S21 and S31 of 6-18 GHz Lange coupler.	161
Figure 4.114 Phase difference between coupled and isolated ports.	161
Figure 4.115 6-18 GHz I/Q discriminator.	163
Figure 4.116 Output of 6-18 GHz I/Q Discriminator (zoomed around 12 GHz). ...	164
Figure 4.117 Outputs of medium tier 3 and 6-18 GHz I/Q discriminator around 15 GHz in nested form.	164
Figure 4.118 Differences of output pairs in 6-18 I/Q discriminator in nested form with medium tier 3.	165
Figure 4.119 Return loss of port 1 in 6-18 GHz I/Q discriminator.	165
Figure 4.120 Return loss of port 2 in 6-18 GHz I/Q discriminator.	166
Figure 4.121 Fabricated 2-6 GHz I/Q Discriminator.	166
Figure 4.122 Fabricated 2-6 GHz I/Q Discriminator.	167
Figure 4.123 Fabricated 6-18 GHz I/Q discriminator detector outputs.	167
Figure 4.124 Detector outputs of 6-18 GHz I/Q discriminator when a 6 inch cable is used (zoomed around 12 GHz).	168
Figure 4.125 Detector outputs of fabricated 6-18 GHz I/Q discriminator (zoomed around 12 GHz).	168
Figure 4.126 Insertion losses with respect to the port 1 (ADS version).	169
Figure 4.127 Insertion losses with respect to the port 1 (fabricated discriminator).	169
Figure 4.128 Insertion losses with respect to the port 2 (ADS version).	170
Figure 4.129 Insertion losses with respect to the port 2 (fabricated discriminator).	170
Figure 4.130 Differential phase response between output arms when the input is given from port 1 (ADS version).	171
Figure 4.131 Differential phase response between output arms when the input is given from port 1 (fabricated discriminator).	171

Figure 4.132 Differential phase response between output arms when the input is given from port 2 (ADS version).....	172
Figure 4.133 Differential phase response between output arms when the input is given from port 2 (fabricated discriminator).....	172
Figure 4.134 Final frequency discriminator in ADS.....	17474
Figure 4.135 Coarse tier and medium tier 1 outputs in nested form.....	175
Figure 4.136 Diplexer output of coarse tier.....	175
Figure 4.137 Medium tier 1 and medium tier 2 outputs in nested form (zoomed around 10 GHz).....	176
Figure 4.138 Medium tier 2 and medium tier 3 outputs in nested form (zoomed around 12 GHz).....	176
Figure 4.139 Medium tier 3 and 2-6 GHz I/Q discriminator outputs in nested form (zoomed around 5 GHz).....	177
Figure 4.140 Medium tier 3 and 6-18 GHz I/Q discriminator outputs in nested form (zoomed around 12 GHz).....	177
Figure 4.141 Return loss of the final structure.....	178

LIST OF ABBREVIATIONS

A/D	: Analog to Digital
ADS	: Advanced Design System
ALU	: Arithmetic Logic Unit
DC	: Direct Current
DFD	: Digital Frequency Discriminator
DIFM	: Digital Instantaneous Frequency Measurement
ECM	: Electronic Countermeasures
ESM	: Electronic Support Measures
EW	: Electronic Warfare
HFSS	: High Frequency Structural Simulator
HPF	: High Pass Filter
IFM	: Instantaneous Frequency Measurement
LPF	: Low Pass Filter
OC	: Open Circuit
PDW	: Pulse Descriptor Word
RMS	: Root Mean Square
SC	: Short Circuit
SNR	: Signal to Noise Ratio
TL	: Transmission Line
UBW	: Unambiguous Bandwidth

CHAPTER 1

INTRODUCTION

1.1 Frequency Discrimination Overview

Instantaneous Frequency Measurement (IFM) receivers are among the essential components in Electronic Warfare (EW) systems and frequency discriminators form the heart of the most IFM receivers. Especially in broadband operations, as well as digital processing, analog processing of the input RF signal is necessary for IFM structures.

In order to accomplish to design a suitable IFM structure, the way of operation and fundamental requirements of frequency discrimination process must be well understood. A simple block diagram of an IFM is given in Figure 1.1 as an example.

The operation of a digital frequency discriminator is basically as follows:

1. Input signal entering to the system is divided into several paths.
2. Divided signals enter phase discriminators. Here, the phase shifts are applied to each incoming signal.
3. Phase shifted signals are mixed with a reference signal. Output of this mixing process contains DC voltage values which changes according to input signal's frequency are obtained.
 - The reference signal used in this mixing process may be the original input signal or one of the phase shifted signals or a specific signal generated by a local oscillator in the system.

4. The output DC values obtained from the mixing process are sampled by A/D converters.
5. Arithmetic Logic Unit (ALU) first solves possible ambiguities then estimates the input signal's frequency and creates a pulse descriptor word (PDW) for the IFM receiver.
 - Estimation of input frequency can be done by using pre-installed look-up tables into system. These tables may contain the relationship between voltage, phase and frequency. On the other hand both in ambiguity solution and estimation processes obtained DC values may be used in sorting algorithms and/or simple mathematical/trigonometric equations.

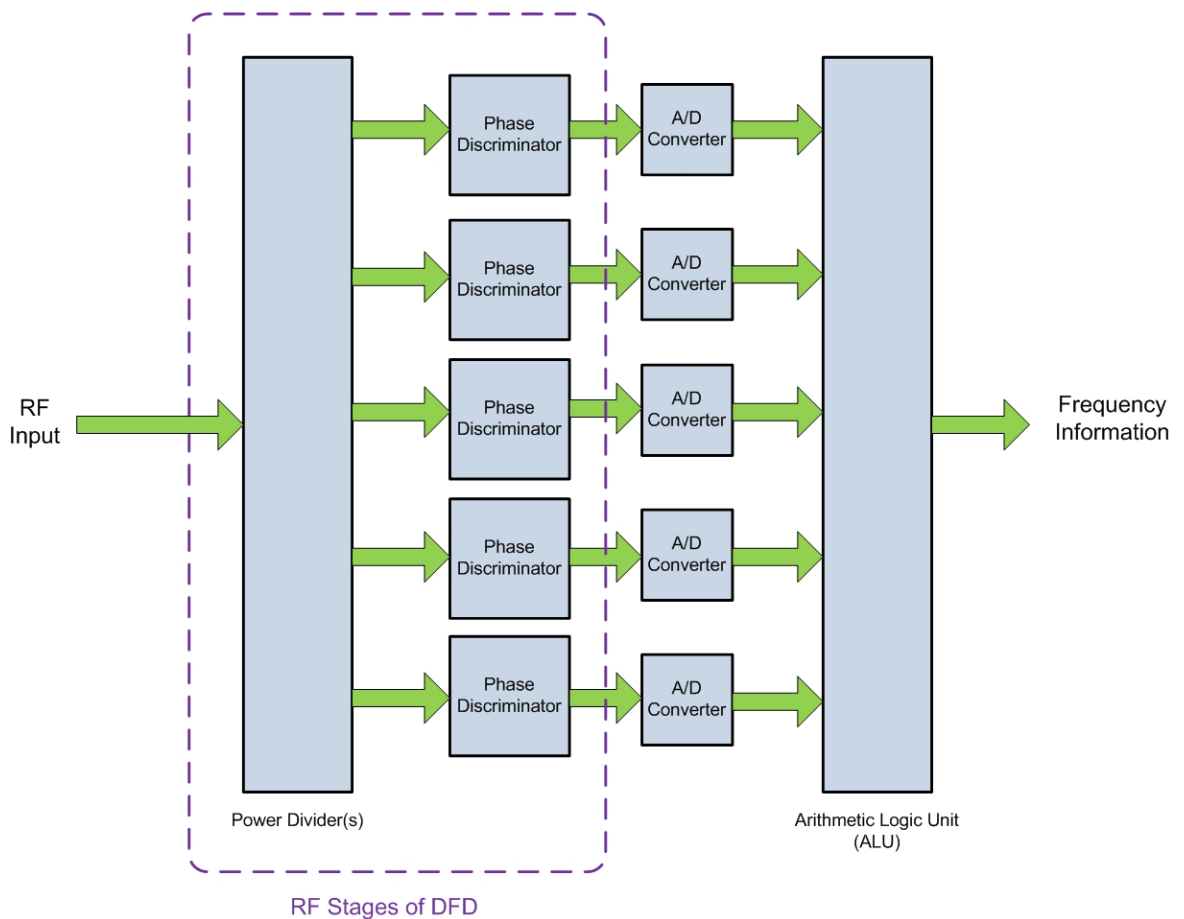


Figure 1.1 Basic block diagram of an IFM.

1.2 A Short History of IFM

The first radar system was introduced in the United States and Britain in 1930s [1] and played an important role during World War II for military uses [2]. Ever since then, its applications have comprehensively developed to other areas including Electronic Warfare (EW).

EW systems cover a very wide range of equipment to intercept radar or communication signals and to recognize and possibly locate threat emitters and their military platforms to gain a tactical advantage. The Electronic Support Measures (ESM) function is one of the key parts of an EW system. For ESM applications, frequency is reckoned to be the most important radar parameter. It is a very good descriptor of an emitter and therefore it is used in sorting and de-interleaving processes in especially dense signal environments. By this way, correlation of similar emitter reports from different stations and emitter identifications/classifications can be done. Knowing the frequency of possible enemy emitters has also an important role in active Electronic Countermeasures (ECM) systems to define correct operating band for noise or deception responses, optimizing output power and jammer effectiveness. Thus, accurate real time indication of the carrier frequency of radar signals is an essential link in EW concept. So microwave receivers have become an important research area because of their applications in EW. Accordingly, the importance of using microwave frequency discriminators in EW receivers is also increasing as the complexity of the signal environment continues to advance and the need for better signal information is required to perform the even more demanding EW functions.

Several different types of frequency analysis receiver are available at the present time, but none satisfies all the requirements placed by today's operational scenarios. Judging from the number of suppliers, however, the digital instantaneous frequency measuring (IFM) receiver, based on delay line discriminators, comes the closest and has become a major EW building block over the past 20 years [3].

The first practical delay line frequency discriminator circuit for wideband measurement of pulsed microwave signals was demonstrated by S. J. Robinson at Mullard Research Laboratories (MRL, later to become Philips Research Laboratories) in 1957 [4]. Application to EW receivers in an analogue form followed almost immediately. Robinson used a Polar Discriminator to generate analogue voltages which deflected a spot on a CRT screen. In these structures, the input signal amplitude was obtained from the magnitude of the vector appearing on the X-Y plane and the angle of this vector was changing linearly proportional to the input signal frequency. Modern discriminator components have evolved considerably over the years, but their operation is essentially the same. Video outputs are produced synchronously with the input RF signal and they are processed to generate sinusoidal video functions of frequency.

Further developments, such as digitization of video signals and combining multiple parallel discriminators with various delay line lengths naturally followed yielding digital frequency discriminators (DFDs). Nowadays, digital frequency discriminators are the most used discriminators in modern receivers.

1.3 IFM Structures

1.3.1 Time Domain Frequency Measurement

The simplest method of frequency measurement is the frequency counter. Figure 1.2 shows a simplified counter arrangement where input RF is amplified and used to drive a binary counter via a gate controlled by a timing circuit. After the timing interval the count stored in the counter is proportional to the RF input frequency. High resolution and accuracy are possible by using a long timing interval and high stability reference clock in the timer.

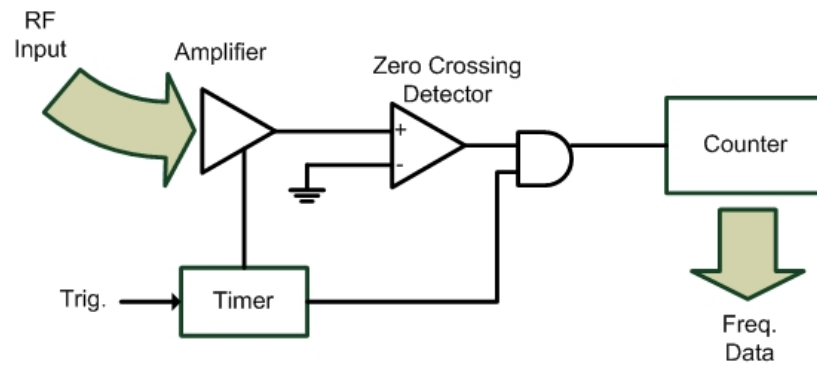


Figure 1.2 Simplified Frequency Counter

When EW requirements are considered, using such a counter is insufficient for measuring emitter frequency with a high resolution. Also the operating frequency band is limited to a few hundred MHz by the counter logic circuits so that RF down conversion would be required, adding to the complexity. But other than EW operations, frequency counters are still in use for basic applications [5].

1.3.2 Frequency Domain Discriminators

1.3.2.1 High-Pass / Low-Pass Discriminator

Most discriminators used in EW systems employ frequency domain circuits where frequency information is derived from the frequency selective characteristic of a microwave circuit. Since the required frequency information is at video bandwidths (<100 MHz) the frequency selective circuits include detectors outputting video signals only. Figure 1.3 shows how a low-pass filter followed by a detector can be used to discriminate between frequencies lying in the skirt region of the filter.

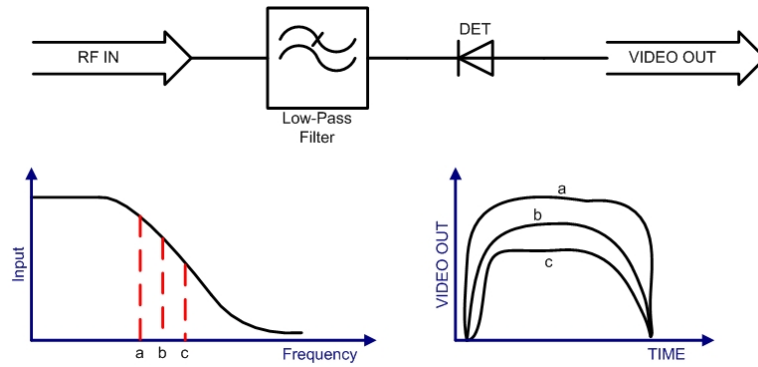


Figure 1.3 Low-pass discriminator.

The detected amplitude, however is also a function of the input signal amplitude, hence the arrangement shown in Figure 1.4 is used to remove the amplitude dependence by taking the ratio of the two detected outputs.

This simple arrangement has been used in low cost Radar Warners, it is restricted to very coarse frequency measurement only and mainly used in channelized activity detectors. Still efforts continue to improve the resolution of filter based discriminators like the one studied in [6], [7] and [8].

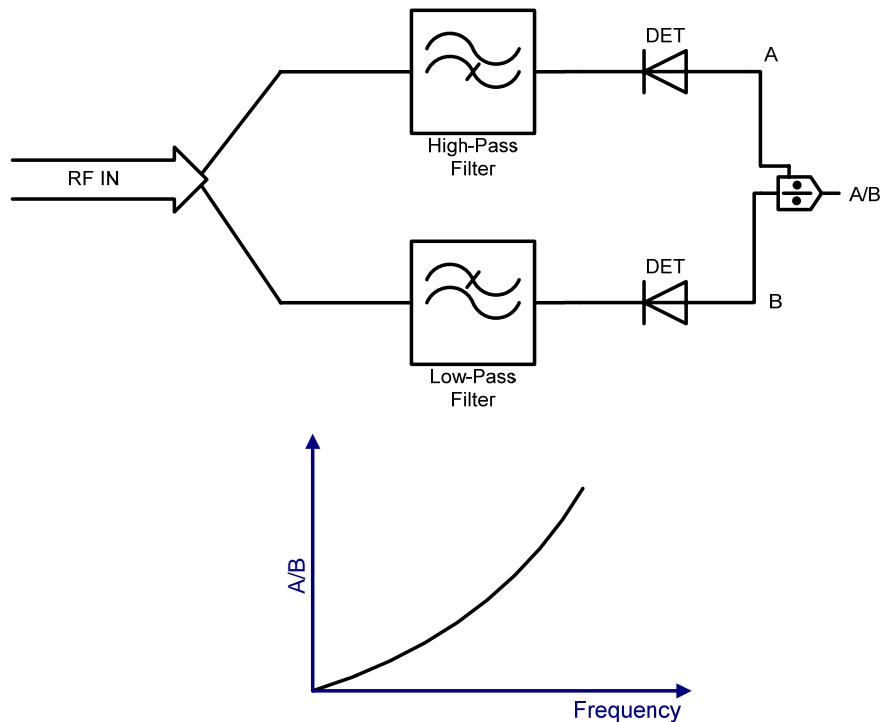


Figure 1.4 Ratio discriminator.

1.3.2.2 Delay Line Discriminator

Delay-line discriminators form the heart of most modern IFM receivers. They generate the basic signals which vary as functions of frequency across the defined operating band. The optimum output shape for a discriminator is a sinusoidal output voltage as a function of input frequency.

Most of the delay line discriminators are based on the principle of combining together two signal paths of different lengths to generate constructive and destructive interference which is detected as given below.

$$\left. \begin{aligned} V_1 &= 1 - \sin(\omega T) \\ V_2 &= 1 + \sin(\omega T) \end{aligned} \right\} \text{Quadrature} \quad (1.1)$$

$$\left. \begin{aligned} V_3 &= 1 + \cos(\omega T) \\ V_4 &= 1 - \cos(\omega T) \end{aligned} \right\} \text{In-Phase}$$

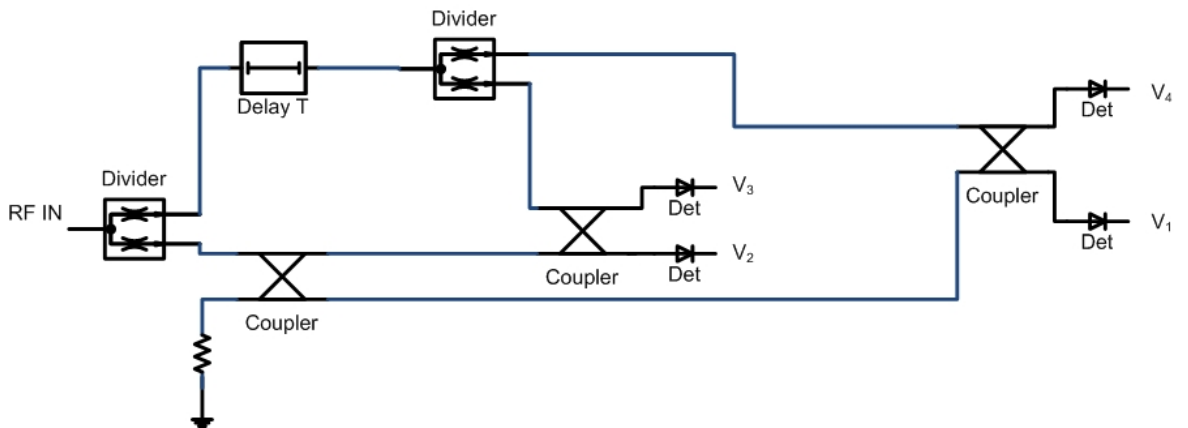


Figure 1.5 Delay line discriminator using 90 degree hybrid couplers.

The fidelity of the video outputs depend on the losses in the delay element, matching/isolation of the splitters/combiners, matching/transfer characteristics of the detectors and other various practical circuit imperfections.

Choosing the delay lines are another subject that must be considered. Using long delay lines may cause unequal power division. According to that, gain equalizers must be used in order to compensate the loss of the delay element. Because large imbalances of power arrived to the detectors may lead to video output offsets and large phase errors.

On the other hand, the hybrid couplers become extremely difficult to manufacture when designed for ultra-broadband operation since very tight couplings are required. Alternative structures are also considered about delay line concept like the one presented in [9].

1.3.2.3 Three-Phase Discriminator

As described for the I/Q discriminator in the above section, although very commonly used in IFMs, other than using 4 outputs, only three video outputs are sufficient to convey unambiguous 360 degree phase information.

Figure 1.6 shows the ideal outputs of a three-phase discriminator where the three video outputs vary sinusoidally vs frequency and phased 0, 120, 240 degrees. Discriminators with these characteristics may be designed using very simple structures operating over large bandwidths as studied in [10].

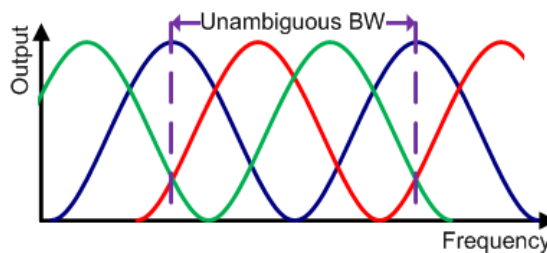


Figure 1.6 Three-Phase Discriminator Output

Figure 6 shows the conceptual schematics of a reflection mode discriminator where a short circuited transmission line is fed from a source of resistance R_s . The resistance

R_L represents the video detector diode which is used to detect the amplitude of the combined incident and reflected voltages.

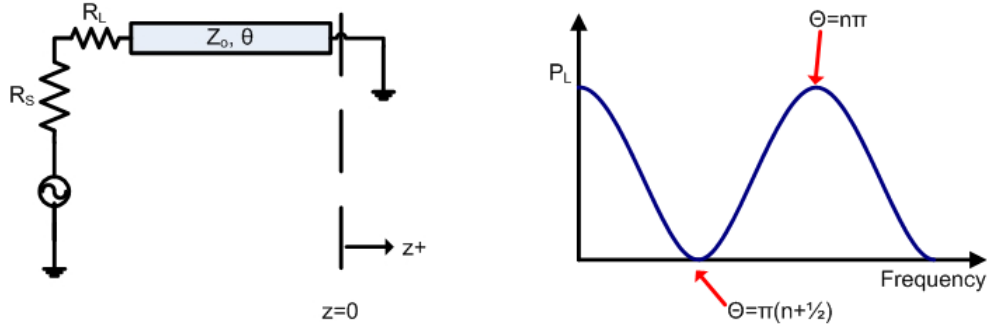


Figure 1.7 Reflection-mode Discriminator

The expression for the voltage at any point over the transmission line is given by equation (1.2). Here $V^+ e^{-j\beta z}$ represents the incident wave propagating in +z direction and $V^- e^{+j\beta z}$ represents reflected wave propagation in -z direction. β is the phase constant and “z” is the distance to the load which is located at $z=0$. Γ is the voltage reflection coefficient with θ being the phase angle of the reflection coefficient. $\Gamma(0)$ stands for the reflection at the load.

$$\Gamma(z) = \frac{V^- e^{+j\beta z}}{V^+ e^{-j\beta z}} = \Gamma(0) e^{+2j\beta z} \Rightarrow \Gamma(0) = |\Gamma(0)| e^{j\theta} = \rho e^{j\theta} \quad (1.2)$$

The total voltage over the line and its magnitude are given as follows.

$$V = V^+ e^{-j\beta z} + V^- e^{+j\beta z} \Rightarrow \Gamma(0) = \frac{V^-}{V^+} \Rightarrow V^+ (e^{-j\beta z} + \Gamma(0) e^{+j\beta z}) \quad (1.3)$$

$$|V| = |V^+| |e^{-j\beta z} + \Gamma(0) e^{+j\beta z}| \quad (1.4)$$

Magnitude of the total voltage at the position $z=-d$ of R_L is formulated through equations (1.5) to (1.8).

$$|V| = |V^+| |e^{+j\beta l} + \Gamma(0)e^{-j\beta l}| = |V^+| |1 + \Gamma(0)e^{+2j\beta l}| |e^{+j\beta l}| \Rightarrow |e^{+j\beta l}| = 1 \quad (1.5)$$

Here, $\Gamma(0)$ in equation (1.5) is equal to 1 as given in equation (1.6).

$$\Gamma(0) = \rho e^{j\theta} \Rightarrow |e^{+j\beta l}| = 1 \quad (1.6)$$

So the voltage value will be;

$$\begin{aligned} |V| &= |V^+| |e^{+j\beta l} + \rho e^{j(\theta-2\beta l)}| \\ &= |V^+| \sqrt{(1 + \rho \cos(\theta - 2\beta l))^2 + (\rho \sin(\theta - 2\beta l))^2} \end{aligned} \quad (1.7)$$

$$\begin{aligned} |V| &= |V^+| \sqrt{(1 + \rho)^2 - 2\rho(1 - \cos(\theta - 2\beta l))} \\ &= |V^+| \sqrt{(1 + \rho)^2 - 4\rho \sin^2(\beta l - \theta/2)} \end{aligned} \quad (1.8)$$

The minimum and maximum voltages will occur according to the sine function in the equation above.

When $\sin^2(\beta l - \theta/2) = 0 \Rightarrow (\beta l - \theta/2) = n\pi$, $|V_{\max}|$ will be;

$$|V_{\max}| = |V^+| (1 + \rho) \quad (1.9)$$

And when $\sin^2(\beta l - \theta/2) = 1 \Rightarrow (\beta l - \theta/2) = (2n + 1)\pi/2$, $|V_{\min}|$ will be;

$$|V_{\min}| = |V^+| (1 - \rho) \quad (1.10)$$

So, considering the simple circuit shown in Figure 1.7, when the frequency of the source is such that the line length is a multiple of half wavelength the power dissipated in R_L will be a maximum and conversely at odd multiples of quarter wavelengths the line will appear open circuit and no power will be absorbed in R_L .

Now by combining three of these networks, and replacing R by series mounted detectors the circuit shown in Figure 1.8 is formed, which is the basis of the Reflection Mode Three-Phase Discriminator.

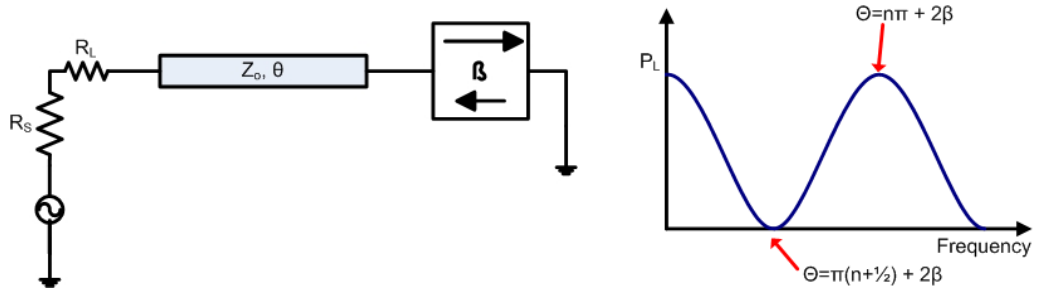


Figure 1.8 Reflection Discriminator with Phase Shifter

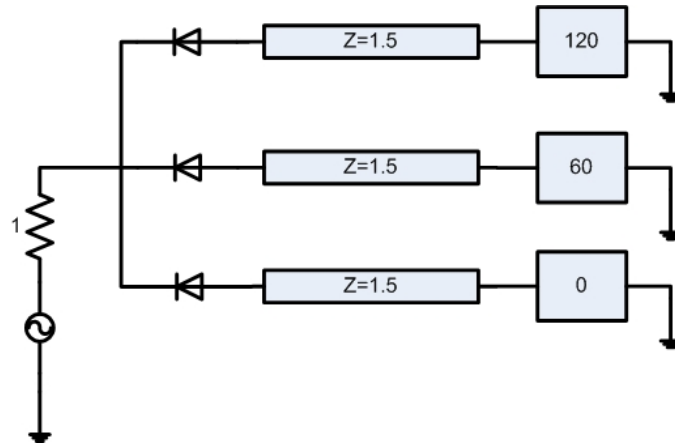


Figure 1.9 Three-phase discriminator.

The impedance levels required for a 50 ohm feed are 75 ohm detector resistances and 75 ohm lines and phase shifters, as developed in equations (1.11) to (1.16).

$$Z_{in} = Z_1 // Z_2 // Z_3 \Rightarrow Z_{in} = 1 \quad (1.11)$$

$$Z_1 = Z_2 = Z_3 = Z_L = Z_{line+shifter} + Z_{Detector} \quad (1.12)$$

$$Z_{line+shifter} = Z_{Detector} = Z \quad (1.13)$$

$$Z_{in} = Z_L // Z_L // Z_L \Rightarrow Z_{in} = \left(\frac{Z_L}{2} \right) // Z_L \quad (1.14)$$

$$Z_{in} = \frac{\left(\frac{Z_L}{2} \right) Z_L}{\left(\frac{Z_L}{2} \right) + Z_L} = \frac{\left(\frac{Z_L}{2} \right)}{\frac{3}{2}} = \frac{Z_L}{3} = 2 \left(\frac{Z}{3} \right) \quad (1.15)$$

$$Z = Z_{in} \left(\frac{3}{2} \right) \quad (1.16)$$

The discriminator will then be matched at the input port. All available power will be split between the three detectors equally. The structure is explained and presented by a figure (Figure 1.10) below. Here, assume that the input wave is $A \cos(\omega t)$

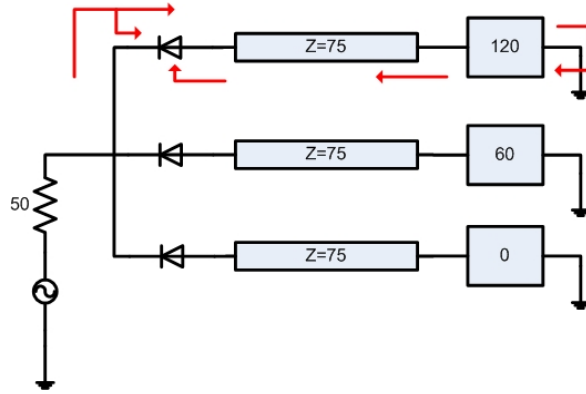


Figure 1.10 Reflection discriminator signal paths.

1. An input wave packet is split equally three ways. So the input will be $\frac{A}{\sqrt{3}} \cos(\omega t)$ at each branch.
2. Half of each wave is absorbed from detectors at the branches.
3. The remaining power, $\frac{A}{\sqrt{6}} \cos(\omega t)$, propagates to the lines and phase shifters.
4. At each branch, incoming waves will be delayed $\left(\frac{\omega \tau}{2} \right)$, reflected back from the phase shifters with a phase shift and delayed again. So the reflected waves at the

common feed will be $\frac{A}{\sqrt{6}}\cos(\omega t + \omega \tau + 240)$, $\frac{A}{\sqrt{6}}\cos(\omega t + \omega \tau + 120)$, and $\frac{A}{\sqrt{6}}\cos(\omega t + \omega \tau)$

5. The mutual phase difference between the reflected waves will create a virtual earth at the common feed. This situation can be explained as follows.

$$V_{\text{common_feed_reflected}} = \underbrace{B \cos(\omega t + \omega \tau + 240)}_{\text{term1}} + \underbrace{B \cos(\omega t + \omega \tau + 120)}_{\text{term2}} + \underbrace{B \cos(\omega t + \omega \tau)}_{\text{term3}} \quad (1.17)$$

Here, the trigonometric identity given below can be used

$$\cos(\alpha \pm \beta) = \cos(\alpha)\cos(\beta) \mp \sin(\alpha)\sin(\beta) \quad (1.18)$$

then the summation terms 1 and 2 will be respectively;

$$\begin{aligned} B \cos(\alpha + 240) &= B(\cos(\alpha)\cos(240) - \sin(\alpha)\sin(240)) \\ &= B\left(\sin(\alpha)\frac{\sqrt{3}}{2} - \cos(\alpha)\frac{1}{2}\right) \end{aligned} \quad (1.19)$$

$$\begin{aligned} B \cos(\alpha + 120) &= B(\cos(\alpha)\cos(120) - \sin(\alpha)\sin(120)) \\ &= B\left(-\cos(\alpha)\frac{1}{2} - \sin(\alpha)\frac{\sqrt{3}}{2}\right) \end{aligned} \quad (1.20)$$

Here, $\alpha = \omega(t + \tau)$. If we sum the terms above with the term3, then the result will be equal to;

$$V_{\text{common_feed_reflected}} = \text{term1} + \text{term2} + \text{term3} = 0 \quad (1.21)$$

So the reflected waves will only see the 75 ohm detectors and they will be absorbed.

6. Detectors will act as a “single balanced mixer”. So incident and reflected waves will be mixed. At each branch, mixed waves will have DC values, $C \cos(\omega \tau + 240)$, $C \cos(\omega \tau + 120)$ and $C \cos(\omega \tau)$. Thus, it is seen that these DC values are related to the input frequency from which the frequency information can be extracted.

1.4 Scope of the Thesis

In this thesis, RF sections of a multi tier instantaneous frequency measurement (IFM) receiver operating in 2-18 GHz range is targeted, with possible fabrication of some of the critical components. Presented structure is simple, compact, highly reproducible and can be used in IFM receivers for airborne applications.

The design and simulation stages are completed successfully. Some components are also fabricated yielding the expected results. The block diagram of the designed RF section of the IFM is shown in Figure 1.11. The structure contains a series of discriminator tiers operating in parallel to give the required resolution unambiguously over the operating band. It has the following blocks: One coarse tier, three medium tiers and one fine tier. These tiers are separated according to their frequency resolution measurement capabilities and each tier is used to resolve the ambiguity of the adjacent tier.

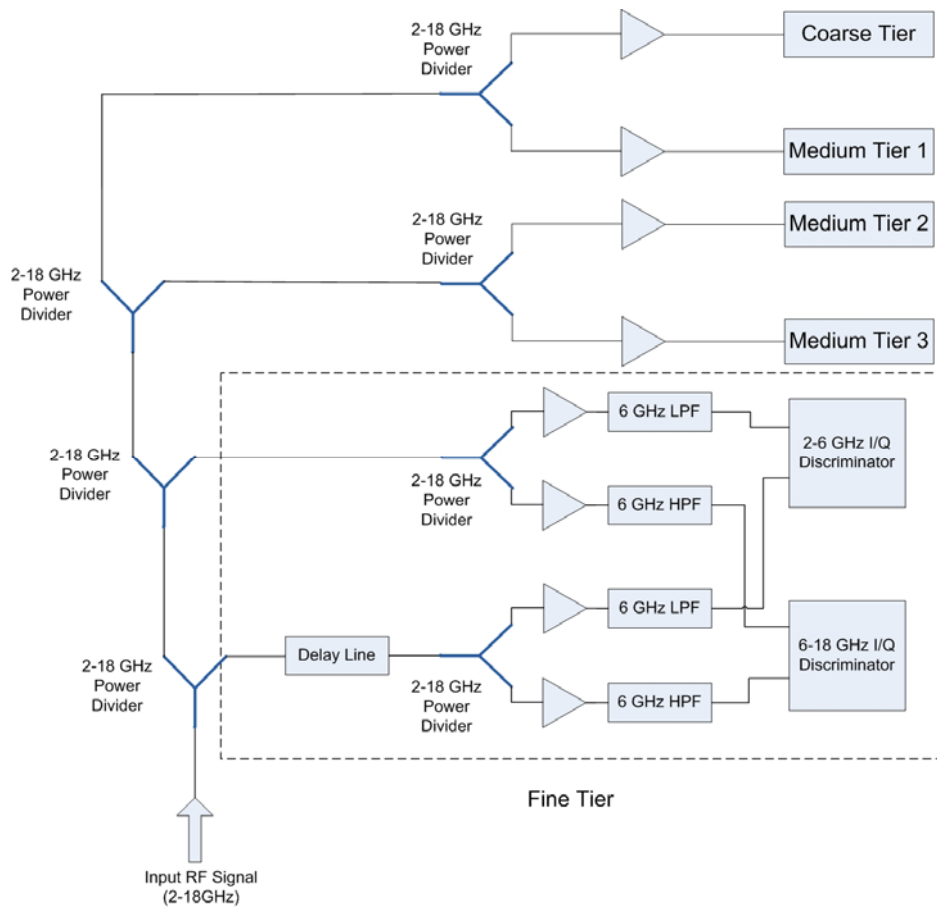


Figure 1.11 Basic block diagram of the discriminator.

The most critical components for the RF part of an IFM are phase discriminators (also called as phase correlators). These structures are used to employ phase shifting networks and delay lines which are used to insert different phases to the incoming signal. As will be detailed in the succeeding chapters, much of the efforts in this thesis are directed to the design and realization of phase shifters, resulting in novel reflective phase shifter structures operating successfully over the targeted frequency band. Presented phase shifting technique is used coarse and medium tiers. These tiers cover the determined frequency range in a single band. According to the theory of operation, an ambiguity in coarse tier is not tolerated. Due to this reason, in addition to the reflective phase shifting network, a 10 GHz diplexer is used in order to get a hint about whether the input signal's frequency is below 10 GHz or not. Unlike the other tiers, because reflective phase shifters would necessitate unacceptably long delay lines, fine tier is designed by using a more conventional approach by using I/Q discriminators and employing Lange directional couplers. However couplers are usable only up to around 1.5 octaves. For this reason fine tier has two different discriminator structures which operate in 2 – 6 GHz and 6 – 18 GHz frequency ranges.

The designed structure seems to be able to measure the input signal's frequency with 1 MHz resolution and 0.28 MHz accuracy (rms) under the assumption that 8 bit A/Ds are used in the sampling process, an input SNR of 0dB and 20 MHz video bandwidth. In addition to the whole system design of the RF part, coarse and fine tiers shown in Figure 1.11 are also fabricated and measured.

1.5 Outline of the Thesis

The thesis is organized as follows:

This introduction chapter is followed by Chapter 2 which introduces the basic concepts for frequency discriminator design. Background theory is given for a typical frequency discriminator structure. Fundamental criteria for a discriminator

such as measurement resolution and accuracy, number of phase shifting tiers and phase margin are discussed by presenting necessary derivations and calculations.

Chapter 3 describes various phase shifter network alternatives as candidates to be used in the frequency discriminator. Simulations and optimizations performed by using Advanced Design System 2006A[®]. Discussions and comparisons are made according to these simulations and additional calculations. At the end of this chapter, the appropriate structure is decided, designed and simulated.

Chapter 4 presents the components of the frequency discriminator. The choice of fabrication materials is discussed. Designs, simulations and layout drawing are given. In that chapter, simulations are done by using ADS[®] and in addition to that, for a specific problem HFSS[®] is also used. Solutions to probable problematic subjects that can be encountered in realization process are explained. Measurement results of manufactured components are also presented and discussed in this chapter.

Chapter 5 summarizes the work presented in this thesis by mentioning the important points of design and fabrication steps.

Chapter 6 gives the conclusions about the thesis done and the possible future works.

CHAPTER 2

BASIC CONCEPTS

2.1 Signal Spectra and Instantaneous Frequency

The spectral components $S(\omega)$ of a time domain signal $s(t)$ can be calculated by using the Fourier transform

$$S(\omega) = \int_{-\infty}^{\infty} s(t)e^{-j\omega t} dt \quad (2.1)$$

Figure 2.1 shows the spectrum of a pulse of an RF signal with carrier frequency f_0 Hz and duration T seconds

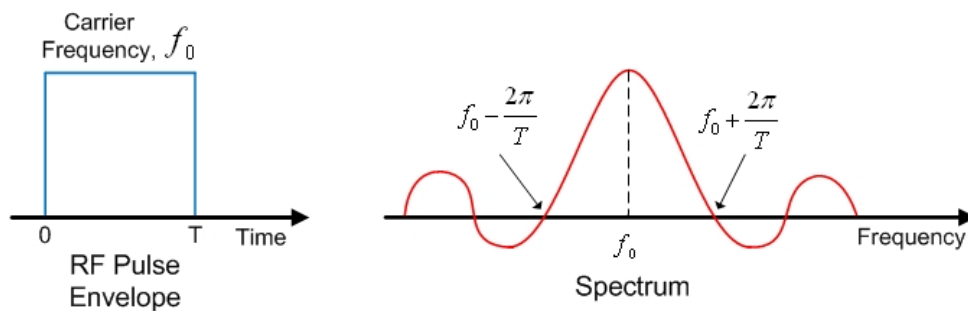


Figure 2.1 Spectrum of an RF Pulse

Although the amplitude of the spectrum is maximum at the carrier frequency, as T reduces the spectrum widens and that makes the exact determination of f_0 more uncertain. This introduces the fundamental constraint on frequency measurements: The uncertainty degree of a frequency measurement is inversely related to the

duration of the measurement time. The term “instantaneous frequency” when interpreted literally is thus meaningless and needs to be defined in a more practical way. This can be done by assuming that the signal $s(t)$ can be expressed as

$$s(t) = A(t)e^{j\theta(t)} \quad (2.2)$$

and that $A(t)$ is a slowly varying function of the time relative to $\theta(t)$, the instantaneous phase. Now the instantaneous frequency is defined as

$$F_{inst} = \frac{d\theta(t)}{dt} \quad (2.3)$$

The restriction imposed on $A(t)$ is normally well satisfied in most practical cases for two reasons as follows: the video bandwidths (signal envelope bandwidth) for most signals of interest are much smaller than the carrier frequency and amplifiers with limiting characteristics are normally required dynamic range compression, hence amplitudes are limited to a constant level. Although the instantaneous frequency is now defined at an instant in time, the measurement of rate of change of phase still requires a finite time interval.

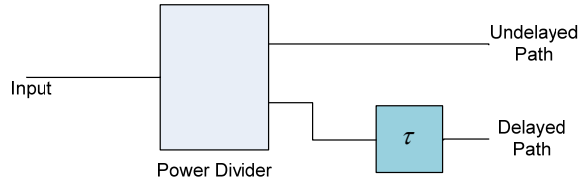
2.2 Principle of Operation

Consider a sinusoidal wave which is split into two paths by a power divider as shown in Figure 2.2a. Here, one of the divided signals is delayed a constant time with respect to the other one. This time delay creates a phase difference between the outputs of two paths. Figure 2.2b and Figure 2.2c show delayed and undelayed versions of different sinusoidal waves. As presented in this figure, for the same time delay, phase angles change with respect to the frequency. The relative delayed phase angles are

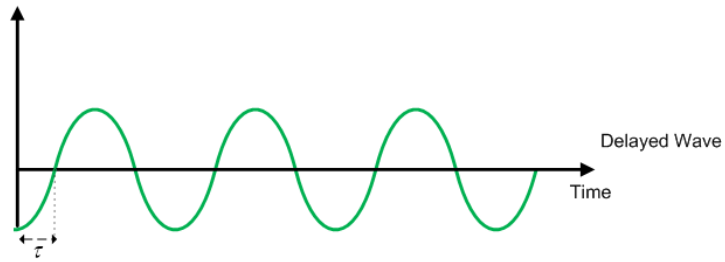
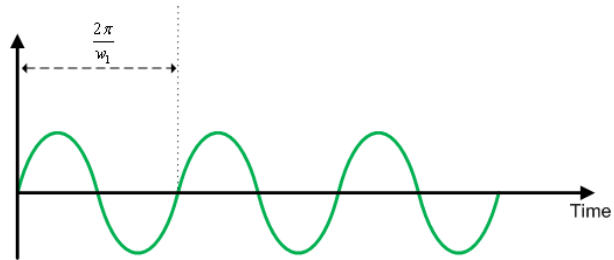
$$\theta_1 = \omega_1 \tau \quad (2.4)$$

$$\theta_2 = \omega_2 \tau \tag{2.5}$$

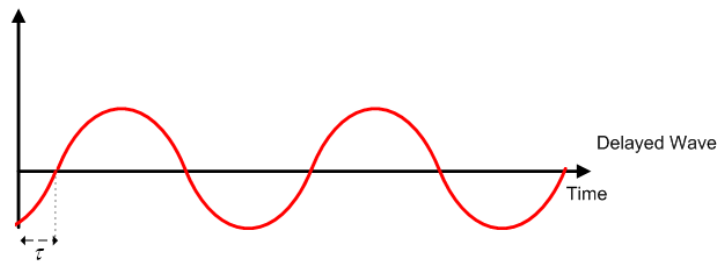
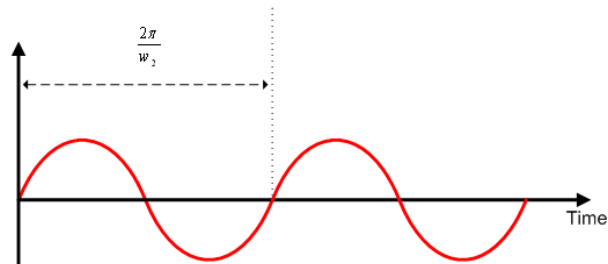
Since $\omega_1 > \omega_2$, then $\theta_1 > \theta_2$



(a) Schematic diagram



(b) Signal with Angular Frequency ω_1



(c) Signal with Angular Frequency ω_2 ($\omega_1 > \omega_2$)

Figure 2.2 Phase relation of sinusoidal waves with constant time delay

Equations (2.4) and (2.5) show that the phase angle is directly proportional to the input signal frequency. In an IFM receiver, a proper delay line τ is introduced. By measuring the phase delay between the undelayed and delayed signal, the frequency of the input signal is obtained. Since the amplitude of the signal does not affect the relative phase angle, the signal strength can be measured at the same time [11].

An example of a frequency measurement circuit in a practical IFM receiver is given in Figure 2.3. The incoming signal is divided into delayed and undelayed paths. Both of these signals are fed into a phase correlator which has four outputs, and each of them is followed by a detector. The outputs of the detectors are connected to the inputs of two differential amplifiers. The differential amplifier is used to take the difference of its two input signals. If one input is V_1 and the other one is V_2 , then the output of the differential amplifier $V_0 = A(V_1 - V_2)$ where A is the amplification factor. The outputs of the differential amplifiers can be either digitized or directly displayed on a scope to obtain the frequency information.

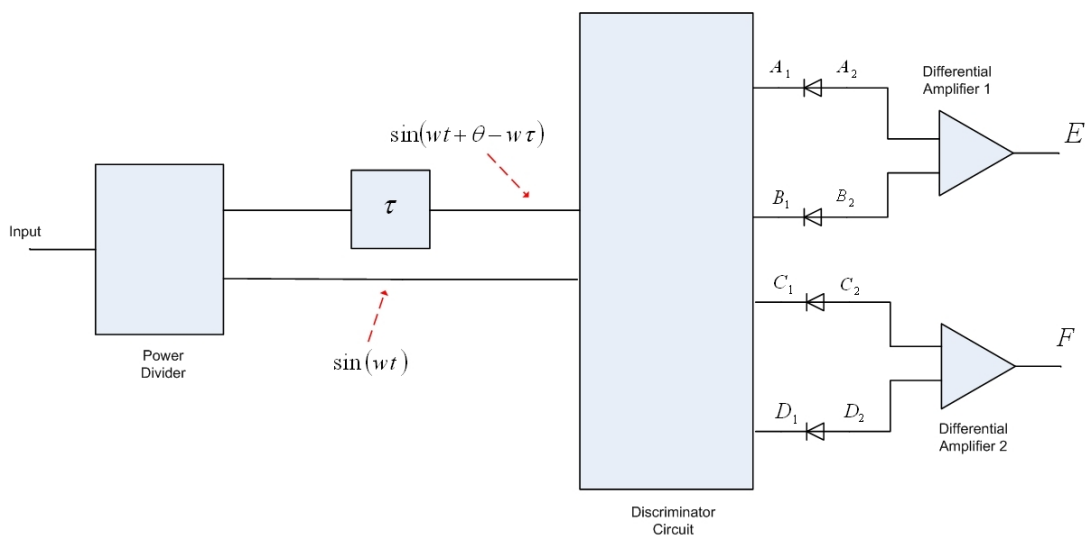


Figure 2.3 Basic frequency measurement circuit of an IFM receiver [11].

A typical frequency discriminator (also called as phase correlator or phase discriminator) is a passive component which contains usually four hybrid circuits. Its function is to introduce constant phase angles to each of the two input signals and combine them in a certain way. These discriminator circuits may have different

designs. A general discussion will be presented here by using Figure 2.3 to refer to the signal at each point. In order to provide a universal concept on the phase discriminator, the following steps are taken [11]:

1. The signals are known.
2. The desired outputs at E and F are specified.
3. The detectors are square law devices followed by low-pass filters.
4. With the input and output specified, signals at A_1 , B_1 , C_1 and D_1 are assigned so that after the detectors and differential amplifiers, the outputs will match the desired ones at E and F .
5. For simplicity, neglect the amplitude on each signal and assume that all amplitudes are units. Then assume that the input signal is

$$\sin(\omega t + \theta) \tag{2.6}$$

where ω is the angular frequency and θ is its phase angle. At the input of the phase discriminator, the two signals are $\sin(\omega t + \theta)$ and $\sin(\omega t - \omega \tau + \theta)$, where τ is the delay time introduced on one of the two outputs from the power divider. Assume that desired E and F are

$$E = \sin(\omega \tau) \tag{2.7}$$

$$F = \cos(\omega \tau) \tag{2.8}$$

Here the relative amplitude of E and F can be measured to determine $\omega \tau$, which in turn determines the frequency of the input signal, because τ is a known value. In order to obtain the equations (2.7) and (2.8), the terms $\sin(\omega \tau)$ and $\cos(\omega \tau)$ must be present at the inputs of differential amplifiers E and F . The required outputs from

the discriminator can be designed as follows. The input that can produce $\sin(w\tau)$ after a square law detector is

$$A_1 = \pm[\sin(wt + \Phi_A) + \cos(wt - w\tau + \Phi_A)] \quad (2.9)$$

or

$$A_1 = \pm[\sin(wt - w\tau + \Phi_A) - \cos(wt + \Phi_A)] \quad (2.10)$$

The input that will produce $-\sin(w\tau)$ is

$$B_1 = \pm[\sin(wt - w\tau + \Phi_B) + \cos(wt + \Phi_B)] \quad (2.11)$$

or

$$B_1 = \pm[\sin(wt + \Phi_B) - \cos(wt - w\tau + \Phi_B)] \quad (2.12)$$

The input that will produce $\cos(w\tau)$ is

$$C_1 = \pm[\cos(wt - \Phi_C) + \cos(wt - w\tau + \Phi_C)] \quad (2.13)$$

or

$$C_1 = \pm[\sin(wt + \Phi_C) - \sin(wt - w\tau + \Phi_C)] \quad (2.14)$$

The input that will produce $-\cos(w\tau)$ is

$$D_1 = \pm[\cos(\omega t + \Phi_D) - \cos(\omega t - \omega \tau + \Phi_D)] \quad (2.15)$$

or

$$D_1 = \pm[\sin(\omega t + \Phi_D) - \sin(\omega t - \omega \tau + \Phi_D)] \quad (2.16)$$

where Φ_A , Φ_B , Φ_C and Φ_D are phase angles at the output of the phase discriminator. Equations through (2.9) to (2.16) can be treated actually as two sets of equations: (2.9)/(2.10) and (2.11)/(2.12) form one set, (2.13)/(2.14) and (2.15)/(2.16) form another set.

The outputs from detectors are the square of the input signals. Thus;

$$\begin{aligned} A_2 &= A_1^2 \\ &= 2 \sin(\omega t + \Phi_A) \cos(\omega t - \omega \tau + \Phi_A) + \sin^2(\omega t + \Phi_A) \\ &\quad + \cos^2(\omega t - \omega \tau + \Phi_A) \\ &= \sin(\omega \tau) + \sin(2\omega t - \omega \tau + 2\Phi_A) + 1 \\ &\quad + \frac{1}{2} \cos 2(\omega t - \omega \tau + \Phi_A) - \frac{1}{2} \cos 2(\omega t + \Phi_A) \end{aligned} \quad (2.17)$$

or

$$\begin{aligned} A_2 &= A_1^2 \\ &= -2 \sin(\omega t - \omega \tau + \Phi_A) \cos(\omega t + \Phi_A) + \sin^2(\omega t - \omega \tau + \Phi_A) \\ &\quad + \cos^2(\omega t + \Phi_A) \\ &= \sin(\omega \tau) - \sin(2\omega t - \omega \tau + 2\Phi_A) + 1 \\ &\quad + \frac{1}{2} \cos 2(\omega t + \Phi_A) - \frac{1}{2} \cos 2(\omega t - \omega \tau + \Phi_A) \end{aligned} \quad (2.18)$$

Similarly

$$\begin{aligned}
B_2 &= B_1^2 \\
&= -\sin(wt) + \sin(2wt - w\tau + 2\Phi_B) + 1 \\
&\quad - \frac{1}{2}\cos 2(wt - w\tau + \Phi_B) + \frac{1}{2}\cos 2(wt + \Phi_B)
\end{aligned} \tag{2.19}$$

or

$$\begin{aligned}
B_2 &= B_1^2 \\
&= -\sin(w\tau) - \sin(2wt - w\tau + 2\Phi_B) + 1 \\
&\quad - \frac{1}{2}\cos 2(wt + \Phi_B) + \frac{1}{2}\cos 2(wt - w\tau + \Phi_B)
\end{aligned} \tag{2.20}$$

$$\begin{aligned}
C_2 &= C_1^2 \\
&= \cos(w\tau) + \cos(2wt - w\tau + 2\Phi_B) + 1 \\
&\quad - \frac{1}{2}\cos 2(wt + \Phi_C) + \frac{1}{2}\cos 2(wt - w\tau + \Phi_C)
\end{aligned} \tag{2.21}$$

or

$$\begin{aligned}
C_2 &= C_1^2 \\
&= \cos(w\tau) - \cos(2wt - w\tau + 2\Phi_C) + 1 \\
&\quad - \frac{1}{2}\cos 2(wt + \Phi_C) - \frac{1}{2}\cos 2(wt - w\tau + \Phi_C)
\end{aligned} \tag{2.22}$$

$$\begin{aligned}
D_2 &= D_1^2 \\
&= -\cos(w\tau) - \cos(2wt - w\tau + 2\Phi_D) + 1 \\
&\quad + \frac{1}{2}\cos 2(wt + \Phi_D) + \frac{1}{2}\cos 2(wt - w\tau + \Phi_D)
\end{aligned} \tag{2.23}$$

or

$$\begin{aligned}
D_2 &= D_1^2 \\
&= -\cos(w\tau) + \cos(2wt - w\tau + 2\Phi_D) + 1 \\
&\quad - \frac{1}{2}\cos 2(wt + \Phi_D) - \frac{1}{2}\cos 2(wt - w\tau + \Phi_D)
\end{aligned} \tag{2.24}$$

In equations through (2.17) to (2.24), the terms $\sin(w\tau)$ and $\cos(w\tau)$ are constants (or in other words, DC voltages from the output of the detector), since w is a constant (angular frequency of the incoming signal) and τ is a constant (the delay time in the phase discriminator). All of the other terms (e.g. $\cos 2(wt - w\tau + \Phi_C)$ and $\sin(2wt - w\tau + 2\Phi_A)$, etc.) are the high frequency terms, and their frequency doubles that of the input signal. These high frequency terms can be filtered out by the low-pass filters formed at the outputs of the detectors. Therefore, the actual signals at the inputs of the differential amplifiers are

$$A_2 = 1 + \sin(w\tau) \quad (2.25)$$

$$B_2 = 1 - \sin(w\tau) \quad (2.26)$$

for the top amplifier (amplifier 1 in Figure 2.3) and

$$C_2 = 1 + \cos(w\tau) \quad (2.27)$$

$$D_2 = 1 - \cos(w\tau) \quad (2.28)$$

for the bottom amplifier (amplifier 2 in Figure 2.3). At the outputs of the amplifiers, these constant terms cancel out.

$$E = 2 \sin(w\tau) \quad (2.29)$$

$$F = 2 \cos(w\tau) \quad (2.30)$$

These are the desired results. They can be either displayed in a polar form or digitized and fed into a digital processor. For a polar display, $x = E = 2 \sin(w\tau)$ and $y = F = 2 \cos(w\tau)$. Then the angle of the polar display is

$$\theta = \tan^{-1}\left(\frac{x}{y}\right) = w\tau \quad (2.31)$$

Thus, the frequency w is linearly proportional to the angle θ . Next section will present an actual network that will provide the required phase discriminator outputs (A_1 , B_1 , C_1 and D_1) to fulfill the equations (2.9) through (2.16) and get the desired result given in (2.31).

2.3 Phase Discriminators

In this section a typical discriminator circuit is presented by using the same structure given in Figure 2.3. Figure 2.4 shows a basic discriminator which contains one power divider, one delay line, three 90 degree hybrid couplers, one 180 degree hybrid coupler, four detectors and two differential amplifiers. In order to simplify the discussion, the input is assumed as $2\sqrt{2}\cos(wt)$, where the phase angle θ is assumed to be zero. For the 90 degree coupler, a signal going through the direct path will have 90 degree phase while going through the diagonal path, the delay line is 180 degrees. Thus the phase difference between two outputs is 90 degrees. For the 180 degree coupler, phase difference between the signals passing through the direct path and the diagonal path is 180 degree.

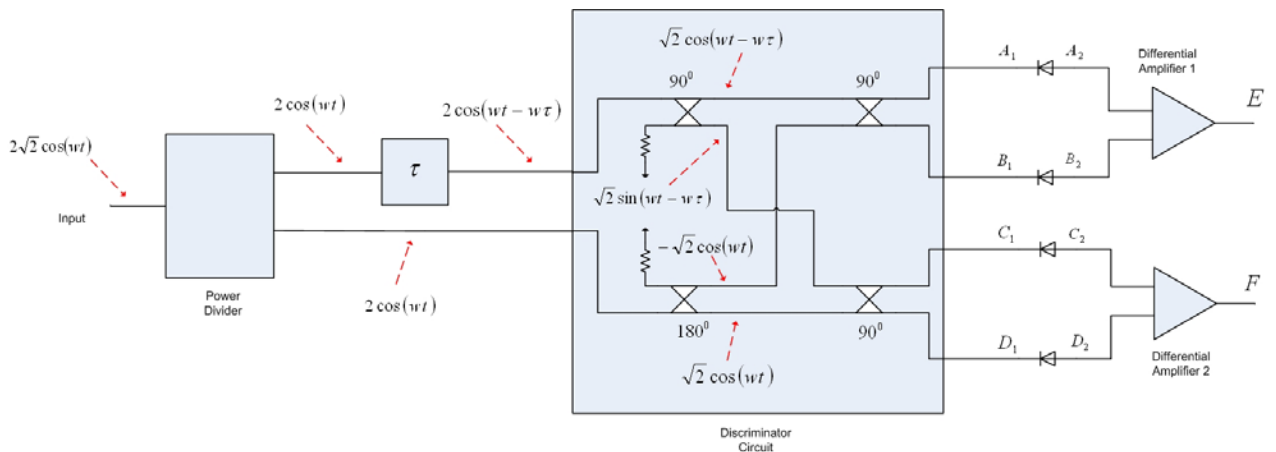


Figure 2.4 An example of a frequency discriminator [11].

The amplitude of the signal decreases by factor $\sqrt{2}$ whenever it passes through either a power divider or a phase shifter. The signal flow can be traced as follows: After the input signal is divided into two paths, delayed and undelayed signals are obtained. After they pass through the 90 degree and 180 degree hybrid couplers four terms which are $\sqrt{2}A\cos(\omega t - \omega\tau)$, $\sqrt{2}A\sin(\omega t - \omega\tau)$, $\sqrt{2}A\cos(\omega t)$ and $-\sqrt{2}A\cos(\omega t)$ obtained as shown in Figure 2.4. The next two 90 degree couplers are used to combine these signals.

$$A_1 = A\cos(\omega t - \omega\tau) - A\sin(\omega t) \quad (2.32)$$

$$B_1 = A\sin(\omega t - \omega\tau) - A\cos(\omega t) \quad (2.33)$$

$$C_1 = A\sin(\omega t - \omega\tau) + A\sin(\omega t) \quad (2.34)$$

$$D_1 = -A\cos(\omega t - \omega\tau) + A\cos(\omega t) \quad (2.35)$$

where (2.32) is equivalent to (2.12), (2.33) is equivalent to (2.10), (2.34) is equivalent to (2.14) and (2.35) is equivalent to (2.15). At outputs of the detectors, the only terms of interest are the square law outputs. They can be written as

$$A_2 = A^2 \cos^2(\omega t - \omega\tau) - 2A^2 \cos(\omega t - \omega\tau)\sin(\omega t) + A^2 \sin^2(\omega t) \quad (2.36)$$

$$B_2 = A^2 \sin^2(\omega t - \omega\tau) - 2A^2 \sin(\omega t - \omega\tau)\cos(\omega t) + A^2 \cos^2(\omega t) \quad (2.37)$$

$$C_2 = A^2 \sin^2(\omega t - \omega\tau) - 2A^2 \sin(\omega t - \omega\tau)\sin(\omega t) + A^2 \sin^2(\omega t) \quad (2.38)$$

$$D_2 = A^2 \cos^2(\omega t - \omega\tau) - 2A^2 \cos(\omega t - \omega\tau)\cos(\omega t) + A^2 \cos^2(\omega t) \quad (2.39)$$

The outputs at the detectors considering the filter action can be written as

$$A_2 = A^2 - A^2 \sin(w\tau) \quad (2.40)$$

$$B_2 = A^2 + A^2 \sin(w\tau) \quad (2.41)$$

$$C_2 = A^2 + A^2 \cos(w\tau) \quad (2.42)$$

$$D_2 = A^2 - A^2 \cos(w\tau) \quad (2.43)$$

At the outputs of the differential amplifiers 1 and 2

$$E = B_2 - A_2 = 2A^2 \sin(w\tau) \quad (2.44)$$

$$F = C_2 - D_2 = 2A^2 \cos(w\tau) \quad (2.45)$$

If the outputs E and F are displayed on a x-y axis, then the angle θ

$$\theta = \tan^{-1}\left(\frac{E}{F}\right) = \tan^{-1}(\tan(w\tau)) = w\tau \quad (2.46)$$

In order to keep the frequency in the unambiguous region, θ must be kept within 2π . For example, if the receiver covers frequency range from f_1 to f_2 then

$$\theta_1 = 2\pi f_1 \tau \quad (2.47)$$

$$\theta_2 = 2\pi f_2 \tau \quad (2.48)$$

where the angle θ_1 corresponds to f_1 and θ_2 corresponds to f_2 .

When $\theta_2 = \theta_1 + 2k\pi$ where k is a constant,

- If $k \leq 1$, there is no frequency ambiguity among the frequency range f_1 and f_2
- If $k = 1$, the receiver will provide the maximum frequency resolution.

For example, if $f_1 = 2GHz$ and $f_2 = 4GHz$ then from (2.47) and (2.48) one obtains

$$\theta_2 - \theta_1 = 2\pi = 2\pi(f_2 - f_1)\tau \quad (2.49)$$

$$\tau = \frac{1}{2 \times 10^9} = 0.5ns \quad (2.50)$$

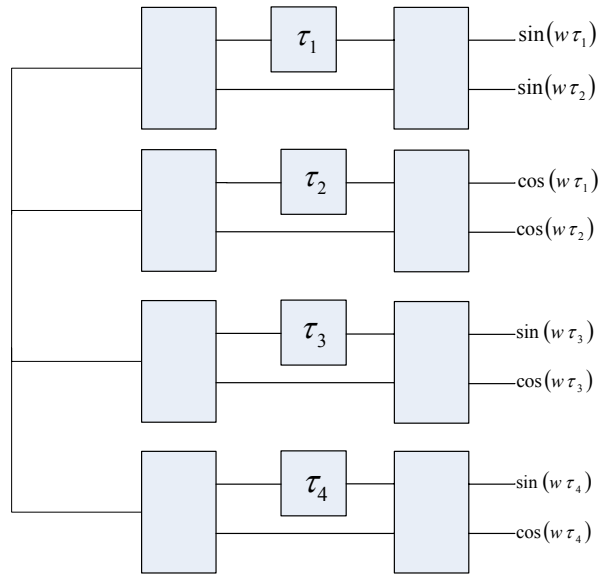
So the maximum delay time without ambiguity should be 0.5ns.

From the above discussion of IFM receivers, note that in the receiver design there is no special filter to limit the RF bandwidth. The frequency resolution generated by the receiver is not from any narrow bandwidth system such as in a superhet receiver. The frequency information is generated by comparison of the phase relation of the delayed and undelayed signals. Both parts are wide bandwidth; therefore, the receiver is basically referred to as a “wide bandwidth” system.

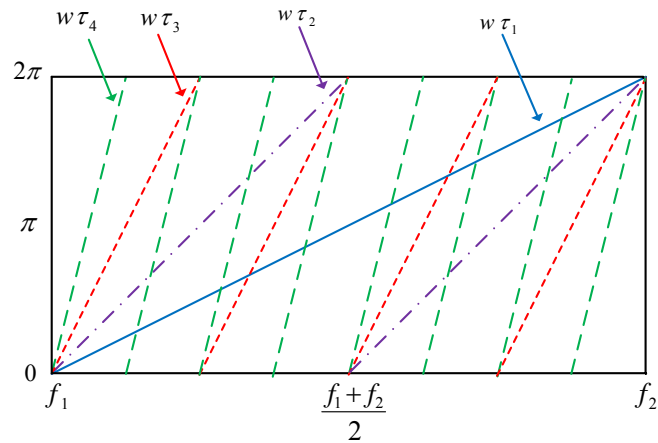
2.4 Frequency Resolution

A receiver with one delay line of the maximum length without causing unambiguous frequency reading can not generate desired frequency accuracy and resolution. The common approach to improve the frequency resolution is to use multiple delay lines [11]. An example such an arrangement is shown in Figure 2.5a. The input signal is separated into four parallel paths. Following each of the four paths there is a discriminator and each discriminator has a different length delay line. The shortest delay line (τ_1) is short enough not to produce frequency ambiguity, where $\tau_4 > \tau_3 > \tau_2 > \tau_1$ are used to generate desired frequency resolution. Here, in general, τ_4 , τ_3 and τ_2 are multiples of τ_1 . Figure 2.5b shows the result of the output $w\tau$

versus frequency for different lines. In this special case, relation between the delay lines is $\tau_4=2\tau_3=4\tau_2=8\tau_1$. It is obvious that $w\tau_1$ does not have any ambiguity problem in the frequency band f_1 to f_2 . However, the slope of $w\tau_1$ is rather flat and it is difficult to measure $w\tau$ angle and predicate the frequency accurately. As can be seen from the delay line relationship, for this example, by using multiple delay lines frequency resolution is improved 8 times than using only one delay line.



(a) Four frequency measurement circuits



(b) $w\tau$ vs frequency for four delay lines.

Figure 2.5 IFM receiver with multiple delay lines.

So finer frequency resolution can be obtained through the longer delay line with ambiguities resolved by sequential or parallel measurements on shorter delay lines.

The longest delay line that can be used in an IFM receiver depends on the minimum pulse handling capability. The delay line time must be shorter than the shortest pulse receiver can handle, otherwise the delayed portion and the undelayed portion of the signal can not overlap. Thus, the phase angle between them can not be measured. The length of the delay line is also very critical to the frequency measurement accuracy. This situation is explained in the following section.

In fact, the frequency resolution is not only determined by the longest delay line in the system but also it changes according to digitization of the finest channel. So for delay T and M quantization levels (i.e. $2^N = M$, N is the bit number) the resolution will be

$$\Delta F = \frac{1}{T.M} \text{ Hz} \quad (2.51)$$

Quantizing the last channel with large M enables higher resolution but it also causes degradation in noise performance. Moreover, increase in T improves the resolution and noise performance but this time hardware complexity increases and minimum pulse width limitations get tighter.

2.5 Frequency Accuracy and SNR

Noise arising from the detectors is assumed negligible so an effective RF input signal to noise ratio may be calculated as follows [3].

$$S_{RF} = \frac{P_s}{KTB_R F} \quad (2.52)$$

where,

S_{RF} is the signal to noise ratio in the RF stage

B_R is the RF noise bandwidth

F is the noise figure of the input amplifier

K is Boltzman constant

T is the temperature

Video signal/noise ratios can be calculated using standard correlation theory [12] and relate to the in-phase (S_i) and quadrature noise (S_q);

$$S_i = \frac{S^2}{2(1+\rho)S + \left(\frac{B_R}{B_V} - \frac{1}{2}\right)} \quad (2.53)$$

$$S_q = \frac{S^2}{2(1-\rho)S + \left(\frac{B_R}{B_V} - \frac{1}{2}\right)} \quad (2.54)$$

where $S = \frac{P_s}{KTB_V F}$ and ρ is a measure of sin-cos correlation $\rho = \frac{\sin(w_v \tau)}{w_v \tau}$

Here B_V is video signal bandwidth, w_v is video signal angular frequency and τ is time delay.

RMS phase noise for a discriminator can be calculated from the following equation.

$$\theta_{rms,noise} = \frac{1}{\sqrt{S_q}} \quad (2.55)$$

Using equation (2.54) above, (2.56) is obtained.

$$\theta_{rms,noise} = \frac{\sqrt{2(1-\rho)S + \left(\frac{B_R}{B_V} - \frac{1}{2}\right)}}{S} \quad (2.56)$$

Here the parameter S can be written in terms of (2.52).

$$S = \frac{P_s}{KTB_v F} = S_{RF} \frac{B_R}{B_v} \quad (2.57)$$

$$\theta_{rms,noise} = \frac{\sqrt{2(1-\rho)S_{RF} \frac{B_R}{B_v} + \left(\frac{B_R}{B_v} - \frac{1}{2}\right)}}{S_{RF} \frac{B_R}{B_v}} \quad (2.58)$$

$$\theta_{rms,noise} = \frac{1}{S_{RF}} \sqrt{\left(\frac{B_v}{B_R}\right)^2 \left[2(1-\rho)S_{RF} \frac{B_R}{B_v} + \frac{B_R}{B_v} \left(1 - \frac{B_v}{2B_R}\right) \right]} \quad (2.59)$$

Here, $B_v \ll B_R$. So the term $\frac{B_v}{2B_R}$ is nearly zero in the equation above. Under this

assumption phase noise equation will become:

$$\theta_{rms,noise} = \frac{1}{S_{RF}} \sqrt{\frac{B_v}{B_R} \left[2 \left(1 - \frac{\sin(w_v \tau)}{w_v \tau}\right) S_{RF} + 1 \right]} \quad (2.60)$$

$$w_1 - w_2 = \frac{2\pi}{\tau} \Rightarrow UB_{fine\ tier} = \frac{1}{\tau} \quad (2.61)$$

$$\rho = \frac{\sin(w_v \tau)}{w_v \tau} = \frac{\sin\left(\frac{w_v}{UB_{fine\ tier}}\right)}{\left(\frac{w_v}{UB_{fine\ tier}}\right)} \quad (2.62)$$

$$\theta_{rms,noise} = \frac{1}{S_{RF}} \sqrt{\frac{B_v}{B_R} \left(\left[2 \left(1 - \frac{\sin\left(\frac{w_v}{UB_{fine\ tier}}\right)}{\left(\frac{w_v}{UB_{fine\ tier}}\right)}\right) S_{RF} + 1 \right] \right)} \quad (2.63)$$

If w_v is a lot smaller than $UB_{fine\ tier}$ the expression simplifies to:

$$\theta_{rms,noise} = \frac{1}{S_{RF}} \sqrt{\frac{B_v}{B_R}} \quad (2.64)$$

And the rms frequency accuracy will be:

$$\Delta f_{rms} = \frac{\theta_{rms,noise}}{\pi} UB_{fine\ tier} \quad (2.65)$$

2.6 Number of Tiers, Inter Tier Ratio and Phase Margin

Given a limit to the accuracy with which the line phases can be determined, there is a finite limit to the number of ambiguities that can be resolved. When ambiguity-resolution processing fails, large errors corresponding to one or more long-line 2π cycles occur. In a good receiver design, the probability of this happening should be minimal [3].

Consider two discriminators with delay-line lengths in the ratio 1:n where n will be referred to as inter tier ratio. At a given input-signal frequency, the actual line phases, assuming no system errors, are related by

$$\Phi_n' = n\Phi_1 \quad (2.66)$$

In general Φ_n' will contain an integer I ($I \leq n$) multiple of 2π which can not be known from a single measurement (hence the ambiguities) which gives the remainder Φ_n . So Φ_n' will be

$$\Phi_n' = \Phi_n + 2\pi I \quad (2.67)$$

$$I = \frac{1}{2\pi} [n\Phi_1 - \Phi_n] \quad (2.68)$$

If ambiguity is taken into account, then (2.68) will be;

$$I + dI = \frac{1}{2\pi} [n(\Phi_1 + d\Phi_1) - (\Phi_n + d\Phi_n)] \quad (2.69)$$

In order to prevent ambiguity breakdown, I must not deviate more than $\pm \frac{1}{2}$ from its true value. If (2.68) is subtracted from (2.69), permitted discriminator phase error can be found.

$$(I + dI) - (I) = \left(\frac{1}{2\pi} [n(\Phi_1 + d\Phi_1) - (\Phi_n + d\Phi_n)] \right) - \left(\frac{1}{2\pi} [n(\Phi_1) - (\Phi_n)] \right) \quad (2.70)$$

$$|dI| = \left| \frac{1}{2\pi} [n(d\Phi_1) - (d\Phi_n)] \right| \leq \frac{1}{2} \quad (2.71)$$

$$|[n(d\Phi_1) - (d\Phi_n)]| \leq \pi \quad (2.72)$$

Here, the worst case is to make phase errors which are in “opposite direction” at consecutive delay lines. So the equation above will be;

$$[n(d\Phi_1) - (-d\Phi_n)] = [n(d\Phi_1) + (d\Phi_n)] \leq \pi \quad (2.73)$$

On the other hand, phase errors expected operationally are usually of same magnitudes ($d\Phi_1 = d\Phi_n = d\Phi$). So phase tolerance can be found by the equation given below.

$$[n(d\Phi) + (d\Phi)] \leq \pi \Rightarrow \Delta\theta_{\max} = \frac{\pi}{(1+n)} \quad (2.74)$$

$$n = \left(\frac{UBW_{coarse_tier}}{UBW_{fine_tier}} \right)^{1/(N-1)} \quad (\text{inter tier ratio}) \quad (2.75)$$

UBW_{coarse_tier} and UBW_{fine_tier} are the unambiguous bandwidth of coarse tier and fine tier respectively and N is the number of total tier in the system.

CHAPTER 3

DIFFERENTIAL PHASE SHIFTER DESIGN

Differential phase shifters are among the key components in an instantaneous frequency measuring (IFM) device. In differential phase shifters the signal is split into two or more paths with equal amplitudes. The aim is to get constant phase differences between the outputs of the paths over a wide frequency band. Common phase discriminator structures use 4 different video outputs from their phase shifter networks. These DC voltages are then used to find the input frequency by the help of simple trigonometric equations as described in Chapter 2. However theoretically only 3 video outputs are enough to resolve the phase ambiguities and find the input frequency by making a magnitude comparison between them. Therefore in this thesis phase discriminator structures with 3 paths yielding 3 video outputs will be used. One of the paths is used as reference while the other two paths are formed by phase shifter branches which give +120 degrees and -120 degrees phase difference compared to the reference line, as described in section 1.3.2.3 as the Three Phase Discriminator.

In this chapter various differential phase shifter configurations will be studied to get a structure which can work over the frequency band of 2-18 GHz and has minimal realization difficulties.

Broad-band phase and amplitude balance can be achieved by using various configurations of phase shifters [13] – [21]. Historically the first and the most commonly used phase shifters are Schiffman phase shifters formed by a reference line and a folded multi-section coupled line [13] – [14]. In this chapter several different Schiffman phase shifter topologies are designed for wideband operation.

Inspection of the results revealed the drawbacks and realization difficulties of especially parallel coupled line sections. Then another approach is inspected which uses 180 degree hybrids to avoid parallel coupled lines [26]. Finally, inspired from this approach, a simpler design technique is developed which uses uncoupled stepped transmission lines with OC and SC terminations yielding much simpler topologies. Similar topologies are known to be used by Filtronic and Sage Laboratories (merged with Filtronic since 1998). This technique is used in the design of the IFM.

3.1 Schiffman Phase Shifter

The basic Schiffman's phase shifter, shown in Figure 3.1 consists of two separate TEM transmission lines, one of which is a length of uncoupled line named as reference line. The other is a C-section, consisting of a pair of parallel coupled transmission lines shorted to each other at one end. The coupled section is a one-quarter wavelength long at the center frequency. An octave wide 90-degree differential phase shifter can be designed in this way [13]. In order to construct a component for multioctave operation, Schiffman used plurality of such coupled line sections interconnected in cascade as shown in Figure 3.2 [13] – [14].

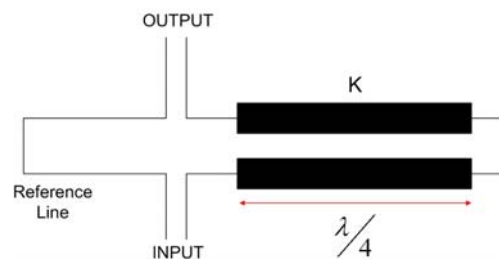


Figure 3.1 Schiffman's single-section phase shifter.

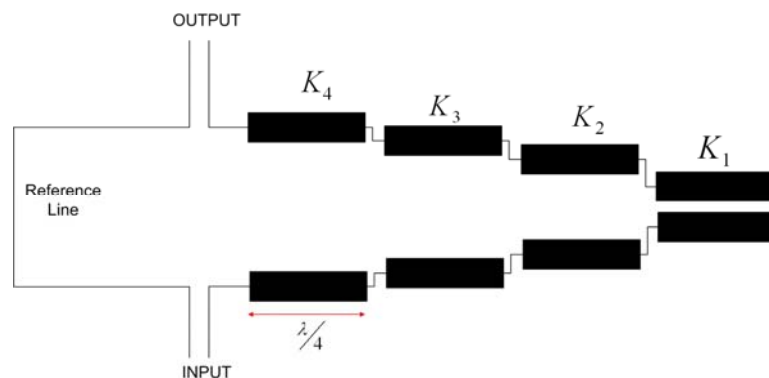


Figure 3.2 Schiffman's four-section phase shifter.

Right after Schiffman's work, many papers have been devoted to the problems of optimum synthesis of broadband differential phase shifters. However, recently only one type of structure for the multi-section phase shifter has been considered particularly. It is a cascade of coupled sections of equal lengths (one quarter wavelength at the center of operating frequency) and different coupling coefficients. The equality of the section lengths allows one to obtain an analytical solution of the phase shifter synthesis problem. Shelton and Mosko [21] described an approximate synthesis procedure based on a first order reflections theory; Zysman and Matsumoto [23] have investigated some analytic properties of cascaded C-sections and Edward G. Cristal presented an investigation of the analytic properties of cascaded commensurate transmission line C-sections and he gave a general exact synthesis procedure for realizing cascaded commensurate transmission line C-sections to describe their phase characteristics.

Jones and Bolljahn [24] showed that the condition that a single C-section be matched at all frequencies is

$$Z_o = \sqrt{Z_{oe}Z_{oo}} \quad (3.1)$$

where Z_o is the termination impedance, Z_{oe} is the even-mode impedance of the coupled lines and Z_{oo} is the odd-mode impedance of the coupled lines.

Equation (3.1) is also the condition for a pair of coupled lines to be a directional coupler. Thus, the C-section may be regarded as a directional coupler with two adjacent ports connected by a zero length line. This analogy carries over directly to cascaded transmission line C-sections which may be considered as cascaded transmission line directional couplers having adjacent ports of the last one connected by a zero length line.

3.2 Schiffman-Type Phase Shifter Alternatives

In this section, alternative phase shifter networks are presented. These structures can be considered as variations of the basic Schiffman networks. These networks are evaluated by their performance and manufacturability. The designs are carried out by optimization on ADS simulator. Ideal transmission lines are used to reduce the simulation/optimization time. The transmission line impedances are normalized with respect to the port impedances. With the development of optimization methods it is possible to design various types of phase shifter networks easily. Optimization converges always for any starting set of step impedances.

3.2.1 Three Section Schiffman Phase Shifter

In this alternative, 3 section Schiffman phase shifter is considered in a stepped impedance form [14]-[20]-[21]. Figure 18 shows the reference line and phase shifter branches in ADS format. Reference line is a uniform line of unity impedance with matched terminations. It has six sections, each with 90 degrees electrical length at 10 GHz. Phase shifter branch-1 and branch-2 are responsible for creating +120 and -120 degrees of phase difference with respect to reference line respectively. Phase differences are defined as follows:

$$\begin{aligned} \text{Phase}(RL) - \text{Phase}(PSB_1) &\approx 120^\circ \\ \text{Phase}(PSB_2) - \text{Phase}(RL) &\approx -120^\circ \end{aligned} \tag{3.2}$$

where;

RL: Reference Line

PSB_1: Phase Shifter Branch 1

PSB_2: Phase Shifter Branch 2.

Phase shifter branch 1 and phase shifter branch 2 have three sections. There are uncoupled lines of unity impedance at their input and output. Then two folded coupled line sections are appended as shown in the figure. The coupled line sections

of phase shifter branch 1 have even mode impedances $z_{e1} \approx 1.46$ and $z_{e2} \approx 3.54$ ohms (normalized). The odd mode impedances are $z_{o1} = 1/z_{e1}$ and $z_{o2} = 1/z_{e2}$. Phase shifter branch 2 odd mode impedances are $z_{o1} \approx 0.59$ and $z_{o2} \approx 1$ with even mode impedances being $z_{e1} = 1/z_{o1}$ and $z_{e2} = 1/z_{o2}$. The uncoupled lines are used for adjusting the phase differences. Their lengths are 30 degrees for phase shifter branch 1 and 150 degrees for phase shifter branch 2. All these parameters are calculated by optimization on ADS. The resulting phase difference between phase shifter 1 and reference line is shown in Figure 3.4. Phase difference is 120 ± 6 degrees in 4.35 GHz – 15.5 GHz frequency bandwidth. In Figure 3.5, the phase difference between reference line and phase shifter branch 2 is shown. It is approximately -120 ± 6 degrees in 6.25 GHz – 13.65 GHz frequency bandwidth which is almost 4 GHz narrower than the other one. Besides the bandwidth mismatch, it has too large ripples and realization of the coupled line section of phase shifter branch 1 is difficult. Therefore this alternative is discarded.

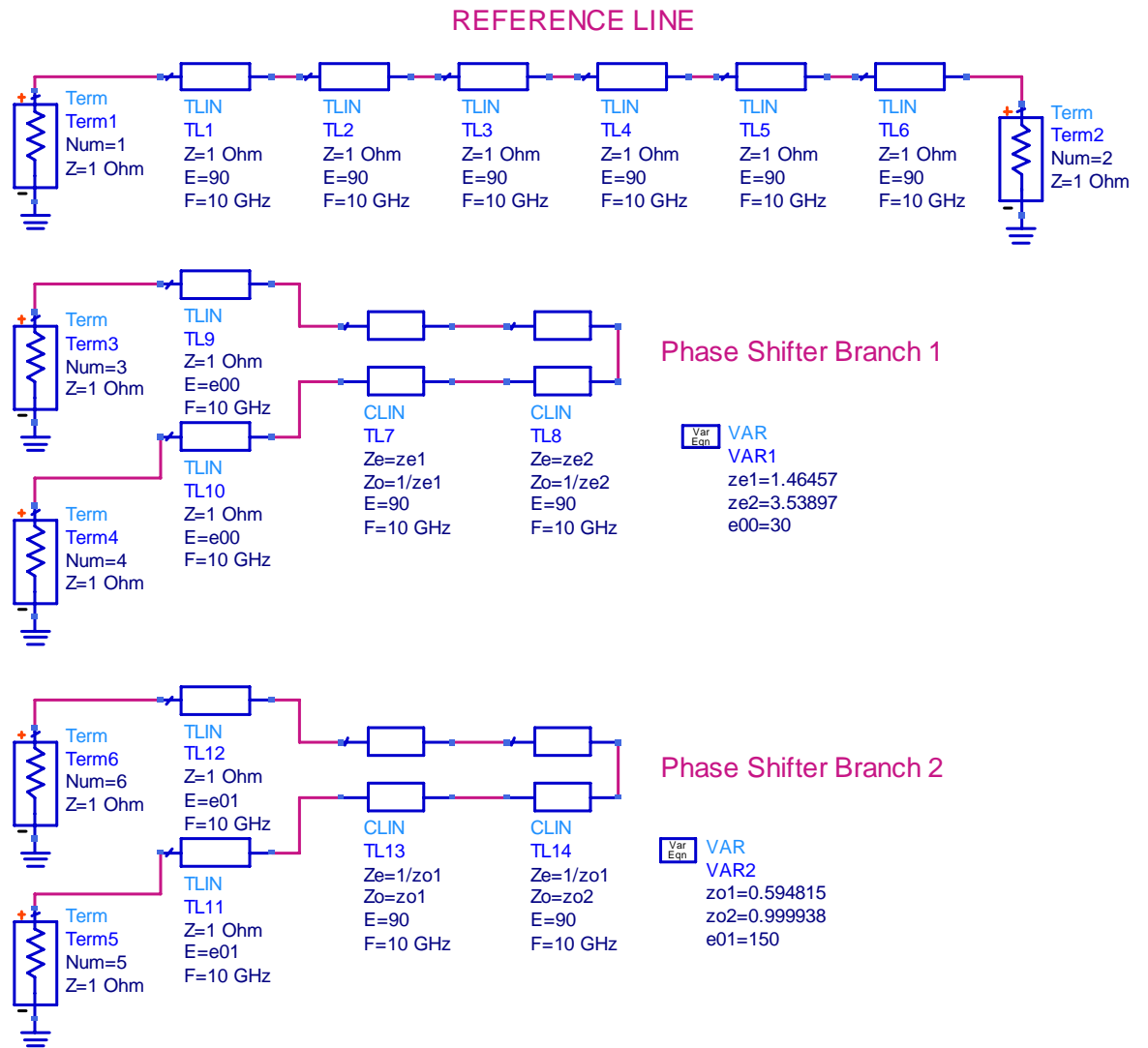


Figure 3.3 3 section Schiffman phase shifter.

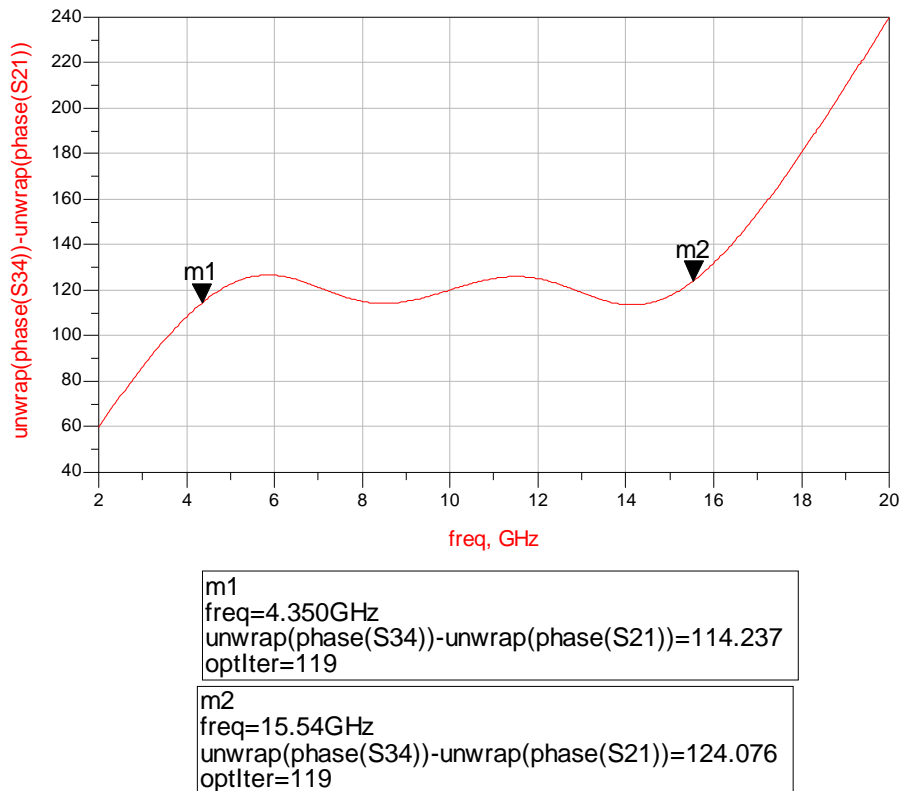


Figure 3.4 Phase difference between phase shifter branch 1 and reference line.

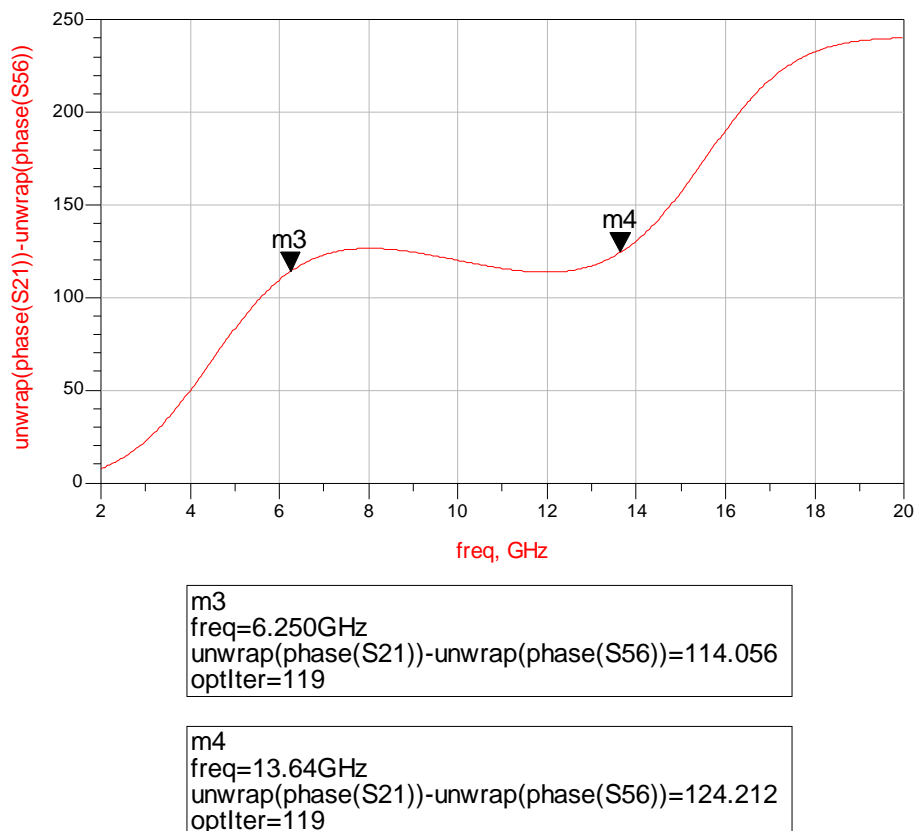


Figure 3.5 Phase difference between reference line and phase shifter branch 2.

3.2.2 Four Section Schiffman Phase Shifter

In this alternative to get a better phase response in a wider frequency bandwidth, an extra Schiffman section is inserted to each phase shifting branch given in the design above. The reference line number of sections is increased to eight. The new version of the circuit is optimized giving the impedances shown in Figure 3.6.

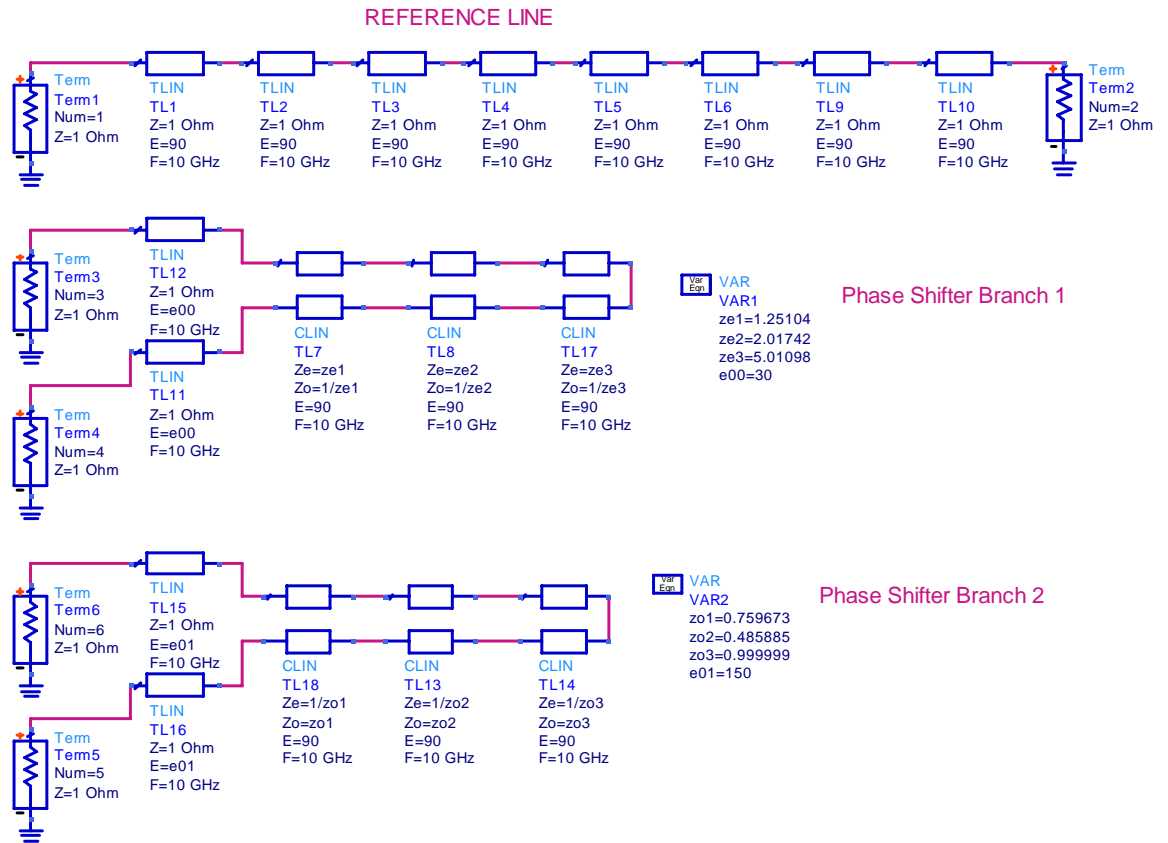


Figure 3.6 4 section Schiffman phase shifter.

Figure 3.7 shows the phase difference between phase shifter branch 1 and reference line. The phase difference is 120 ± 3 degrees in a frequency bandwidth from 3.6 GHz to 16.3 GHz. It is seen that phase ripple is decreased to ± 3 degrees in a wider bandwidth than the previous circuit. In Figure 3.8, the phase difference between reference line and phase shifter branch 2 is presented. The phase difference is -120 ± 5 degrees in a frequency bandwidth from 4.3 GHz to 16.5 GHz which is

nearly 2 GHz narrower than branch-1. Thus, phase ripple is decreased to ± 5 degrees over a wider bandwidth compared to the previous alternative.

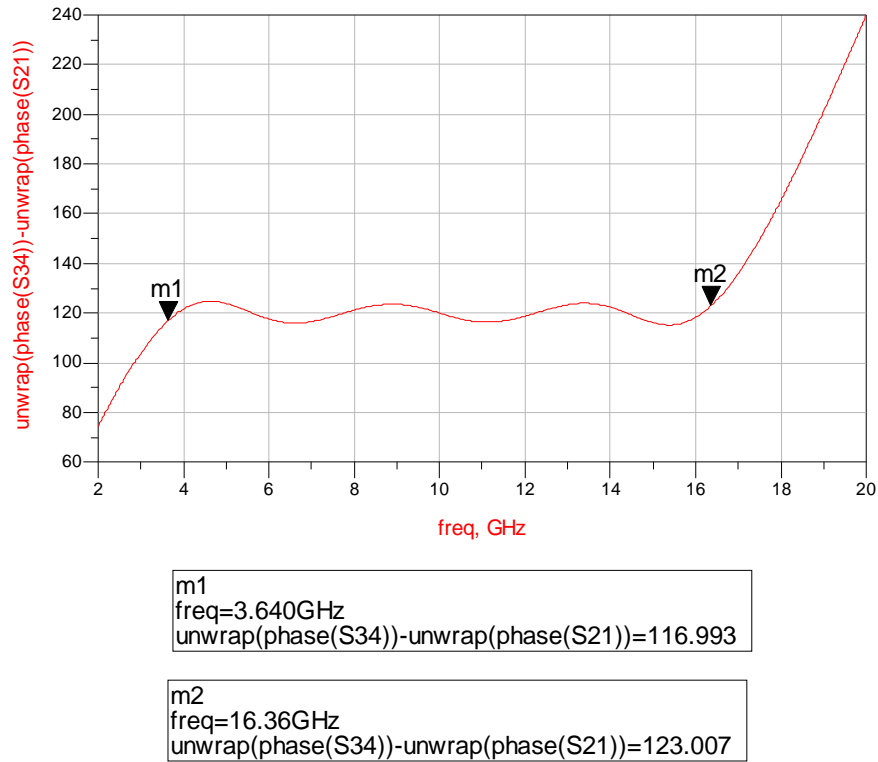


Figure 3.7 Phase difference between phase shifter branch 1 and reference line.

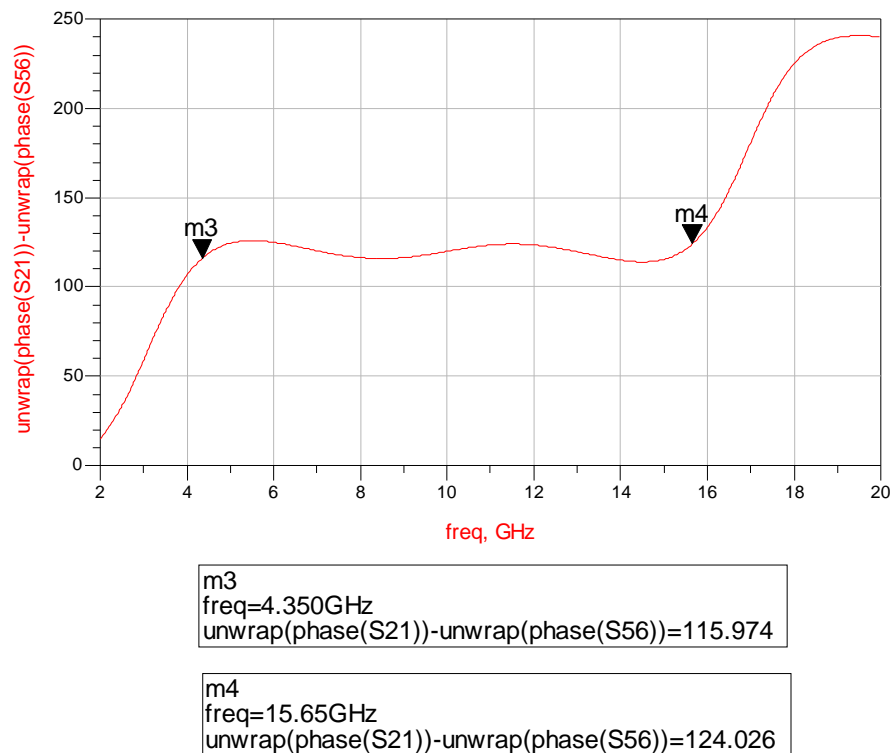


Figure 3.8 Phase difference between reference line and phase shifter branch 2.

The results presented in this alternative are not bad. However the phase ripple of phase shifter branch 2 needs improvement and also the coupled line section with $ze3 \approx 5$ and $zo3 = 1/ze3 \approx 0.2$ of phase shifter branch 1 is difficult to realize, necessitating broad side coupling. Therefore this alternative is also discarded.

3.2.3 Five Section Schiffman Phase Shifter

Figure 24 shows five section Schiffman phase shifter networks obtained by optimization.

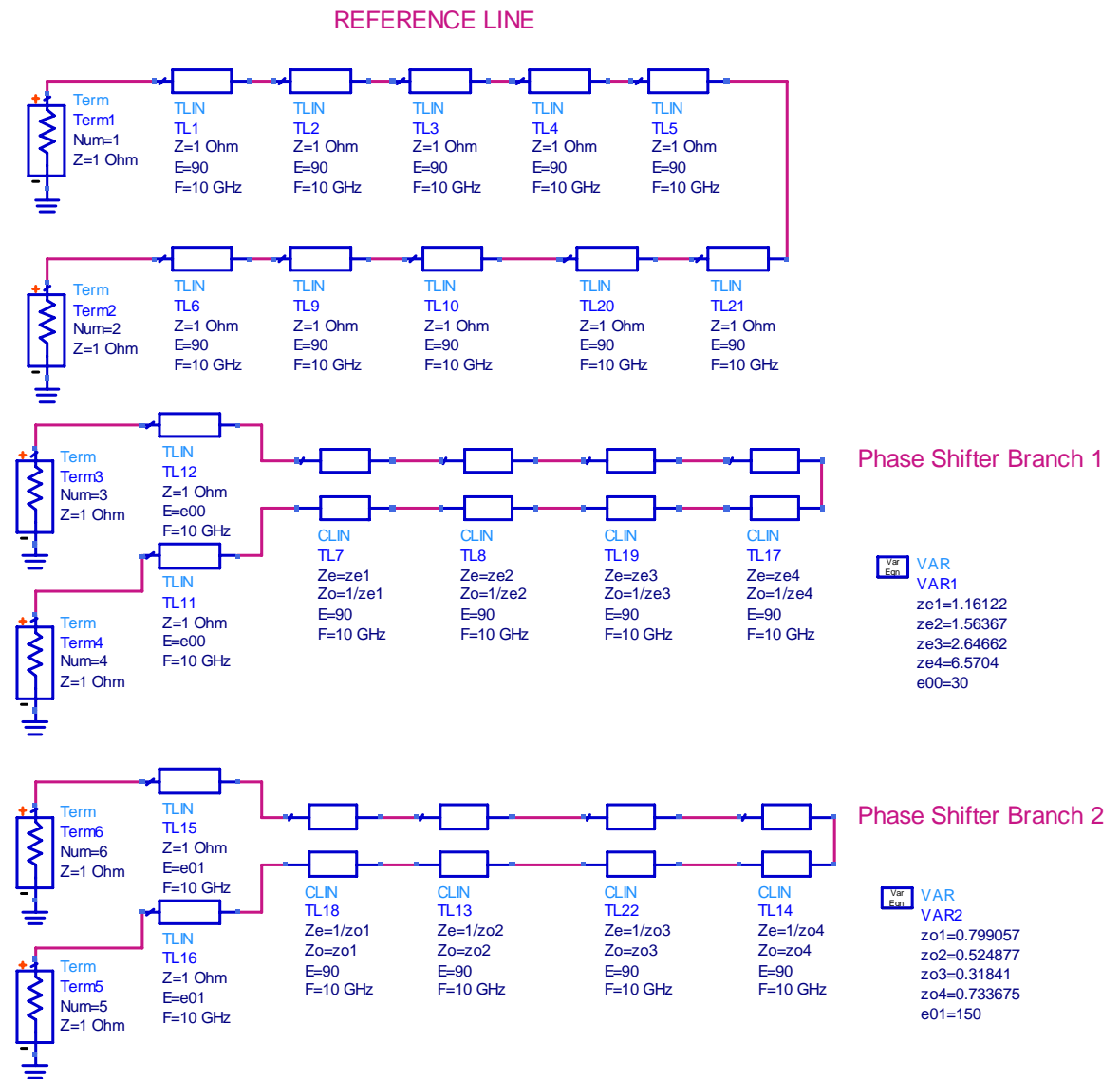


Figure 3.9 5 section Schiffman phase shifter.

As expected, the phase differences for both phase shifter branches are better than the previous cases. Figure 3.10 shows the phase difference between the phase shifter branch 1 and reference line. The approximate relative phase difference is 120 ± 3 over the band from 3 GHz to 17 GHz. Phase ripple is the same as the previous case with a 1.3 GHz wider bandwidth.

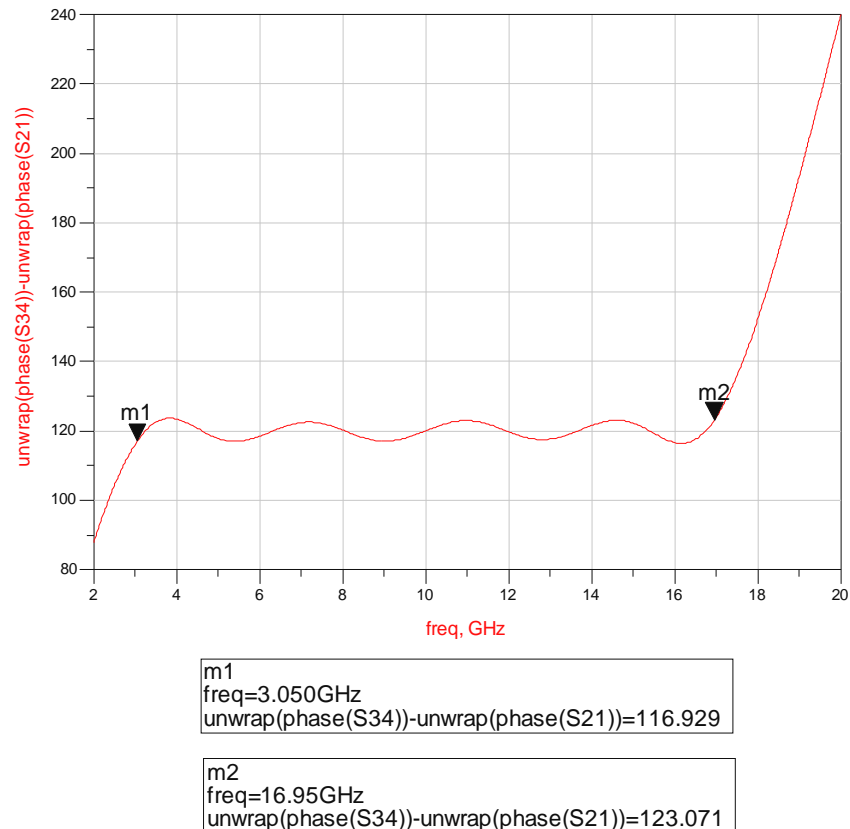


Figure 3.10 Phase difference between phase shifter branch 1 and reference line.

In Figure 3.11, phase difference between reference line and phase shifter branch 2 is shown. Relative phase difference is nearly -120 ± 3 over the band from 3.6 GHz to 16.3 GHz, 1 GHz wider than phase shifter branch 2 of the four section case.

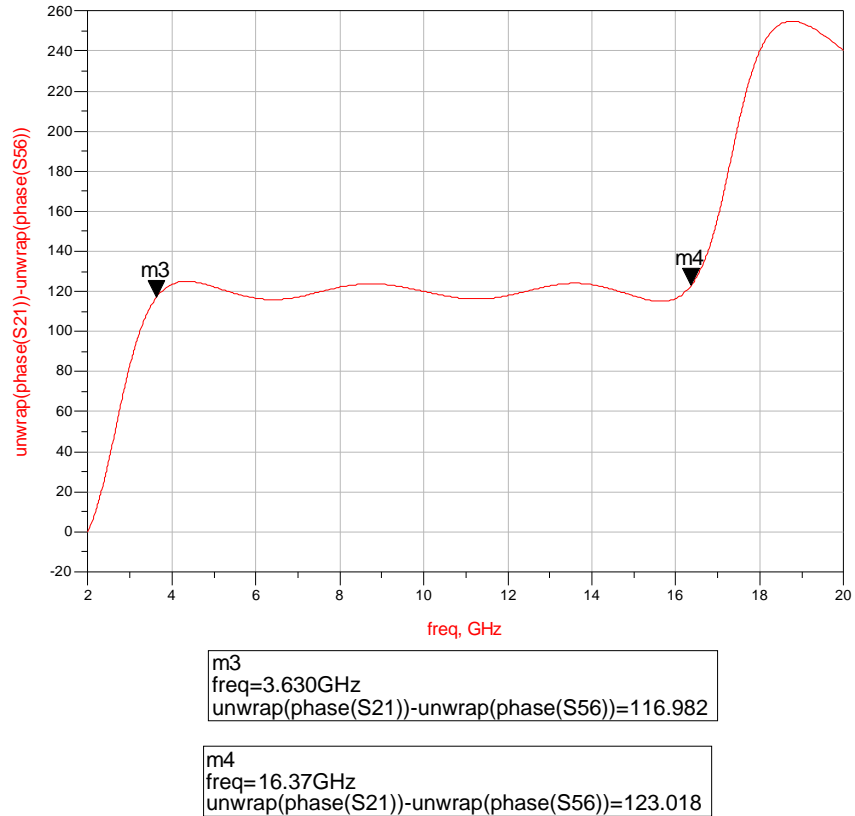


Figure 3.11 Phase difference between reference line and phase shifter branch 2.

Overall results are better than all the previous cases. However fabrication problem for phase shifter branch 1 with $z_{e4} \approx 6.6$ ohms and $z_{o4} = 1/z_{e4} \approx 0.15$ still exists.

3.2.4 Six Section Schiffman Phase Shifter

Figure 27 shows the results of optimization trials for six section phase shifter network.

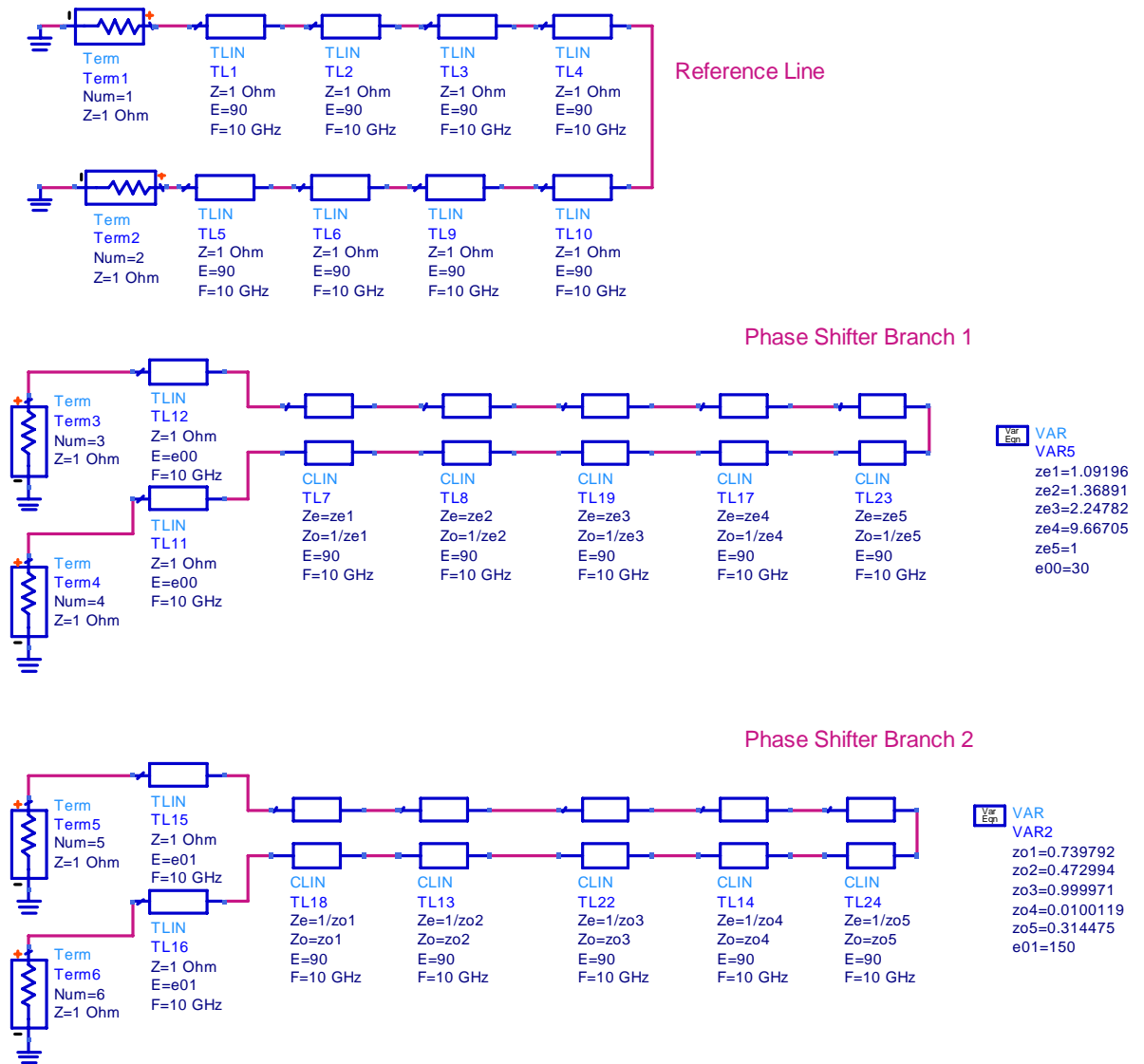


Figure 3.12 6 section Schiffman phase shifter

The differential phase of branch 1 is 120 ± 1 degrees in 2.64 GHz – 17.36 GHz band, a better phase ripple over a wider band compared to the previous cases (Figure 28). Differential phase of branch-2 is shown in Figure 29. It is -120 ± 3 which is same as the five section case. However this ripple is valid over a narrower bandwidth, from 4.39 GHz to 15.61 GHz.

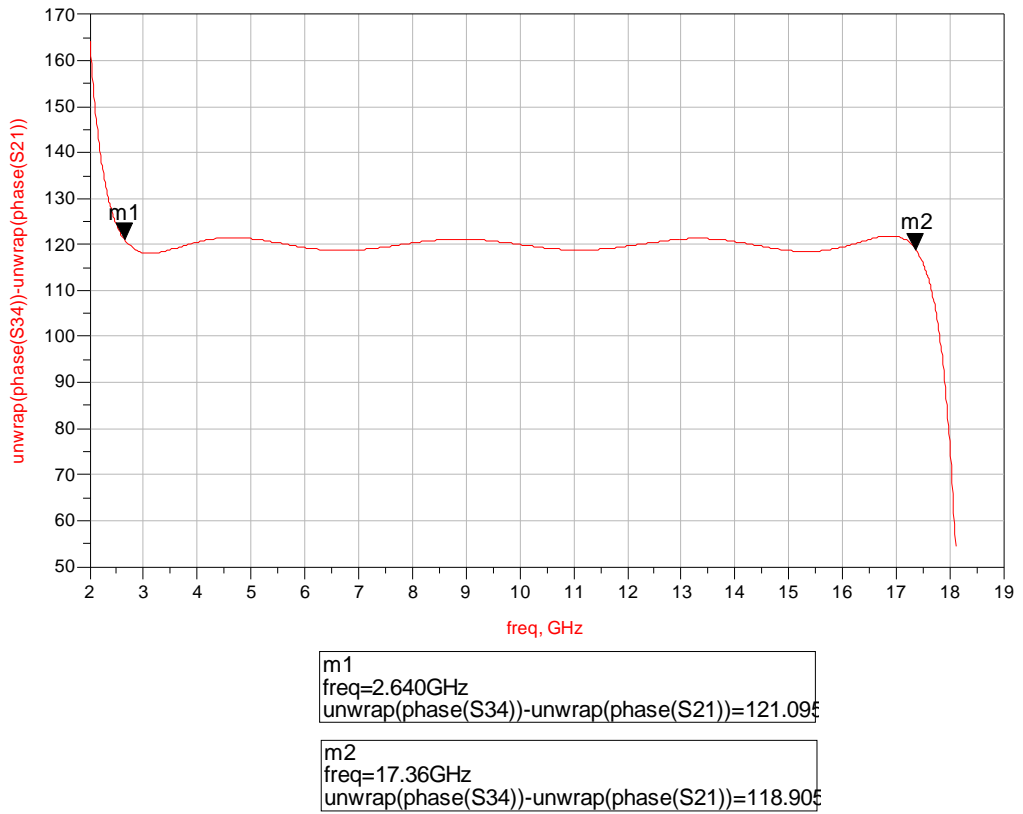


Figure 3.13 Phase difference between phase shifter branch 1 and reference line.

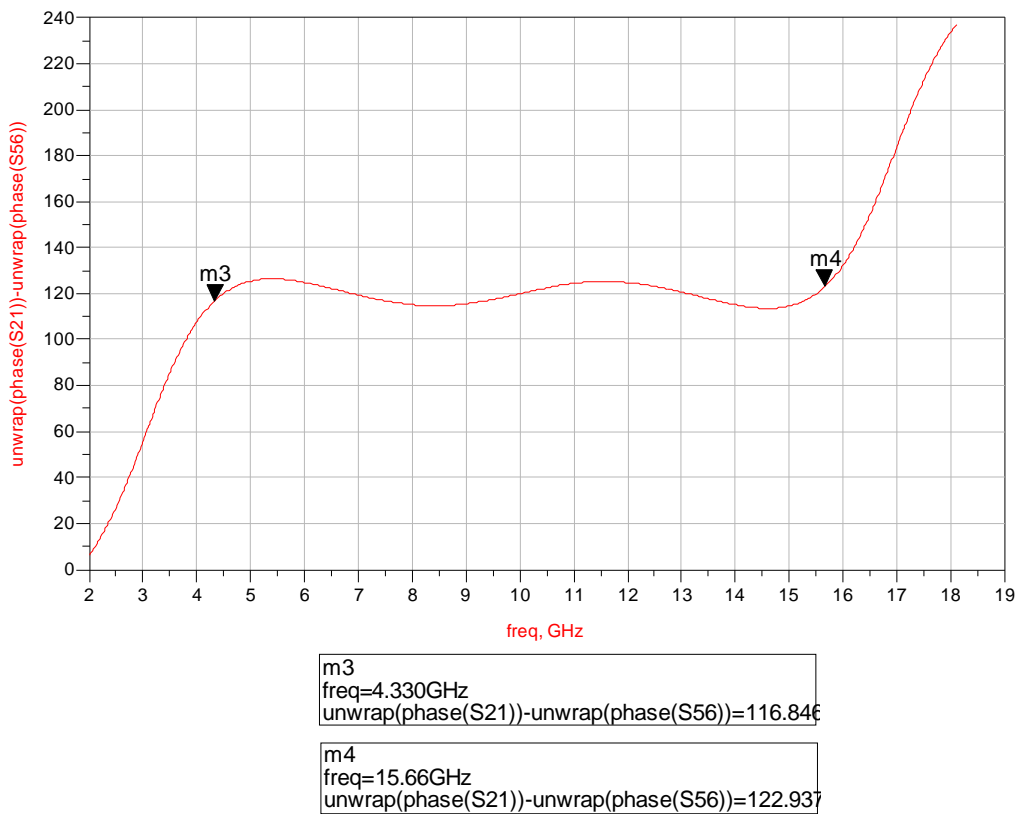


Figure 3.14 Phase difference between reference line and phase shifter branch 2.

Because of the tight couplings in TL 17 ($ze4 \approx 9.6, ze4 = 1/zo4 \approx 0.1$) in phase shifter branch 1 fabrication problem still exists and for TL 14 ($zo4 \approx 0.01, ze4 = 1/zo4$) in phase shifter branch 2 it is impossible. Further, when the phase responses are considered, this phase shifter structure has no significant advantage over the five section case. Until this alternative, increasing the number of sections made the phase responses better. But from this point, adding more sections will not serve purpose. In short, this alternative seems to be the actual limit of the number sections that can be used in phase shifter branches. For this reason different types of phase shifters are considered, as described in the following sections.

3.2.5 Schiffman Class II Phase Shifter

Figure 3.15 shows a topology which is named as Schiffman Class II phase shifter. A five section phase shifter is studied to get insight. The most important advantage in comparison of Schiffman's original circuit is the reduced length of components [19].

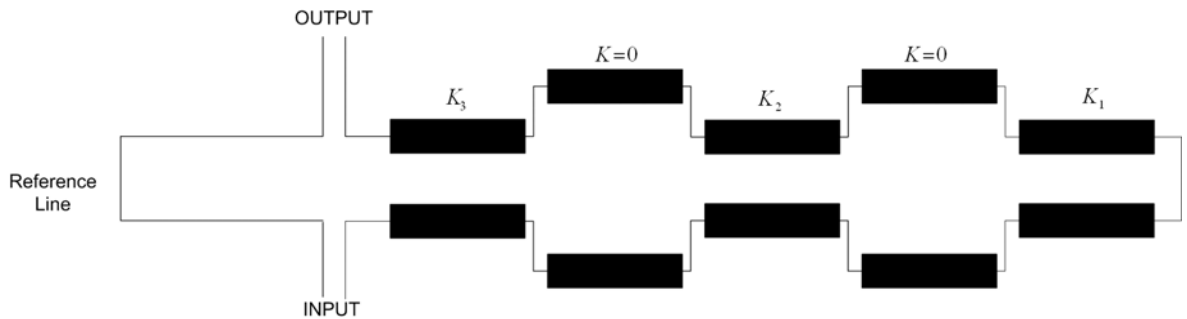


Figure 3.15 Five-section phase shifter of Class II.

Figure 3.16 shows the ADS design of a Class II phase shifter branches with reference line. It includes three separate two ports with ideal transmission lines which are reference line, phase shifter branch 1 and phase shifter branch 2. As can be seen in Figure 3.16, the transmission lines near to the termination ports have different electrical length. These lines are used to get the required ± 120 relative phase shift. The other uncoupled/coupled lines are quarter-wave long at the center of operating frequency (i.e. 10 GHz).

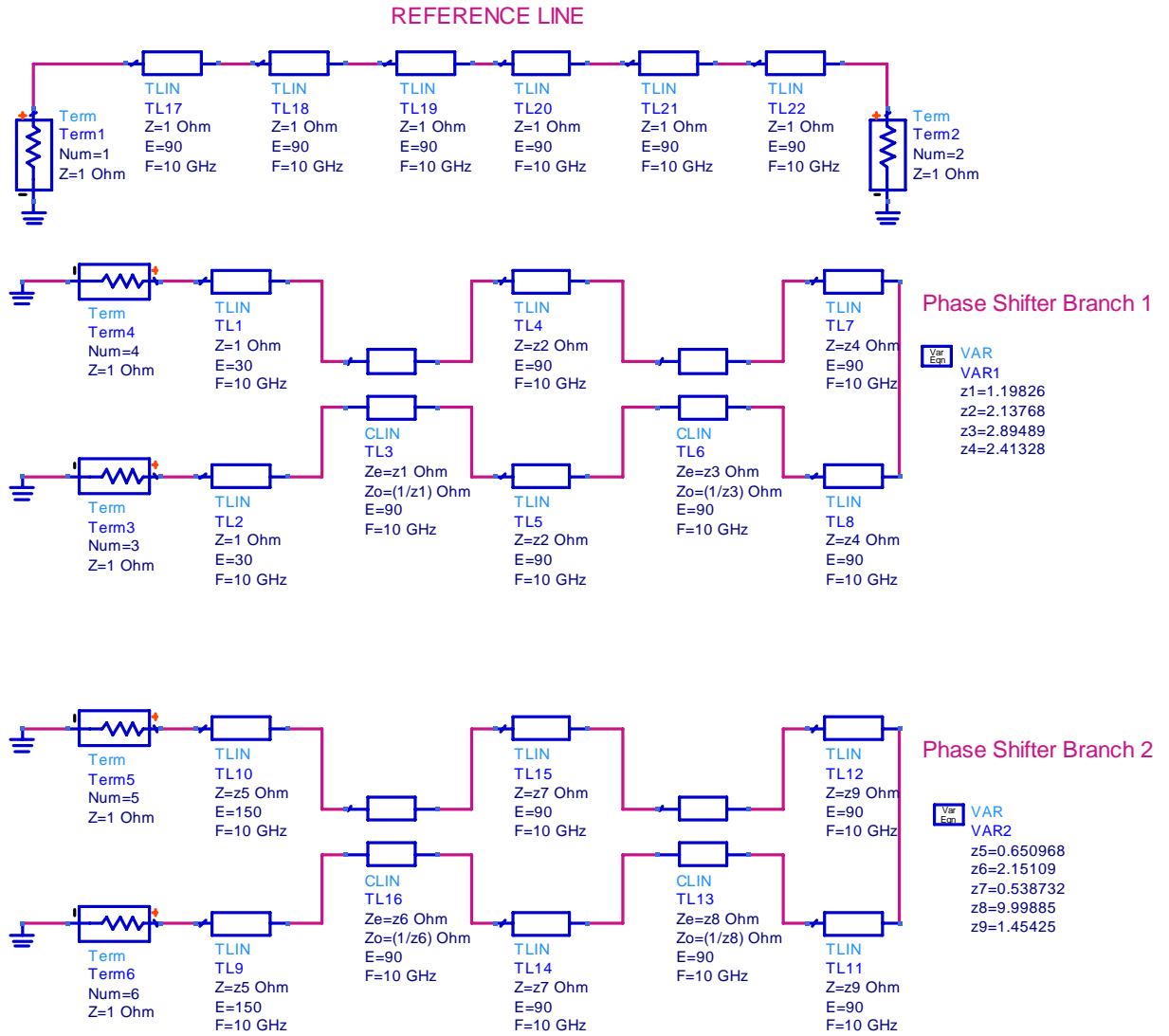


Figure 3.16 Five-section phase shifter of Class II, ADS Design.

In Figure 3.17, the phase difference between phase shifter 1 and reference line is presented. Here, relative phase shift in branch 1 changes between 120 ± 6 degrees in a frequency bandwidth of nearly 4.4 GHz – 15 GHz. Figure 3.18 shows the phase difference between the reference line and phase shifter branch 2. Compared to the result given in Figure 3.17, the situation is much worse. The ripple in phase difference is similar (i.e. approximately -120 ± 6 degrees) however this phase difference is valid for nearly 4.3 GHz – 10.1 GHz frequency bandwidth which is 4.8 GHz narrower than the previous one. The phase difference results obtained using these approaches are not as good as desired. In addition to this, it is nearly impossible to fabricate phase shifter branch 2 because of the tight coupling of TL13.

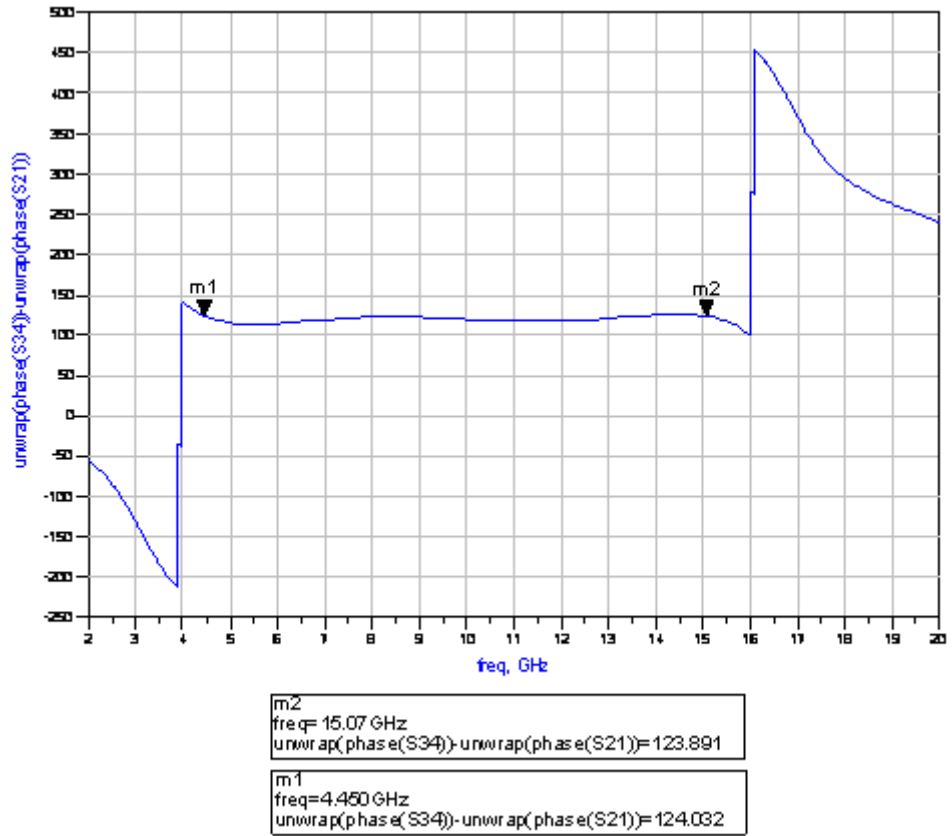


Figure 3.17 Phase difference between phase shifter branch 1 and reference line.

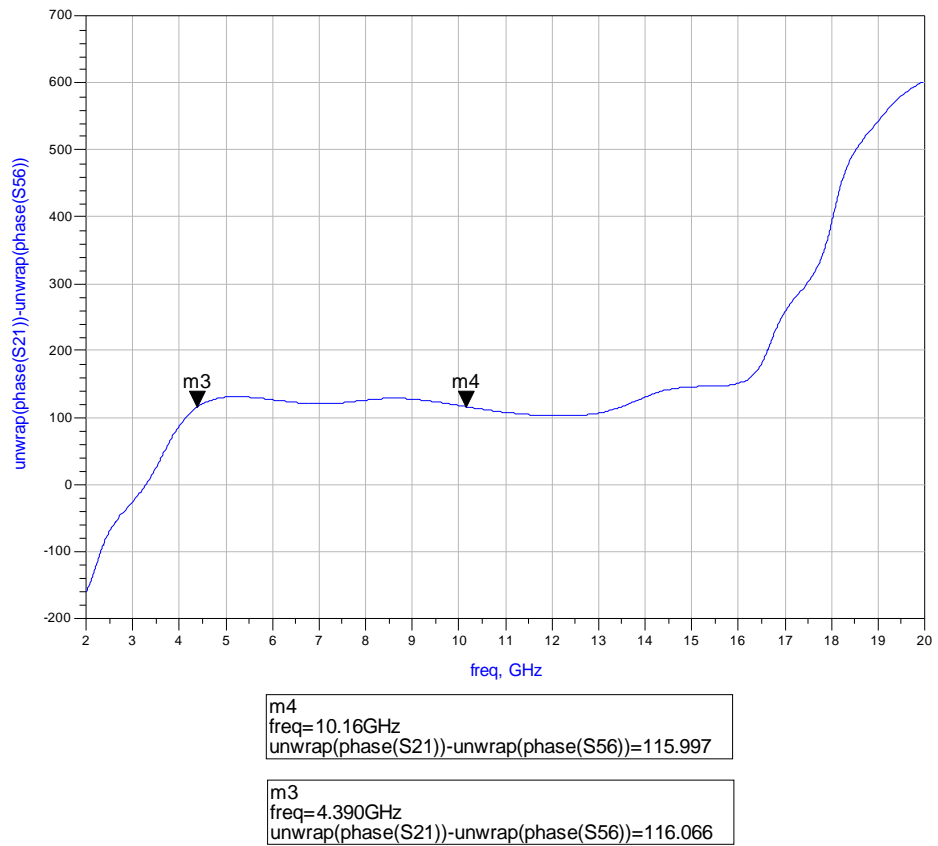


Figure 3.18 Phase difference between reference line and phase shifter branch 2.

3.2.6 Tandem Connected Schiffman Phase Shifter

Figure 3.19 shows the topology named as tandem connected phase shifter. It consists of a reference line and a set of coupled line sections connected as shown in the figure. The use of cascaded two ports was considered in [19] and [24]. According to [24], using several coupled sections can be used to decrease the maximum coupling coefficient between the lines as shown in Figure 3.20.

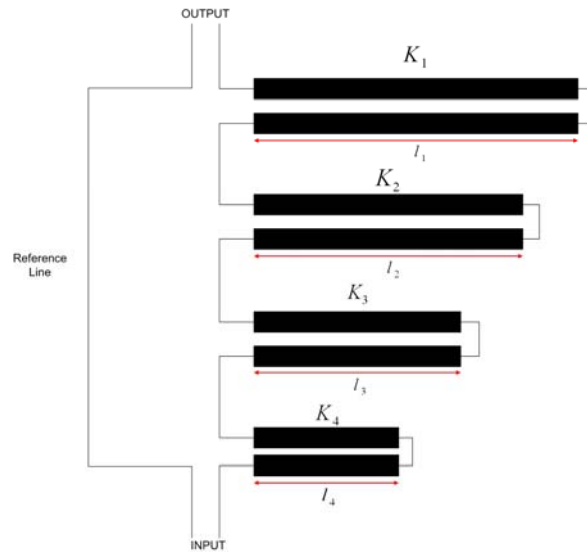


Figure 3.19 Four element tandem connected phase shifter.

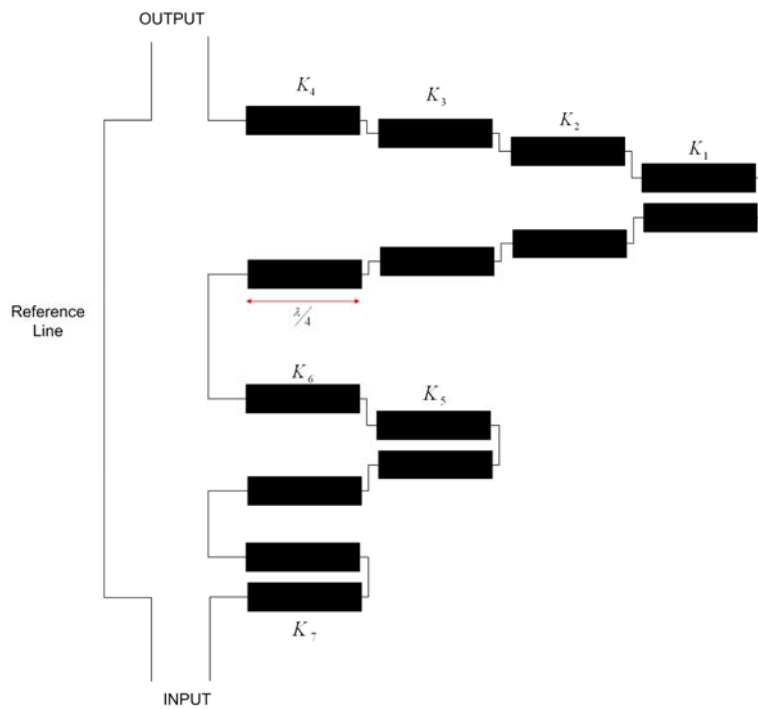
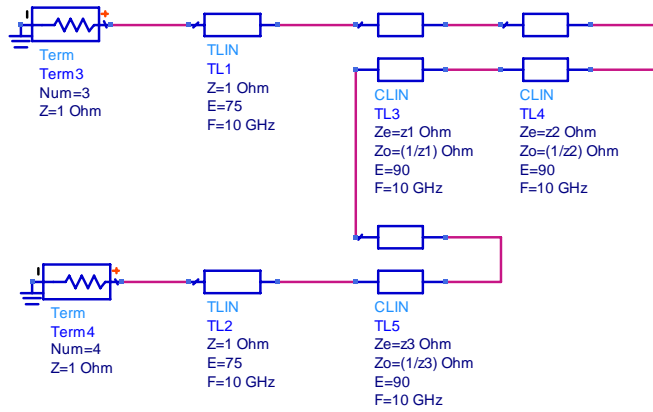
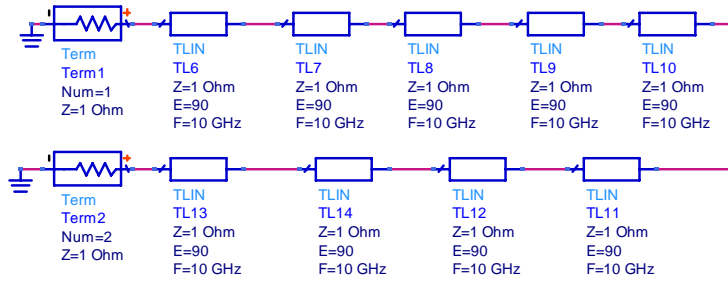


Figure 3.20 Tandem connection of different two ports to reduce of maximum coupling coefficient.

In order to test this approach for maximum bandwidth and impedance levels, several simulations accompanied by optimization are performed. One result is presented in Figure 3.21. Actually, this structure is like a hybrid of Class II and tandem connected coupled lines. Each phase shifting branch has both tandem and series connected coupled lines and uncoupled lines. The differential phase of branch-1 is 120 ± 6 degrees in 3.2 GHz – 16.65 GHz band (Figure 3.22). Differential phase of branch-2 is -120 ± 6 degrees in a band of 3 GHz – 17 GHz which is slightly wider than the other branch (Figure 3.23). Impedances of coupled lines are realizable. However the ripple in the phase difference in both phase shifting arms need improvement.

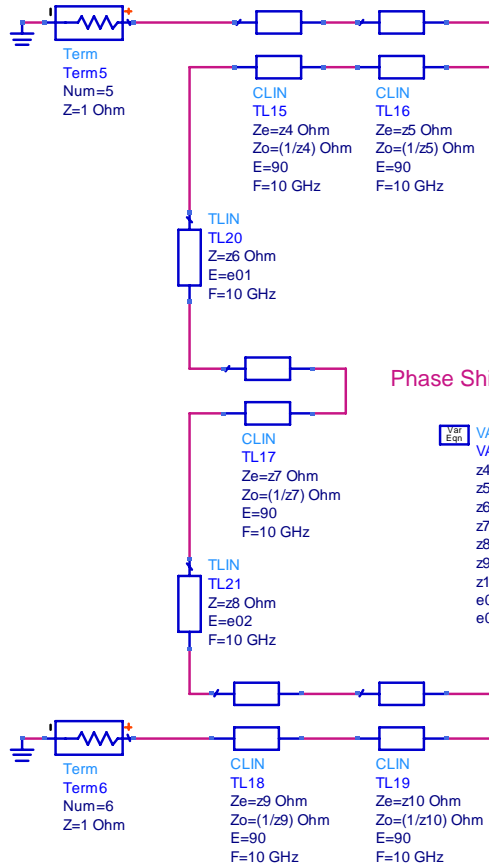
The search for better phase shifter alternatives are continued in the succeeding sections.

REFERENCE LINE



Phase Shifter Branch 1

VAR
Eqn VAR1
z1=1.78824
z2=2.00298
z3=2.94098



Phase Shifter Branch 2

VAR
Eqn VAR2
z4=6.36482
z5=1.02564
z6=2.12364
z7=3.23631
z8=2.28635
z9=1.83714
z10=2.87121
e02=12
e01=11

Figure 3.21 Phase shifter networks in tandem connection.

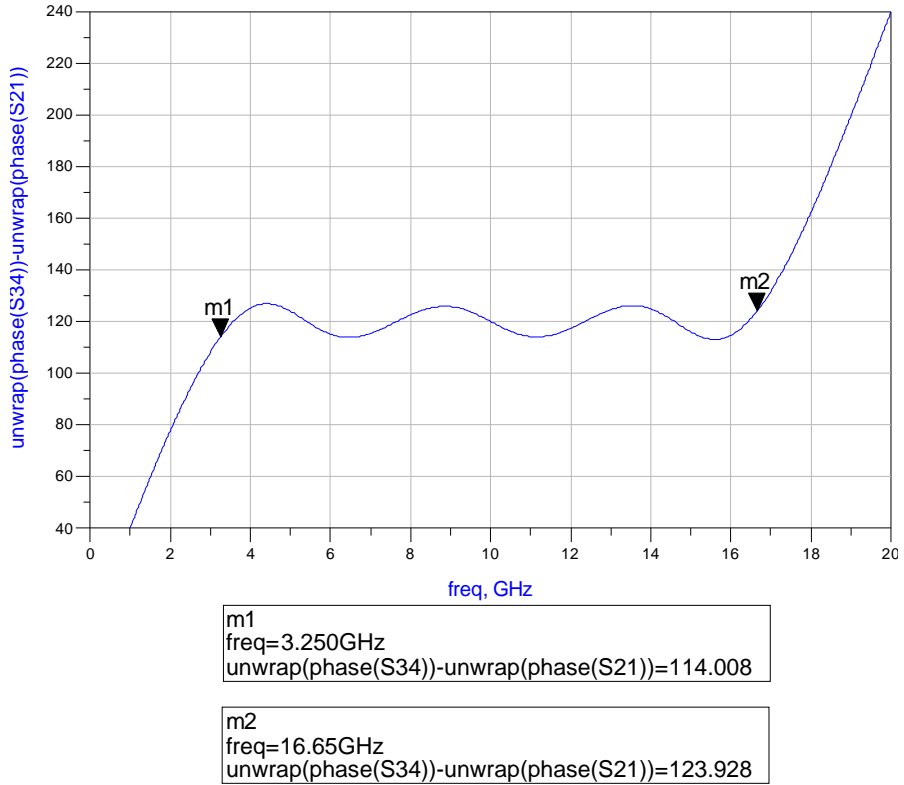


Figure 3.22 Phase difference between phase shifter branch 1 and reference line.

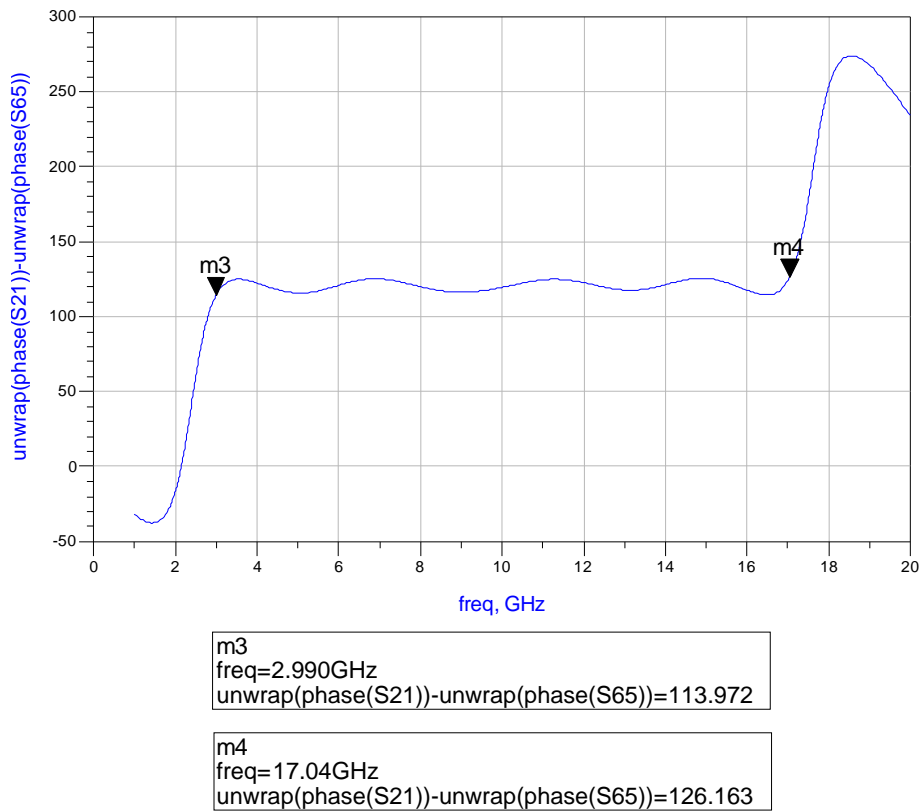


Figure 3.23 Phase difference between reference line and phase shifter branch 2.

3.3 Reflective Phase Shifters

3.3.1 Phase Shifters Using 0° - 180° Hybrids and Uncoupled OC and SC Stepped Lines

The Schiffman type phase shifters described in the previous cases involve parallel coupled lines which may cause realization problems. A simpler phase shifter topology can be obtained using 0° - 180° degree hybrid as follows.

Figure 3.24 describes the definitions and operation of a 0° - 180° hybrid on a Rat Race directional coupler type topology. When power is fed from port-1 it is split into two, one half going to port-2 and the other half to port-4, with both signals having 90° degrees phase shift. Port-3 is isolated. Thus, this type of operation is named as in-phase power division (Figure 3.24.a). If power is fed from port-3 then one half of the power goes to port-4 with 90° degree phase shift while the other half goes to port-2 with 270° degree phase shift, with no signal at port-1. Thus the signals at ports 2 and 4 are 180° degrees out of phase (Figure 3.24.b). This device can be used to find sum and difference of two signals if two signals are fed from the isolated ports as presented in Figure 3.24.c and d.

Figure 3.25.a describes the operation of a two section Schiffman phase shifter. The input signal is split into even and odd excitations. Under even mode excitation the even mode half of the circuit becomes a stepped impedance line with an OC termination. Impedances of the steps are the even mode impedances of the coupled line sections. Under odd mode excitation the odd mode half becomes also a stepped impedance line, but with a SC termination. Step impedances are the odd mode impedances of the coupled line sections. Reflected signals from the even and odd mode half circuits are combined to form the output signal with a phase shift set by the even and odd mode impedances of the sections [26].

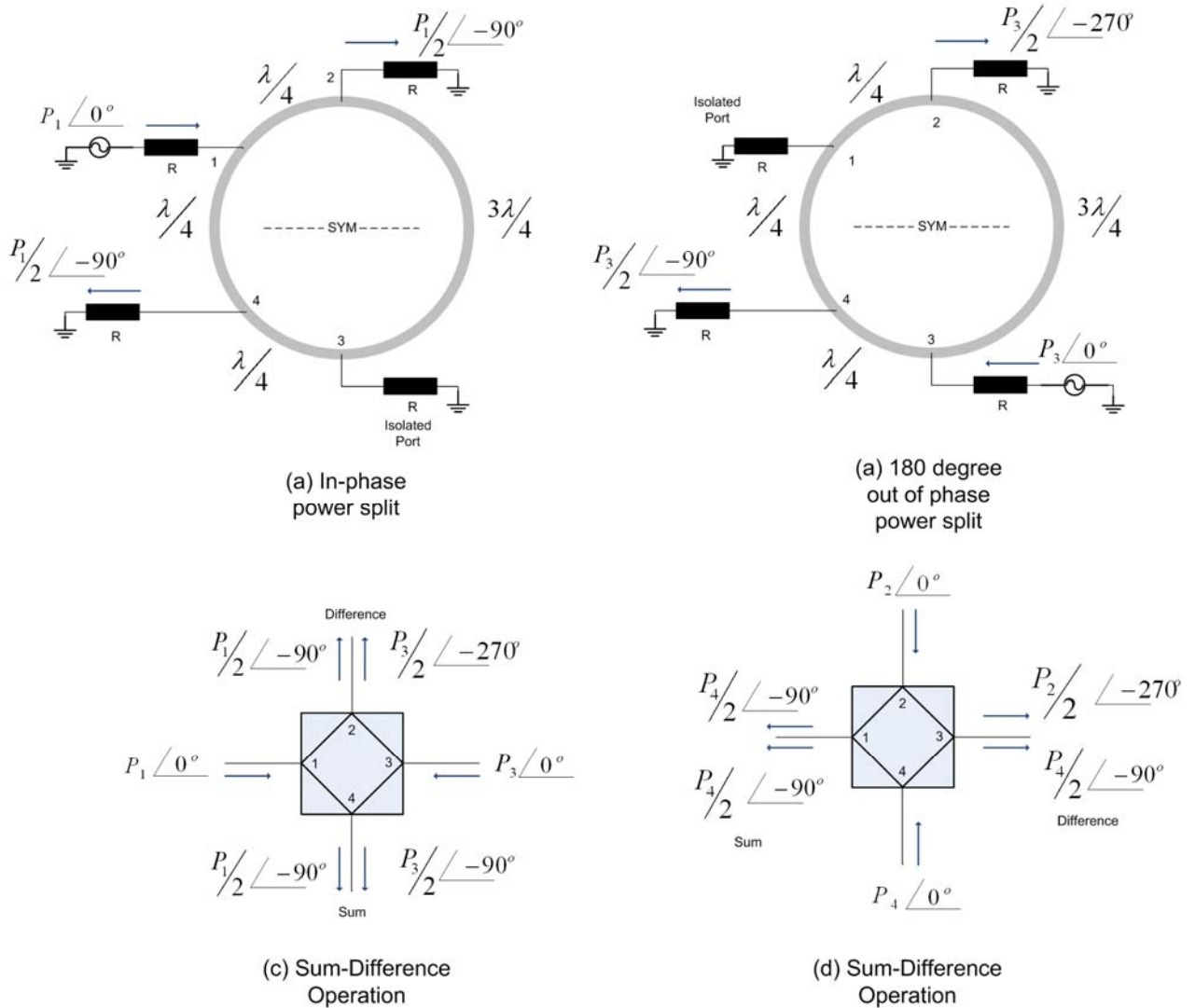


Figure 3.24 Operation and use of 0° - 180° hybrid.

The same phase shift can also be obtained by connecting the even and odd mode half circuits to the isolated ports, for example port-2 and port-4 of a 0° - 180° hybrid as described in Figure 3.25.b. The signal fed from port-1 is split in phase to port-2 and port-4 of the hybrid. The signals reflected from the SC and OC terminations of the stepped lines back to ports 2 and 4. The reflected signals have 180° phase difference because of the SC and OC terminations. Therefore they cancel at port-1 and combine at port-3. The signal at port-3 will have the same phase shift as the Schiffman phase shifter because it is formed by the reflections from the same even and odd half stepped impedance sections. This device is named as reflection mode phase shifter with a 180° hybrid. This approach seems to avoid parallel coupled lines, but

actually the design of a 180 degree directional coupler which can operate over 2-18 GHz band is as difficult as the Schiffman type coupled line phase shifters. Therefore this approach is not studied in this thesis. However it helped to open a way for using phases of reflected signals from OC and SC stepped uncoupled lines, as discussed next.

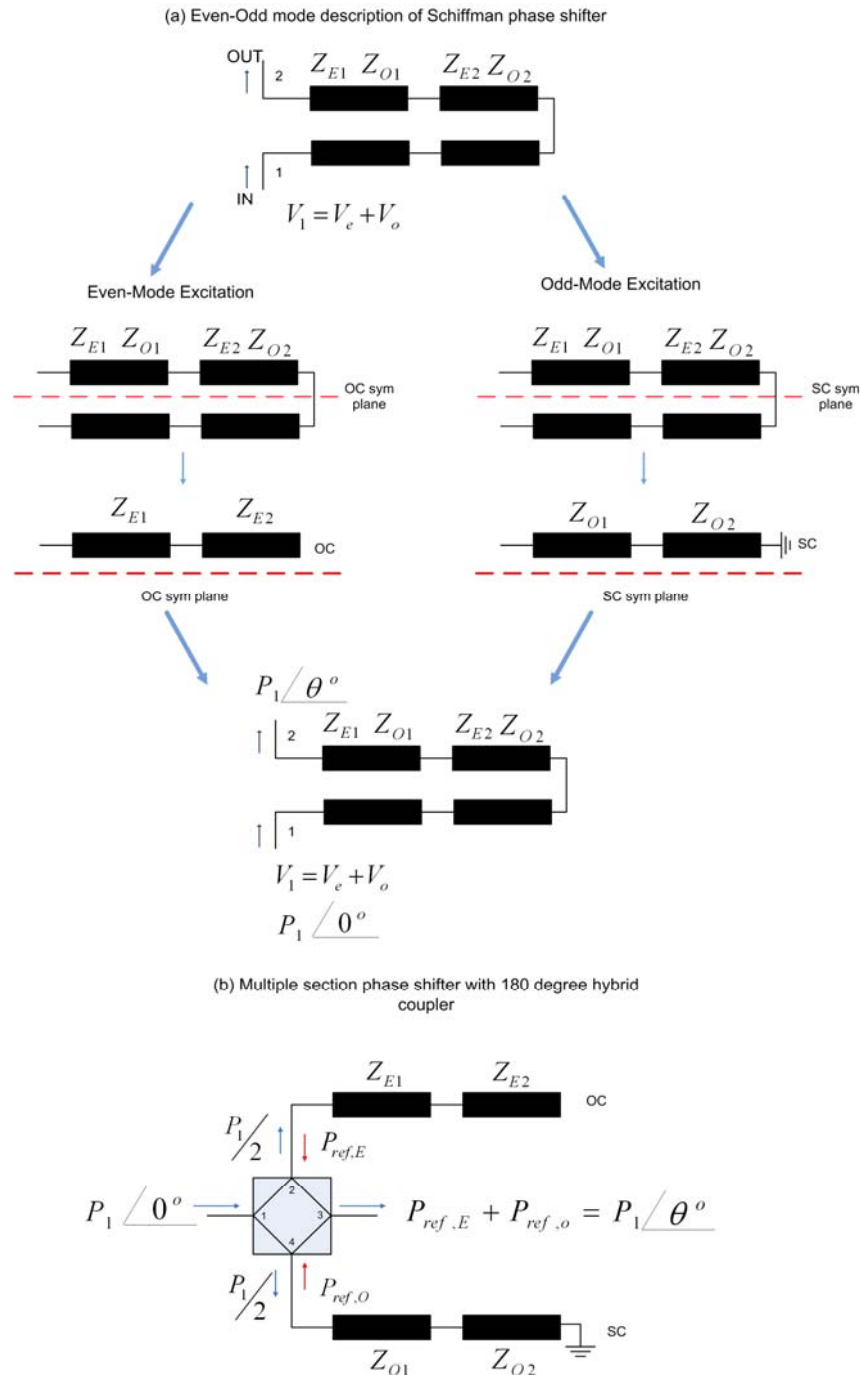


Figure 3.25 (a) Even-Odd mode decomposition of a Schiffman phase shifter. (b) Multiple section phase shifter with 180 degree hybrid coupler and uncoupled stepped transmission lines.

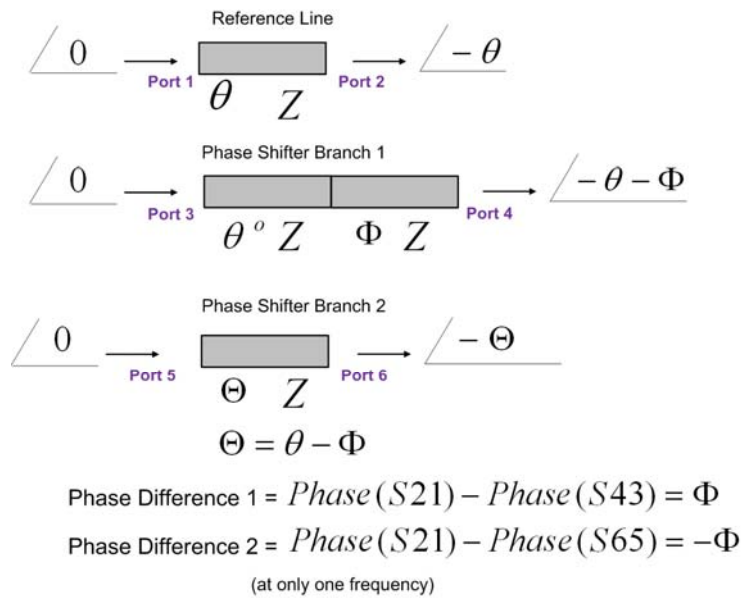
3.3.2 Phase Shifters Using Reflections from Stepped SC and OC Line Sections

The idea given by the phase shifter employing 180° hybrid can be extended to form much simpler differential phase shifter topologies. This idea gives a hint that using appropriate reflective phase shifting branches instead of coupled lines of any kind (including 180° degree hybrid coupler) is sufficient to get desired differential phase shift. Actually this approach was first used in [10], but without any details. Therefore, in this section, a systematic and general approach will be described leading to simple and easy to realize topologies.

3.3.2.1 Reflective Uniform Phase Shifters

In this section, uniform phase shifters in reflective form will be investigated. First transmission and reflective type phase shifters will be compared as starting point. After that reflective type phase shifters and some possible alternatives will be presented. Here, the discussions are made under the assumption that mentioned electrical lengths in the below figures/explanations/examples are smaller than or equal to 90° . Desired phase shifts can also be obtained by using transmission lines which have electrical lengths greater than 90° , but this assumption is made so that the signs of phase shifts are consistent with each other. Figure 3.26 represents the starting point of the discussion. In this figure, the relationship between transmission (Figure 3.26.a) and reflection (Figure 3.26.b) type phase shifting networks which provide the same differential phase shifts is shown. Notice that, the length of phase shifter branch 2 (Θ) is shorter than the reference line. This design is only valid if the desired phase shift is smaller than the length of reference line (θ) at the operating frequency, otherwise a longer transmission line must be used in phase shifter branch 2. Comparison given in Figure 3.26 shows that for reflective phase shifting branches, employing only the half length of each section with respect to the corresponding ones in transmission type phase shifter is sufficient to get the same phase shift. Of course this phase shift is only valid in a specific frequency.

(a) Transmission type differential phase shifter



(b) Reflection type differential phase shifter
(branches are OC ended)

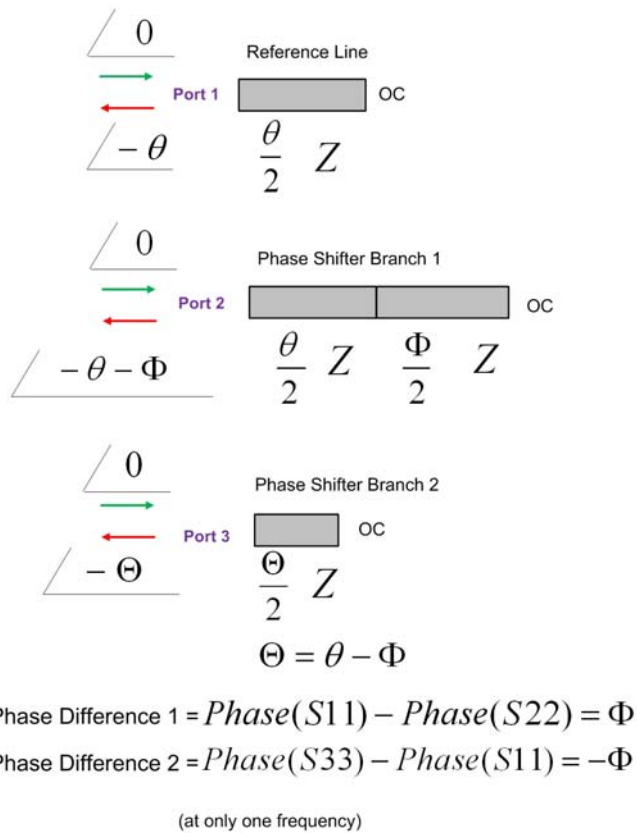


Figure 3.26 The concept for differential phase shifter design using reflected signals.

Let's discuss the situation given in Figure 3.26 with an example: The structure in Figure 3.27 is a transmission type phase shifter. Notice that, the electrical lengths θ , Φ and Θ are equal to 90, 60 and 30 degrees at 10 GHz respectively.

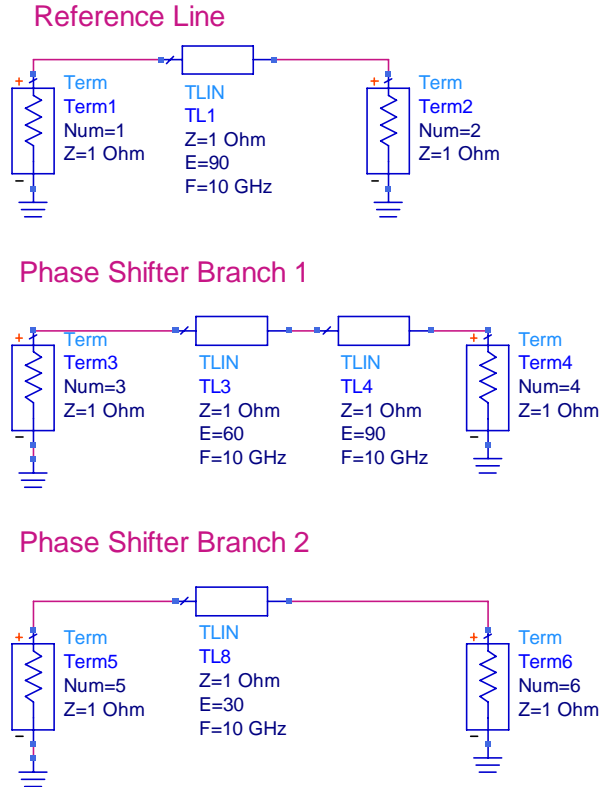


Figure 3.27 Transmission type phase shifter structure.

The phase response of each branch is:

$$Phase(RL)@10GHz = -90^\circ$$

$$Phase(PSB_1)@10GHz = -60^\circ - 90^\circ = -150^\circ \quad (3.3)$$

$$Phase(PSB_2)@10GHz = -30^\circ$$

where;

RL: Reference Line

PSB_1: Phase Shifter Branch 1

PSB_2: Phase Shifter Branch 2.

According to (3.3) the differential phase responses will be

$$\begin{aligned} \text{Phase}(RL) - \text{Phase}(PSB_1) &= 60^\circ @ 10\text{GHz} \\ \text{Phase}(RL) - \text{Phase}(PSB_2) &= -60^\circ @ 10\text{GHz} \end{aligned} \tag{3.4}$$

The results given in (3.4) are also simulated in ADS. Related responses are given in Figure 3.28 and Figure 3.29.

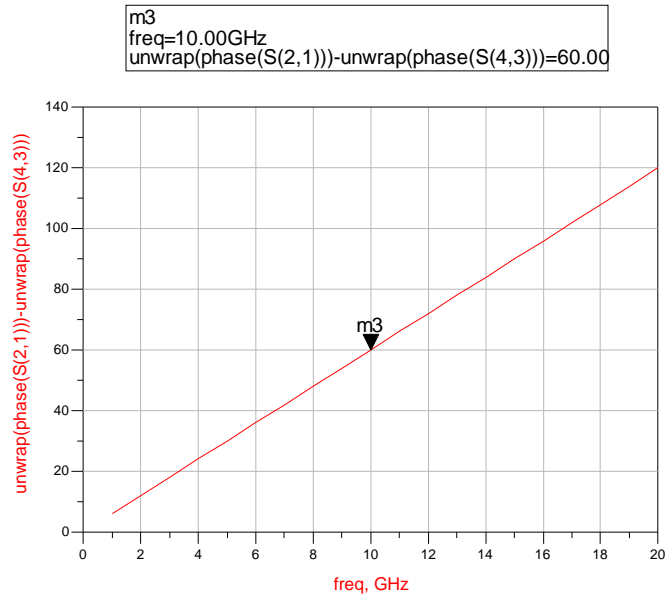


Figure 3.28 Phase difference between phase shifter branch 1 and reference line in transmission type phase shifter.

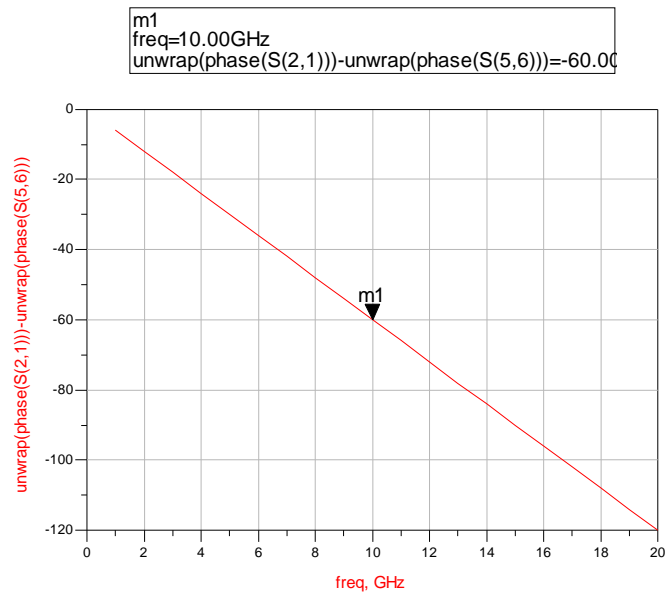


Figure 3.29 Phase difference between phase shifter branch 2 and reference line in transmission type phase shifter.

Reflective phase shifter version of the structure given in Figure 3.27 can be obtained by using only the half lengths of the sections using OC's at the end of each lines (Figure 3.30). For this structure the phase response of each branch is:

$$\begin{aligned}
 \text{Phase}(RL) @ 10\text{GHz} &= -45^\circ - 45^\circ = -90^\circ \\
 \text{Phase}(PSB_1) @ 10\text{GHz} &= 2(-30^\circ - 45^\circ) = -150^\circ \\
 \text{Phase}(PSB_2) @ 10\text{GHz} &= 2(-15^\circ) = -30^\circ
 \end{aligned}
 \tag{3.5}$$

According to (3.5) the differential phase responses will be the same given in (3.4) which are:

$$\begin{aligned}
 \text{Phase}(RL) - \text{Phase}(PSB_1) &= 60^\circ @ 10\text{GHz} \\
 \text{Phase}(RL) - \text{Phase}(PSB_2) &= -60^\circ @ 10\text{GHz}
 \end{aligned}
 \tag{3.6}$$

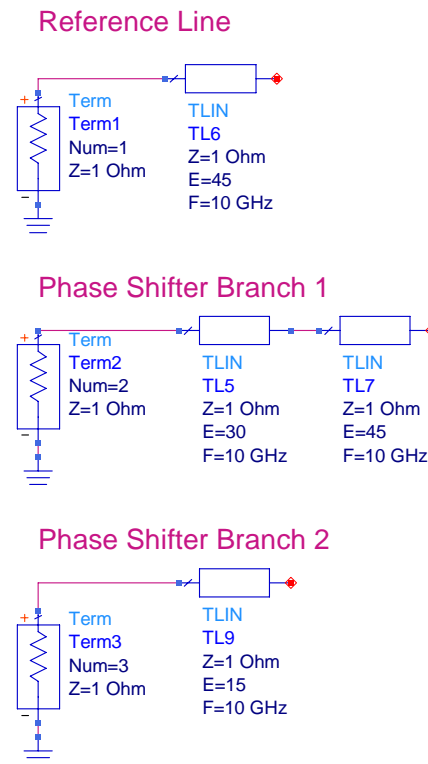


Figure 3.30 OC ended reflection type phase shifter structure.

The results given in (3.6) are also shown in Figure 3.31 and Figure 3.33.

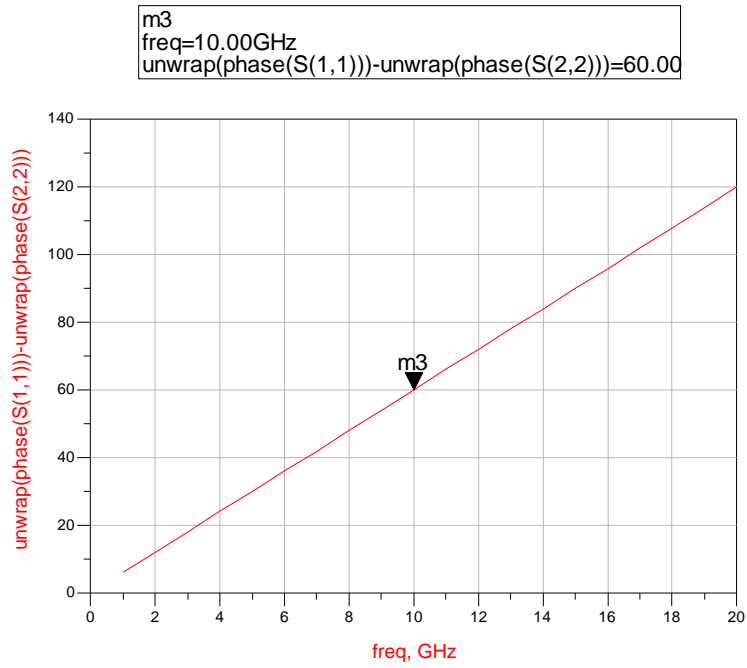


Figure 3.31 Phase difference between phase shifter branch 1 and reference line in OC ended reflection type phase shifter.

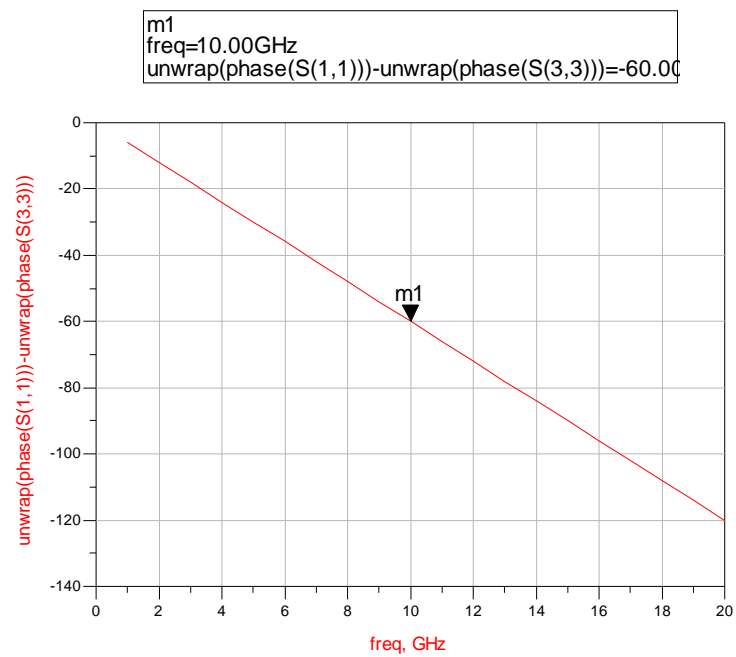
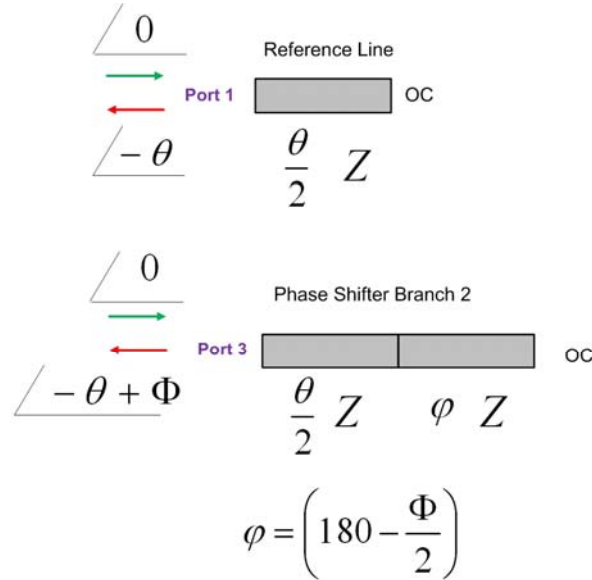


Figure 3.32 Phase difference between phase shifter branch 2 and reference line in OC ended reflection type phase shifter.

Actually the same phase shift can be obtained with various types of phase shifter in reflective form. For example, the length of phase shifter branch 2 can be expanded as shown in Figure 3.33.



$$\text{Phase Difference } 2 = \text{Phase}(S_{33}) - \text{Phase}(S_{11}) = -\Phi$$

(at only one frequency)

Figure 3.33 First alternative of phase shifter branch 2 in the reflection type phase shifter.

In order to obtain the differential phase shift $-\Phi$ the phase of the reflected signal from phase shifter branch 2 must be equal to $-\theta + \Phi$. Here, the reflected signal phase at phase shifter branch 2 is

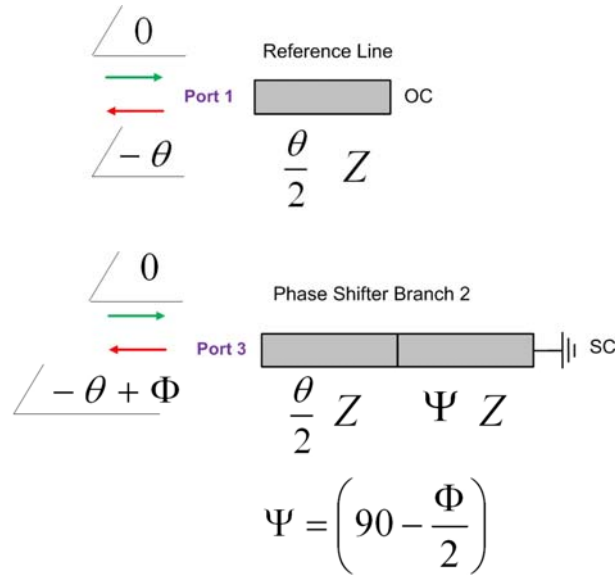
$$\text{Phase}(PSB_2)@10GHz = -2\left(\frac{\theta}{2} + \varphi\right) = -\theta - 2\varphi = -\theta + \Phi \quad (3.7)$$

According to (3.7) φ can be found as follows

$$\begin{aligned} -\theta - 2\varphi &= -\theta + \Phi \Rightarrow -2\varphi = \Phi \Rightarrow 2\varphi = 360^\circ - \Phi \\ \varphi &= 180 - \frac{\Phi}{2} \end{aligned} \quad (3.8)$$

If this design alternative is preferred in the structure given in Figure 3.30 then the length of the line in phase shifter branch 2 must be $\frac{\theta}{2} + \varphi = 45 + 150 = 195$ degrees.

As a second alternative for phase shifter branch 2, the line can be SC ended instead of OC by using an appropriate transmission line (Figure 3.34).



$$\text{Phase Difference 2} = \text{Phase}(S_{33}) - \text{Phase}(S_{11}) = -\Phi$$

(at only one frequency)

Figure 3.34 Second alternative of phase shifter branch 2 in the reflection type phase shifter.

As mentioned above, the reflected signal from phase shifter branch 2 must be equal to $-\theta + \Phi$. Here, the reflected signal phase at phase shifter branch 2 is

$$\text{Phase}(PSB_2)@10GHz = -2\left(\frac{\theta}{2} + \Psi\right) - 180 = -\theta - 2\Psi - 180 \quad (3.9)$$

According to (3.9) Ψ can be found as follows

$$\begin{aligned}
-\theta - 2\Psi - 180 &= -\theta + \Phi \Rightarrow -2\Psi - 180 = \Phi \\
\Rightarrow -2\Psi - 180 + 360 &= \Phi \Rightarrow -2\Psi + 180 = \Phi \\
180 - \Phi &= 2\Psi \Rightarrow \Psi = 90 - \frac{\Phi}{2}
\end{aligned}
\tag{3.10}$$

If second design alternative is preferred in the structure given in Figure 3.30 then the length of the line in phase shifter branch 2 must be $\frac{\theta}{2} + 90 - \frac{\Phi}{2} = 105$ degrees and the line must be SC ended.

3.3.2.2 Simple Reflective Phase Shifters in Stepped Form

As explained above, reflective uniform phase shifters can provide the desired phase shifts at only a single frequency. To obtain a constant differential phase difference over a wider frequency band, these phase shifters must be designed in stepped form. The lines can be OC or SC ended due to the designer's choice. Here, step impedances of the OC and SC ended lines have to be calculated by optimization by placing constraints of phase difference, phase difference ripple and step impedances.

Consider the simple structure shown in Figure 3.35 which represents an example of a uniform reflective phase shifter. Reference line is open circuited line with 1 ohms impedance and 180 degrees electrical length at band center. The reflected signal has a phase of -360 degrees. Another uniform OC line of 1 ohm impedance and 120 degree electrical length is used in the phase shifter. Its reflected signal has -240 degrees. So, the phase difference between reflections is 120 degrees at the center frequency only (Figure 3.36).

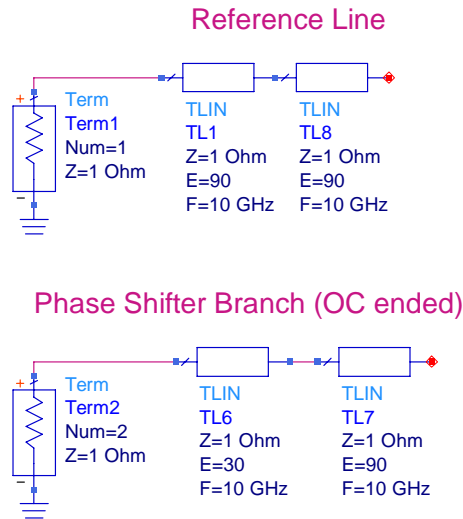


Figure 3.35 Simple reflective phase shifter structure.

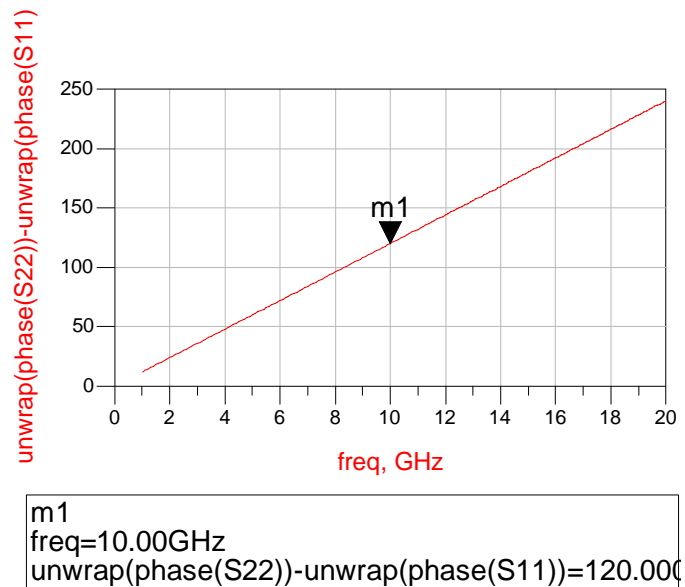


Figure 3.36 Differential phase response of one step reflective phase shifter.

In order to get the desired phase shift in a wider frequency bandwidth, a stepped-impedance structure must be used. Figure 3.37 shows a two step version just to get insight. It is clear that constant phase difference bandwidth widens as the number of sections increase. This fact is used in the following designs by increasing the number of steps.

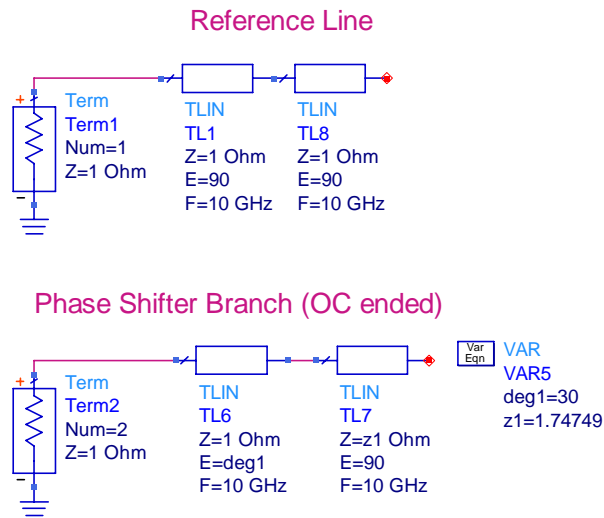


Figure 3.37 Two-step reflective phase shifter structure.

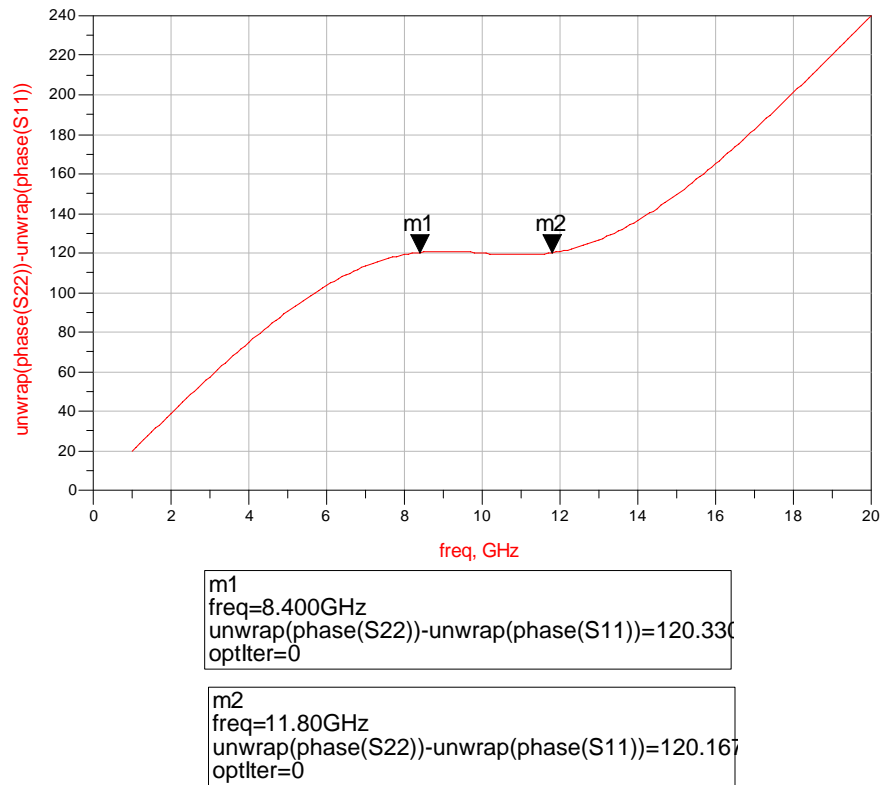


Figure 3.38 Differential phase response of the two-step reflective phase shifter.

3.3.2.3 Multi-Step Reflection Phase Shifters

Phase shifters with multiple steps can be designed by brute force optimization approach by starting with arbitrary initial section impedances. This fact is observed through many design trials. Additionally, it is possible to obtain same differential phase shift with various kind of phase shifting branches and reference lines. Not only these lines can be at any form (i.e. uniform, gradually increasing/decreasing impedance stepped sections or random stepped impedance sections) but also they can be terminated with OC or SC (Figure 3.39). Due to the variety of design alternatives, a set of criteria should be determined by the designer.

3.3.2.3.1 Evaluating the Structural Alternatives

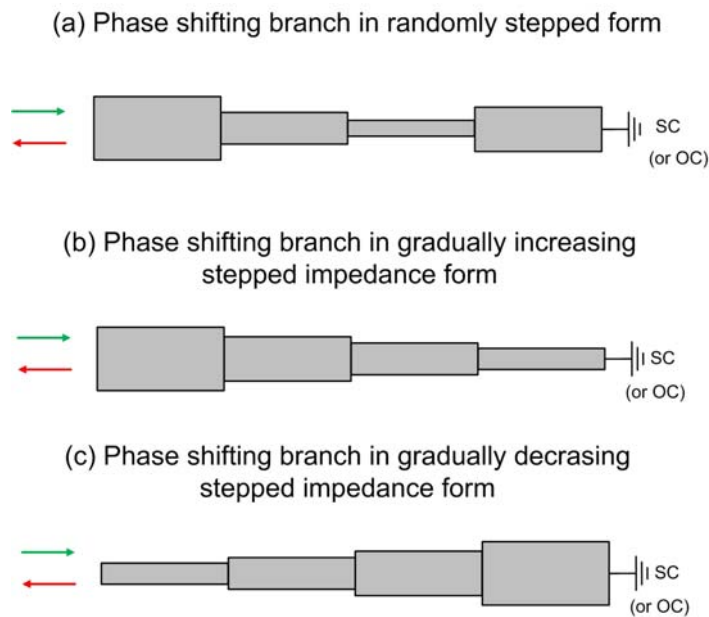


Figure 3.39 Phase shifting branches in alternative forms.

In this thesis, the design rules of phase shifters are determined in order to simplify the phase shifter structures for production process. These rules are listed below.

- Mostly OC ended lines are used to get rid of using additional components like bonding wires and capacitors which are needed to short circuit the lines.

- Uniform reference line is used and phase shifter branches are designed/optimized/tuned according to this reference line.
- According to the choice made for reference line, the phase shifting branches must be in stepped form. Actually this process is an entirely different subject. At this point, the width difference between adjacent sections is very important. In computer simulations this difference may not be a problem. But in practical world, as the difference between adjacent sections increases the response gets worse due to junction discontinuity losses. So before choosing the form of phase shifting branches, the designer should make several simulations to get an insight about which option is suitable. Experiments had shown that generating negative (i.e. $-\Phi$) differential phase shifts seems to be much easier with gradually decreasing step impedances while for positive differential phases ($+\Phi$) increasing step impedances are much easier compared to randomly stepped form. Two reasons can be given for this situation:
 - For gradually increasing/decreasing impedance stepped lines, forming positive/negative reflections coefficients are easier due to the arrangement of sections.
 - According to the transmission line model (Figure 3.40) using random impedance sections may lead to generate a low pass filter effect and this may lead to create a true time delay. Of course this situation depends on the design, but if it happens, obtaining a constant or low ripple phase shift in a wide frequency band becomes harder.

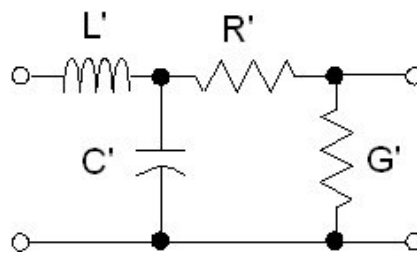


Figure 3.40 Transmission line equivalent model.

After various simulation efforts, with constraints on the number of sections (limited to five or six to keep the longitudinal size small) and realizable widths of line pieces,

gradually increasing/decreasing stepped impedance form is chosen for phase shifting branches as follows:

- For phase shifter branch 1, positive reflection coefficient is needed to obtain $+\Phi$ differential phase shift. So a branch in gradually increasing stepped impedance form will be used.
- For phase shifter branch 2, negative reflection coefficient is needed to obtain $-\Phi$ differential phase shift. So a branch in gradually decreasing stepped impedance form will be used.

3.3.2.3.2 Designing the Phase Shifter

As presented in section 3.2, in a Schiffman type phase shifter the coupling values “gradually changes” as shown in Figure 3.25. When the phase shifter is decomposed into even and odd mode branches, a “gradual increase or decrease” in even/odd mode branch impedance values can be obtained. Thus, although it is possible to start the optimization procedure with an arbitrary set of initial values, the results of Schiffman type phase shifters are used to speed up the convergence.

3.3.2.3.2.1 Reference Line and Phase Shifter Branch 1

The 6-section Schiffman phase shifter discussed at the section 3.2.4 can form the structural basis of phase shifting branches due to its good differential phase response. In Figure 3.41, the reference line and phase shifter branch 1 of this structure is given.

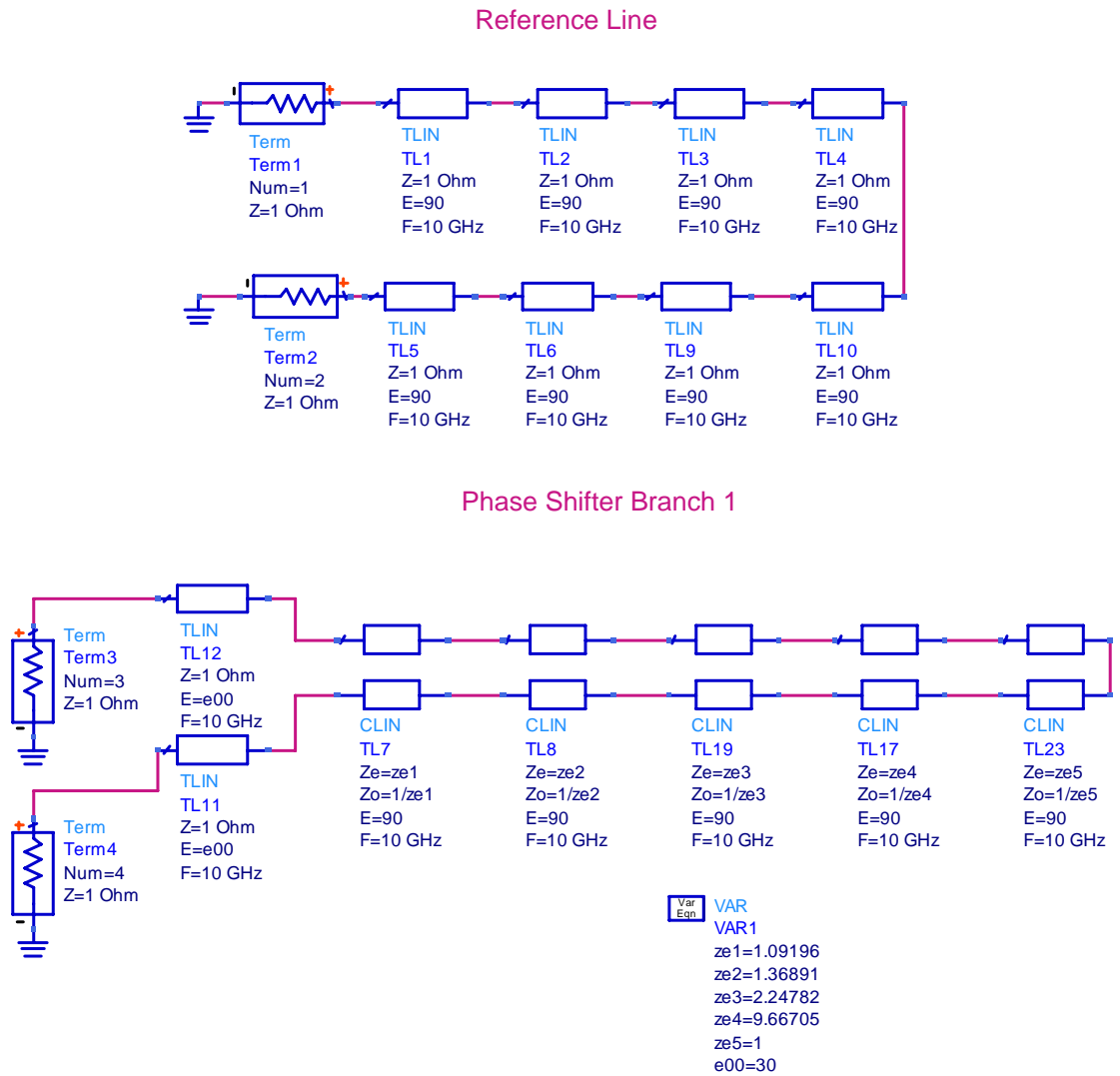


Figure 3.41 Phase shifting structure given in section 3.2.4.

Figure 3.42 shows the decomposed version of the phase shifter branch 1. As expected, the phase difference between even and odd mode branches is 180 degrees at all frequencies (Figure 3.43).

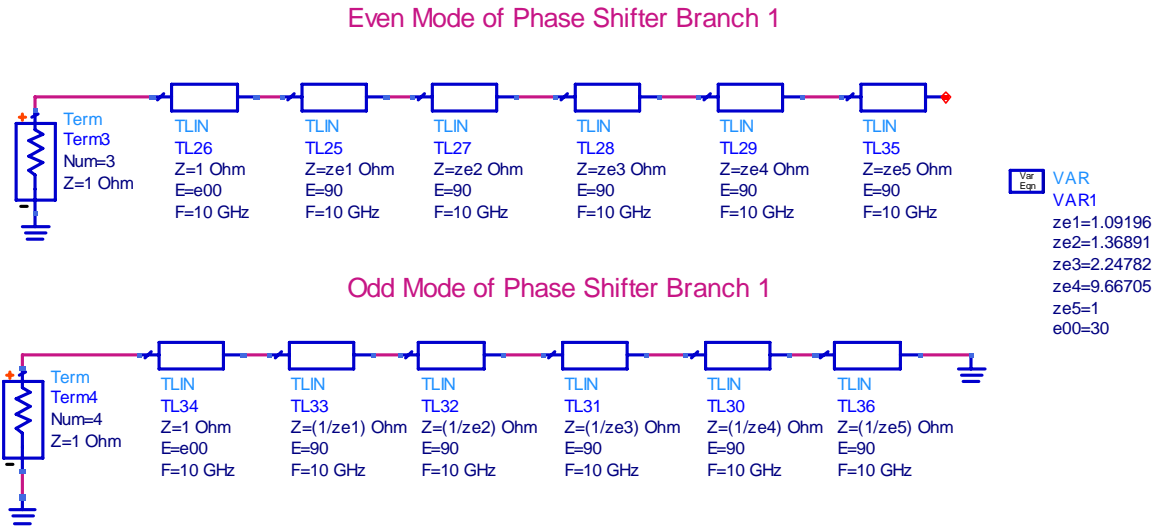


Figure 3.42 Decomposed version of the phase shifter branch 1.

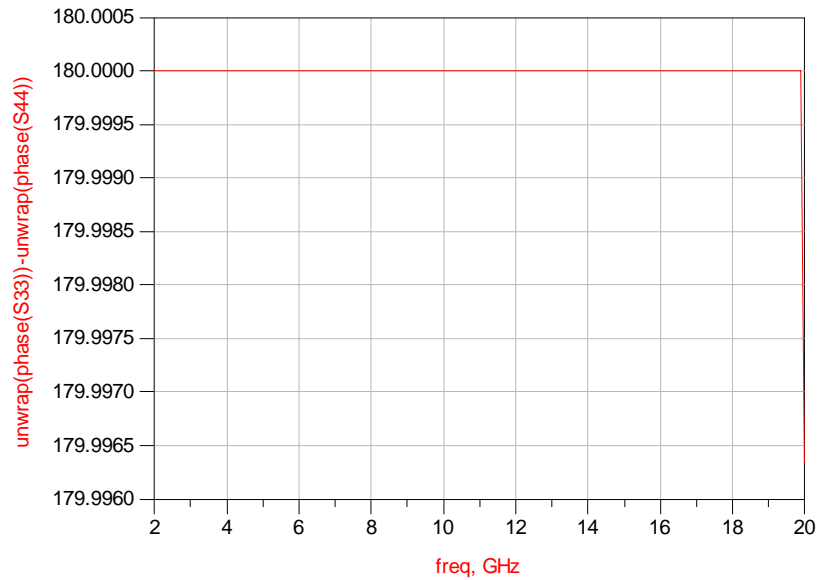


Figure 3.43 The phase difference between the decomposed lines of phase shifter branch 1.

The reference line is also transformed into a reflective form by using the half length of the line and terminating it with open circuit. As can be seen in Figure 3.45, the phase does not change between these two lines.

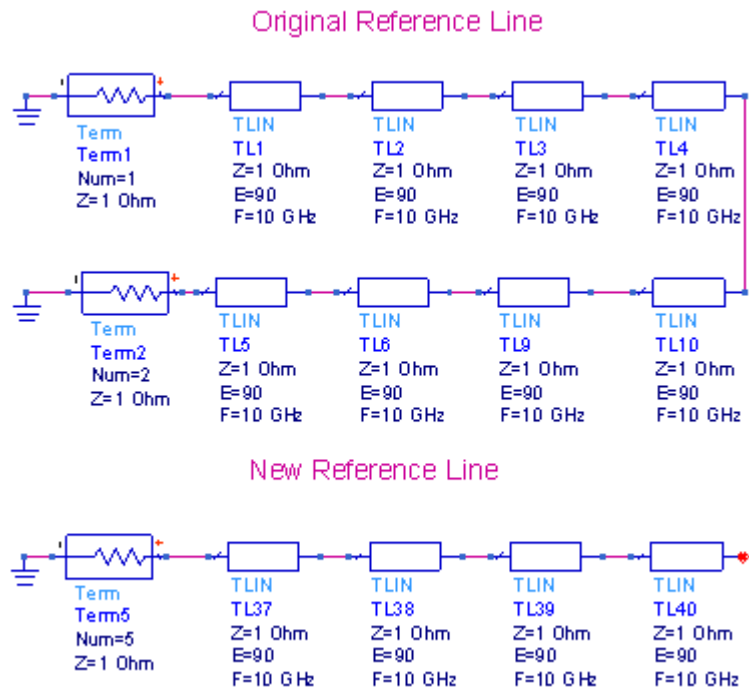


Figure 3.44 Original and new versions of the reference line given in section 3.2.4.

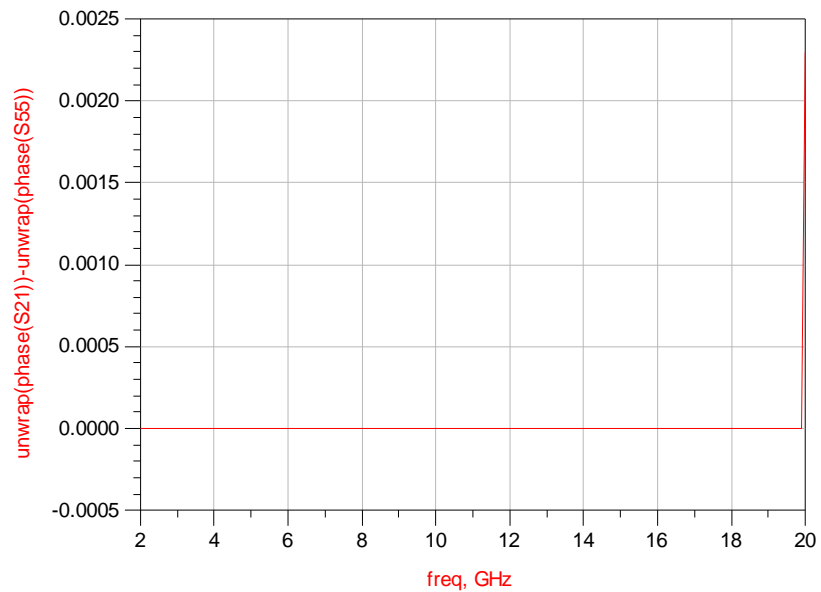


Figure 3.45 Phase difference between the original and new versions of the reference lines.

Since the phase difference between decomposed even and odd mode branches is 180° , calculations can be done using only even mode stepped impedance branch which has the same phase response with the original Schiffman phase shifter branch.

Figure 3.46 shows the new version of the phase shifter discussed above. As expected, the phase response of this structure is same with the one given in Figure 3.13.

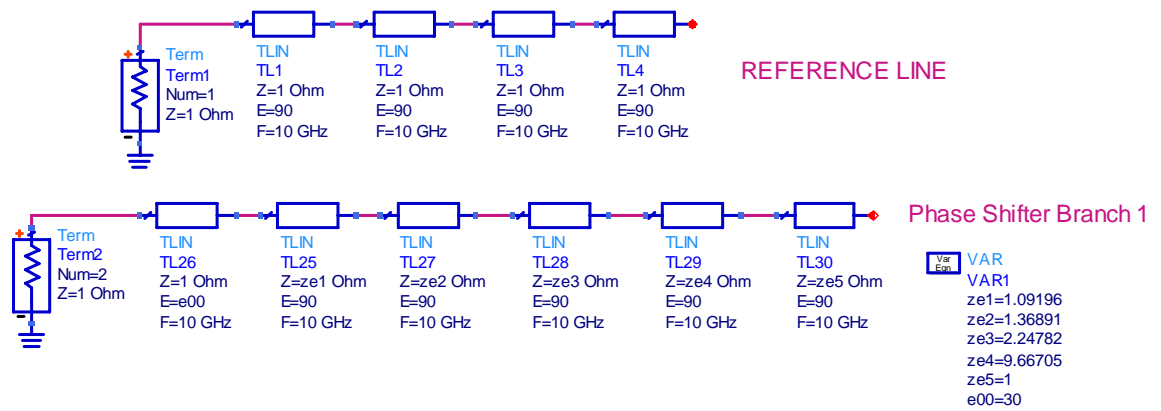


Figure 3.46 Decomposed version of 6 section phase shifter.

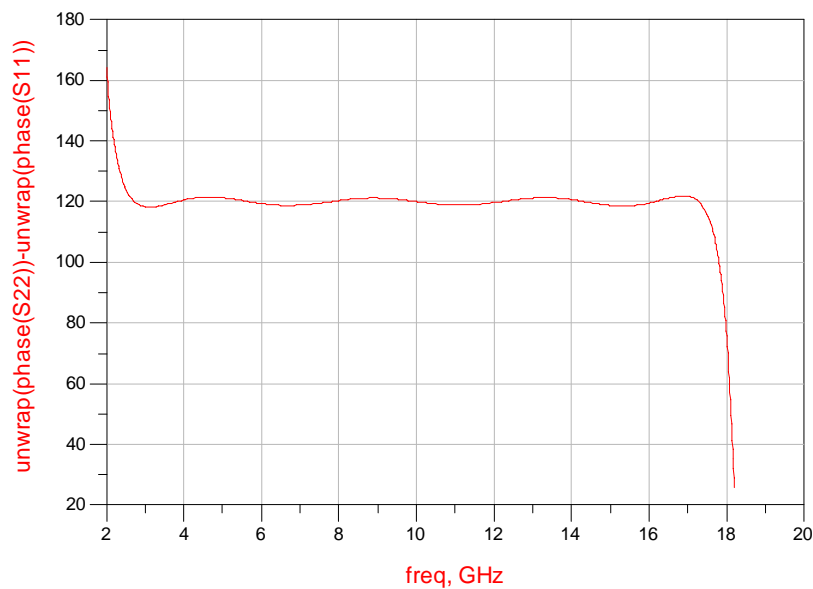


Figure 3.47 Differential phase response of new structure.

Notice that, there is a “gradual” increase in impedance values until the last transmission line in this new phase shifter structure. Here, the impedance ratio (i.e. $ze5/ze4$) between the last two transmission lines is too small. This means that the reflection coefficient (equation (3.11)) between TL30 and TL29 is nearly -1 for the most parts of the frequency band. In other words, for TL29, TL30 acts like a short circuit.

$$\Gamma = \frac{(-j)\cot(\beta l)ze5 - ze4}{(-j)\cot(\beta l)ze5 + ze4} \Rightarrow \beta l = \frac{2\pi \lambda_0}{\lambda} \frac{1}{4} = \frac{\pi f}{2f_0} \quad (3.11)$$

The phase change of the reflection coefficient given in (3.11) is presented in Figure 3.48. It is seen that phase of the reflection coefficient is nearly 180 degree over 2-18 GHz band.

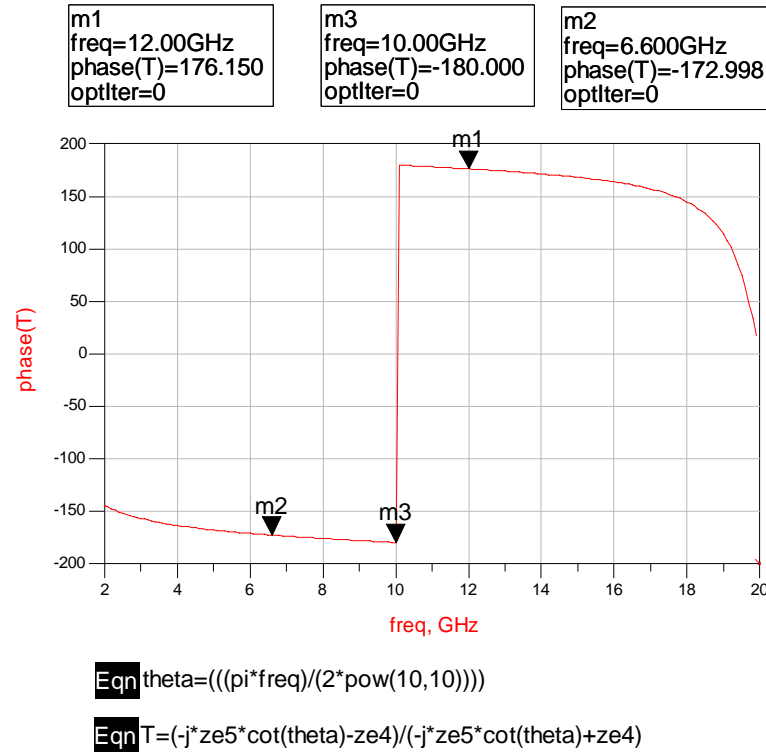


Figure 3.48 Phase of reflection coefficient between TL 29 and TL 30 in phase shifter branch 1.

So if the last transmission line (TL 30) is omitted and TL 28 is short circuited the differential phase response of the new structure (Figure 3.49) would not be affected much as shown in Figure 3.50.

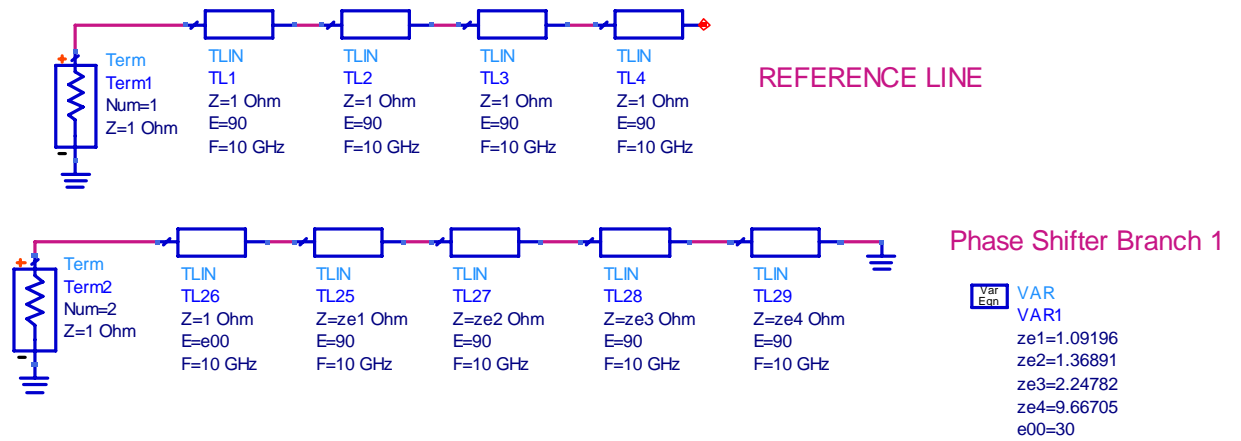


Figure 3.49 Decomposed version of 6 section phase shifter branch 1, with TL30 omitted and structure is short circuited.



Figure 3.50 Differential phase response of the short circuited phase shifter branch 1.

The phase response in Figure 3.50 shows a deformation especially at the edges of defined frequency band due to the changes in the circuit. But this structure gives a hint that a 5 section SC ended phase shifter branch will be sufficient to obtain +120 degree differential phase shift. Indeed after optimization, the final structure is obtained as shown in Figure 3.51 with phase response given in Figure 3.52. The differential phase is 120 ± 1 degrees in 2 GHz – 18 GHz bandwidth.

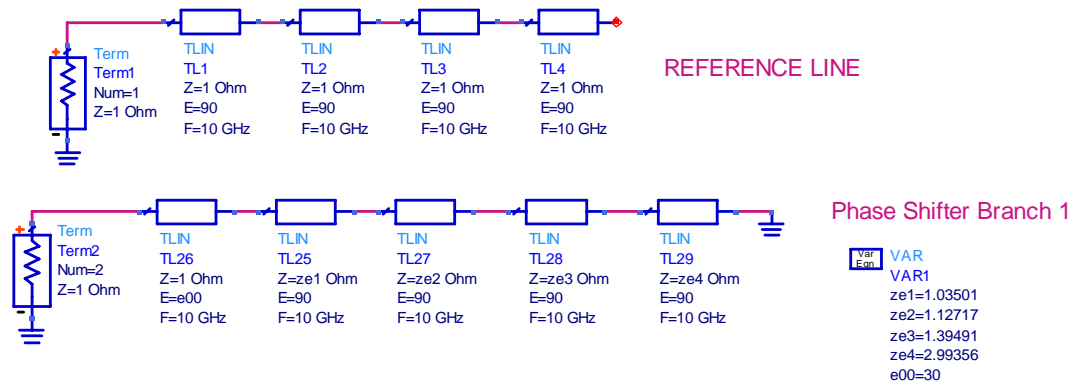


Figure 3.51 Decomposed, shortened and optimized version of the original phase shifter branch 1.

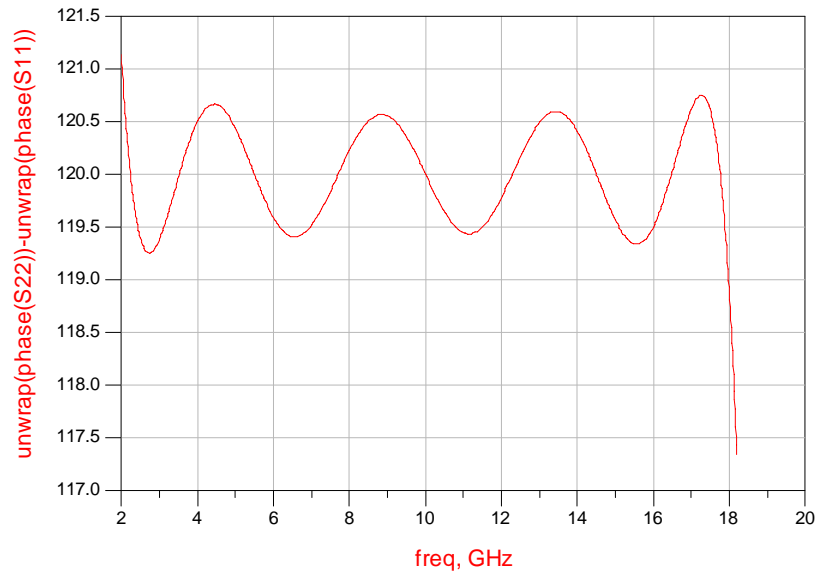


Figure 3.52 Differential phase response of final phase shifter structure for phase shifter branch 1.

3.3.2.3.2.2 Phase Shifter Branch 2

For this branch gradually decreasing stepped impedance form with a SC termination can be used to obtain -120 degree differential phase shift. Since the phase difference between even and odd mode branches of a Schiffman phase shifter is 180 degrees at all frequencies, odd mode half of a Schiffman phase shifter with 60 degrees differential phase can be used as a starting circuit for an optimization process to get the required -120 degrees differential phase shifter with SC termination. The mentioned Schiffman phase shifter odd mode branch with 60 degrees differential

phase shift is given in Figure 3.53 with response shown in Figure 3.54. The odd mode half of this circuit is shown in Figure 3.55. As expected, it has 180 degrees differential phase shift with respect to the even half (Figure 3.56).

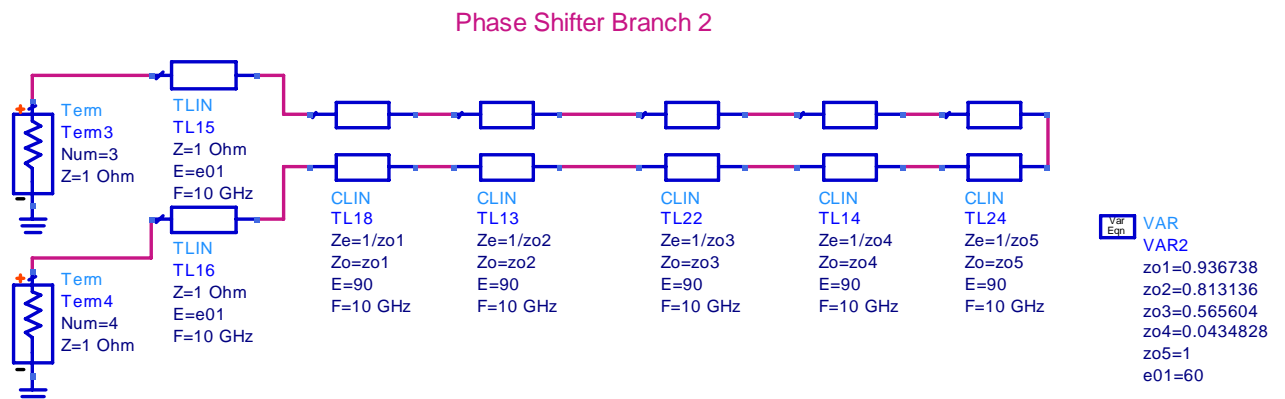


Figure 3.53 Phase shifter branch 2.

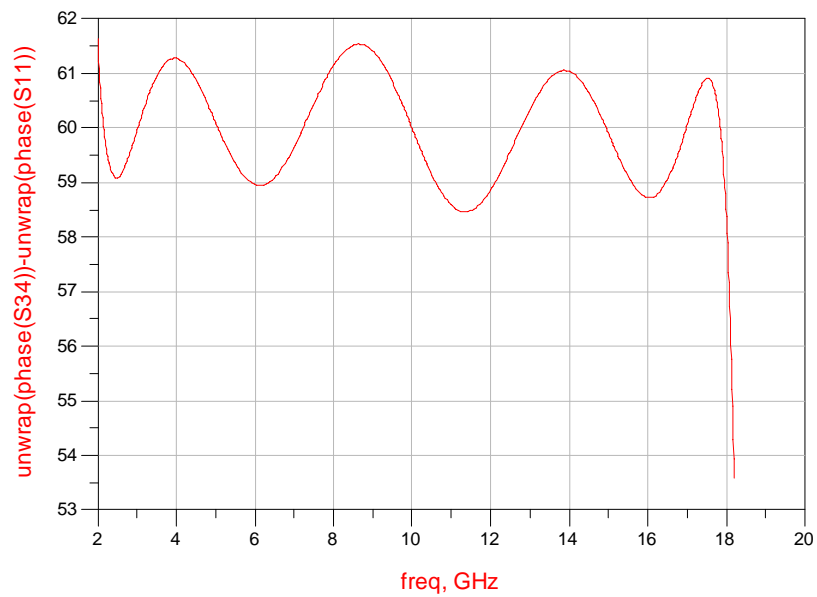


Figure 3.54 Phase difference between reference line and phase shifter branch 2.

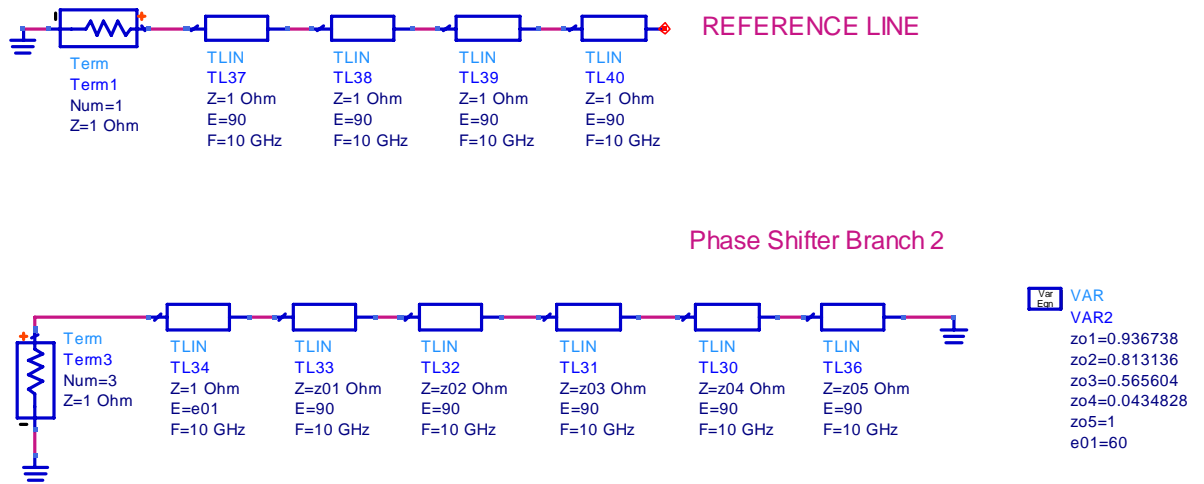


Figure 3.55 Odd mode impedance branch of decomposed phase shifter branch 2.

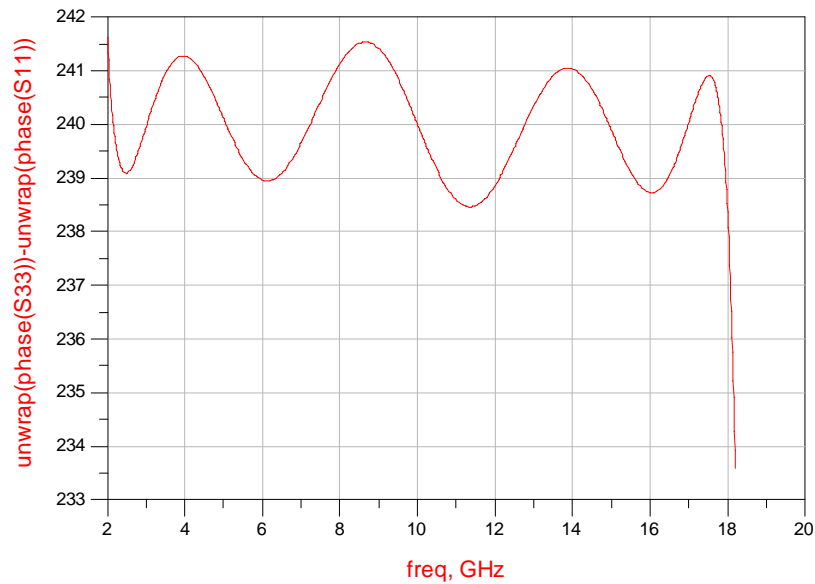


Figure 3.56 Differential phase response of odd mode impedance branch.

It is seen that impedance of the last transmission line (TL 35) is too high compared to the adjacent line (TL 36), acting like an OC. Therefore it is deleted and the branch is terminated in OC leading to negligible effect on the phase, as shown in Figure 3.57 and Figure 3.58.

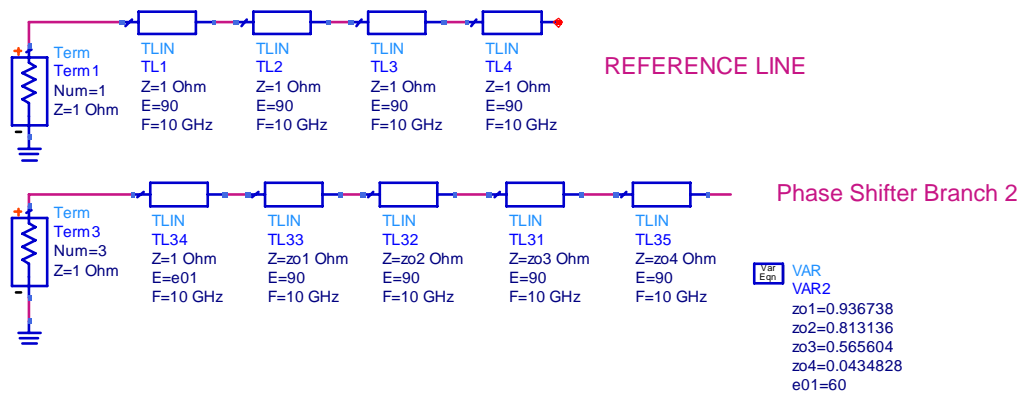


Figure 3.57 Decomposed version of 6 section phase shifter branch 2, TL36 is omitted and structure is open circuited.

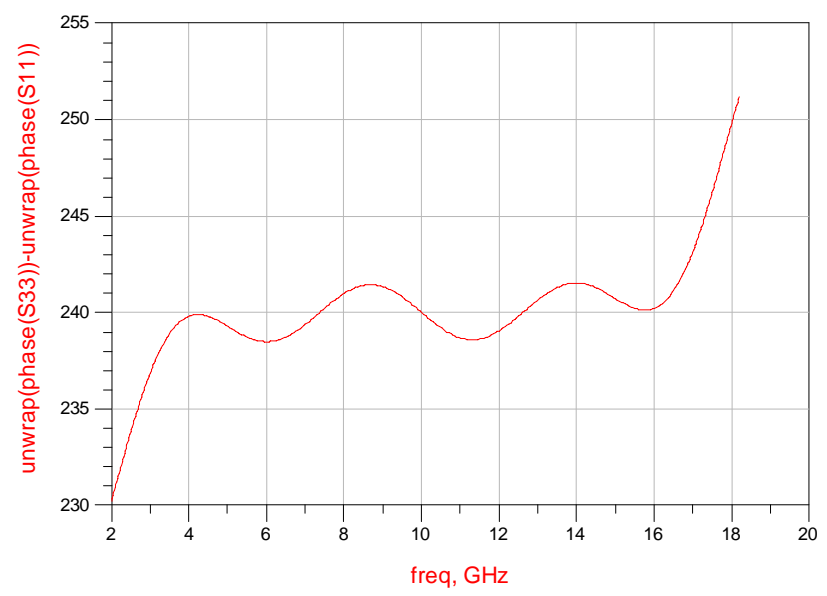


Figure 3.58 Differential phase response of the open circuited phase shifter branch 2.

After optimization process the structure shown in Figure 3.59 is obtained with the differential phase response shown in Figure 3.60. The phase is 240 ± 1 (i.e. -120 ± 1) degrees in 2 GHz – 18 GHz frequency bandwidth.

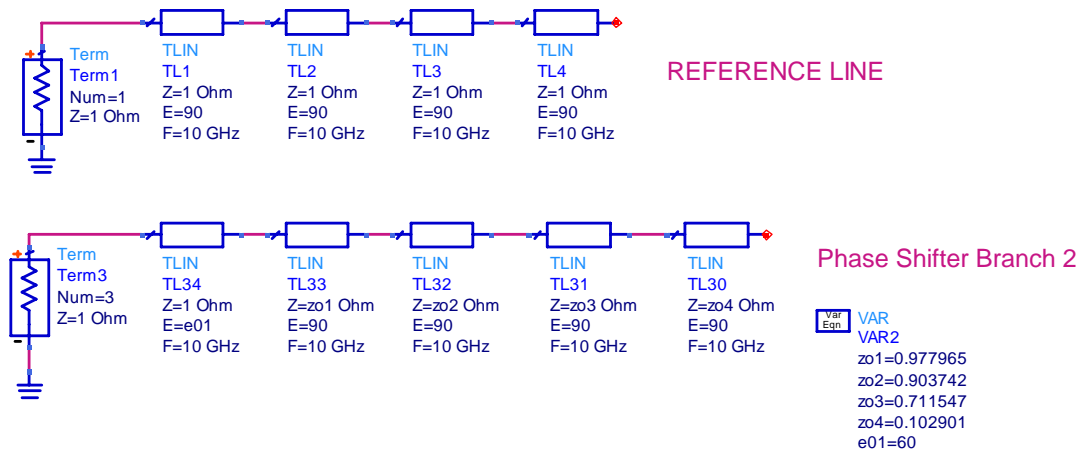


Figure 3.59 Decomposed, shortened and optimized version of the original phase shifter branch 2.

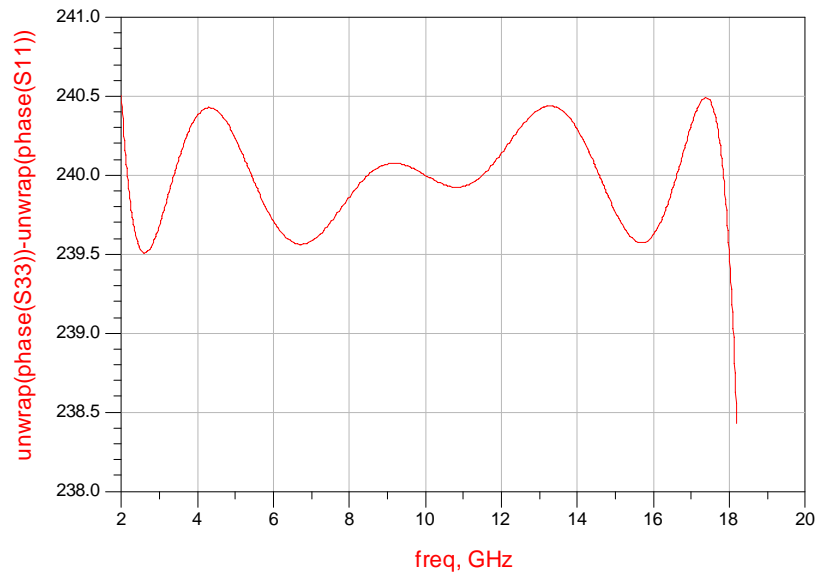


Figure 3.60 Differential phase response of final phase shifter structure for phase shifter branch 1

3.3.2.3.2.3 Final Structure

The final phase shifter network is given in Figure 3.61. Compared to the previous approaches, this circuit has minimum phase ripples over widest frequency band with no implementation difficulties. Therefore this circuit is used in the designed IFM system.

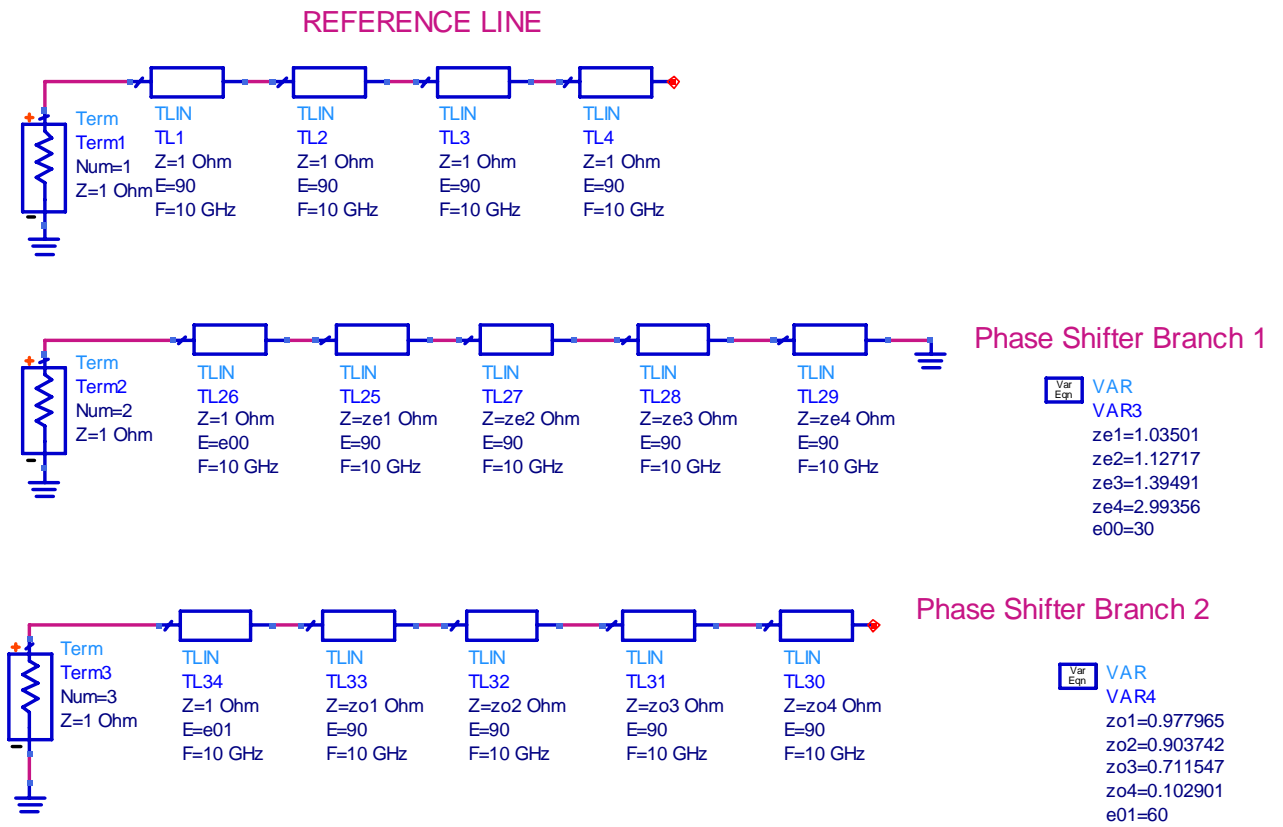


Figure 3.61 Final phase shifting network.

CHAPTER 4

FREQUENCY DISCRIMINATOR DESIGN

The digital instantaneous frequency measurement (DIFM) receiver is the core technique used in wideband EW systems for pulse and CW frequency measurement [27]. As mentioned in Chapter 2, in principle, the input signal frequency of a sinusoidal carrier is recovered by measuring the phase shift across a delay line of known length using a wideband phase discriminator circuit.

Accurate broadband frequency operation is achieved by using multiple frequency discriminators with different delay lines. The discriminator with longest delay line (i.e. fine tier) defines the frequency accuracy, as determined by the phase measurement performance of the basic phase discriminator, while the other discriminators with shorter lines (coarse and medium tiers) are used progressively to resolve longer line phase ambiguities. So a typical IFM receiver structure includes multiple discriminators with different delay lengths. On the other hand, apart from having different delay lengths, the configuration of these discriminators can also be different.

As mentioned in Chapter 2, finding the input frequency depends on the output DC detector voltages of each frequency discriminator structure. Obtained DC voltages are digitized in order to resolve the ambiguities by using look-up tables usually installed in a programmable-read-only-memory (PROM). These values can also be used in simple mathematical/trigonometric equations as presented in section 2.3. Apart from the digital world, the aim of this thesis is only designing the RF part of the system. So, here, the main purpose is to provide the required DC voltage values to the digital card in the system.

In this chapter, RF components of the frequency discriminator are explained with their ADS designs and various simulation results. Coarse and fine tiers of the discriminator are also fabricated and their outputs are measured. These measurement results are also given in related sections.

4.1 Frequency Resolution and Accuracy

For a receiver, an approximate 1 MHz frequency measurement resolution is quite good. As explained in section 2.4, theoretically, frequency resolution depends on two factors: length of the longest delay line and sampling bit number.

$$\Delta F = \frac{1}{TxM} \text{ Hz} \quad (4.1)$$

where;

ΔF = Frequency Resolution

T = Delay

$M = 2^N$ =Quantization Levels (N is the number of bits)

And the relationship between a delay in time and a physical length of a line is

$$L = \frac{Txc}{VF} \text{ meters} \quad (4.2)$$

where;

T = Delay

c = Speed of Light

VF = Velocity Factor

Here velocity factor represents the degradation amount of speed of light in the medium and it is equal to square root of relative dielectric constant of the medium (i.e. $\sqrt{\epsilon_R}$)

According to [3] quantization bit number can be up to 12 bits (i.e. N). But let's take it as 8 bits. So the number of quantization levels will be $M = 2^N = 256$. According to M, to obtain 1 MHz frequency resolution the delay must be;

$$T = \frac{1}{\Delta F \times M} \approx 3.9 \text{ ns} \quad (4.3)$$

Maximum delay line length also affects the frequency measurement accuracy. As given in section 2.5, the frequency accuracy can be defined as follows.

$$\theta_{rms,noise} = \frac{1}{S_{RF}} \sqrt{\frac{B_v}{B_{RF}} \left(2 \left[1 - \frac{\sin\left(\frac{w_v}{UB_{fine\ tier}}\right)}{\left(\frac{w_v}{UB_{fine\ tier}}\right)} \right] S_{RF} + 1 \right)} \quad (4.4)$$

where;

$\theta_{rms,noise}$ is the rms phase noise

S_{RF} is the signal to noise ratio in the RF stage

B_R is the RF noise bandwidth

F is the noise figure of the input amplifier

K is Boltzman constant

T is the temperature

w_v is video signal angular frequency

$UB_{fine\ tier}$ is the unambiguous bandwidth of the fine tier.

If w_v is a lot smaller than $UB_{fine\ tier}$ the expression simplifies to:

$$\theta_{rms,noise} = \frac{1}{S_{RF}} \sqrt{\frac{B_v}{B_{RF}}} \quad (4.5)$$

And the rms frequency accuracy will be:

$$\Delta f_{rms} = \frac{\theta_{rms,noise}}{\pi} UB_{fine_tier} \quad (4.6)$$

So frequency accuracy depends on the maximum delay line length, the input SNR, video bandwidth. Here, video bandwidth is related to the minimum pulse width handling capability of the system [41]. If it is too large then identifying the input signals frequency becomes harder under interference of other signals. If it is too narrow, then detecting the desired signal may be problematic. According to the operational requirements the video bandwidth must be decided by the designer. The presented frequency discriminator design in this thesis can provide 0.28 MHz (rms) frequency measurement accuracy with 20 MHz video bandwidth if 0 dB input SNR is assumed.

4.2 Number of Tiers

For the frequency discriminator in this thesis, number of tiers is decided by making estimation after several simulation efforts. A practical 2-18 GHz coarse tier has an unambiguous bandwidth nearly 14 GHz and making the time delay of the longest line nearly 4ns seems to be reasonable. So the ratio between UBW_{coarse_tier} and UBW_{fine_tier} will be

$$\frac{UBW_{coarse_tier}}{UBW_{fine_tier}} = 56 \quad (4.7)$$

Using fixed inter tier ratio between the tiers, which is usually the case, phase margin and tier ratio is given in Table-1 for different number of tiers. These values are calculated according the equations given in section 0.

Table 1 Number of tiers vs. phase margin relationship.

Number of tiers, n	Inter tier ratio, r	Phase margin, degrees
3	7.48	21.22
4	3.77	37.73
5	2.73	48.26
6	2.23	55.72

As can be seen from the table, phase margin changes rapidly when the system has 5 tiers instead of 4. But this change is smaller between a 5 tier and a 6 tier structure. Thus, in order to build the simplest design, number of tiers is decided to be 5 including 1 coarse, 3 medium and 1 fine tier.

Figure 4.1 basically shows the block diagram of the system. It includes two kinds of phase discriminator structures. Here, coarse and medium tiers rely on “Three Phase Discriminator” model explained in section 1.3.2.3 and fine tier (encircled area) is designed in a more conventional approach like the one given in section 2.3. Details of these tiers will be given in related sub-sections.

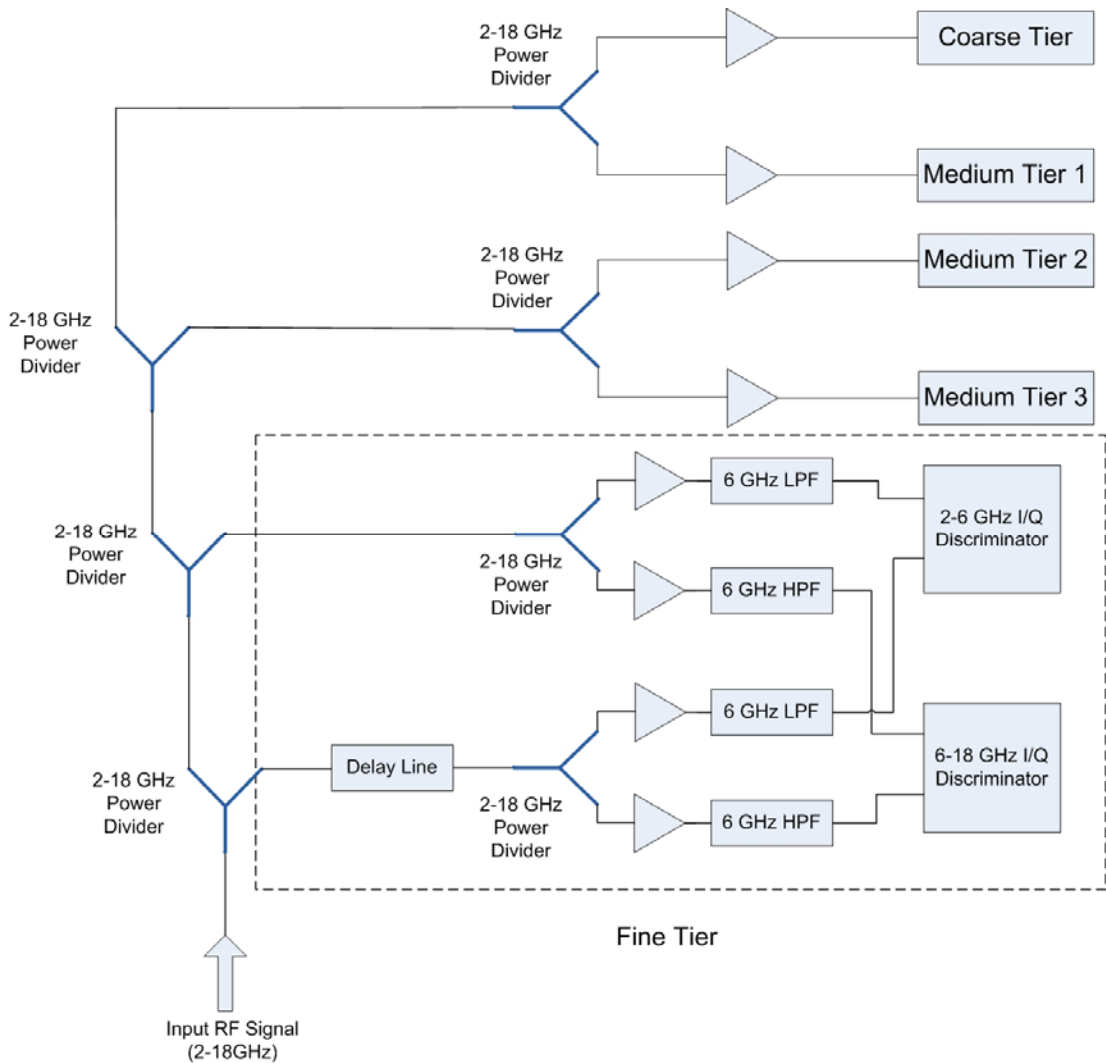


Figure 4.1 IFM discriminator, basic block diagram.

4.3 Choosing the Appropriate Physical Structure and Substrate

The choice of substrate used is also one of the most important tasks that must be taken into consideration. The basic technologies available for realizing microwave discriminators are microstrip, dielectric stripline and suspended stripline. Microstrip on hard substrates is the most commonly used medium but suffers from the high losses and dispersive second order effects compared with stripline. Suspended substrate stripline has the lowest loss but dimensions become excessive especially at lower frequencies.

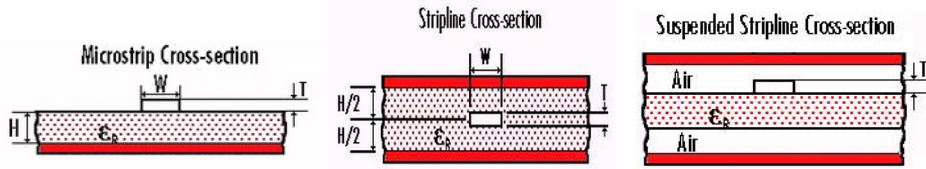


Figure 4.2 Cross-sections of common microwave circuit structures.

The substrate used in high frequency applications, i.e. $f \geq 2\text{GHz}$, should be selected carefully. The attenuation of substrate plays one of the main roles in these applications. The width of the substrate and tangent loss are the other factors that affect the performance of the substrate. Most of the system components in the frequency discriminator design are realized as microstrip circuits on alumina substrate with permittivity $\epsilon_r = 9.8$ and dielectric height 15 mil. Alumina is preferred to reduce the circuit sizes as much as possible. But in medium tier structures the phase shifting networks can be realized on suspended stripline due to low dielectric tolerance and loss. In medium tier simulations Rogers Duroid 5880 is used as substrate.

4.4 Amplifier

In simulations, TriQuint TGA2513 is used as amplifier model. It provides a nominal 16 dBm of output power at 1 dB gain compression with a small signal gain of 17 dB in 2-20 GHz frequency bandwidth.

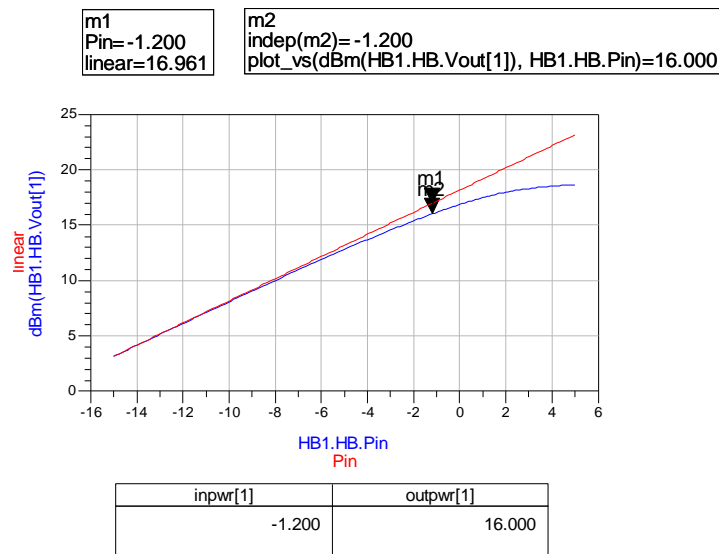


Figure 4.3 1 dB compression point of the amplifier.

4.5 2-18 GHz Power Divider

As can be seen in Figure 4.1, power dividers are the most widely used component in the system. When the cascaded form is considered, the specifications (i.e. matching, isolation and ripple in insertion loss over frequency band) of each power divider become critical in order to keep the consistency between each tier output. To fulfill this need 5 section Wilkinson power divider is designed (Figure 4.4).

Here, it is also important to decide the locations of each amplifier. Actually, unlike the design given in Figure 4.1, less number of amplifiers can be used by placing them “before” each divider. But in this design, to increase the total isolation and matching between each arm, the amplifiers are located after power divider in order to compensate their low output power. This decision is especially important in fine tier when high S11 of each filter in undetermined frequencies (i.e. above 6 GHz for LPF and below 6 GHz for HPF) is considered.

Below, the s-parameters of the related divider are given. Alumina is used as substrate in simulations. The approximate line lengths/widths of sections are 100/3.75 mil, 97/4.85 mil, 123/6.4 mil, 119/8.43 mil and 107.5/10.5 mil respectively. The values of resistive elements (green rectangles in Figure 4.4) are 125 ohm, 288 ohm, 346 ohm, 290 ohm and 364 ohm from left to right. The length and width of the line at port 1 are 115.4 mil and 17.47 mil. The lines at port 2 and port 3 are same in length/width and they are 109.2/12.6 mil.

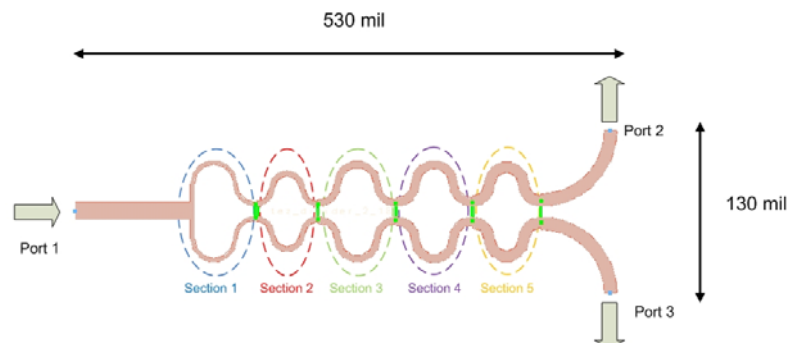


Figure 4.4 5 section Wilkinson power divider layout.

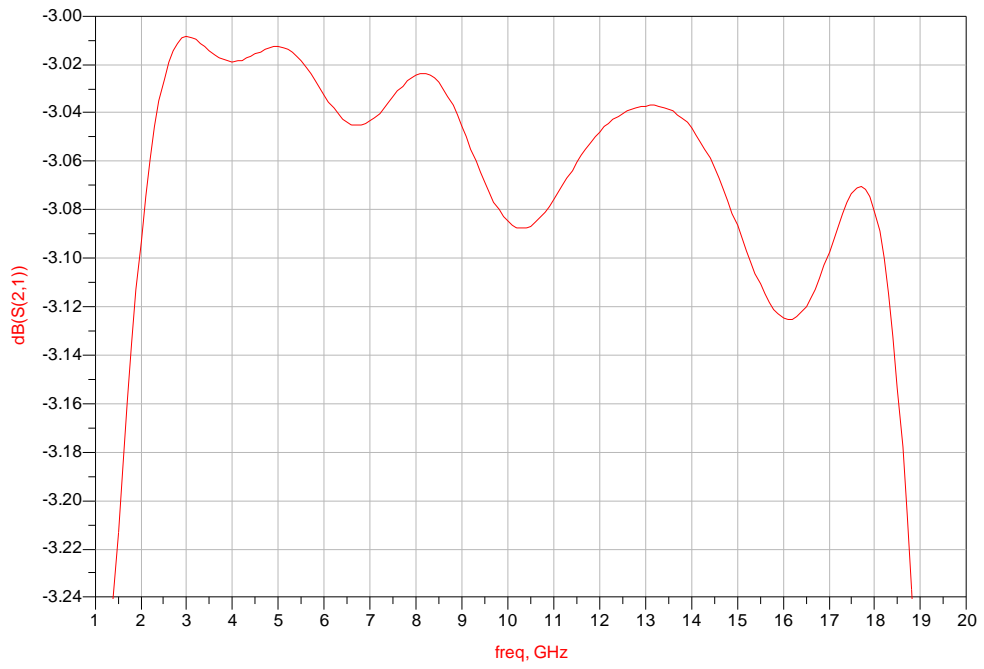


Figure 4.5 Power divider S_{21} , momentum simulation result.

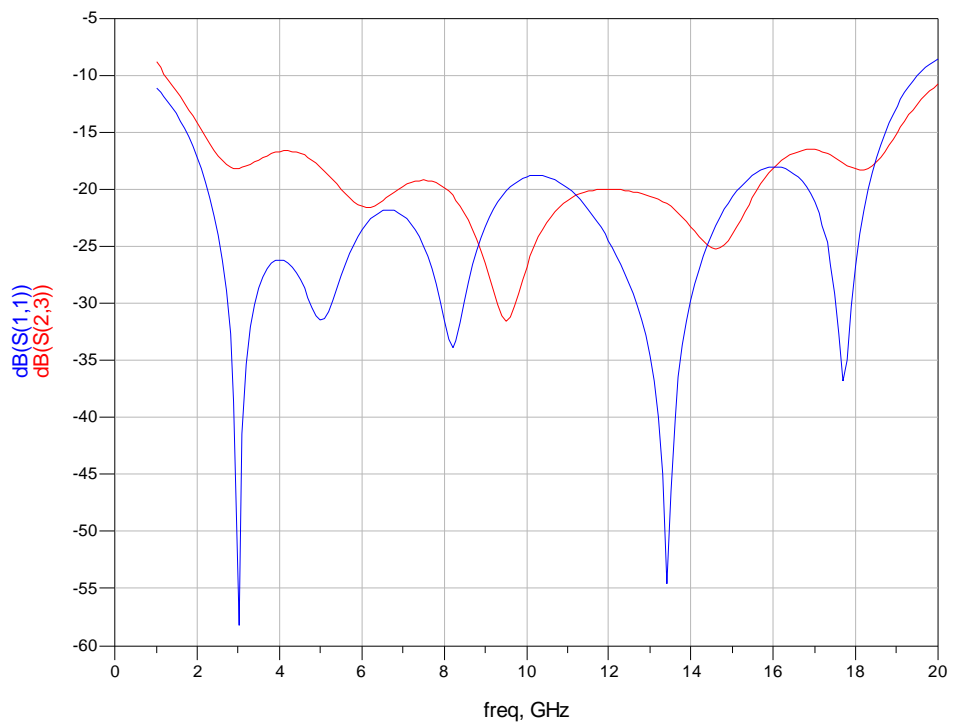


Figure 4.6 Power divider S_{11} and S_{23} , momentum simulation result.

4.6 Schottky Diode

In all the detector structures of each discriminator design in the system, Schottky diodes are used because of the advantages listed below.

- Quick response, it is especially important at high frequencies
- Low noise
- Lower forward voltage drop

In ADS Designs, Aeroflex MSS39,148-B10B is used as diode model. This diode is also used in the realized circuits. Figure 4.7 shows the equivalent of the diode. Here, Diode DF models the forward bias curve, capacitance and transit time. Diode DR models the reverse bias curve. Diode DI isolates diode DR from the circuit when the equivalent model is forward biased.

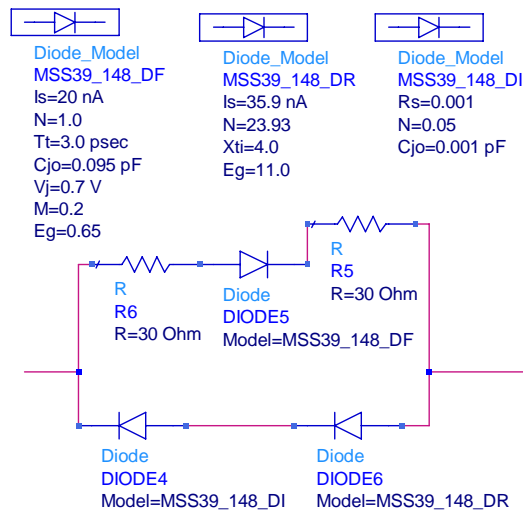


Figure 4.7 Diode equivalent model in ADS.

Schottky diodes need to be matched and in the circuit they are biased to get maximum sensitivity. Figure 4.8 shows the Schottky diode and a 150 ohm parallel resistor. Diode impedance with respect to frequency is given in Figure 4.9. The impedance of diode decreases with frequency because of its capacitance. Figure 4.10 shows the general circuit of a phase shifting tier. R25, R26 and R27 represent the

phase shifting arms. The boxes are the subcircuits which represents the Schottky diodes and parallel resistors (Figure 4.8). Also the three arms are isolated from each other by using resistors in series. These resistors are also used to improve matching (Figure 4.11).

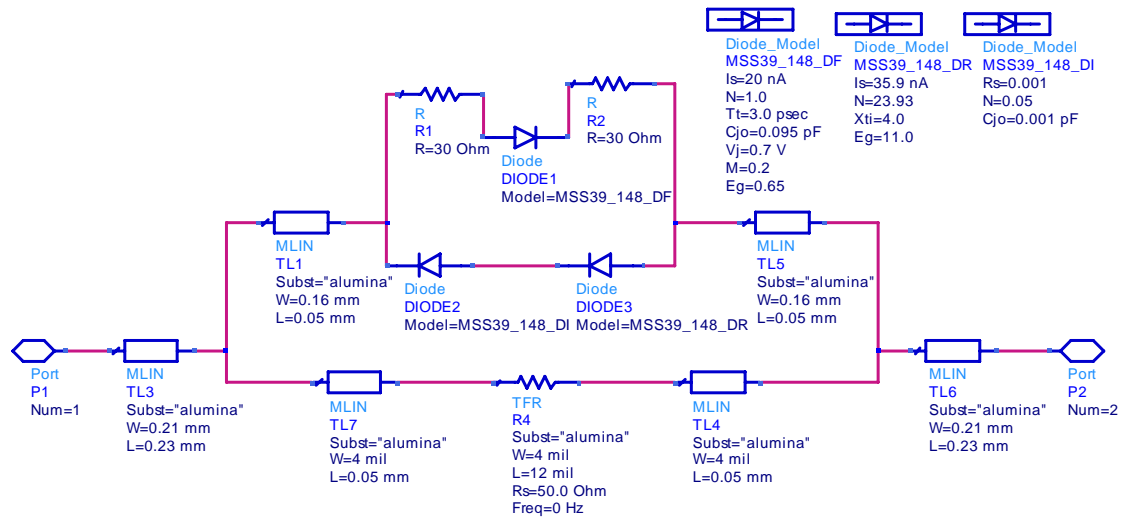


Figure 4.8 Diode model with 150 ohm printed resistor.

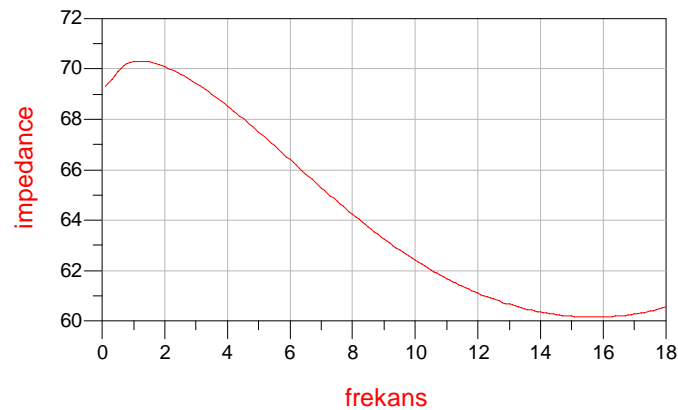


Figure 4.9 Diode impedance vs. frequency.

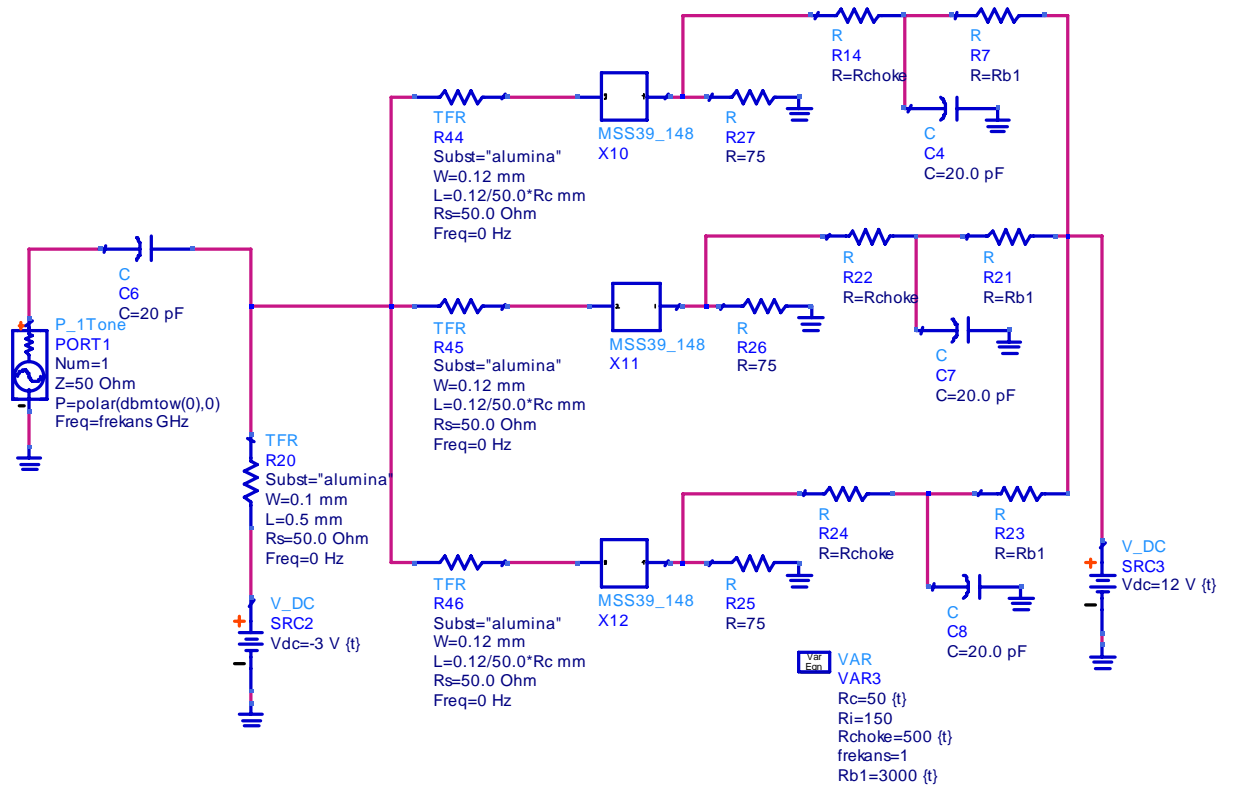


Figure 4.10 Simulated circuit at harmonic balance.

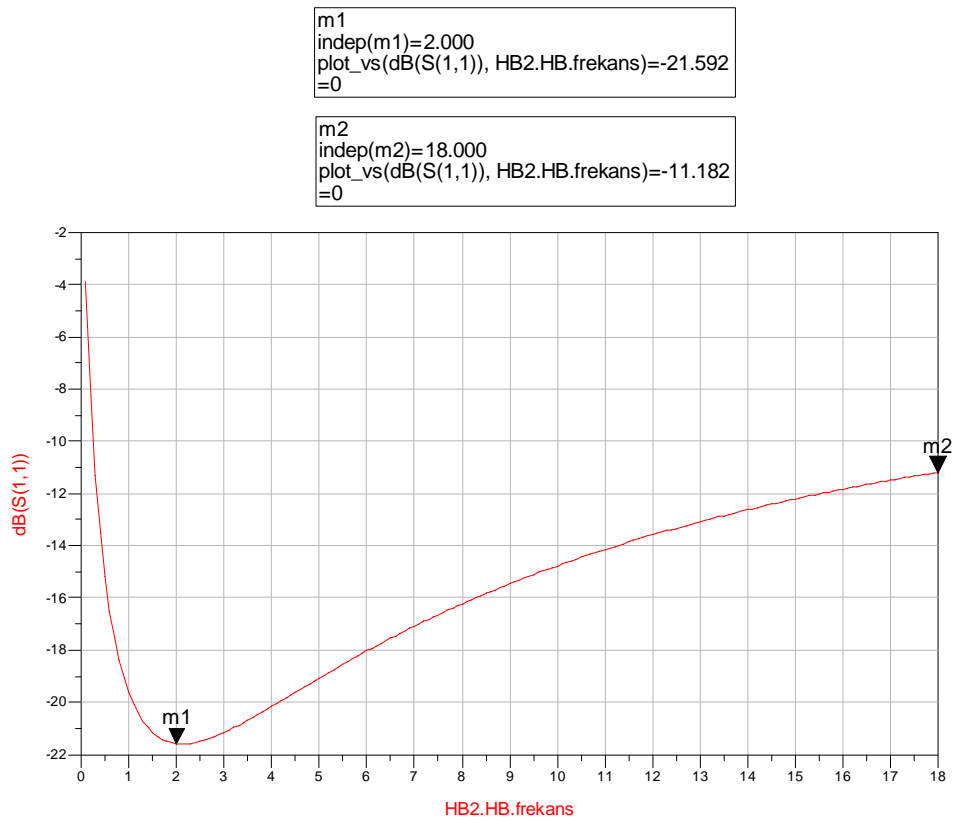


Figure 4.11 Circuit matching.

4.7 Tier Designs

Finding the frequency region of input signal relies on the magnitude comparison between the detector voltages. Every tier starting from the coarse one, provides a reference point (i.e. a specific magnitude sorting) for the following tiers in order to estimate the input signal frequency. The details are given in below sub-sections.

4.7.1 Coarse Tier

In this section, coarse tier of the frequency discriminator and its components are presented. As the name implies, this tier is used to designate the input frequency in a “coarse” region. So the goal while designing the coarse tier is to cover 2-18GHz frequency band with the widest unambiguous bandwidth as possible. This tier is also fabricated. Due to the “coarse” purpose of this tier, the extra losses arising from the use of microstrip instead of a suspended substrate is accepted in order to reduce the circuit size as possible. So the structure is manufactured on alumina substrate. Actually, this is a trade off that the designer must deal with. A suspended substrate structure may be used to reduce the losses, but this time the circuit will be much bigger.

Theoretically, the unambiguous bandwidth in the determined frequency band must be 16 GHz like the one given in Figure 4.12. So when the magnitude comparison approach between the detector outputs is considered, only six different (i.e. $P(3,3) = 3! = 3 \cdot 2 \cdot 1 = 6$) “unique” voltage sorting sets must be present in 2 – 18 GHz frequency range. For the example given in Figure 4.12, mentioned voltage sorting sets are:

1. Blue > Red > Green
2. Red > Blue > Green
3. Red > Green > Blue
4. Green > Red > Blue
5. Green > Blue > Red
6. Blue > Green > Red

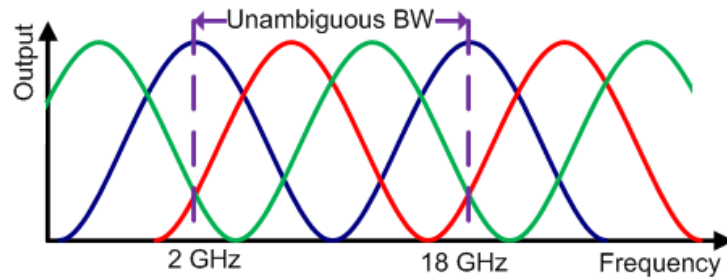


Figure 4.12 Theoretical output of the coarse tier.

Here, it is important to notice that, for the defined frequency band there is only one cycle for each voltage outputs.

In the design efforts it is seen that obtaining a 16 GHz UBW (i.e. 6 unique voltage sorting) is impossible other than that actual detector outputs are like the one given in Figure 4.13 which may lead an ambiguity. As mentioned above, determining the input frequency depends on the result obtained from the previous tiers. But this situation is valid for medium and fine tiers, not for coarse tier. So especially in coarse tier, a problem of this kind most probably can not be resolved. As can be seen from the example output below, the ambiguous regions are at the edges of the frequency band. According to this fact, a 10 GHz diplexer is used in the coarse tier structure in order to know whether or not the frequency of input signal is below/over 10 GHz.

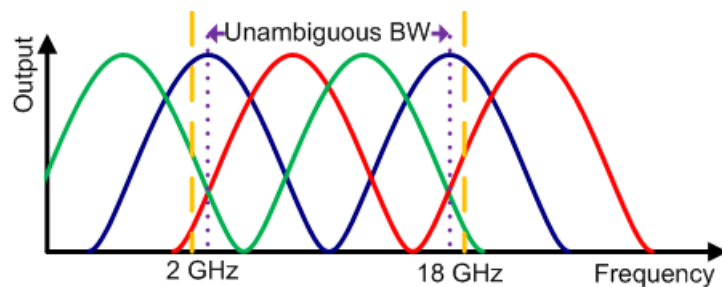


Figure 4.13 Example of actual output of coarse tier.

The general block diagram of coarse tier is shown in Figure 4.14. It operates as follows:

1. Power Divider divides input signal into two halves.
2. One half goes into the 10 GHz diplexer

- a. Diplexer splits the incoming wave in the related frequency point.
 - b. According to input frequency V4 or V5 becomes higher than the other one.
3. The other half goes into 3 branch reflection mode phase shifters.
 - a. Phases between consecutive branches become 120 degree apart.
 - b. Output DC voltages are read from related detectors
4. According to the amplitude relationship between the voltages V1, V2 and V3 and by the help of the diplexer output, a frequency band which includes the input signal frequency is found.

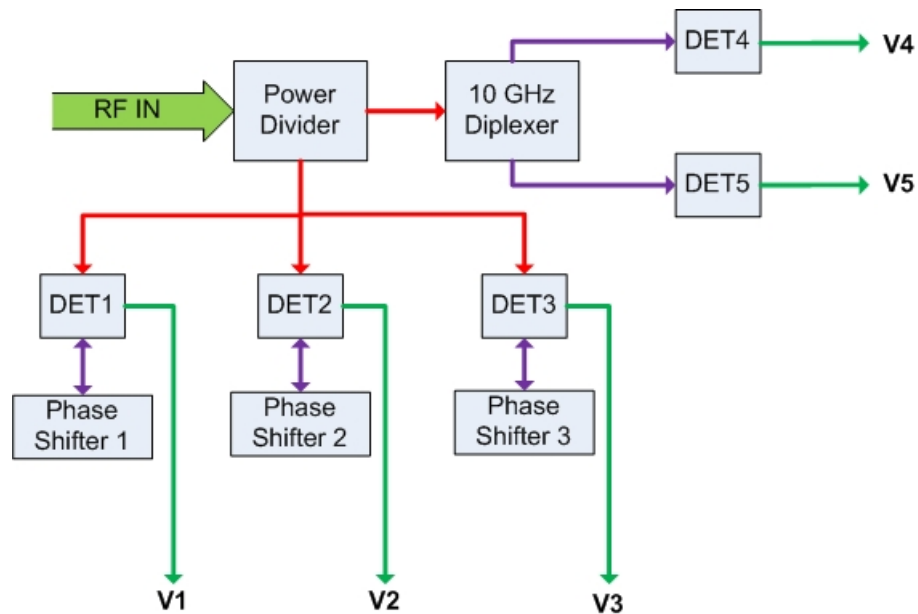


Figure 4.14 General block diagram of coarse tier.

4.7.1.1 Power Divider

In order to use the input signal both in diplexer and phase shifting branches a power divider is needed (Figure 4.14). For this purpose a 4 section Wilkinson power divider is designed (Figure 4.15).

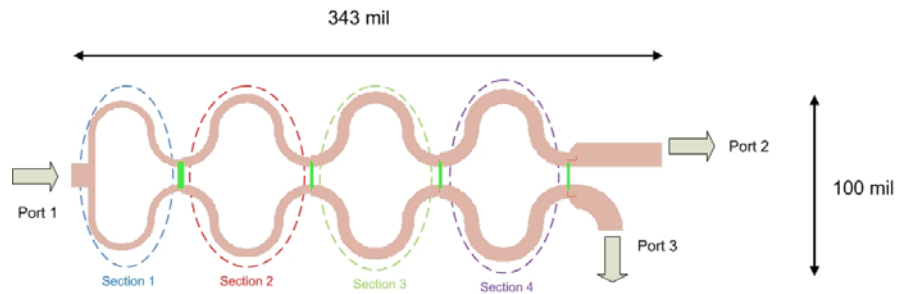


Figure 4.15 4 section Wilkinson power divider layout.

The approximate line lengths/widths of sections are 90.8/4.2 mil, 118.5/5.45 mil, 117.6/7 mil and 116.7/8.72 mil respectively. The values of resistive elements are 382 ohm, 326 ohm, 230 ohm and 147 ohm from left to right. The length and width of the line at port 1 are both 10 mil. The lines at port 2 and port 3 are same in length/width and they are 40/10 mil. The s-parameters of this divider are given below figures.

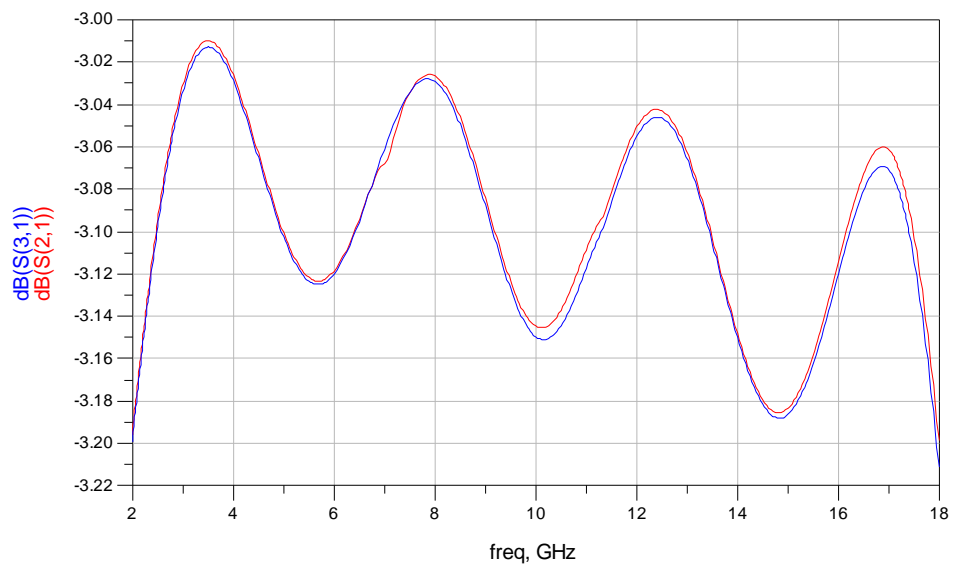


Figure 4.16 Power divider S21, momentum simulation result.

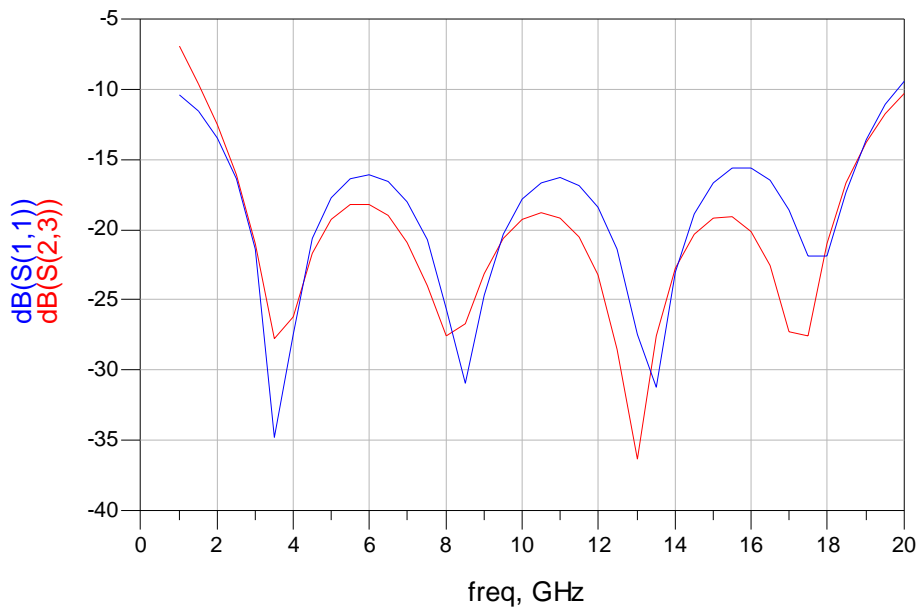


Figure 4.17 Power divider return loss and isolation, momentum simulation result.

4.7.1.2 Diplexer

In diplexer design, a Low-Pass (up to 10 GHz) and a High-Pass (from 10 GHz) filter are used. Here, the main goal is to get sufficient isolation and matching with a minimum number of elements in filter structures (i.e. high pass and low pass).

In high pass section of the diplexer, the designed filter is elliptic. Elliptic filters achieve the smallest order for the same specifications, or, the narrowest transition width for the same filter order, as compared to other filter types. On the negative side, they have the most nonlinear phase response over their pass-band which is not important when the main purpose of using this diplexer in the coarse tier is considered. The theory of work is described below. Figure 4.18 illustrates two commonly used network structures for elliptic function low-pass prototype filters. In Figure 4.18.a, the series branches of parallel-resonant circuits are used for realizing the finite-frequency transmission zeros, since they block transmission by having infinite series impedance (open-circuit) at resonance. For the dual realization form in Figure 4.18.b, the shunt branches of series-resonant circuits are used for implementing the finite-frequency transmission zeros, since they short out

transmission at resonance. Either form may be used, because both give the same response [28].

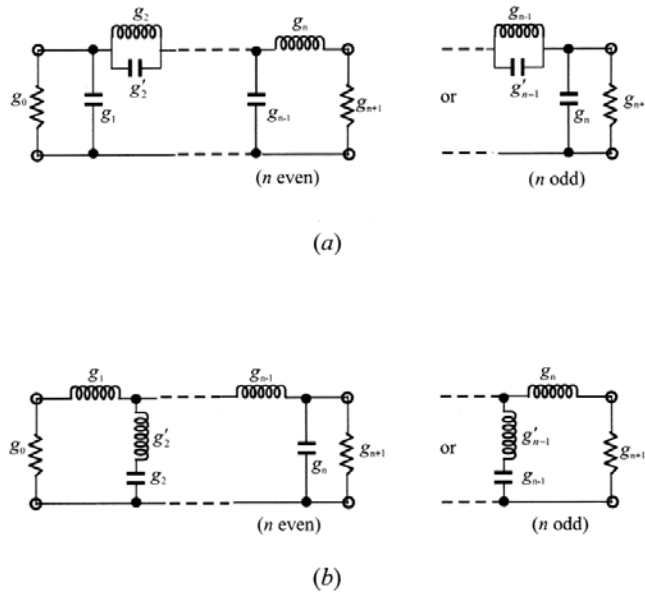


Figure 4.18 Low-pass prototype filters for elliptic function filters with (a) series parallel-resonant branches, (b) its dual with shunt series-resonant branches.

According to the low-pass to high-pass circuit component transformation, inductive and capacitive elements in the circuit transforms into capacitive and inductive elements as shown in Figure 4.19.

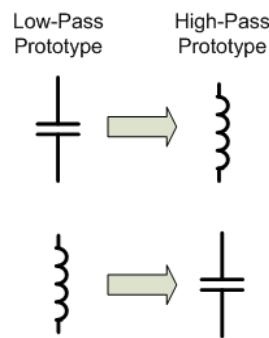


Figure 4.19 Low-pass to high-pass prototype conversion.

Trials showed a third order elliptic filter is enough to get the required specifications and the basic structure of the filter is shown below.

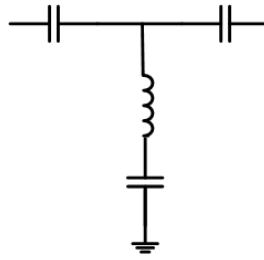


Figure 4.20 10 GHz diplexer, high-pass section.

By the help of related Kuroda Identities, the circuit can be physically realized as described below.

Unit elements are added between the source and the filter, also between the load and the filter. These unit elements only changes the phase, they do not affect the amplitude. This is necessary to manufacture the filter. The new circuit is in Figure 4.21.

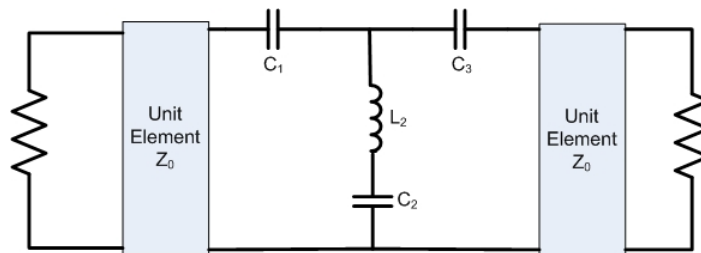


Figure 4.21 10 GHz diplexer, high-pass section with unit elements.

The encircled capacitances in Figure 4.22 (C_1 and C_3) are split into two pieces as shown in Figure 4.23.

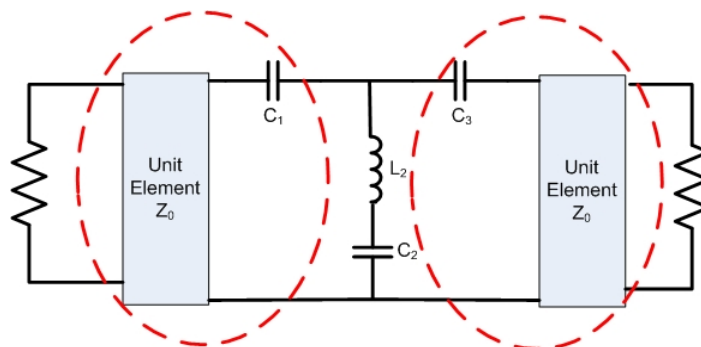


Figure 4.22 10 GHz diplexer, high-pass section, capacitances will be split.

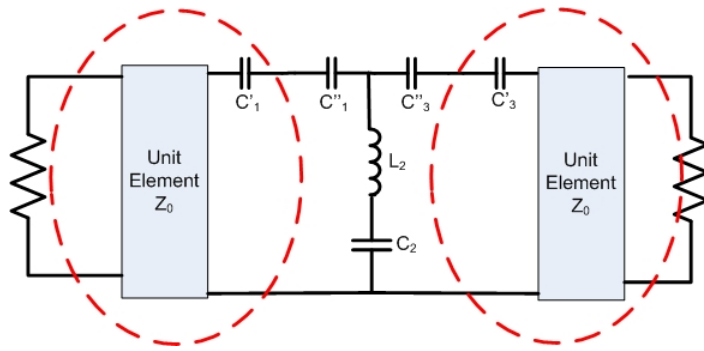


Figure 4.23 10 GHz diplexer, high-pass section, capacitances are decomposed.

Then according to the Kuroda Identity given Figure 4.24, the encircled area is transformed [1].

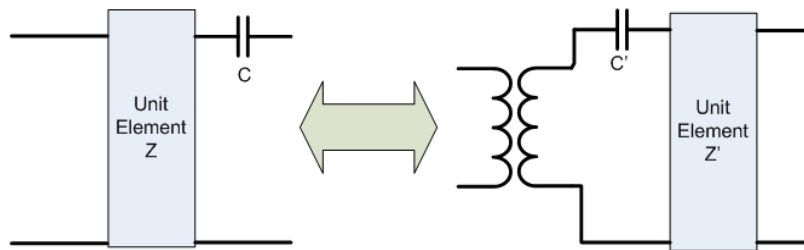


Figure 4.24 Changing capacitance position according to the related Kuroda identity.

The encircled area in Figure 4.25 can be transformed into its coupler form equivalent as given in Figure 4.26 [1].

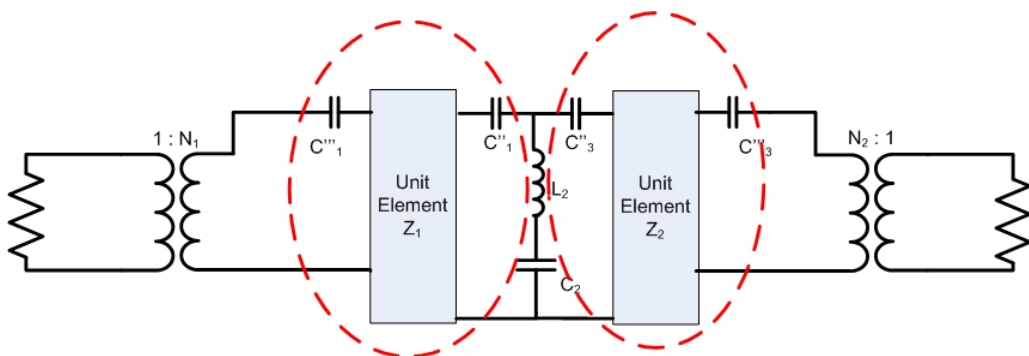


Figure 4.25 The circuit after transformation.

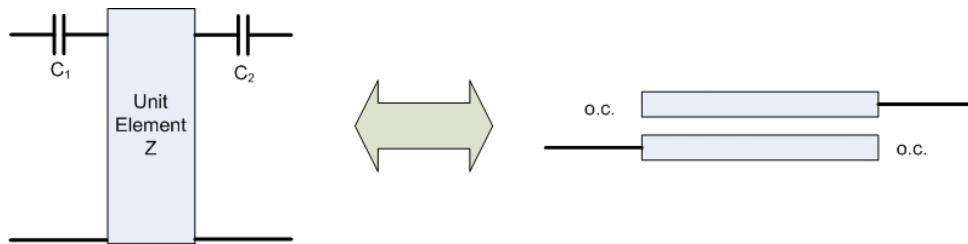


Figure 4.26 Kuroda transformation.

So the final circuit will be the one in Figure 4.27. In this figure, the line spacing, width and length values are also given.

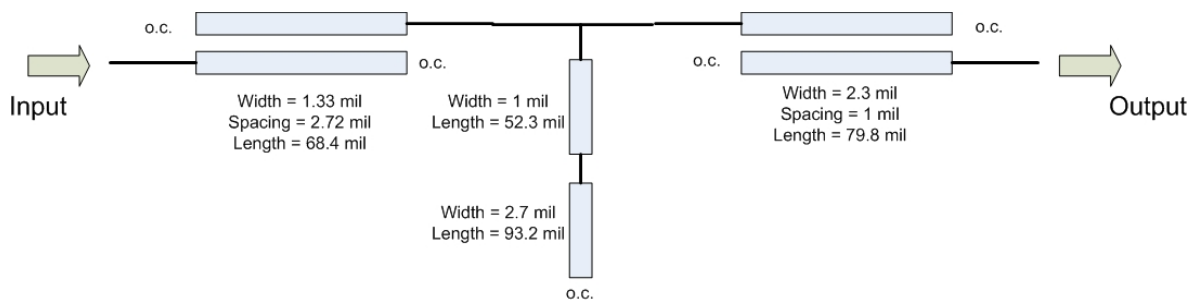


Figure 4.27 10 GHz diplexer, high-pass section.

The layout of the high-pass section is given in Figure 4.28. Here, 2 mil long extra lines are used at the connection points (purple encircled areas) in order to benefit the fringing at the open ends of the coupled lines. By this way, the coupling is increased a little without narrowing the spacing between the lines. On the other hand, the shunt resonator is bended in order fit in a smaller region (green encircled area).

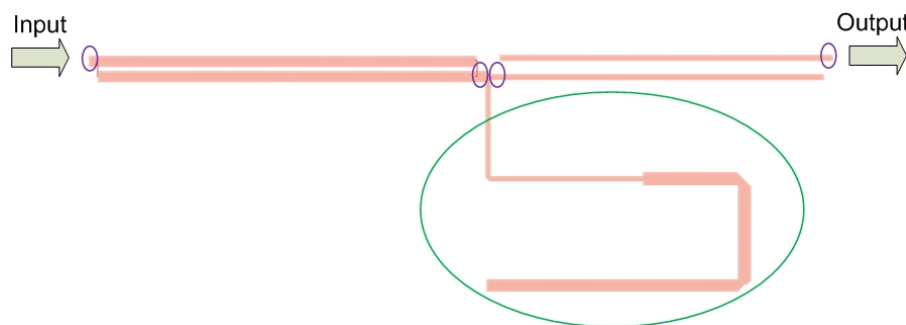


Figure 4.28 High-pass section layout.

In the low pass section of the diplexer, a typical 6th degree Low-Pass Filter is used in low pass section of the diplexer. In Figure 4.29, the width and length values of the lines are also given.

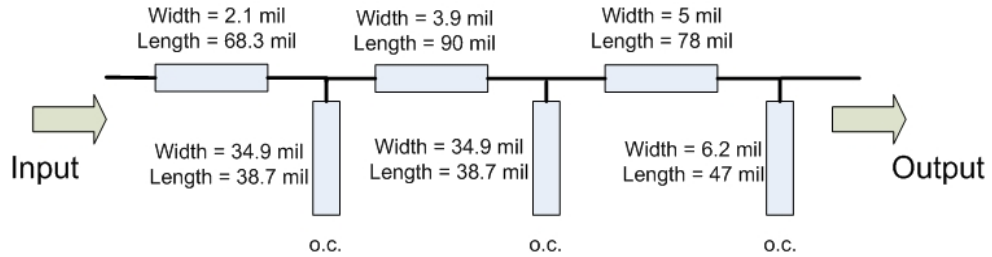


Figure 4.29 10 GHz diplexer, low-pass section.

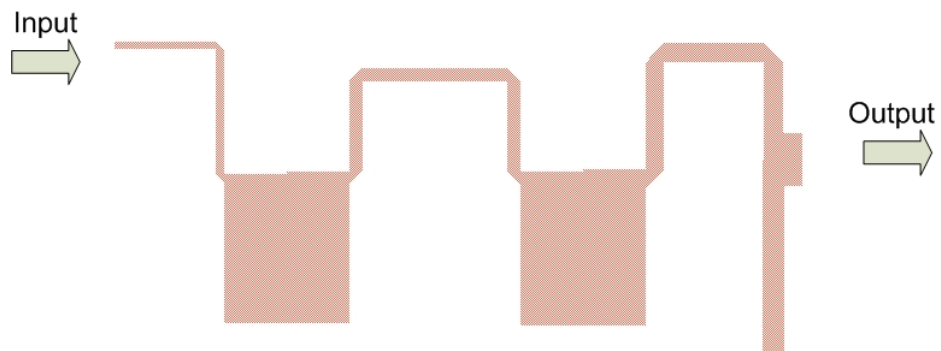


Figure 4.30 Low-pass section layout.

When the HP and LP section described above are joined together the required 10 GHz diplexer is obtained. The final circuit and related outputs are given below.

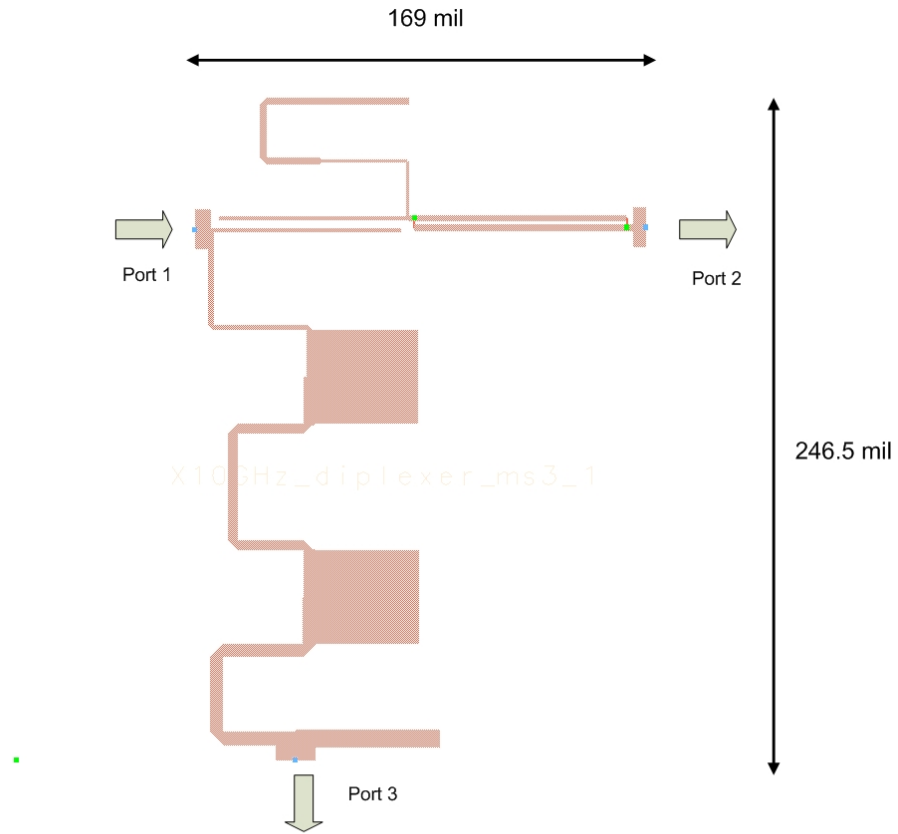


Figure 4.31 Diplexer layout.

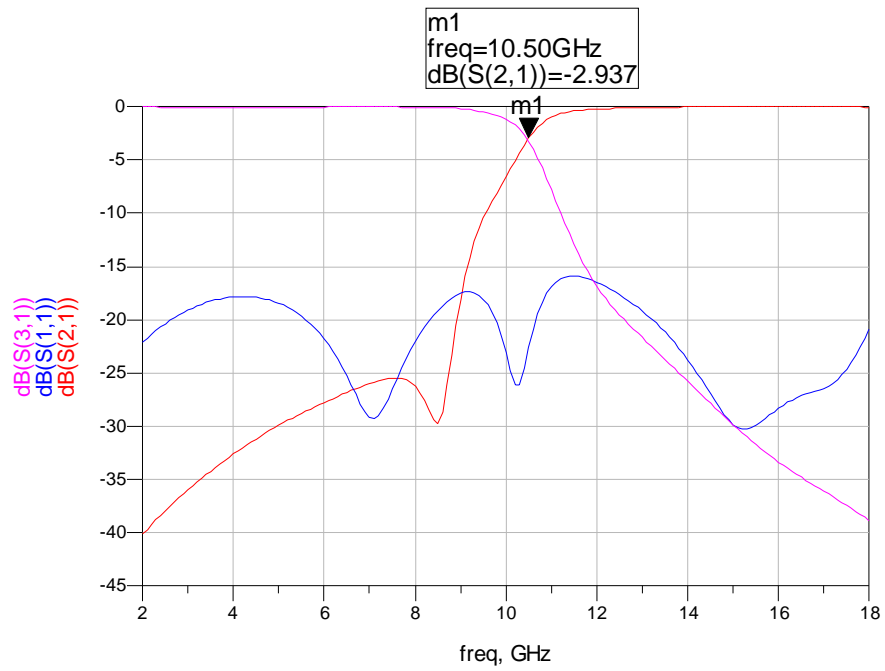


Figure 4.32 Diplexer s-parameters, momentum simulation.

4.7.1.3 Phase Shifter Network

As the number of stepped-impedance section increases better differential phase response can be obtained. Nevertheless, an increase in number of sections creates a decrease in unambiguous bandwidth (section 2.3). The purpose in coarse tier is to get the maximum possible unambiguous bandwidth. Therefore in this tier, 1 section reference line and 2 section phase shifting branches are used. The structure with ideal transmission lines is given in Figure 4.33. When realization process considered, it is difficult to fabricate a transmission line narrower than 1 mil. This situation creates a limit to the transmission line impedances. When alumina is used as a substrate a 1 mil wide transmission line nearly corresponds to 114 ohm. So, in simulations this value is taken as an upper limit for impedance of the sections. Actually, the mentioned limit only affects the last transmission line (i.e. TL4) in the phase shifter branch 1.

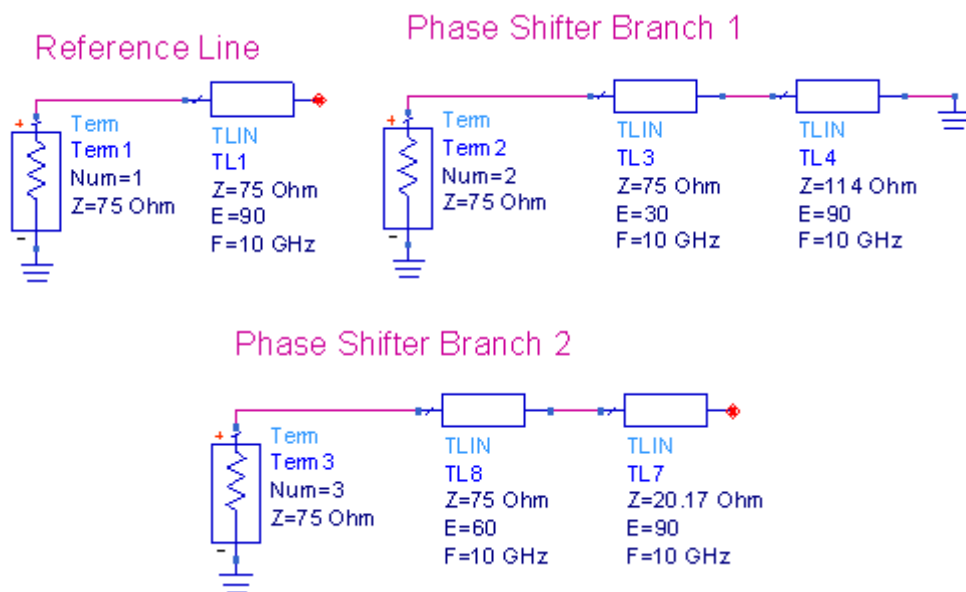


Figure 4.33 Coarse tier with ideal transmission lines.

In Figure 4.34 and Figure 4.35, the differential phase responses for ideal case are given. As can be seen, it is impossible to obtain ± 120 degree phase shift in defined

frequency band. But when the needed unambiguous bandwidth is considered there is no better choice. That is why an extra component, the 10 GHz diplexer, must be used to prevent a possible ambiguity based on the narrow band differential phase shift.

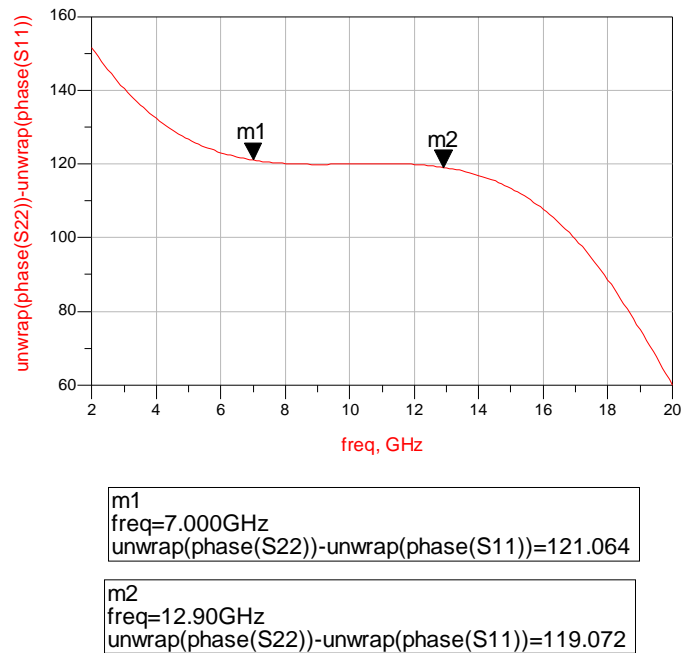


Figure 4.34 Phase difference between phase shifter branch 1 and reference line (with ideal transmission lines).

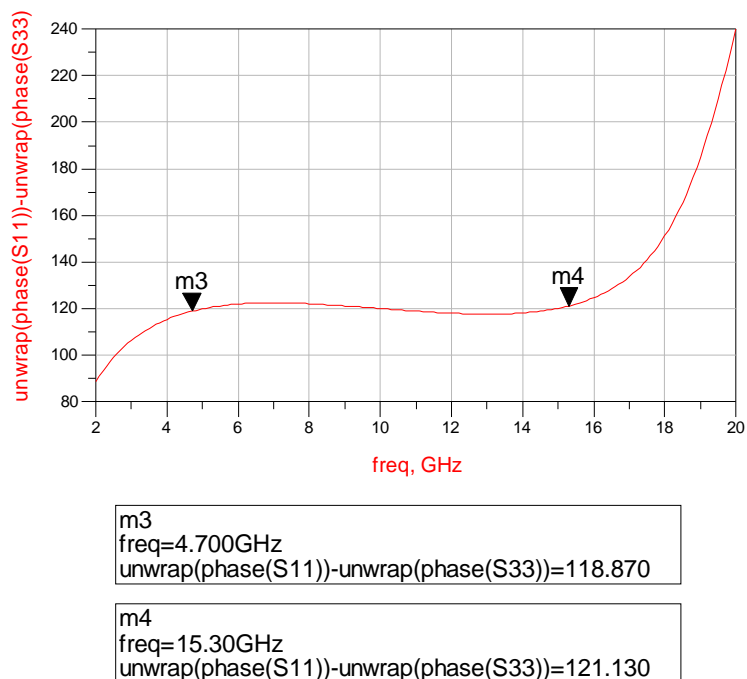


Figure 4.35 Phase difference between reference line and phase shifter branch 2 (with ideal transmission lines).

In Figure 4.36, lossy equivalent of the coarse tier presented above is given. The differential phase responses for this network are given in Figure 4.37 and Figure 4.50, as expected the responses are a little deformed when compared to the ideal case.

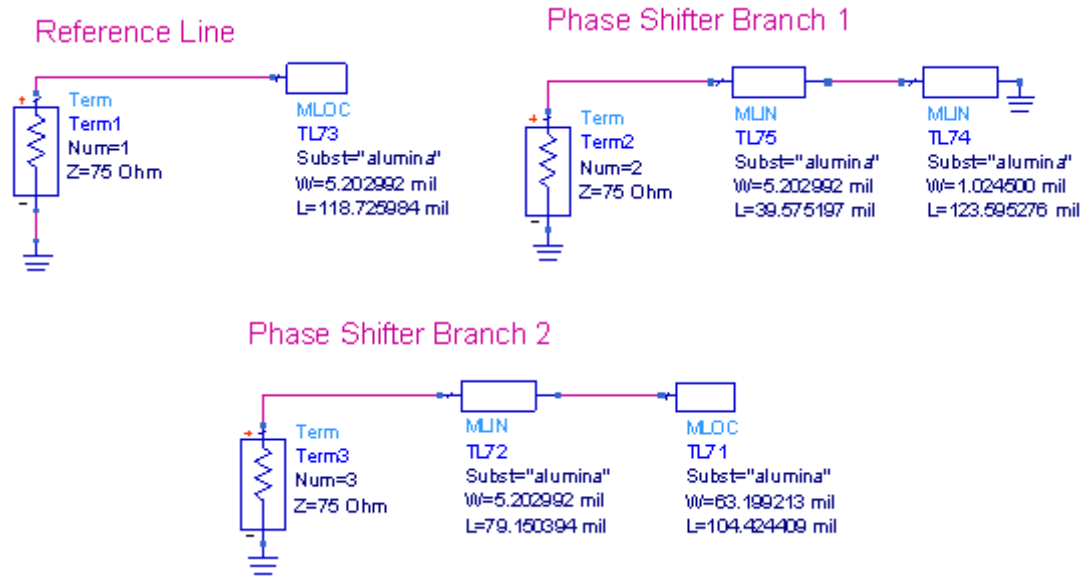


Figure 4.36 Coarse tier with lossy transmission lines.

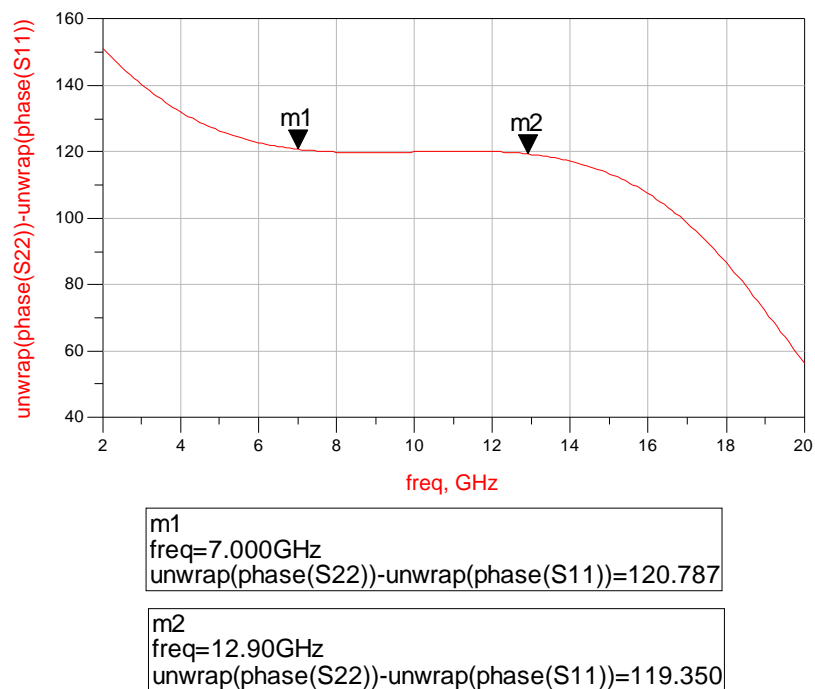
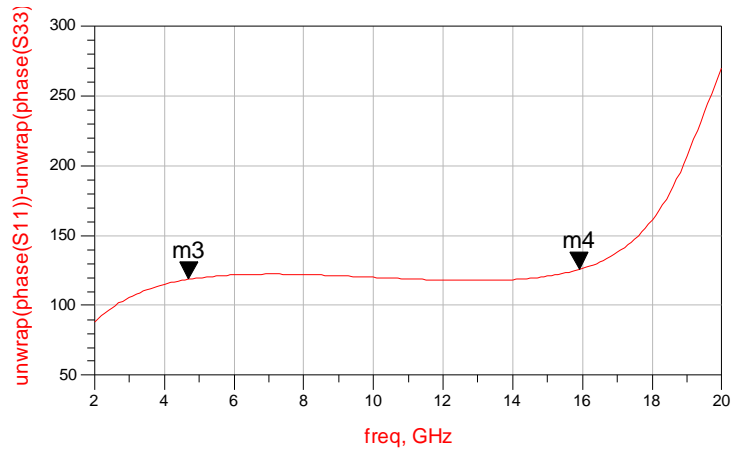


Figure 4.37 Phase difference between phase shifter branch 1 and reference line (with lossy transmission lines).



m3
freq=4.700GHz
unwrap(phase(S11))-unwrap(phase(S33))=118.513

m4
freq=15.90GHz
unwrap(phase(S11))-unwrap(phase(S33))=125.595

Figure 4.38 Phase difference between reference line and phase shifter branch 2 (with lossy transmission lines).

Before designing the lay-out of phase shifting branches, the line with the minimum width is expanded to 1.5 mil instead of 1 mil. The decision of this change is made to stay away from the manufacturing limit. Simulations/optimizations are repeated. The new version of the network and new phase responses are shown in Figure 4.39, Figure 4.40 and Figure 4.41 respectively.

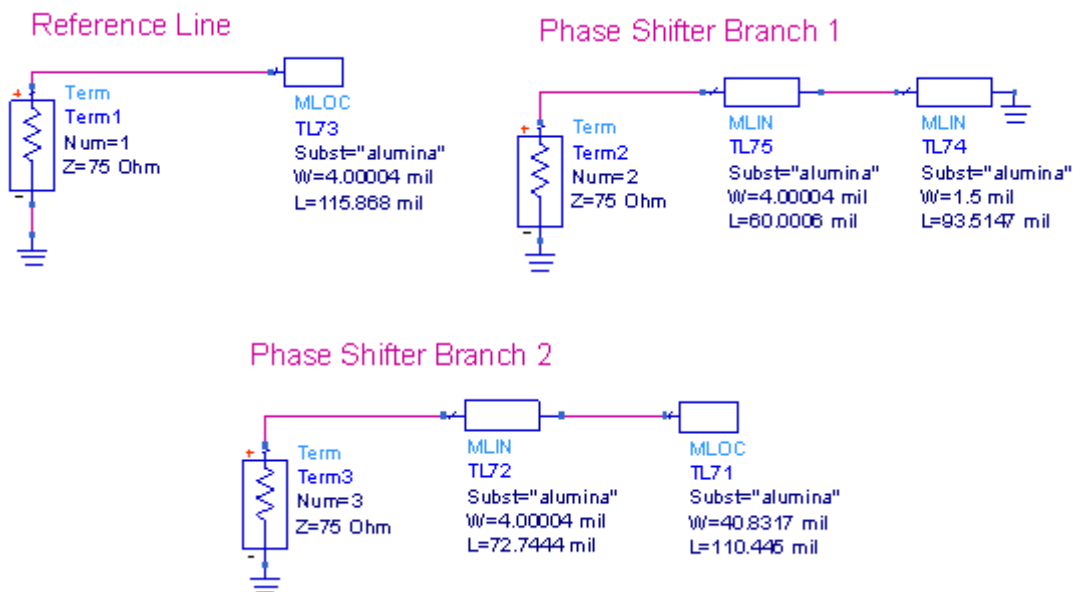


Figure 4.39 Coarse tier phase shifting branches.

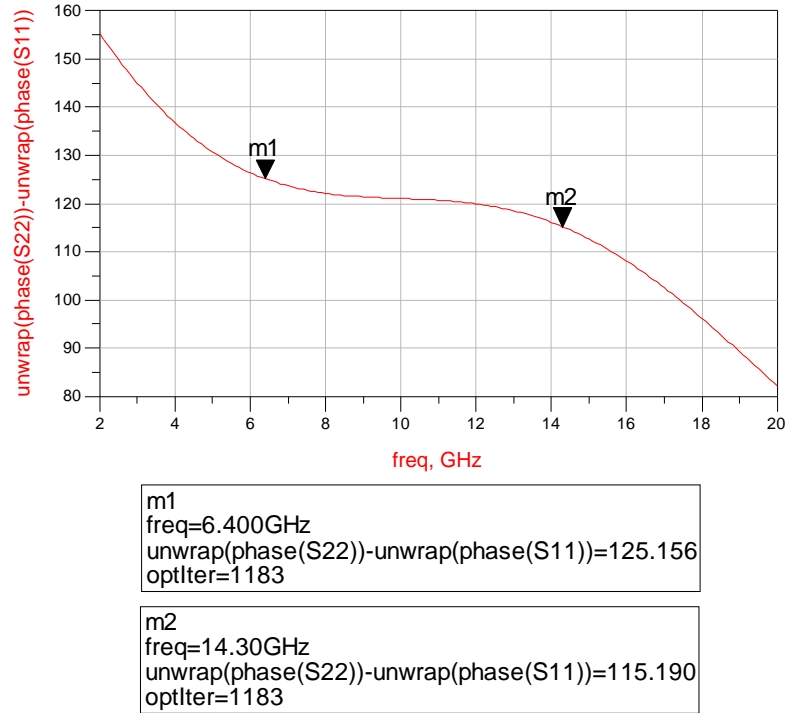


Figure 4.40 Phase difference between phase shifter branch 1 and reference line (new version).

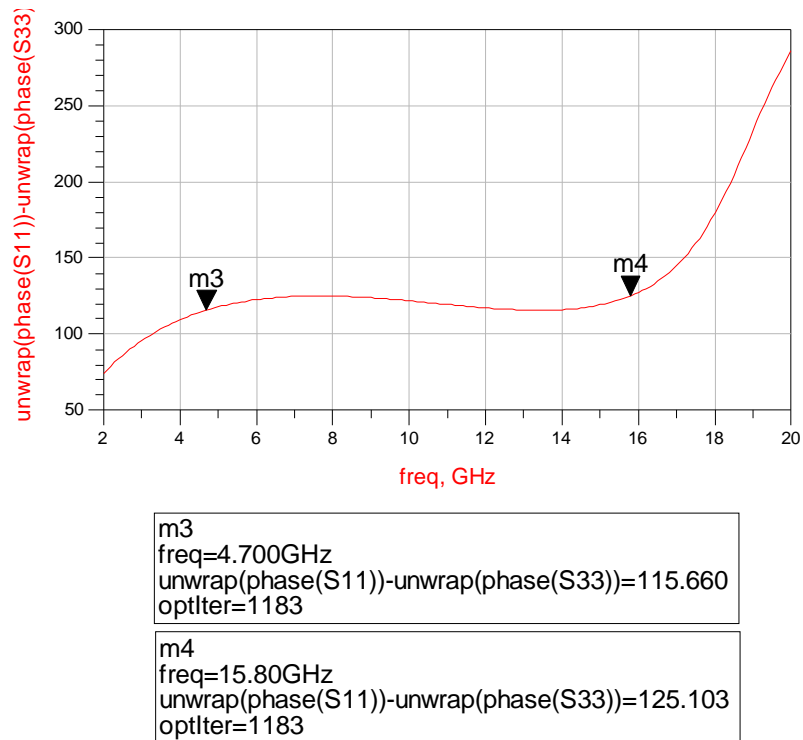


Figure 4.41 Phase difference between reference line and phase shifter branch 2 (new version).

In the new version of the phase shifting structure, this time a new problem is encountered: The discontinuity between the sections in phase shifter branch 2. As can be seen from Figure 4.39, the last section of phase shifter branch 2 is nearly 10 times wider than the previous section. This situation is not a problem in simulation world. But in real life it may cause unexpected losses or a different phase response even if a proper taper is used between these sections. So as a second design decision, the second section of this phase shifting branch is limited to 15 mil and according to this change the simulations are repeated.

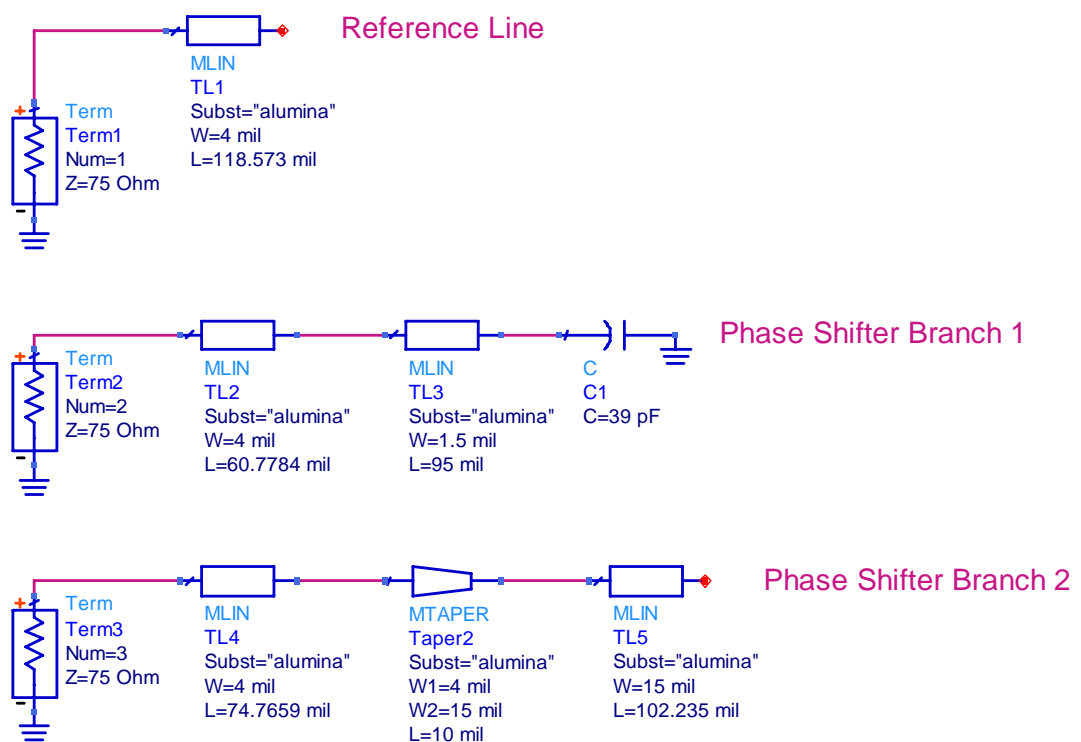


Figure 4.42 Re-optimized version phase shifter network.

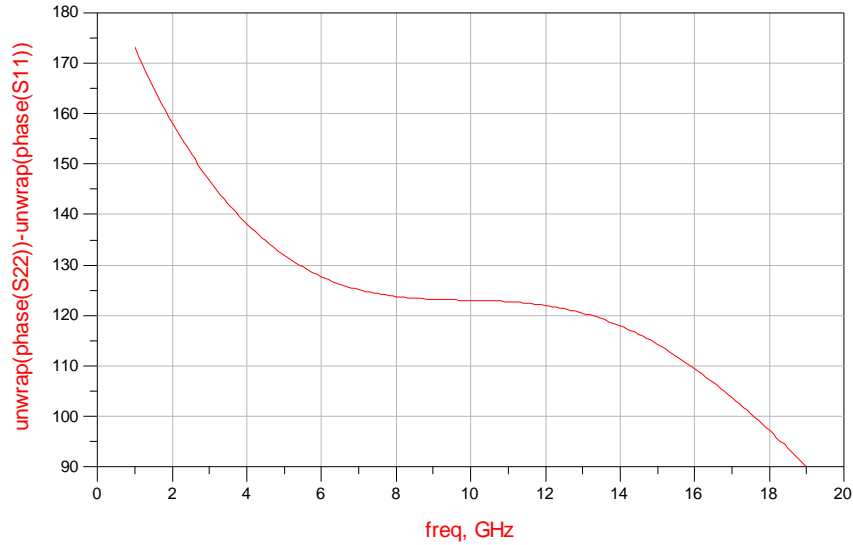


Figure 4.43 Phase difference between phase shifter branch 1 and reference line (re-optimized version).

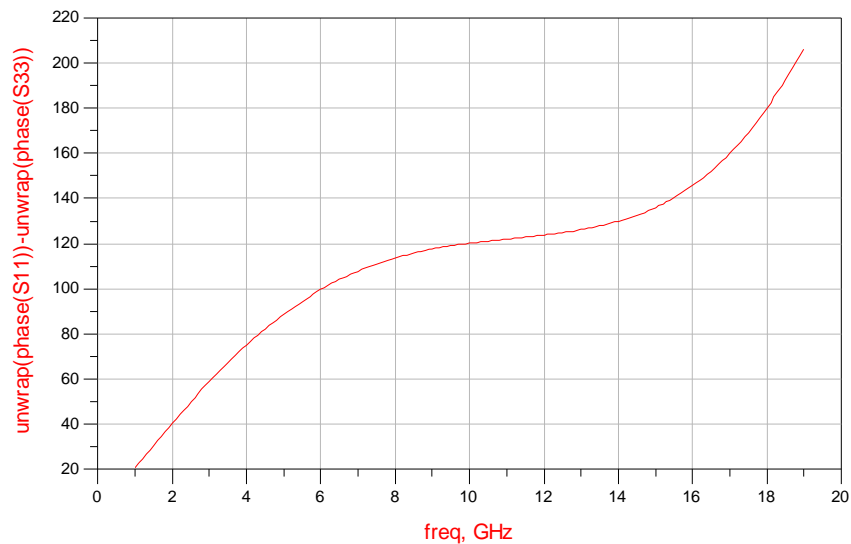


Figure 4.44 Phase difference between reference line and phase shifter branch 2 (re-optimized version).

As explained in at the beginning of this section, coarse tier has two main parts: 10 GHz diplexer and phase shifter. In Figure 4.45, schematic version of phase shifter part is given. Here, the momentum components of phase shifting branches and reference line are used. Orange spots shows the measurement points and green encircled voltages are used to bias the diodes. The sizes between these arms are consistent with each other. Input power is assumed to be 7dBm.

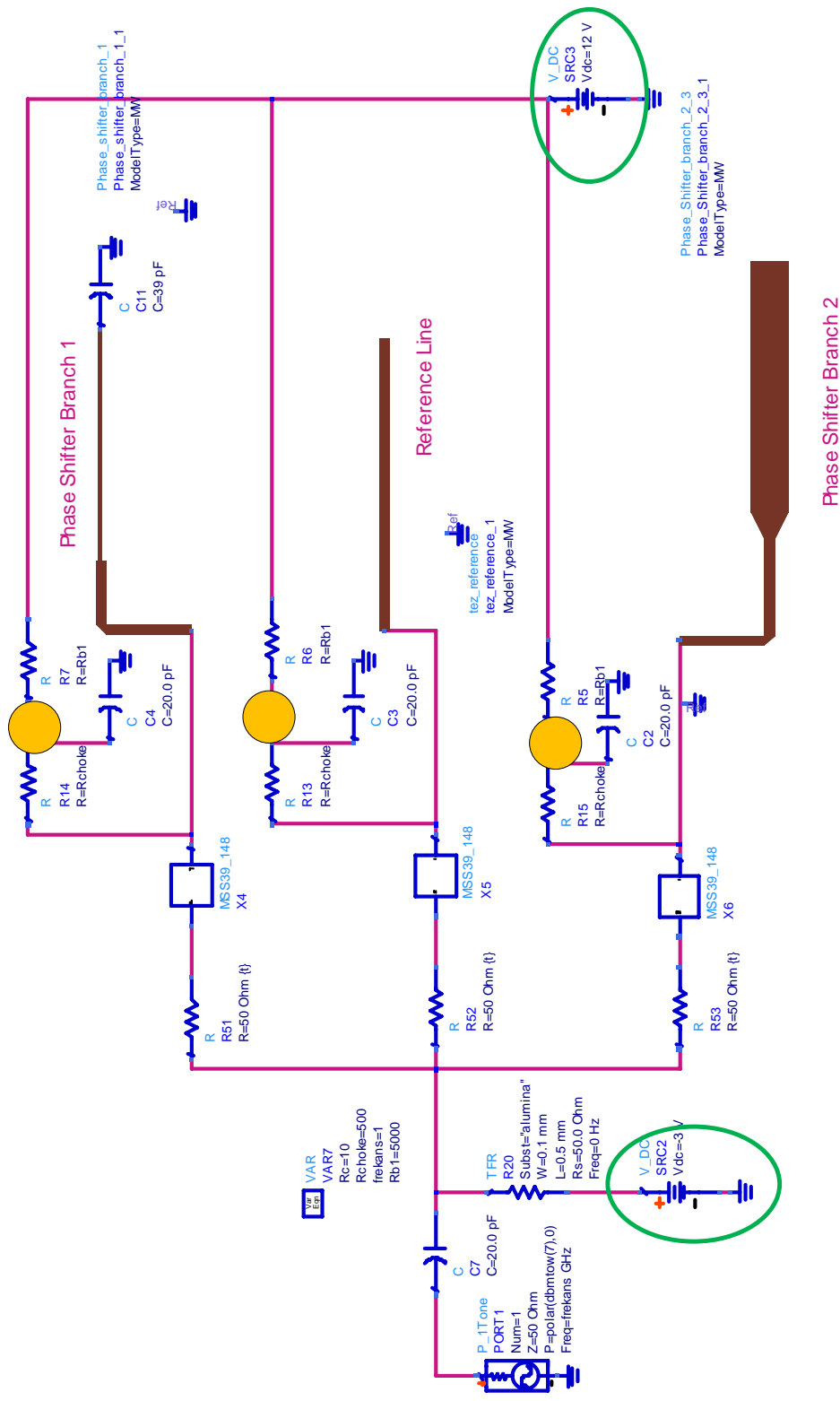


Figure 4.45 Phase shifter part of coarse tier.

In Figure 4.46, detector outputs are shown. As can be seen in this figure, 6 from 8 voltage sorting is different. This explains, again, why a diplexer is used in the coarse tier structure. Mentioned voltage sorting is:

1. Blue > Pink > Red
2. Blue > Red > Pink
3. Red > Blue > Pink
4. Red > Pink > Blue
5. Pink > Red > Blue
6. Pink > Blue > Red
7. Blue > Pink > Red (same with the first one)
8. Blue > Red > Pink (same with the second one)

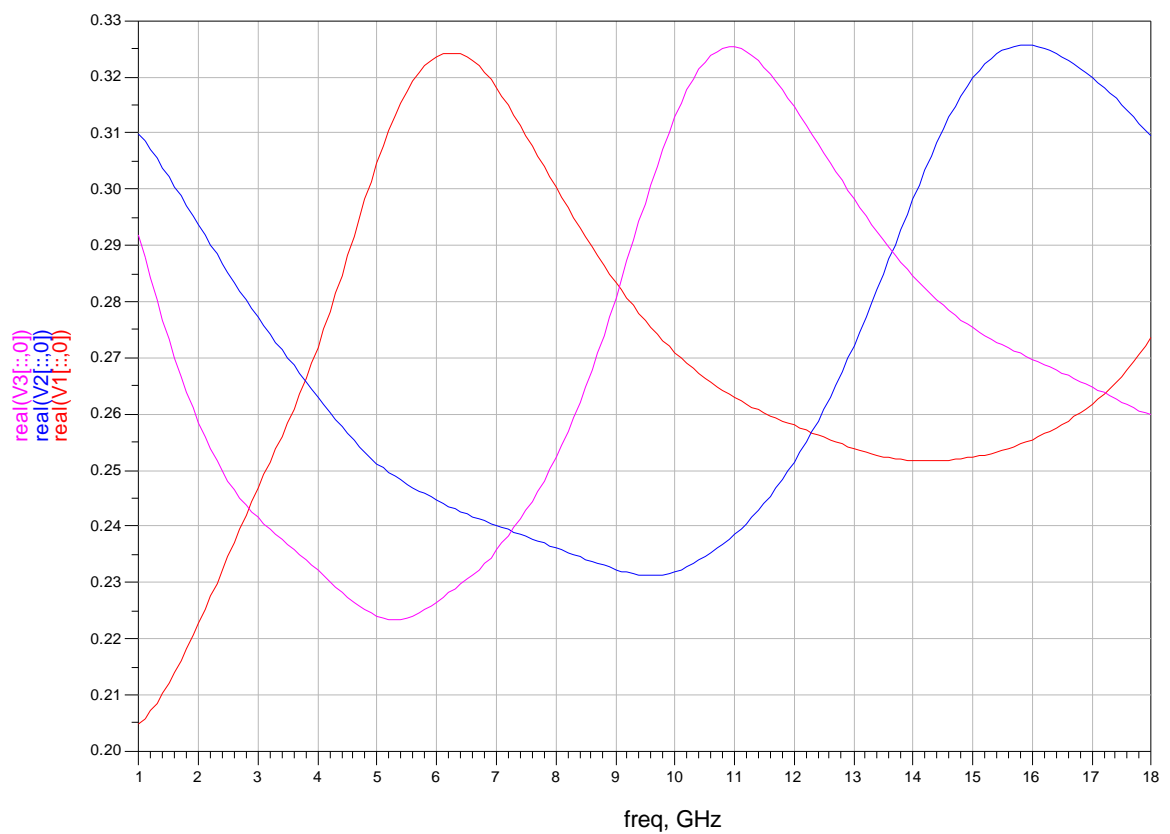


Figure 4.46 Detector outputs.

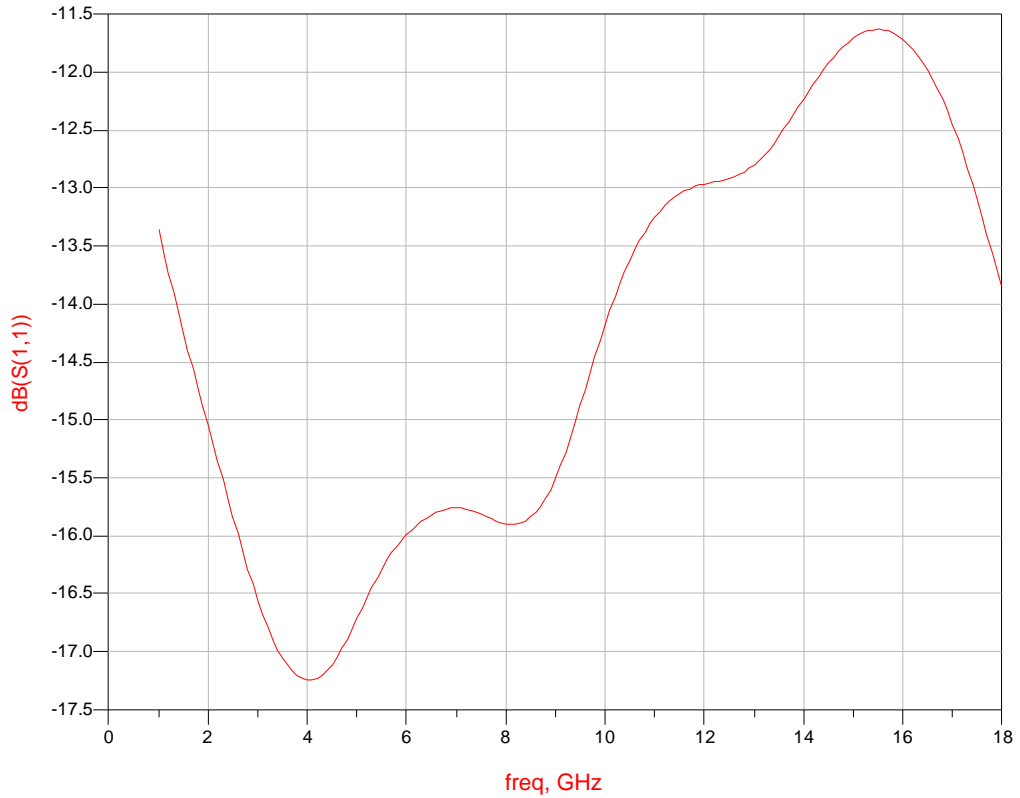


Figure 4.47 S11 of phase shifter part of coarse tier.

4.7.1.4 Final Circuit

Final circuit is presented in Figure 4.48. Blue arrows indicate the bias points for the diodes and orange points are the measurement points. The sizes of momentum components are consistent with each other. The boxes represent the diodes. Additionally, instead of one for each, double bonding wires are used to connect the capacitors in order to reduce the inductance. The real coarse tier card sizes are approximately 480 mil x 718 mil. The simulation results are presented below. Here, like the above section, the input power is assumed to be 7dBm

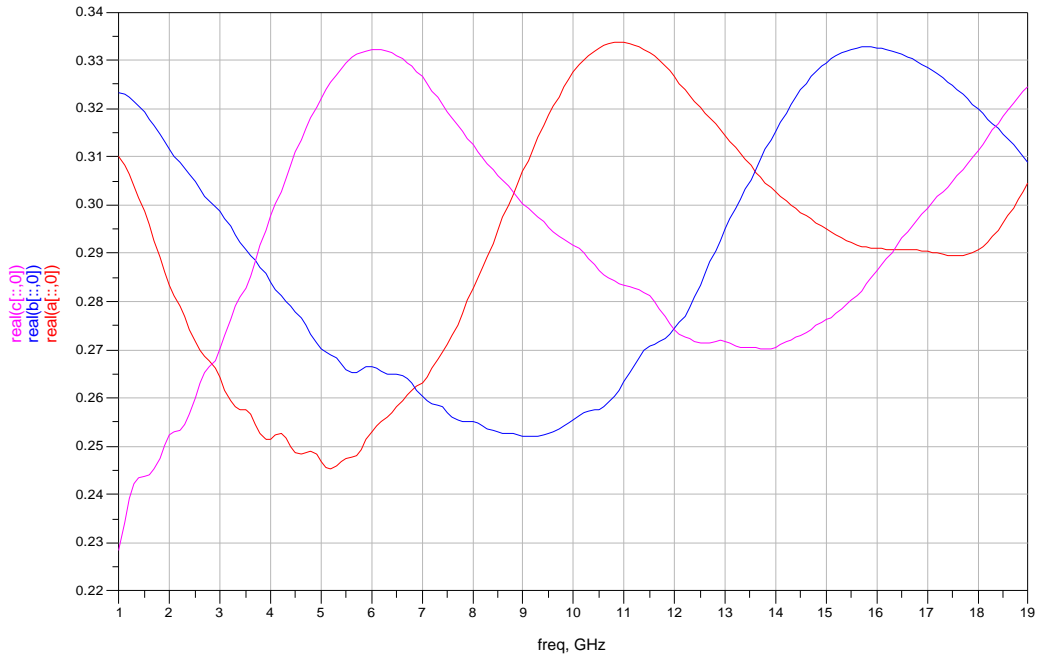
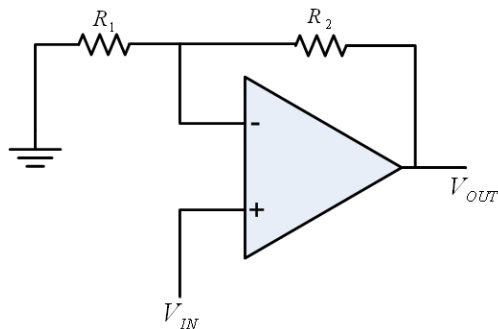


Figure 4.49 Detector outputs of the final circuit.

There are two problematic points in the DC outputs given in Figure 4.49. One of these is the magnitude of voltages. As can be seen from the figure, not only the voltages are small but also voltage change range is too narrow. This situation may be problematic in sorting process. In order to solve this problem, op-amps in non-inverting form can be placed at each output as given in Figure 4.50 [39]. Here, the resistance values R_1 and R_2 are chosen as 100Ω and $1\text{K}\Omega$ respectively. The new output voltage response is given in Figure 4.51.



$$V_{OUT} = \frac{R_1 + R_2}{R_1} V_{IN}$$

Figure 4.50 Non-inverting amplifier.

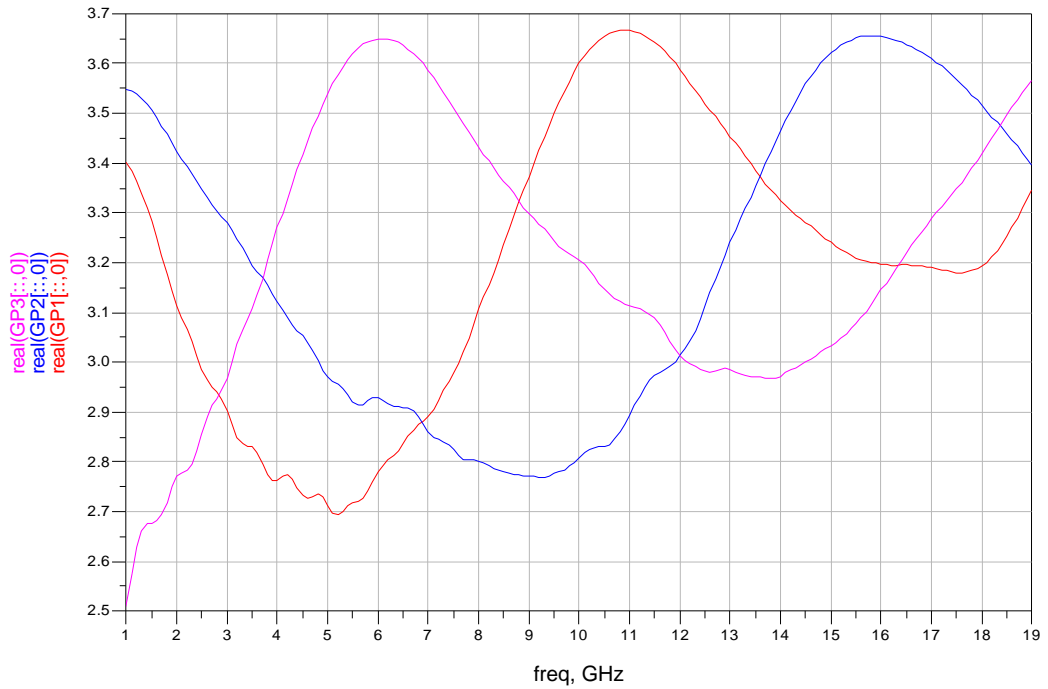


Figure 4.51 Detector outputs with op-amps.

The other problematic point may be change in voltage range with frequency. As can be seen in Figure 4.46, each output voltage cycle becomes narrower as frequency increases. This situation occurs because of the junction capacitance of detector diodes which decreases impedance of the diodes. This in turn leads to narrower output voltage cycles at higher frequencies. However this has no significant effect on the theoretical performance of IFM. This rate of change may be minimized by using a different diode in the actual implementation of the IFM.

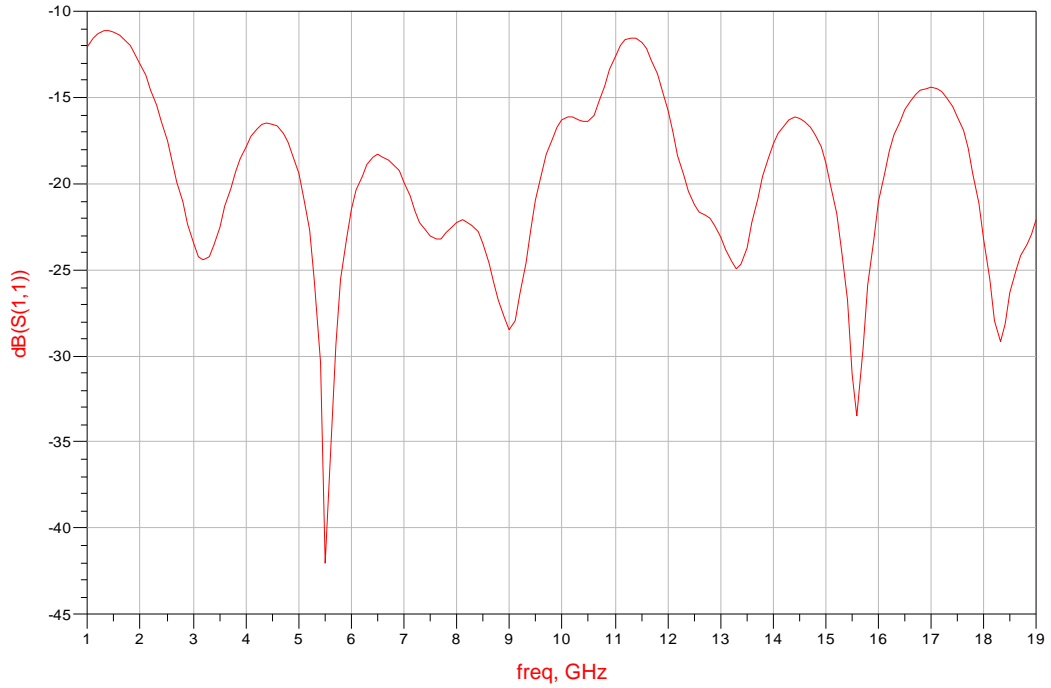


Figure 4.52 S11 of the coarse tier.

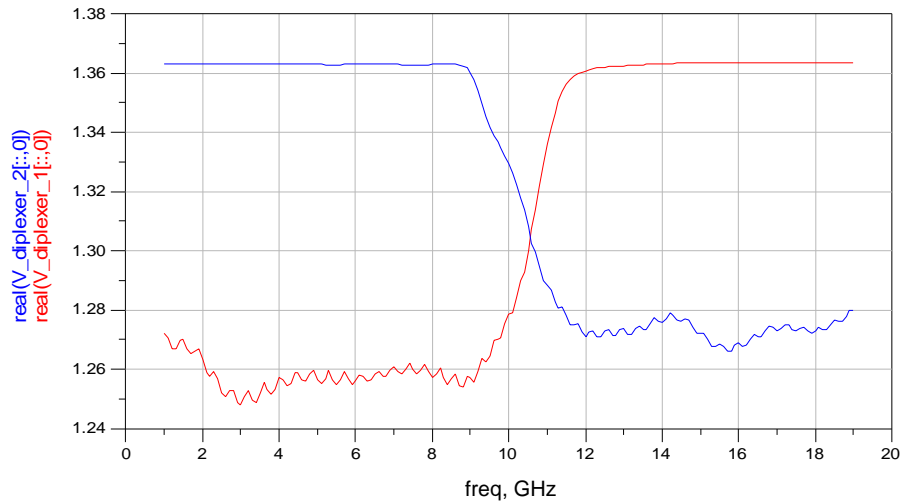


Figure 4.53 Detector outputs at the diplexer.

4.7.1.5 Measurement Results

Figure 4.54 shows the fabricated coarse tier. Detector outputs of this structure are given in Figure 4.55. The major difference between this result and the simulated one

(Figure 4.56), is the extra phase shift in reference line and phase shifter branch 2. This difference may come from the components' non-ideal behaviors and additional layout and measurement effects that are not included in simulations. Still, for the output of the reference line seems to be sufficient. Nevertheless, the output of phase shifter branch 2 could be better. As expected from simulations, there are two same voltage sorting approximately between 3 – 5 GHz and 17 – 18 GHz. This ambiguity can be easily overcome by using the diplexer (Figure 4.57).

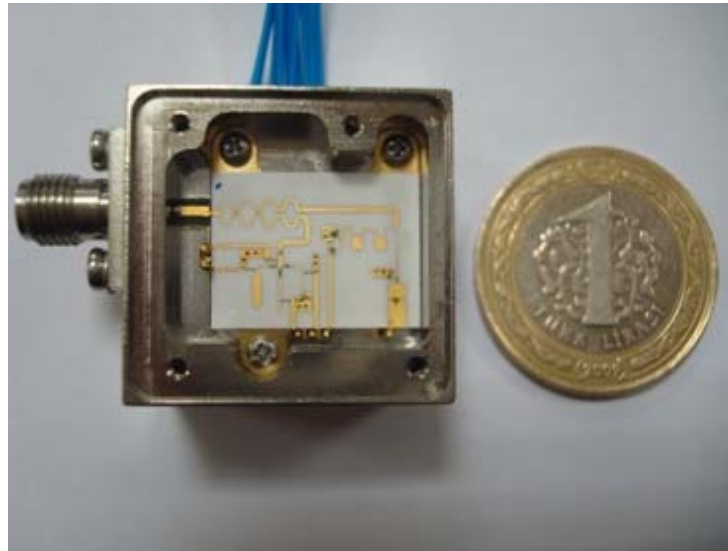


Figure 4.54 Fabricated coarse tier.

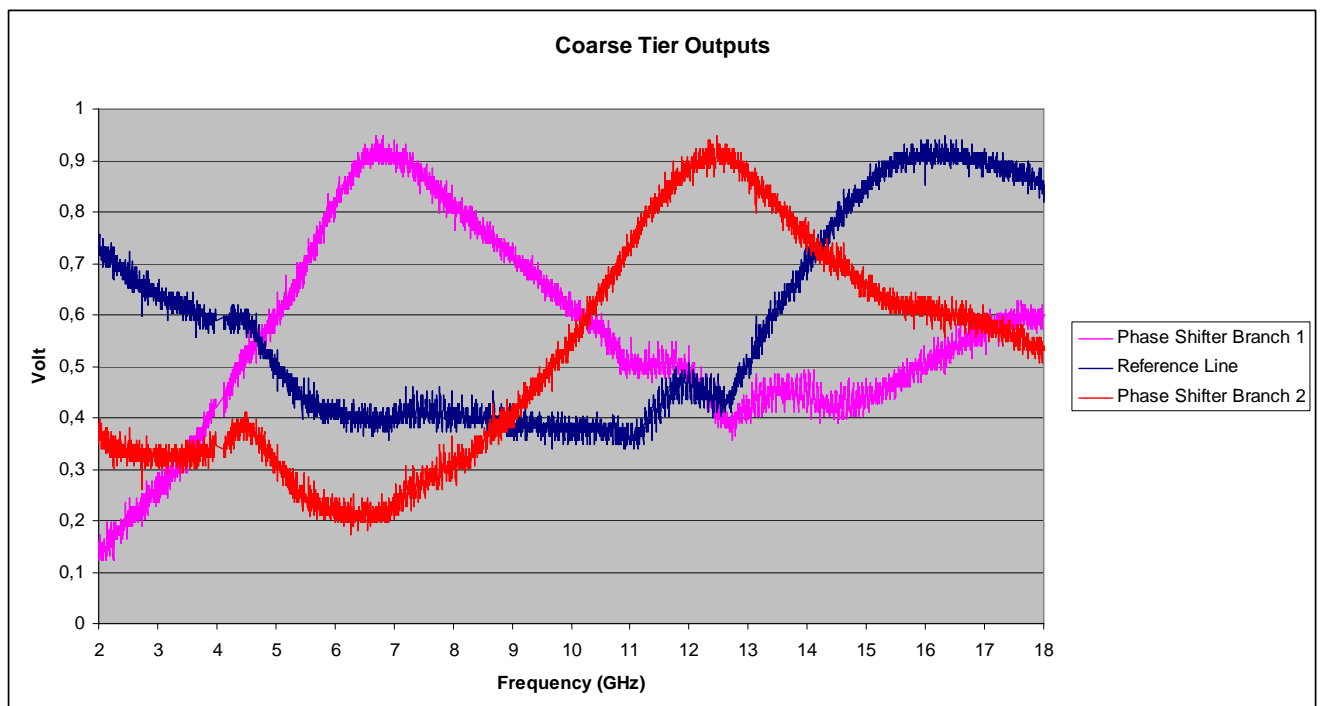


Figure 4.55 Detector outputs of fabricated coarse tier.

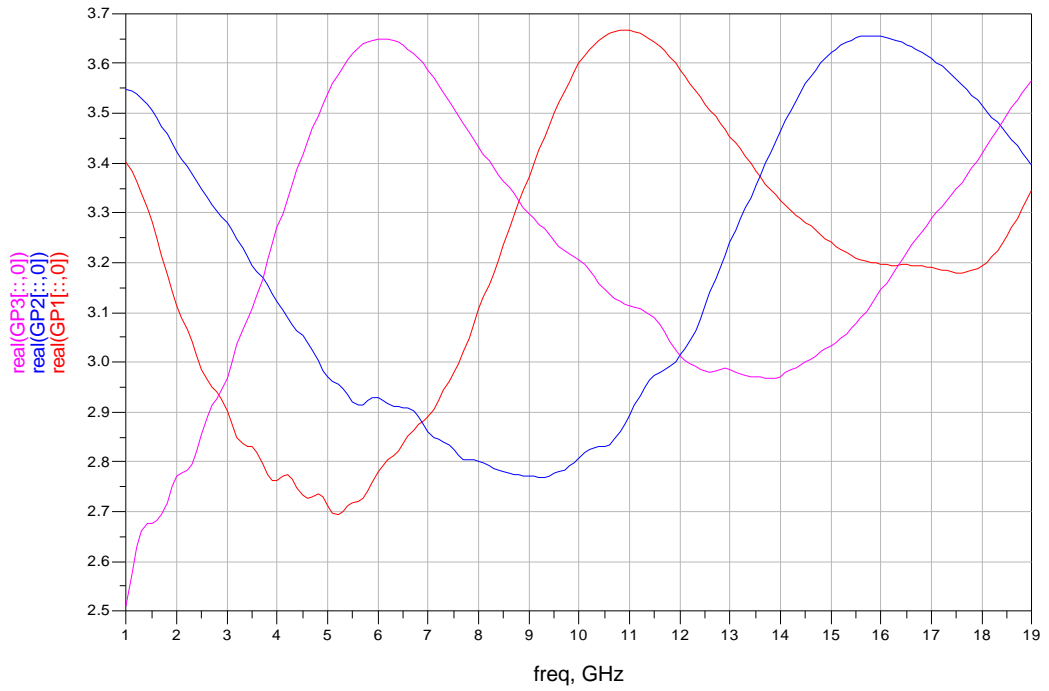


Figure 4.56 Detector outputs of coarse tier in ADS (Momentum result).

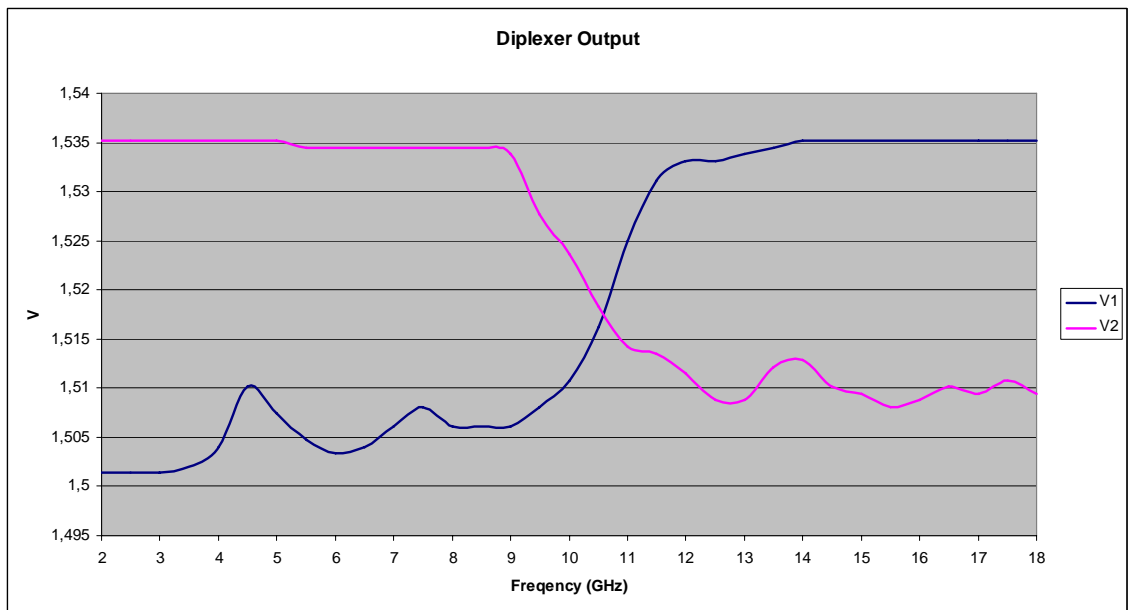


Figure 4.57 Diplexer outputs of fabricated coarse tier.

4.7.2 Medium Tiers

As mentioned in the introduction section of this chapter, more than one phase discriminator tier must be used in order to resolve the possible ambiguities and increase the frequency measurement resolution. Medium and fine tiers are designed to fulfill this purpose. The system has three medium tiers. Only difference between these tiers is the delay line lengths that used before each phase shifting branches. This means, starting from medium tier 1, unambiguous bandwidth of each tier is smaller than the previous one. In other words, every tier is more ambiguous than the previous one. So the number of same voltage sorting increases as the delay line length increases. That is why the output of previous tier(s) is used as a reference point. This reference point gives a hint about which frequency band must be considered. According to that, the delay line lengths of medium and fine tiers are adjusted so that “all three voltage hills” of one tier is fit into “one voltage hill” of the previous tier output. The entire case described here can be explained by an example as follows.

Assume that the input signal frequency is 4 GHz. According to this input frequency, voltage sorting obtained from the coarse tier must be Blue>Red>Green (Figure 4.58). As can be seen from the figure, to the end of the defined frequency band the voltage sorting starts to repeat itself. But by the help diplexer the input, signal frequency can be guessed whether it is below 10 GHz or not. So, according to diplexer output, the input frequency is expected to be between 3 GHz - 5 GHz (Notice that the voltage sorting between 3 GHz - 5 GHz is same).

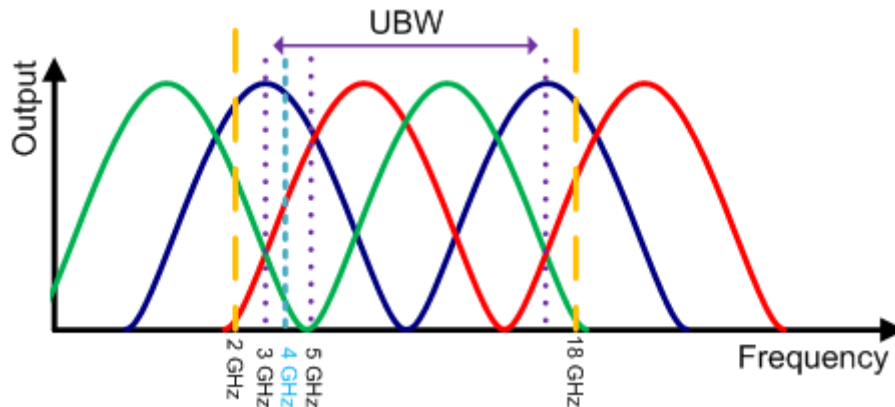


Figure 4.58 Coarse tier detector outputs as an example.

As mentioned above, all three voltage hills of medium tier 1 must fit into one voltage hill of coarse tier. Now consider Figure 4.59: Delay lines in medium tier 1 must be adjusted so that all three voltage hills (purple, orange and brown curves shown between dotted pale blue lines) of this tier are nested into the one hill (for this example it is the red one) of coarse tier as shown in Figure 4.59. According to this arrangement, the output of medium tier one with respect to frequency must be the one given in Figure 4.60. The nested form of the outputs of coarse and medium tiers is given in Figure 4.61.

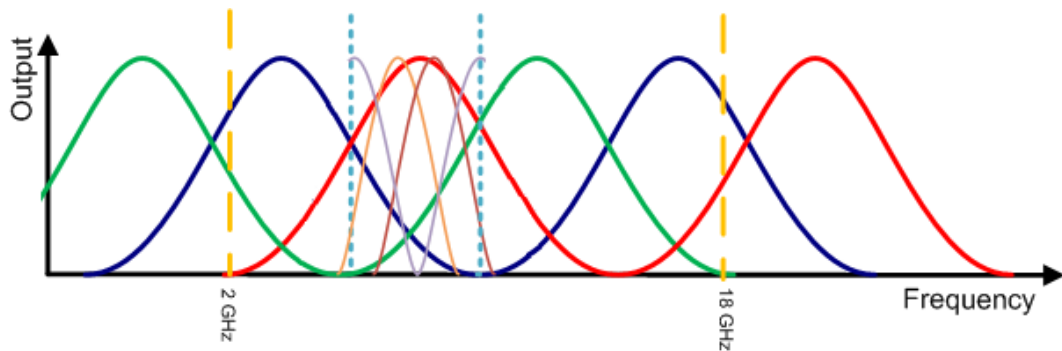


Figure 4.59 Nesting the outputs of medium tier 1 into coarse tier.

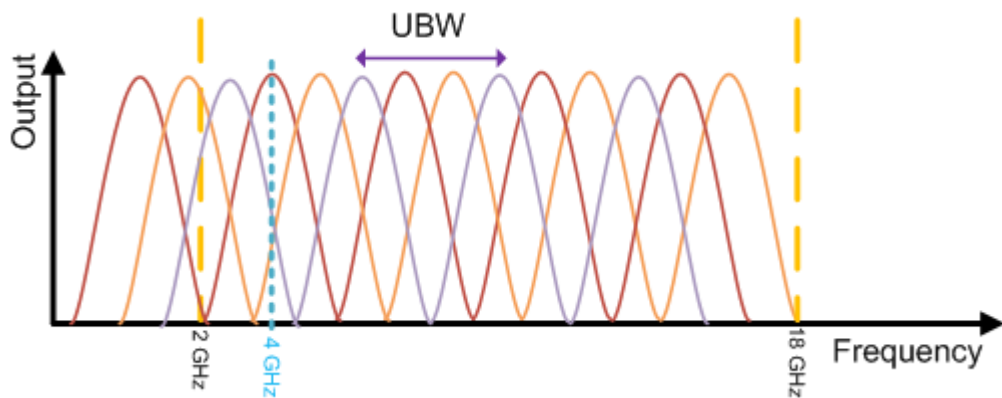


Figure 4.60 Medium tier 1 detector outputs as an example.

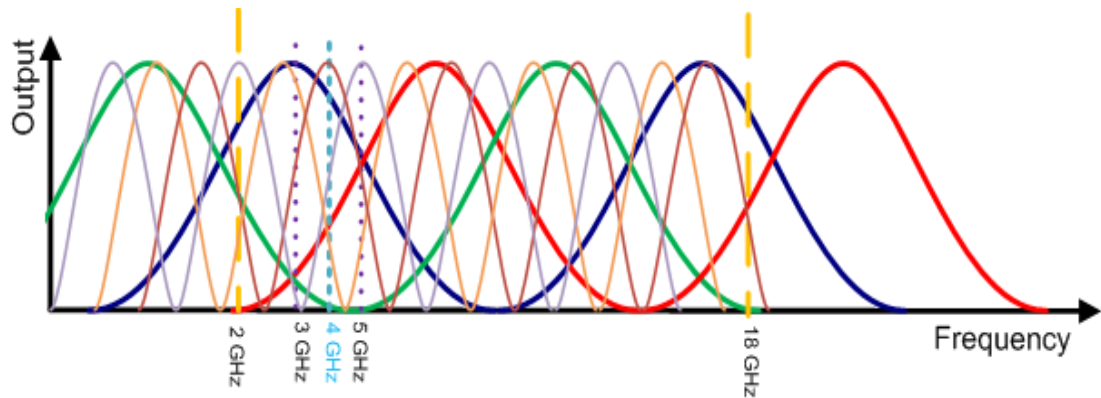


Figure 4.61 Coarse and medium tier outputs in nested form.

Here, according to the input frequency, the voltage sorting obtained from medium tier 1 will be: **Brown>Purple>Orange**. As can be seen from the figure, this voltage sorting is valid for 4 different frequency intervals. In order to find the right one the output of coarse tier must be taken into consideration. By the help of the nested form given in Figure 4.61, which **Brown>Purple>Orange** voltage sorting is the right one for our purpose can be chosen easily.

Like the case presented here, other tiers must be designed and adjusted according to each other's response. By this way, the input signal frequency can be found within the limits of resolution and accuracy.

The design and simulation results are given in below sub-sections for each medium tier. As a design decision, in order to minimize the loss phase shifting branches and delay lines are designed/simulated/optimized on suspended substrate (Rogers 5880). Actually, using suspended substrate also give the opportunity to use/fabricate higher impedance values compared to microstrip. Although the circuit size gets bigger, this choice is also advantageous when the high impedance requirement of the last section of phase shifter 1 is considered. Remember that, the limit of a transmission line impedance is 114 ohm for microstrip (i.e. 1 mil in width), but this time this limit is increased up to 270 ohm. The other parts of the circuit, such as junction point of diodes, can be implemented on microstrip.

Another important thing is the output magnitudes. The only critical thing is to fit the outputs of each tier into the previous one as much as possible. So, actually, the magnitudes of each tier output can be different. But in order to make the figures more understandable, resistive elements is adjusted to equalize all of the output magnitudes of tiers.

4.7.2.1 Medium Tier 1

In differential phase shifter design process presented in section 3.3.2.3, it has already seen that 5 section phase shifter branches are sufficient to obtain a good response. According to the maximum impedance that can be manufactured (i.e. 270 ohm), the simulations for 5 section phase shifting branches are repeated. Figure 4.62 shows the new phase shifting branches with ideal transmission lines. The responses of this structure are presented in following figures.

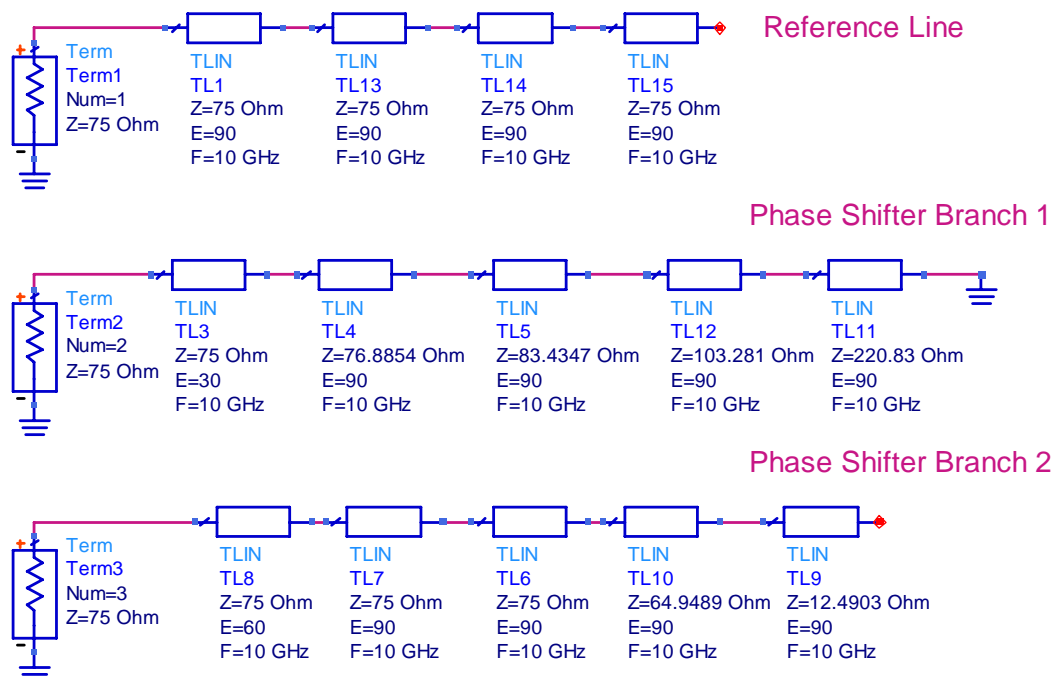
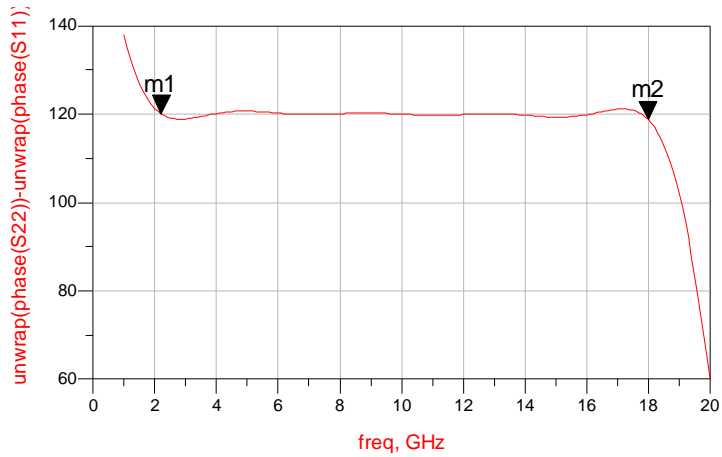


Figure 4.62 Medium tier phase shifting branches with ideal transmission lines.



```

m1
freq=2.200GHz
unwrap(phase(S22))-unwrap(phase(S11))=120.106
optlter=2388

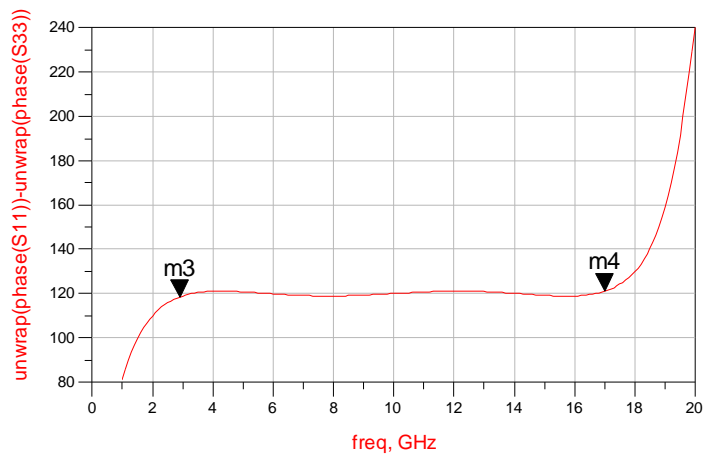
```

```

m2
freq=18.00GHz
unwrap(phase(S22))-unwrap(phase(S11))=118.733
optlter=2388

```

Figure 4.63 Phase difference between phase shifter branch 1 and reference line (with ideal transmission lines).



```

m3
freq=2.900GHz
unwrap(phase(S11))-unwrap(phase(S33))=118.488
optlter=2388

```

```

m4
freq=17.00GHz
unwrap(phase(S11))-unwrap(phase(S33))=121.039
optlter=2388

```

Figure 4.64 Phase difference between reference line and phase shifter branch 2 (with ideal transmission lines).

In Figure 4.65, lossy equivalent of the structure given above is presented. According to these branches the responses given in Figure 4.66 and Figure 4.67 are obtained.

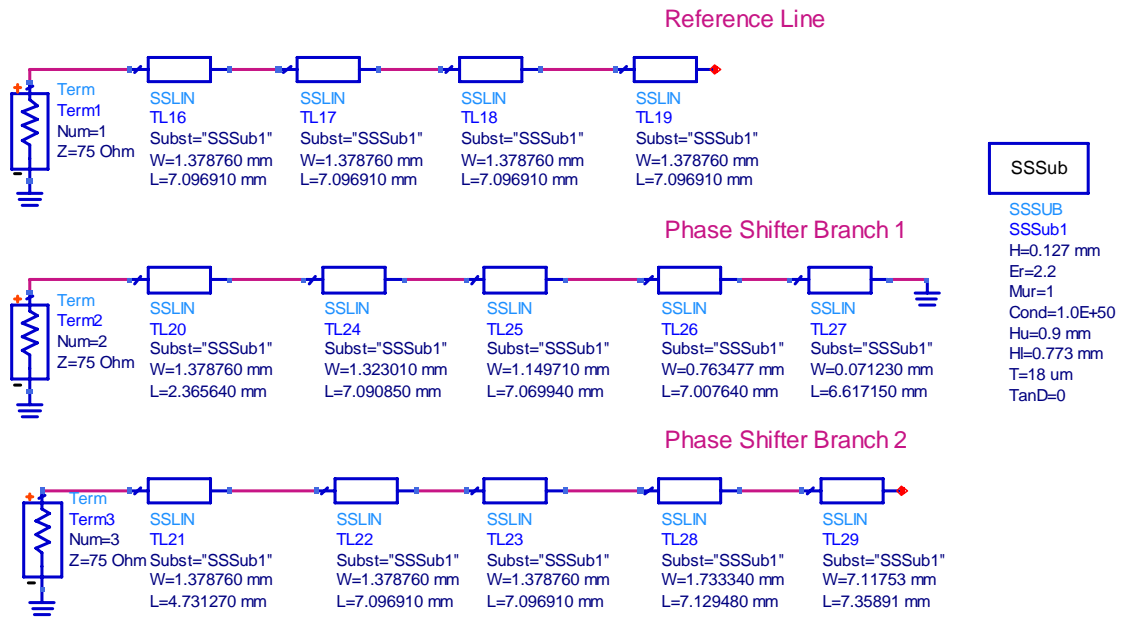
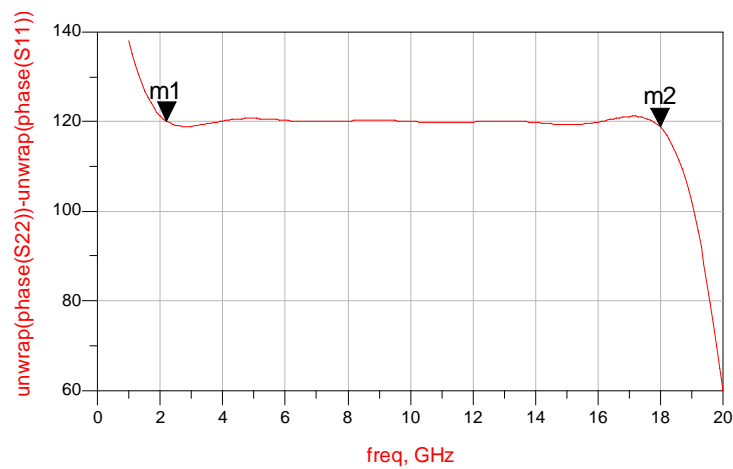


Figure 4.65 Medium tier phase shifting branches with lossy elements.



m1
freq=2.200GHz
unwrap(phase(S22))-unwrap(phase(S11))=120.106
optIter=4349

m2
freq=18.00GHz
unwrap(phase(S22))-unwrap(phase(S11))=118.733
optIter=4349

Figure 4.66 Phase difference between phase shifter branch 1 and reference line (with lossy elements).

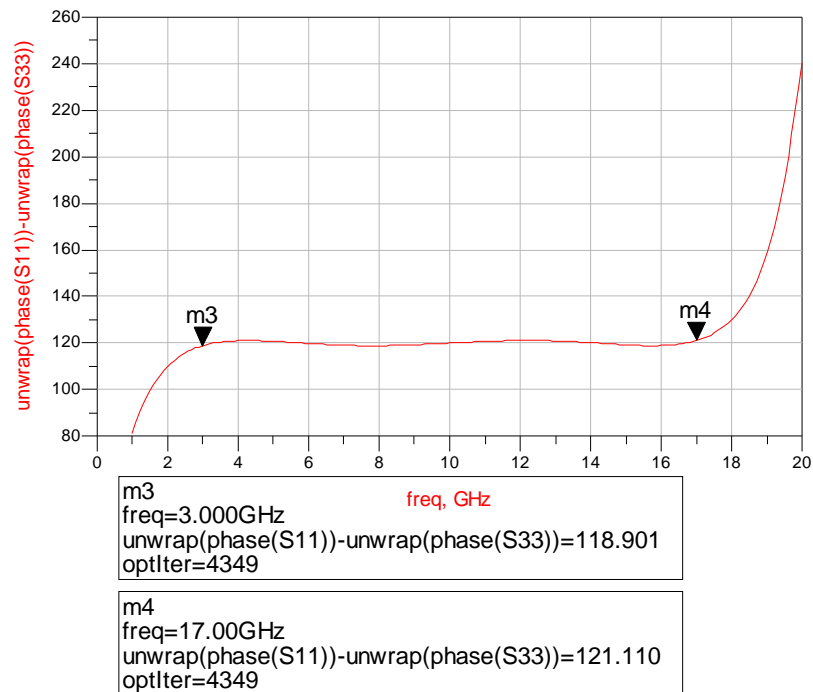


Figure 4.67 Phase difference between reference line and phase shifter branch 2 (with lossy elements).

Although these results are quite sufficient, the discontinuity between the last sections of phase shifter branch 2 may become problematic in real world. Unfortunately it is impossible to decrease the width of the last section by using suspended substrate. But if a microstrip was used for this section, then it would be much thinner than before. So, in a sense, if the substrate at the last section is transformed into a microstrip, then the problem will be eliminated. Starting from this idea, for only the last section, the air spacing at the lower part of the suspended substrate is discarded. A new optimization is applied according to this change. The new version of the structure is given in Figure 4.68. Differential phase responses are given for this modified version in Figure 4.69 and Figure 4.70.

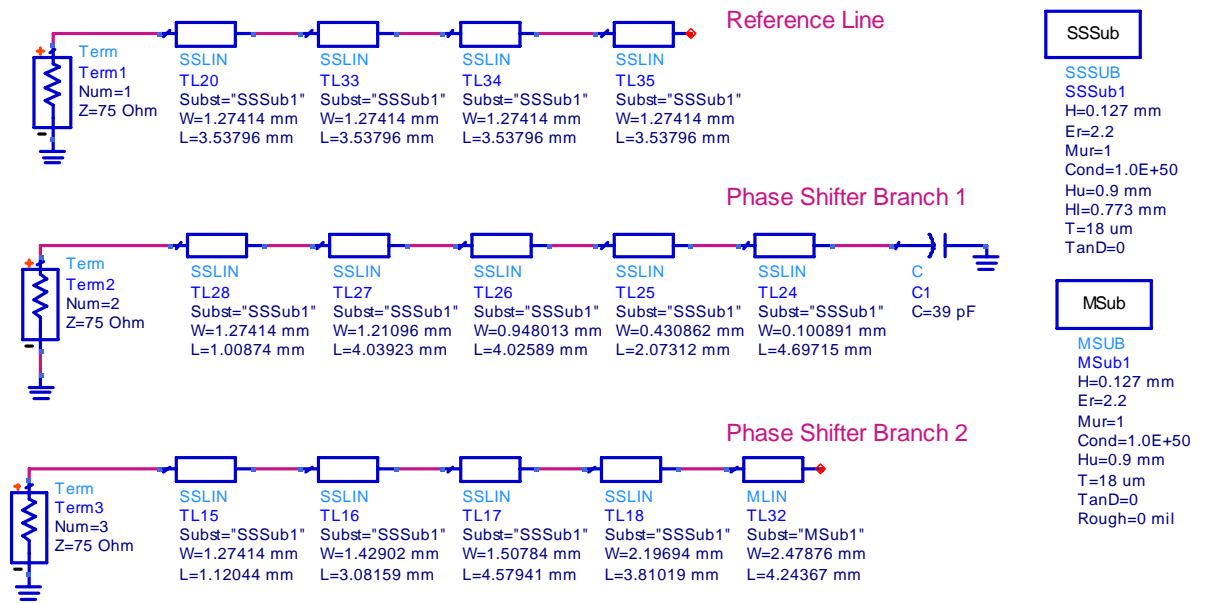


Figure 4.68 New version of the phase shifter structure.

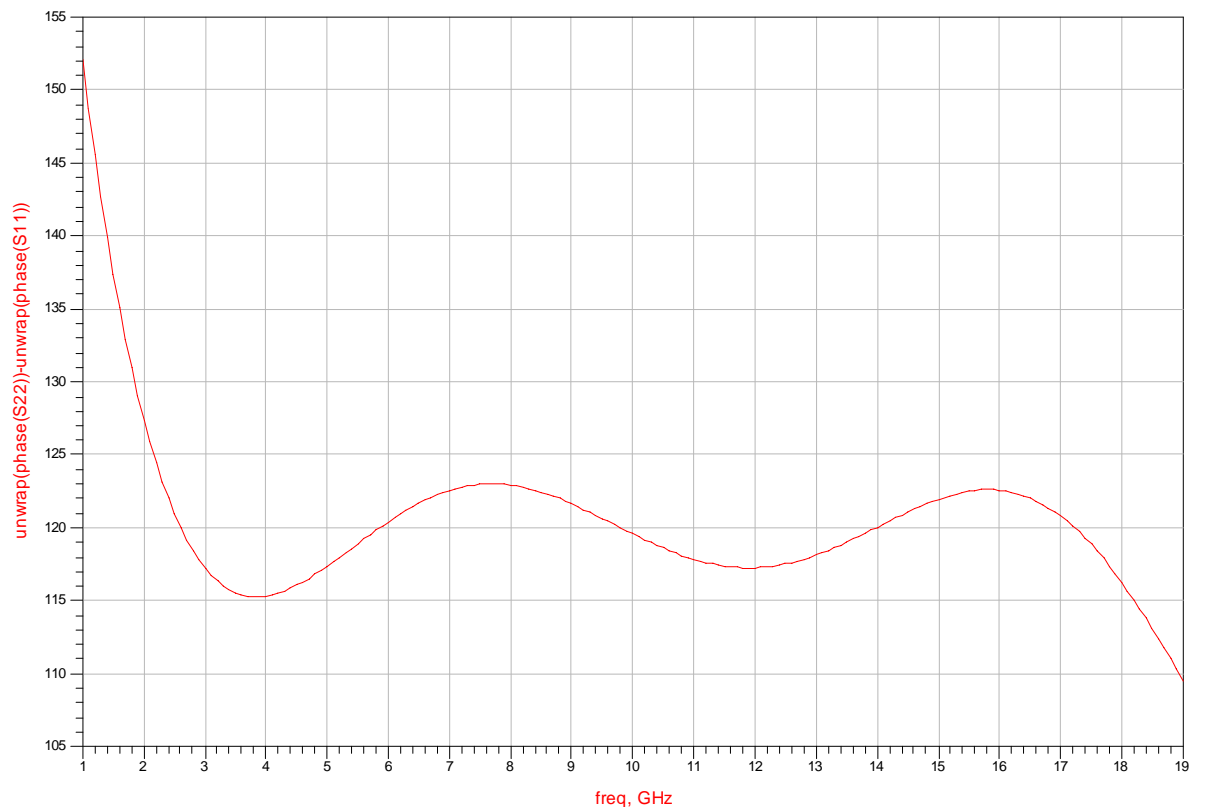


Figure 4.69 Phase difference between phase shifter branch 1 and reference line (modified version).

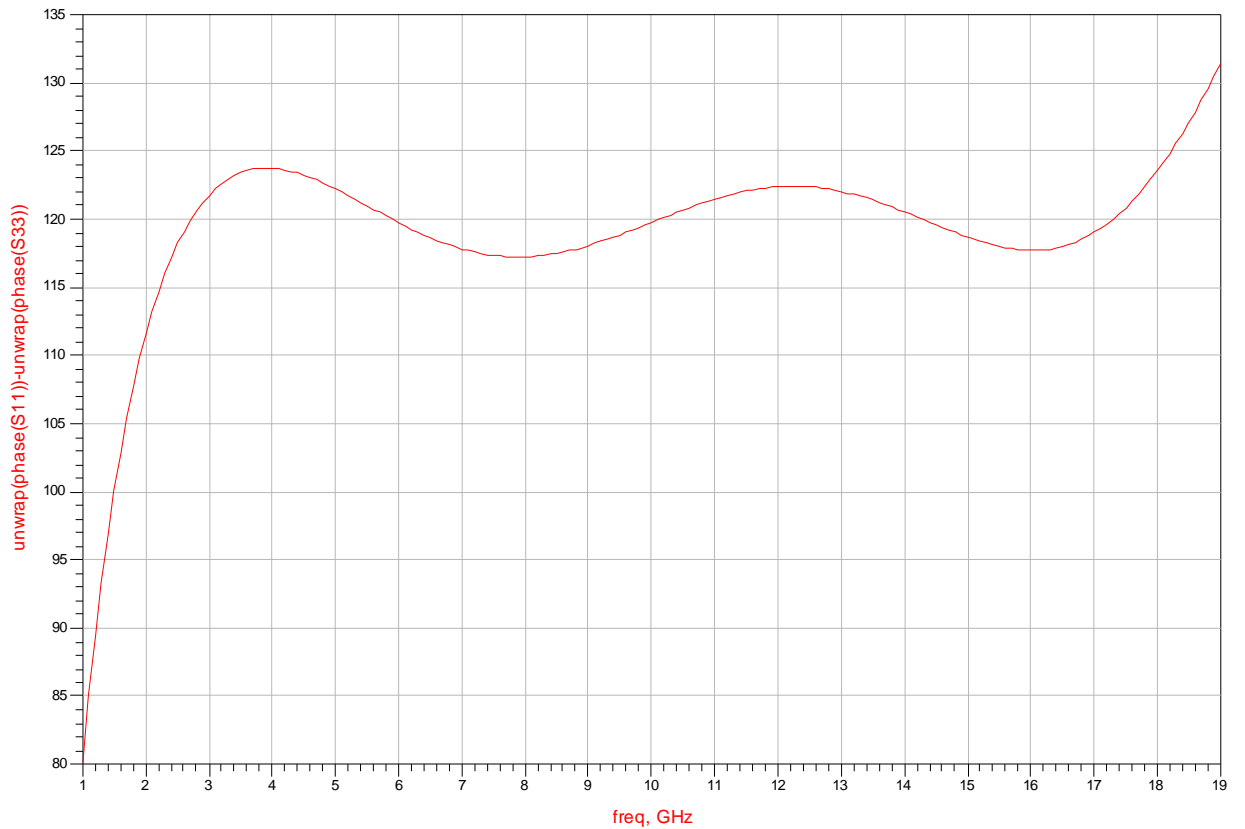


Figure 4.70 Phase difference between reference line and phase shifter branch 2 (modified version).

In order to make a realistic observation, the structure is simulated on 3D EM simulator, HFSS. The simulated structures are given in Figure 4.71, Figure 4.72 and Figure 4.73.

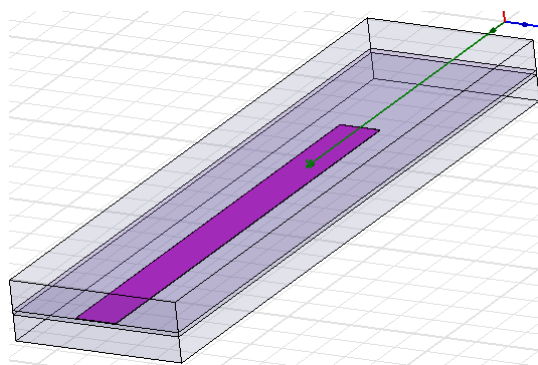


Figure 4.71 Reference line in HFSS.

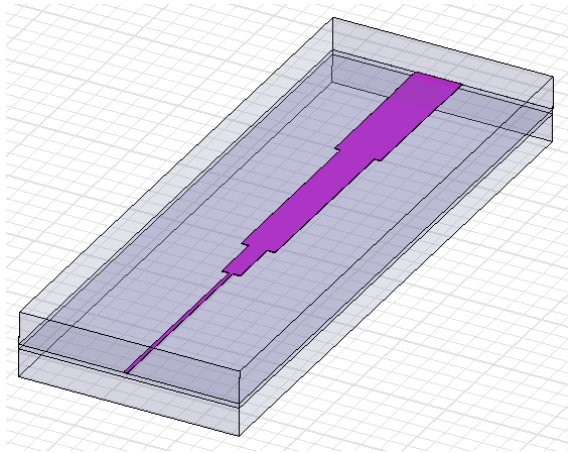


Figure 4.72 Phase shifter 1 in HFSS.

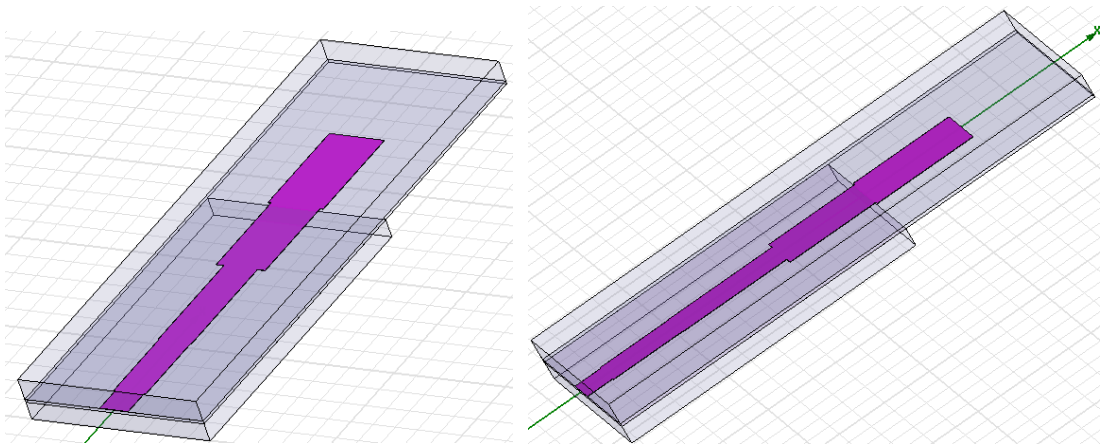


Figure 4.73 Phase Shifter 2 in HFSS from two different angles.

After the simulations in HFSS, S-parameter set of each branch is imported to ADS. The differential phase responses are presented in Figure 4.74 and Figure 4.75.

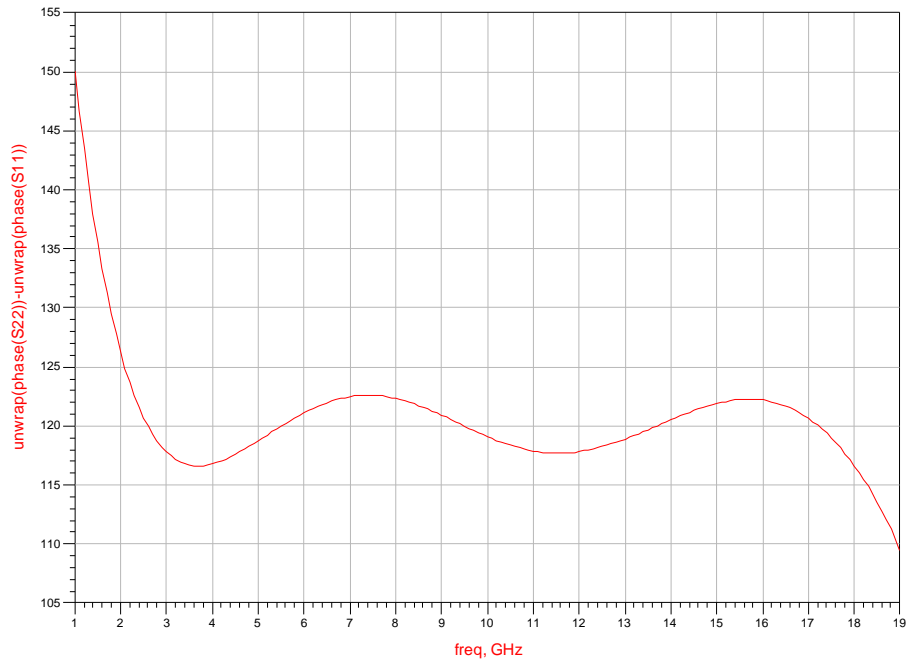


Figure 4.74 Phase difference between phase shifter branch 1 and reference line (HFSS version).

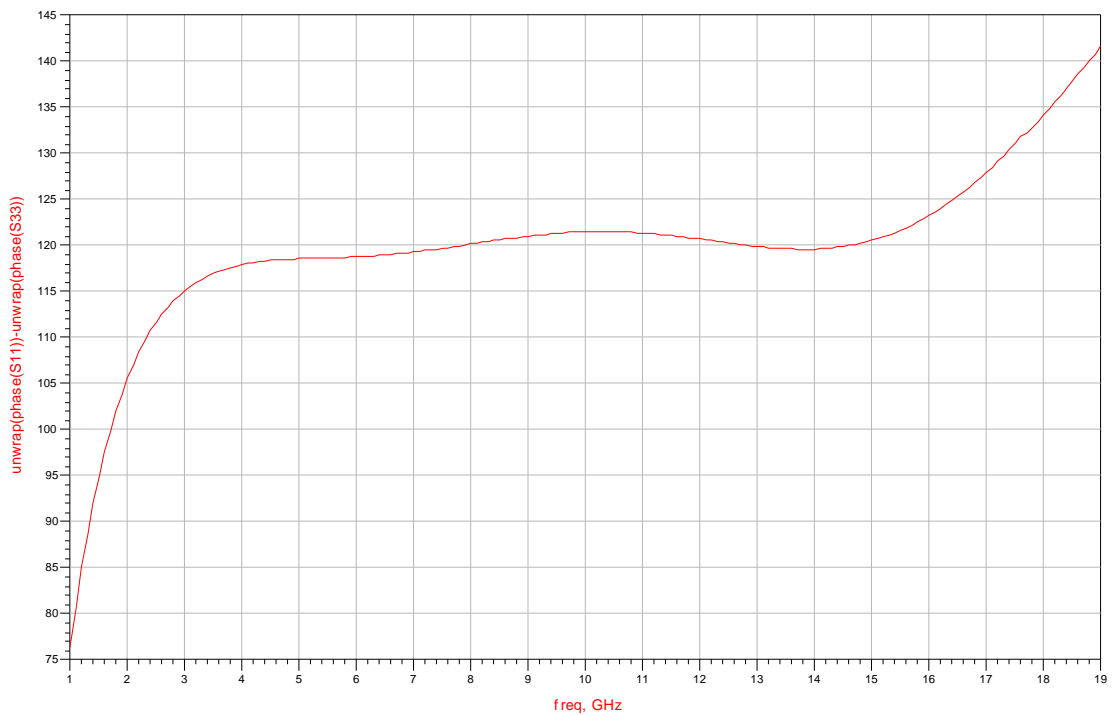


Figure 4.75 Phase difference between reference line and phase shifter branch 2 (HFSS version).

By using the obtained s-parameters form HFSS schematic of medium tier is designed as presented in Figure 4.76. In this figure, purple encircle areas are delay lines, green encircled areas are the bias points of diodes and orange circles are the measurement points

After several adjustment efforts, it has seen that using approximately 11.7 mm delay line length is sufficient for nesting the voltage cycles this tier into the voltage cycles of coarse tier (bold lines) as given in Figure 4.77. Here, delay lines can be implemented on microstrip instead of suspended substrate in order to decrease the length. If the designer chooses this alternative, an approximately 4.8 mm in length and 0.11 mm in width delay lines are sufficient to get the same response. But remember that, the first section of each phase shifting branch is 1.27 mm wide. So, this time the designer must deal with the extra losses as well as the discontinuity between phase shifting branches and delay lines. In this thesis, in order to decrease the loss as much as possible, suspended stripline delays are chosen.

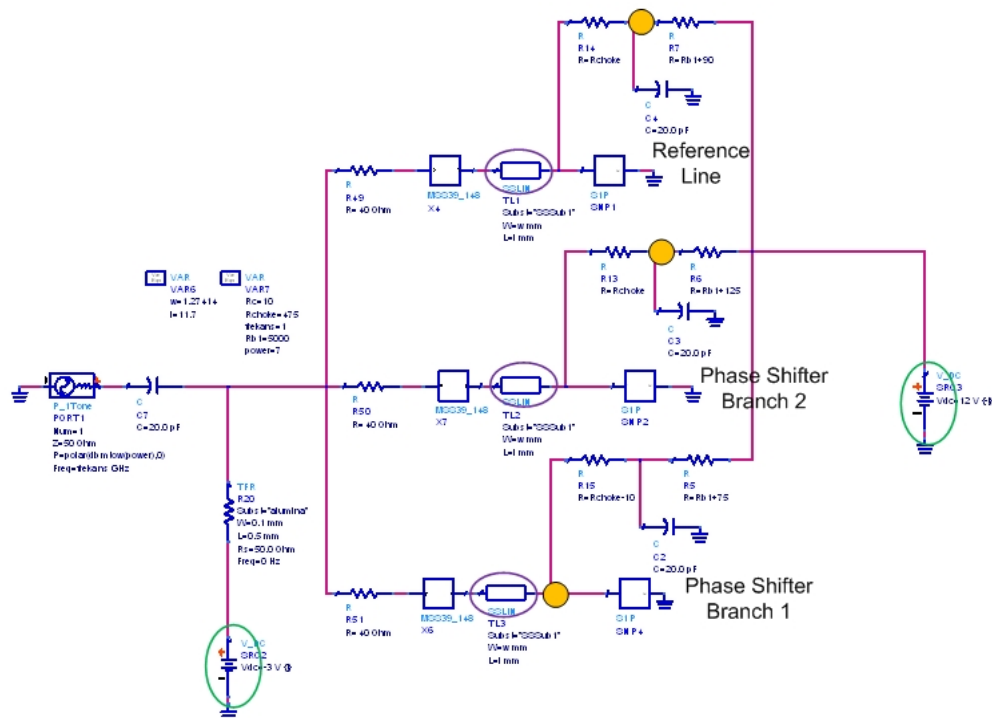


Figure 4.76 Schematic version of medium tier 1.

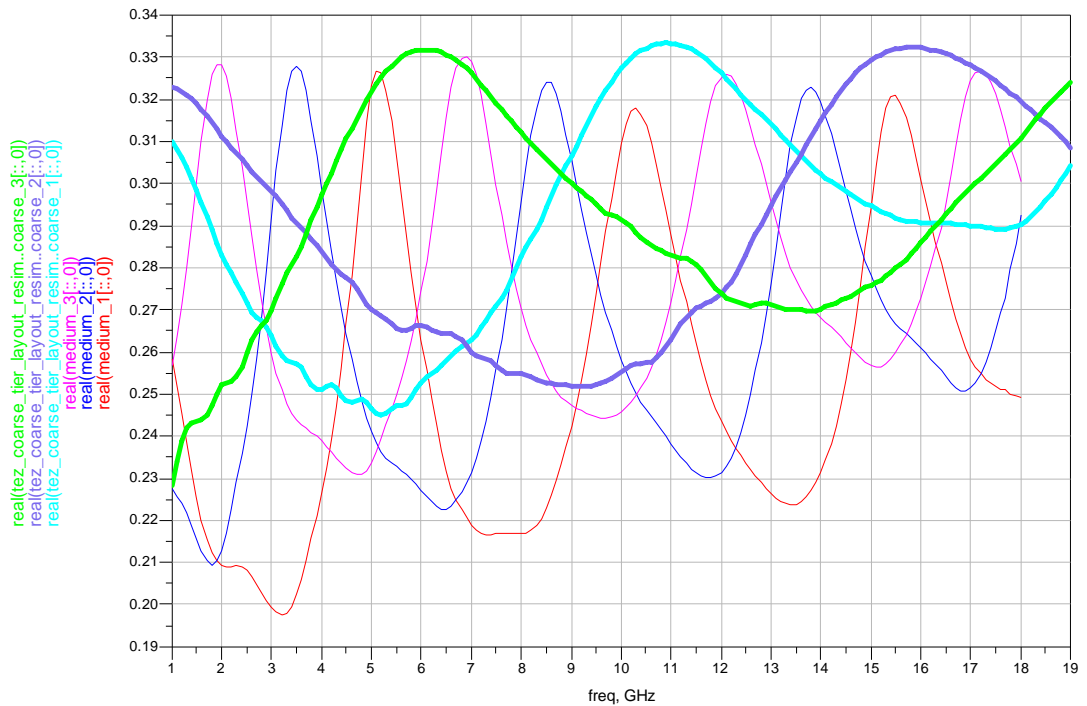


Figure 4.77 Output of medium tier 1 (schematic version) and coarse tier (actual version) in nested form.

A more realistic circuit of medium tier 1 is given in Figure 4.78. In this figure, blue arrows indicate the bias points of diodes, green encircled areas shows the momentum versions delay lines (they are miniaturized to fit the figure in the page) and orange circles are the measurement points. The detector outputs and S11 of this circuit is given in Figure 4.79 and Figure 4.81 respectively.

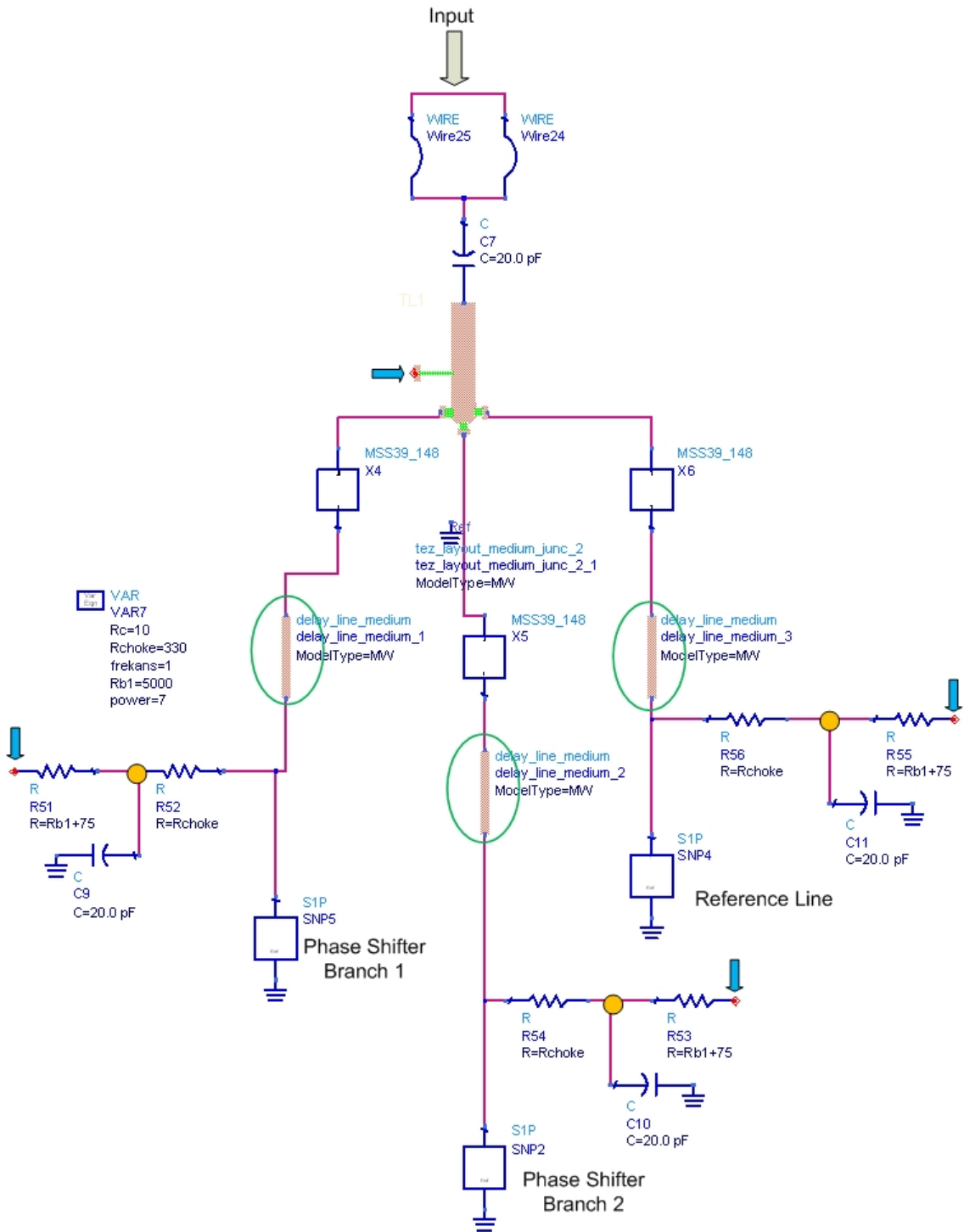


Figure 4.78 Medium tier 1 with HFSS S-parameters and momentum components.

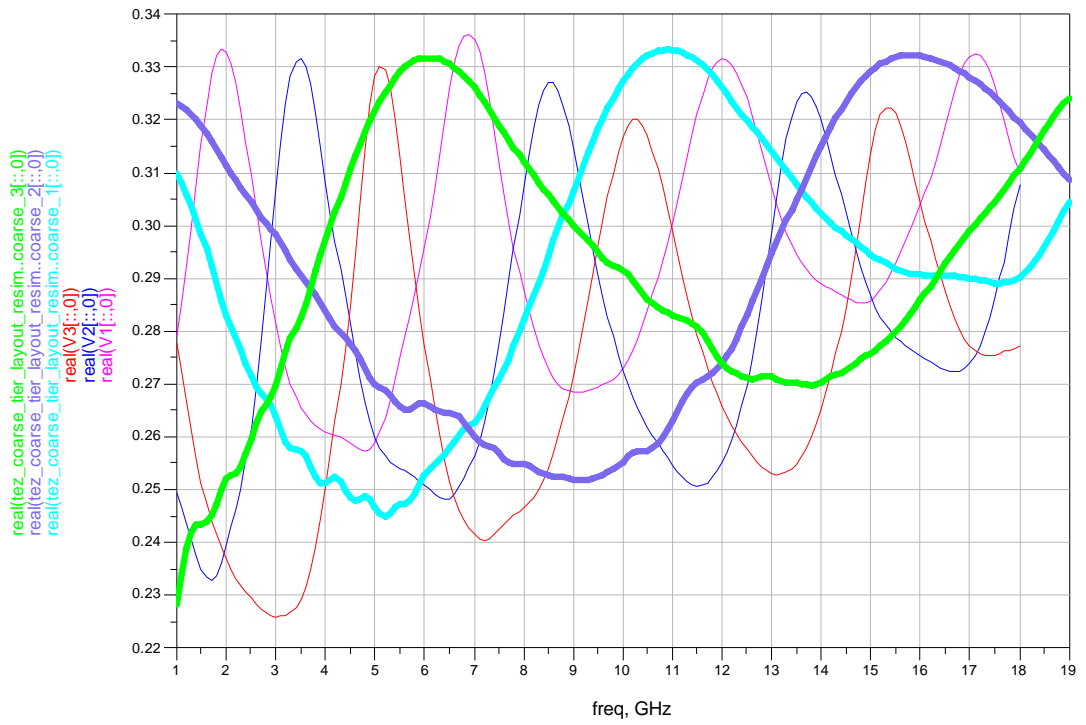


Figure 4.79 Output of medium tier 1 and coarse tier in nested form.

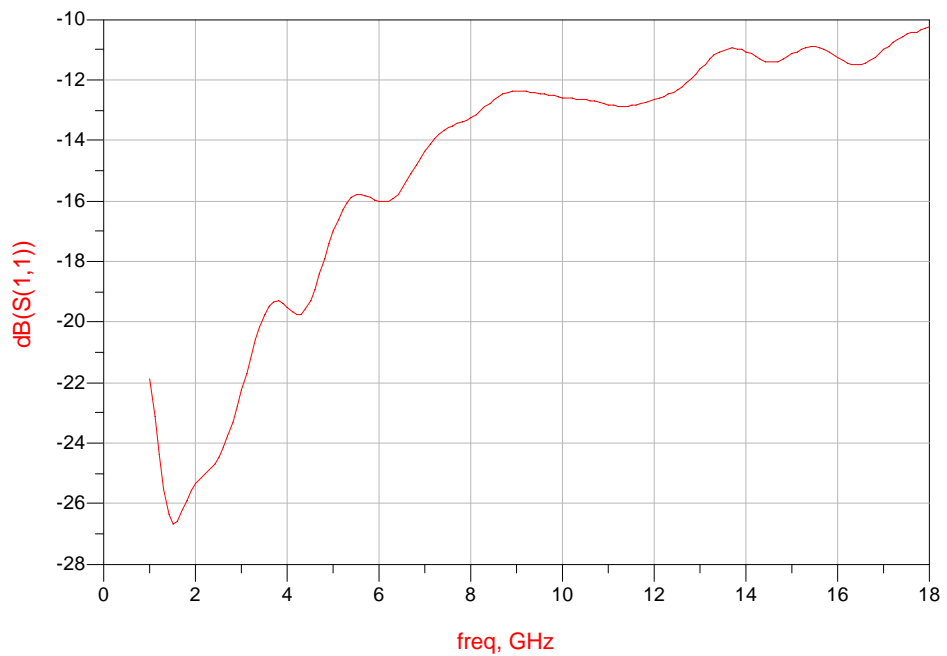


Figure 4.80 S11 of medium tier 1.

4.7.2.2 Medium Tier 2

As described above the only difference between medium tier 1 and medium 2 is the delay line lengths. The simulation efforts for medium tier 2 showed that, using approximately 75.5 mm delay lines are sufficient for fitting the cycles into each other (Figure 4.81).

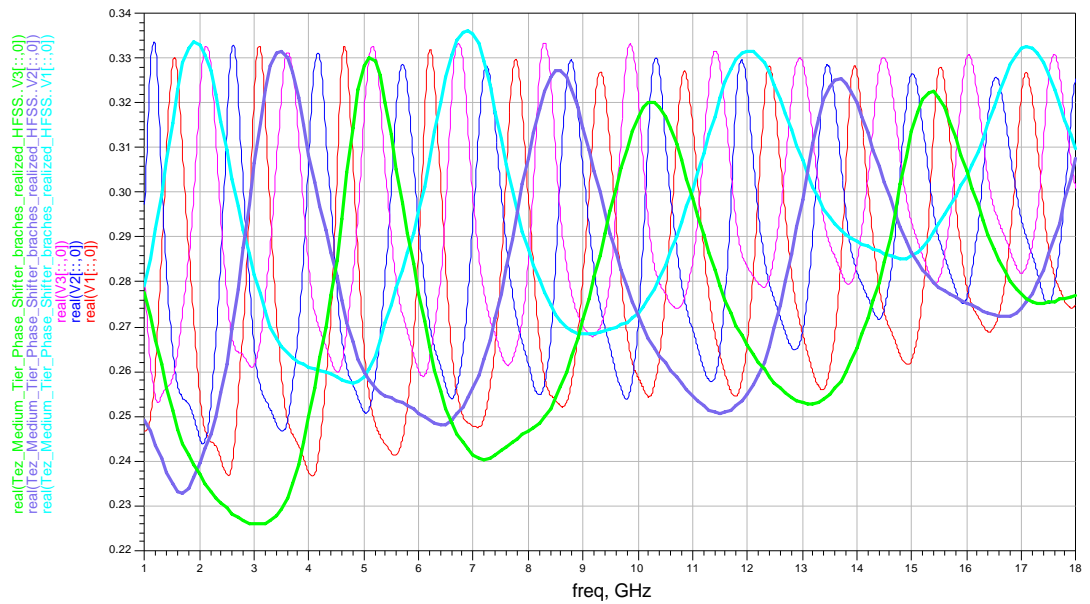


Figure 4.81 Output of medium tier 2 and medium tier 1 in nested form.

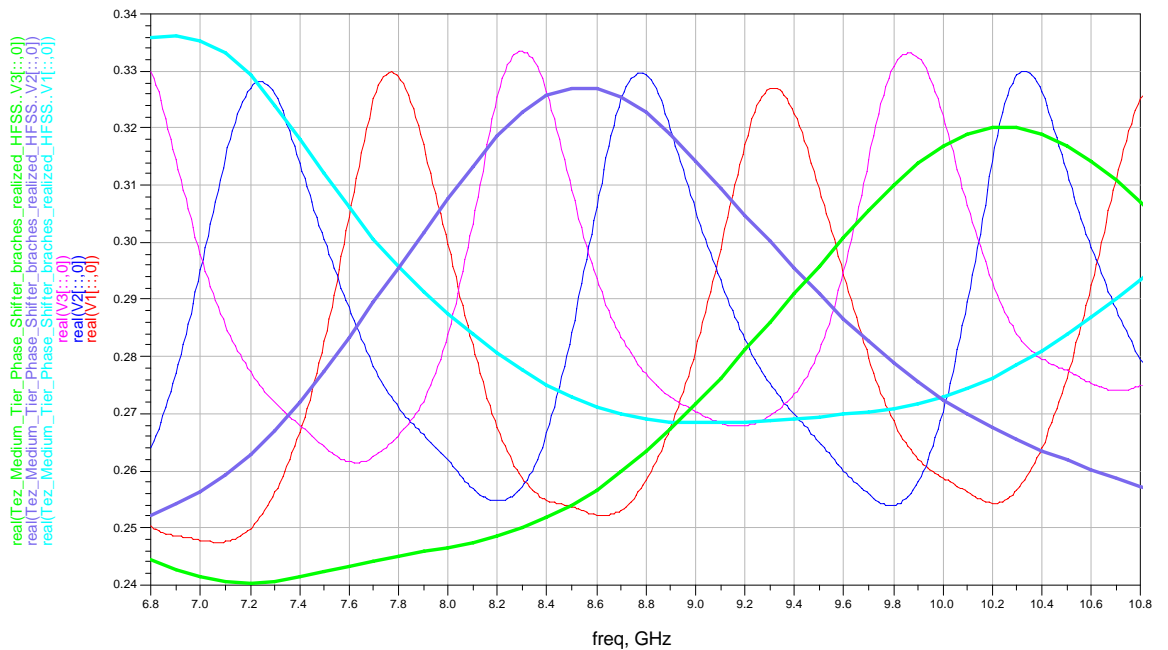


Figure 4.82 Output of medium tier 2 and medium tier 1 in nested form (zoomed around 8.8 GHz).

4.7.2.3 Medium Tier 3

Nesting the cycles into each other becomes harder due to the increase in delay line length. After several simulations, using 285 mm delay lines seems to be good for medium tier 3. The overall response and two zoomed sample figures from this response are given below.

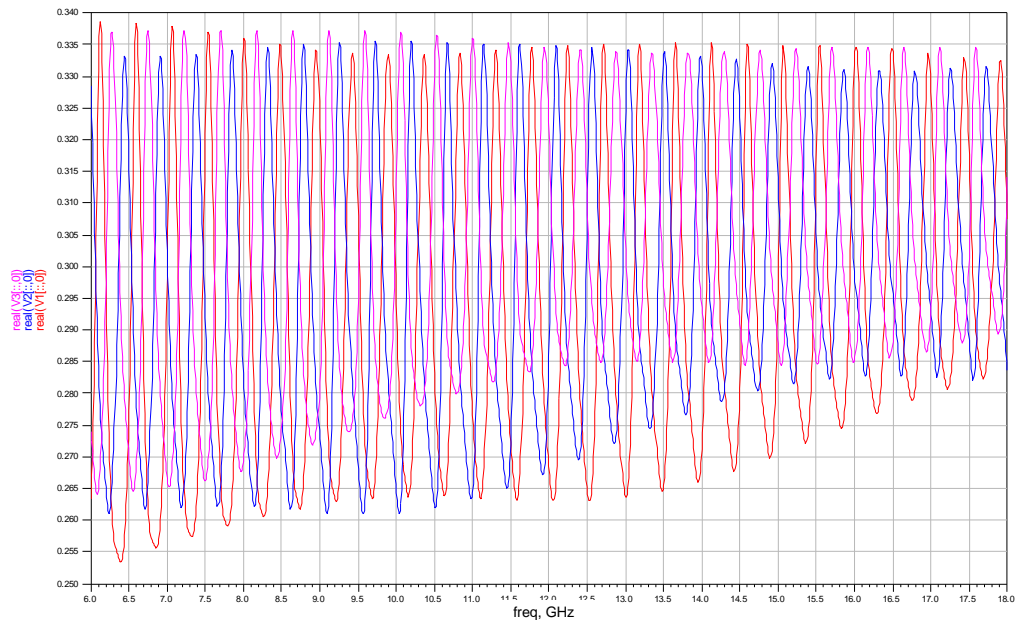


Figure 4.83 Detector outputs of medium tier 3.

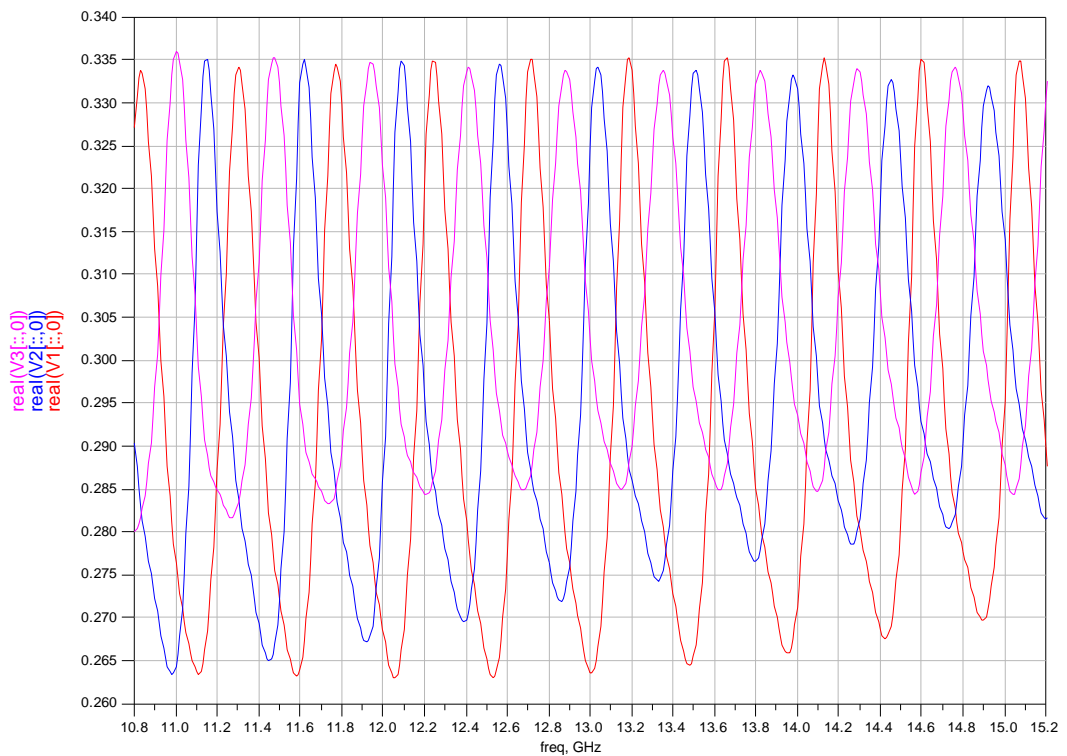


Figure 4.84 Detector outputs of medium tier 3 (zoomed around 13 GHz).

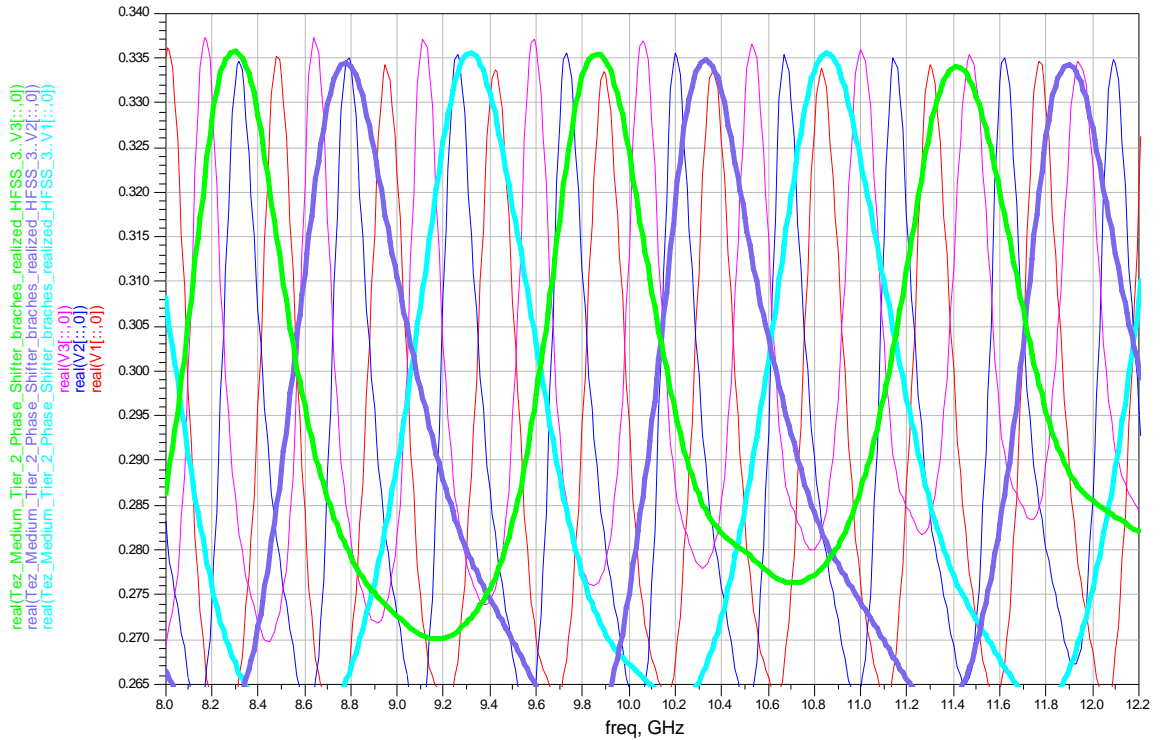


Figure 4.85 Output of medium tier 3 and medium tier 2 in nested form (zoomed around 10 GHz).

4.7.3 Fine Tier

Fine tier is the last tier structure of the system. It has the narrowest unambiguous bandwidth. In other words, fine tier has the longest delay line among all of the tiers. According to that, frequency resolution depends on the delay line length of fine tier (section 2.4, equation (2.51))

As presented in this chapter, three phase discriminator structures require separate delay lines. When the purpose of fine tier is considered, these lines will be very long compared to the other delay lines in medium tiers. But using these long lines/cables will occupy too much space in the circuit. Additionally, nesting the voltage cycles becomes harder as delay line length increases. Due to these two reasons, unlike other tiers, a different approach is applied in the design process of fine tier. The general block diagram of fine tier is given in Figure 4.86. Here, instead of using 2-18 GHz

power dividers, the other option might be to use 6GHz diplexer at the expense of reduced accuracy (due to lower SNR) around the crossover region (5.75-6.25GHz region).

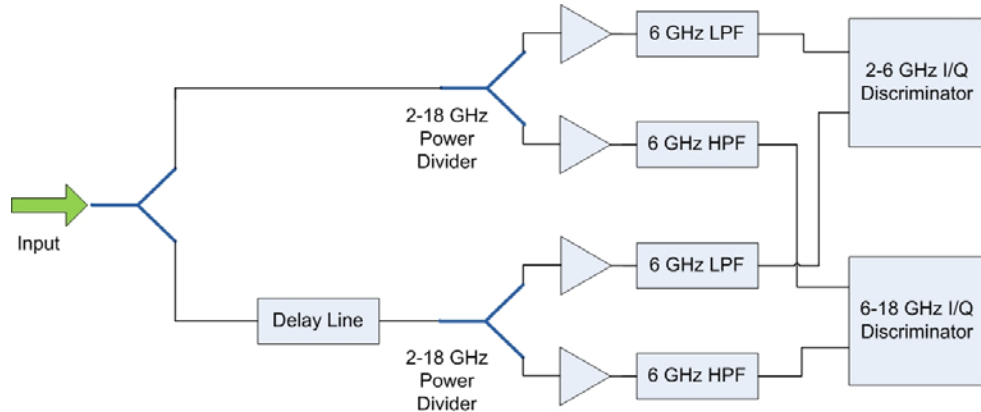


Figure 4.86 General block diagram of fine tier.

Several phase discriminator structures are presented in [30] to [38]. The common point of these structures is the use of 3 dB couplers like the one already examined in section 2.3. However couplers are usable only up to around 1.5 octaves. So it is impossible to cover 2 – 18 GHz frequency band with a single discriminator. Due to this reason, two discriminators are designed which work in 2-6 GHz and 6-18 GHz frequency bands. The structural form is same in both discriminators as given in Figure 4.87. Each discriminator is designed by using three identical Lange couplers and a 3-section standard Wilkinson splitter. These discriminators are also realized on alumina. The measurement results are given in related sub-sections.

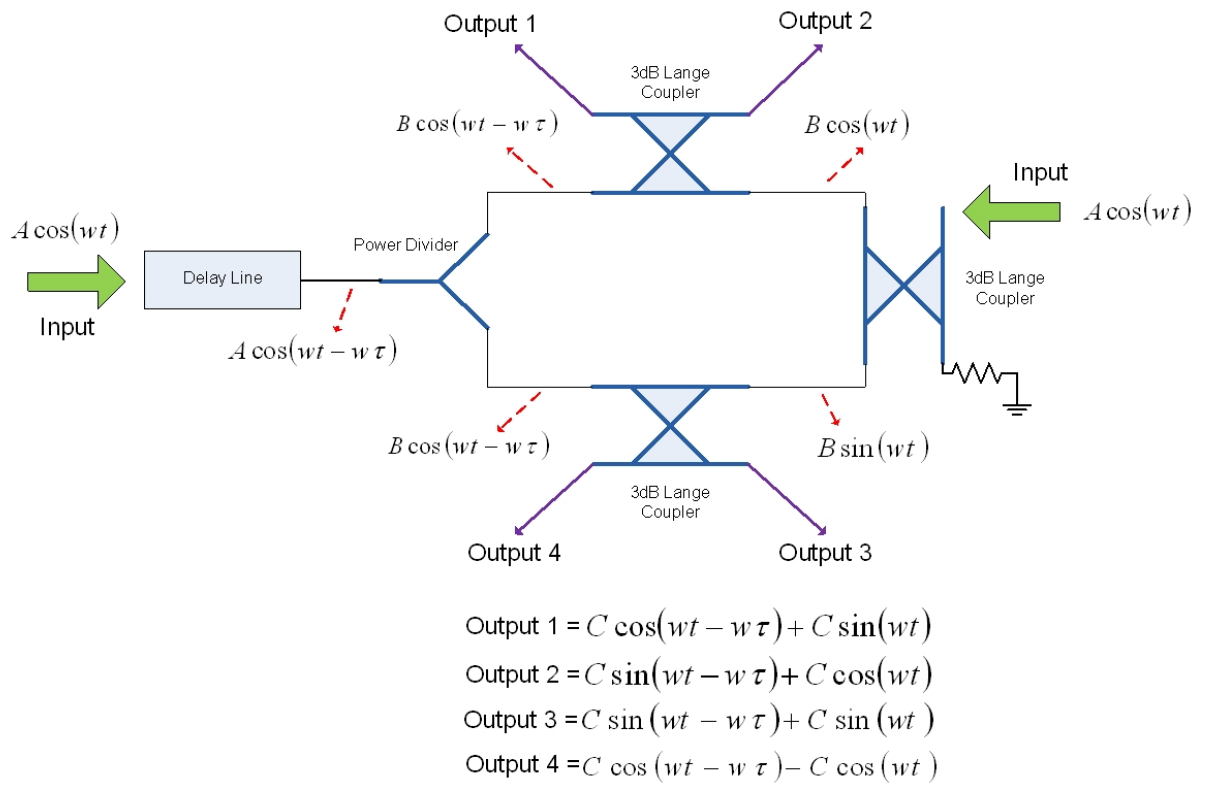


Figure 4.87 Basic block diagram representation of an I/Q discriminator.

According to the design given in Figure 4.87, the outputs of square law detectors will be:

$$A_1 = (\text{Output}_1)^2 = C^2 \cos^2(\omega t - \omega \tau) + C^2 \sin^2(\omega t) + 2C^2 \cos(\omega t - \omega \tau) \sin(\omega t) \quad (4.8)$$

$$A_2 = (\text{Output}_2)^2 = C^2 \sin^2(\omega t - \omega \tau) + C^2 \cos^2(\omega t) + 2C^2 \sin(\omega t - \omega \tau) \cos(\omega t) \quad (4.9)$$

$$A_3 = (\text{Output}_3)^2 = C^2 \sin^2(\omega t - \omega \tau) + C^2 \sin^2(\omega t) + 2C^2 \sin(\omega t - \omega \tau) \sin(\omega t) \quad (4.10)$$

$$A_4 = (\text{Output}_4)^2 = C^2 \cos^2(\omega t - \omega \tau) + C^2 \cos^2(\omega t) - 2C^2 \cos(\omega t - \omega \tau) \cos(\omega t) \quad (4.11)$$

The outputs at the detectors considering the filter action can be written as

$$B_1 = C^2 + C^2 \sin(w\tau) \quad (4.12)$$

$$B_2 = C^2 - C^2 \sin(w\tau) \quad (4.13)$$

$$B_3 = C^2 + C^2 \cos(w\tau) \quad (4.14)$$

$$B_4 = C^2 - C^2 \cos(w\tau) \quad (4.15)$$

From these outputs, θ can be calculated and by using the other tiers' output input signal frequency can be found.

$$E = B_1 - B_2 = 2C^2 \sin(w\tau) \quad (4.16)$$

$$F = B_3 - B_4 = 2A^2 \cos(w\tau) \quad (4.17)$$

$$\theta = \tan^{-1}\left(\frac{E}{F}\right) = \tan^{-1}(\tan(w\tau)) = w\tau \quad (4.18)$$

On the other hand the outputs of discriminators can still be used in voltage sorting to improve the ambiguity solving process. Details will be discussed in related subsections.

4.7.3.1 Filters

High pass and low pass filters are used to provide the required input signals to discriminators. These filters are also fabricated on alumina. Designs, simulation/measurement results of these filters are given in the following subsections.

4.7.3.1.1 6 GHz Low-Pass Filter

8th degree elliptic low pass filter is designed in symmetric form (Figure 4.88). In order to occupy less space open stub at the middle of the filter is separated into two halves (i.e. TL 10 and TL 9).

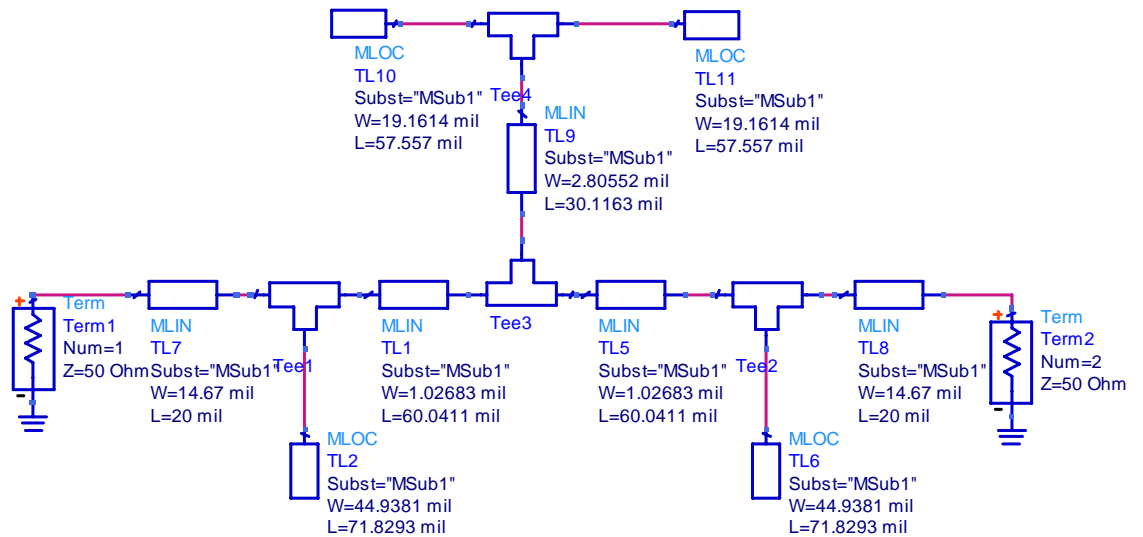


Figure 4.88 Schematic version of low pass filter.

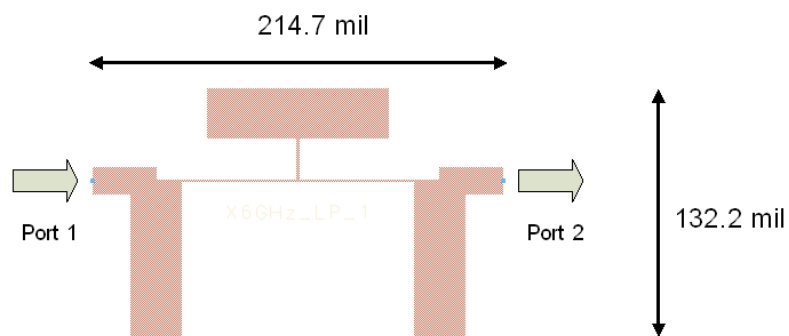


Figure 4.89 Momentum version of low pass filter.

This filter is also fabricated. The S11 and S21 parameters are given in Figure 4.90.

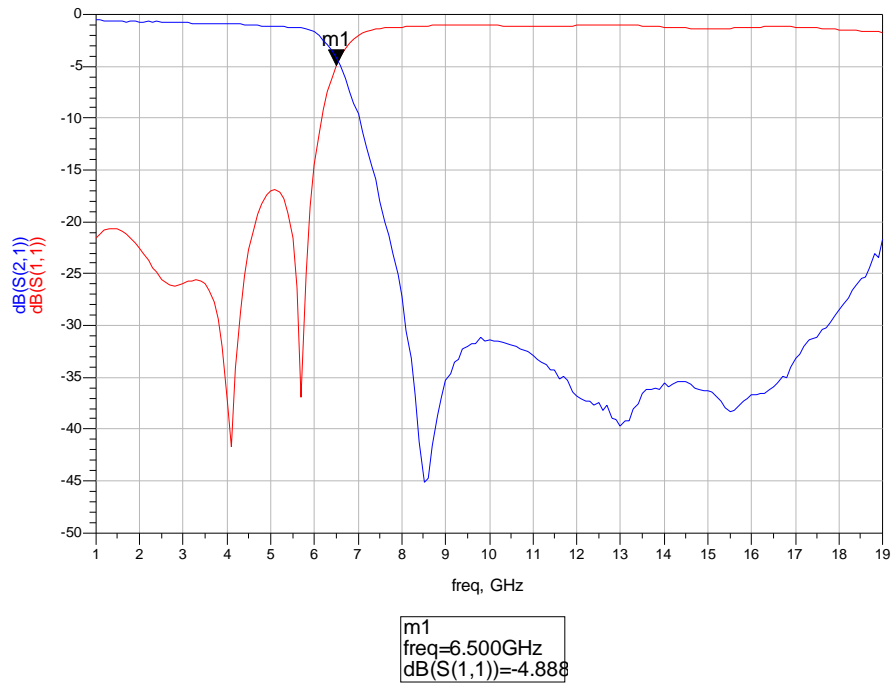


Figure 4.90 Measured response of low pass filter.

4.7.3.1.2 6 GHz High-Pass Filter

Figure 4.91 shows the basic structural design of high pass filter in stub form. To get rid of the red encircled area, the Kuroda transformation given in [40] can be used (Figure 4.92).

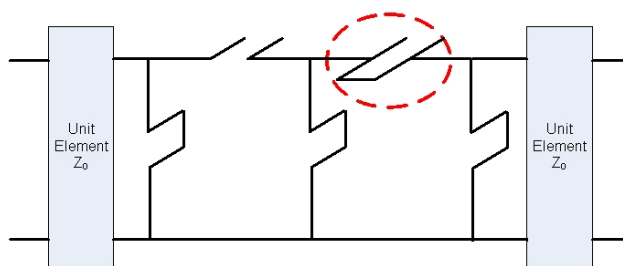


Figure 4.91 6 GHz high pass filter in stub form.

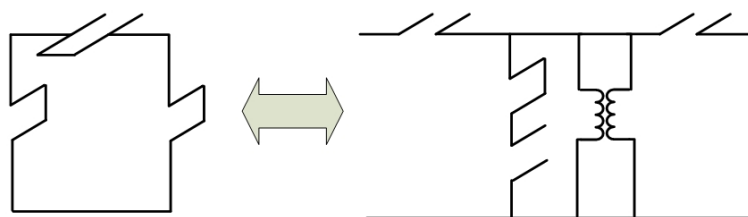


Figure 4.92 Kuroda transformation.

According to this transformation, the high pass filter is designed in ADS (Figure 4.93).

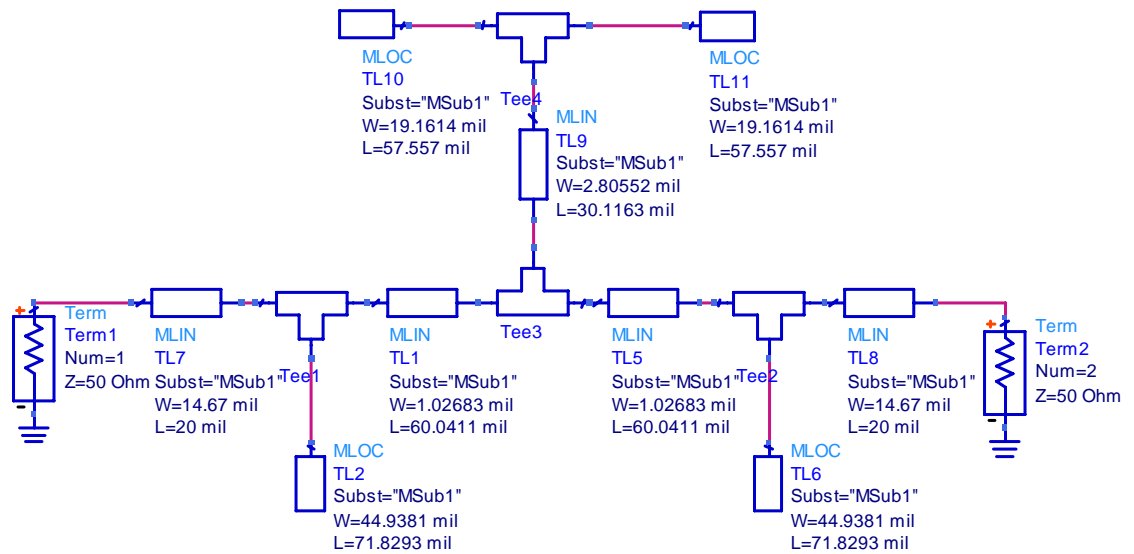


Figure 4.93 Schematic design of 6 GHz high pass filter.

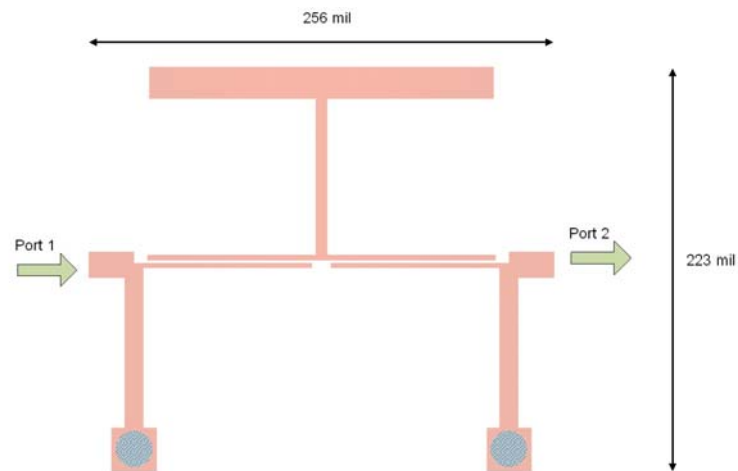


Figure 4.94 Momentum lay out of 6 GHz high pass filter.

This filter is also fabricated. The S11 and S21 parameters are given in Figure 4.95.

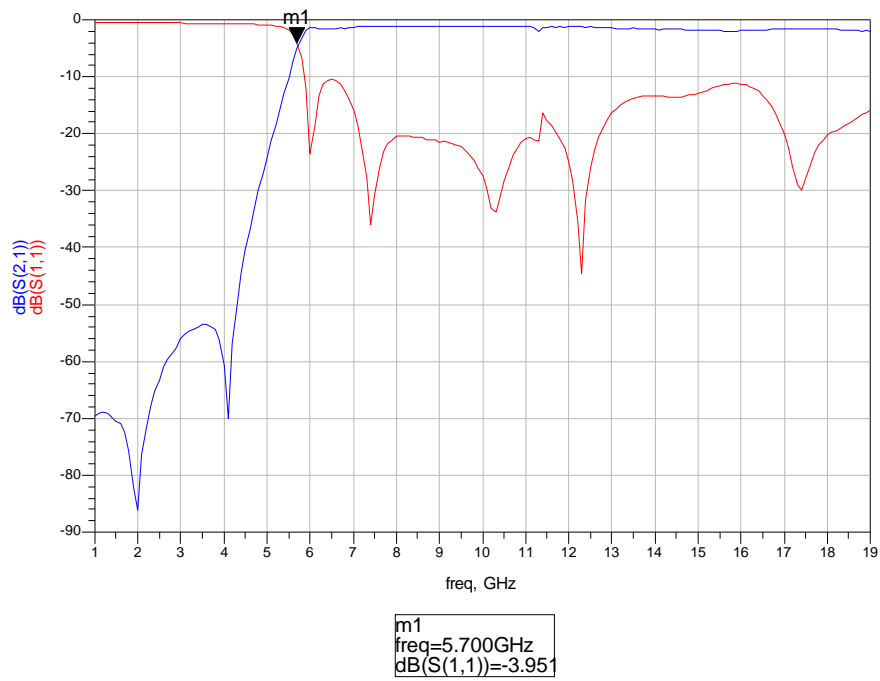


Figure 4.95 Measured response of low pass filter.

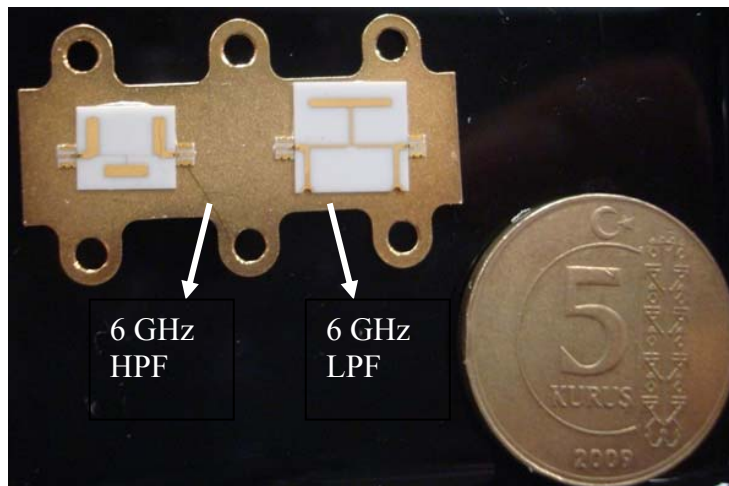


Figure 4.96. Fabricated 6 GHz high pass and low pass filters

4.7.3.2 Delay Line

The maximum time delay of the system is 4ns as decided in section 4.1. This time delay can be obtained by using various ways as follows.

If a structure with $\epsilon_R = 2.2$ (can be suspended substrate or cable) is chosen to minimize the loss, then the length of the delay line will be

$$L = \frac{3.9 \cdot 10^{-9} \cdot 3 \cdot 10^8}{\sqrt{2.2}} \approx 788 \text{ mm} \quad (4.19)$$

But if a structure with $\epsilon_R = 9.8$ (microstrip) is decided to use to reduce the total circuit size, this time the length of the delay line will be

$$L = \frac{3.9 \cdot 10^{-9} \cdot 3 \cdot 10^8}{\sqrt{9.8}} \approx 373 \text{ mm} \quad (4.20)$$

If designer chooses to use a structure other than a cable, in lay-out design step of whole system, instead of reserving a specific area for this delay line, using the empty regions between the other blocks of the system (such as tiers, dividers...etc.) is more reasonable. By this way, relatively little space is used. Or as an alternative, delay line can be designed in different geometric forms, such as spiral, in order to occupy less space on the board. But, actually, using a semi rigid cable seems the most rational choice. By bending the cable much more less space is used compared to a microstrip or a stripline.

The purpose of these calculations above is to create a sense. Depending on the system requirements the designer must decide the frequency resolution. For the simulations given below an approximate 850 mm long delay line with $\epsilon_R = 2.2$ is used. This delay is especially adjusted to 850 mm in order to help in ambiguity resolving process.

4.7.3.3 I/Q Discriminators

As mentioned above, structural form of both of the discriminators is same. Both discriminators have 3 identical Lange couplers and a power splitter. The designs are simulated with 850 mm coaxial cable. The details are given below.

4.7.3.3.1 2-6 GHz I/Q Discriminator

3 section Wilkinson type power divider is designed for this discriminator (Figure 4.97). The momentum simulation results of this discriminator are given in Figure 4.98, Figure 4.99 and Figure 4.100.

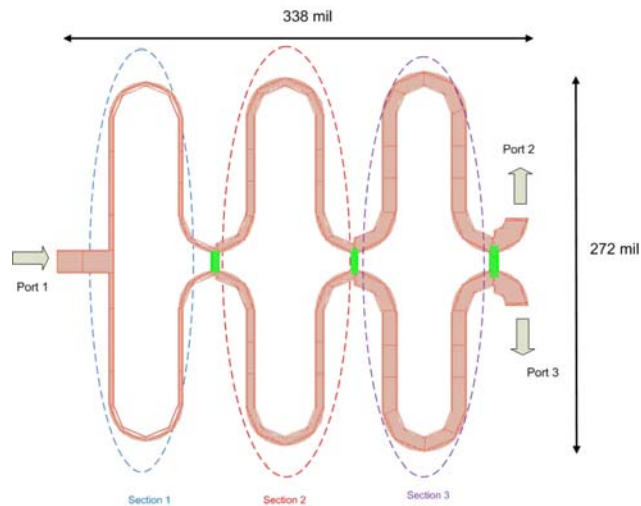


Figure 4.97 2-6 GHz power divider.

The line length of section 1 is approximately 278 mil, the other section line lengths are same which are approximately 286 mil. The line width of each section is nearly 4 mil, 6.5 mil and 11 mil respectively. The values of resistive elements are 131 ohm, 196 ohm and 197 ohm from left to right. The length/width of the line at port 1 is nearly 37 mil / 16 mil. The lines at port 2 and port 3 are same in length/width and they are nearly 25 mil / 16 mil.

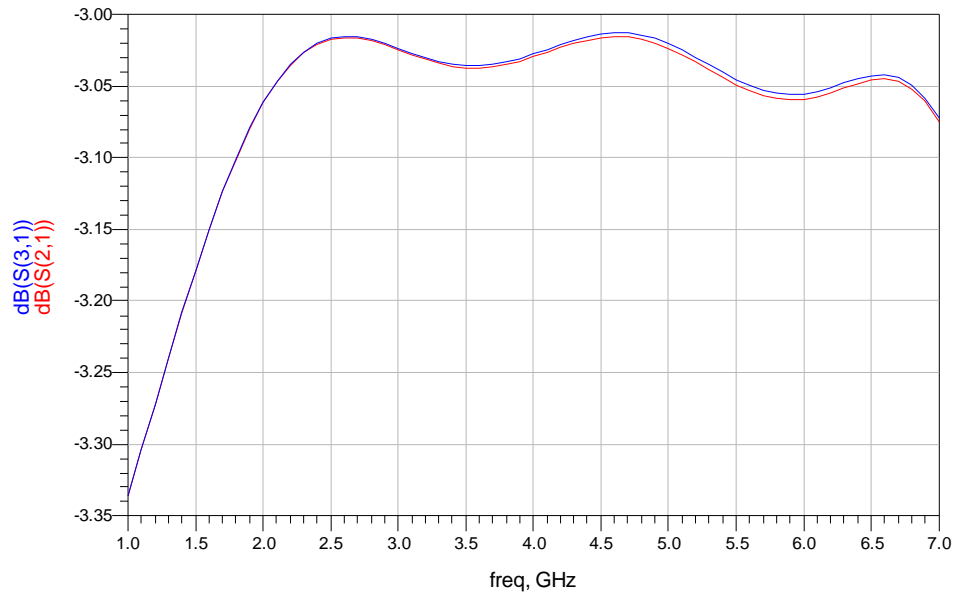


Figure 4.98 S21 and S31 of 2-6GHz power divider.

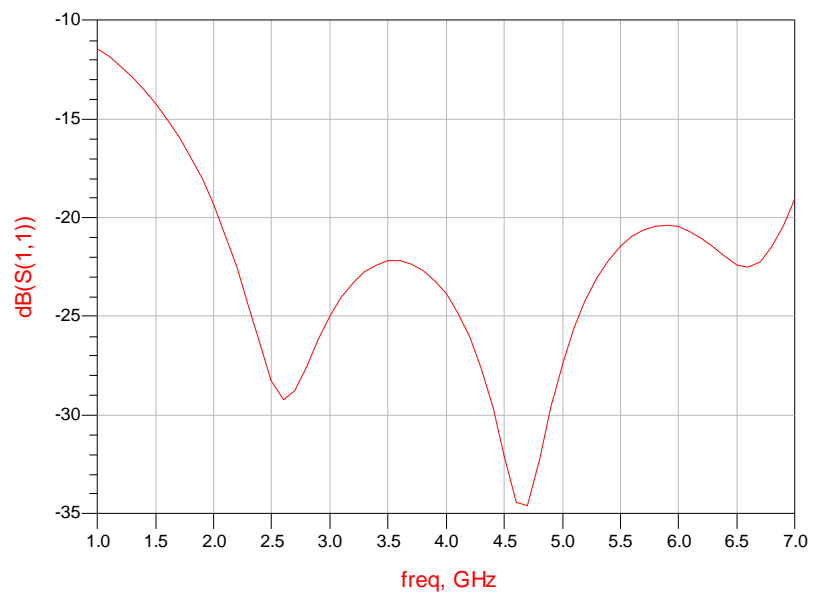


Figure 4.99 S11 of 2-6 GHz power divider.

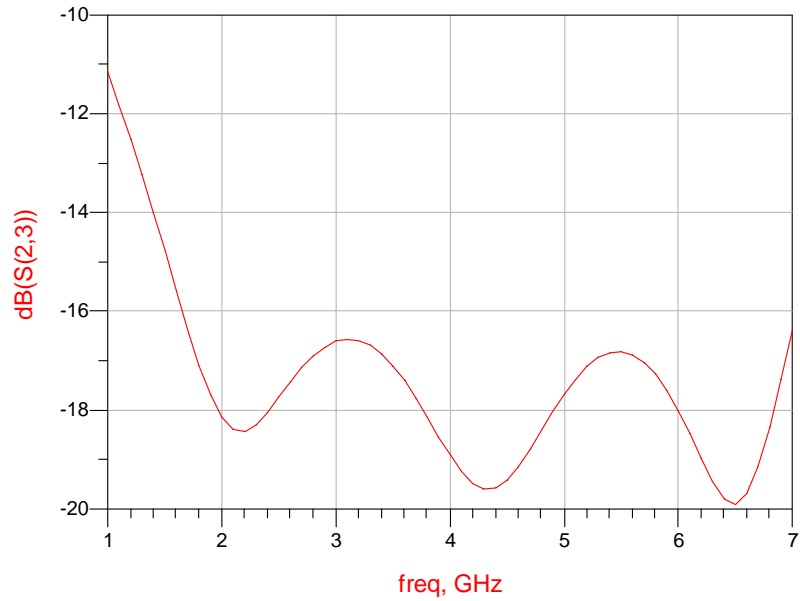


Figure 4.100 Isolation between output ports of 2-6 GHz power divider.

The other component of this discriminator is Lange coupler. A four finger Lange coupler is designed for this purpose. Line widths and lengths are nearly 1.37 mil and 288 mil respectively. The spacing between lines is approximately 1 mil. The momentum layout of this coupler and simulation solutions are given below. As can be seen from Figure 4.101, the response is over-coupled. But it is actually the usual case for wide-band operations.

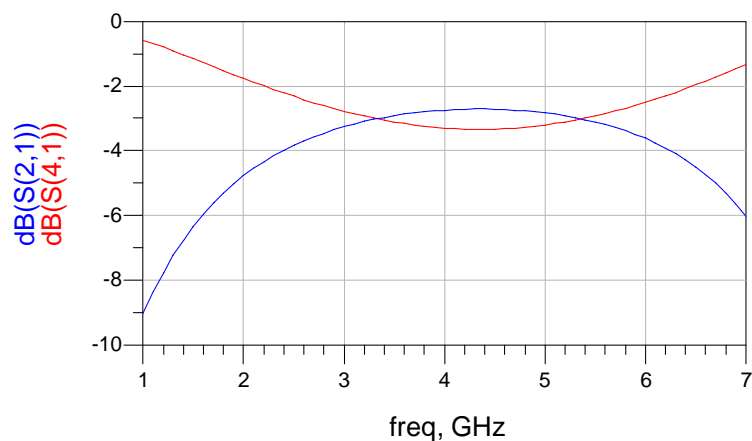


Figure 4.101 Through and coupled ports of 2-6 GHz Lange coupler.

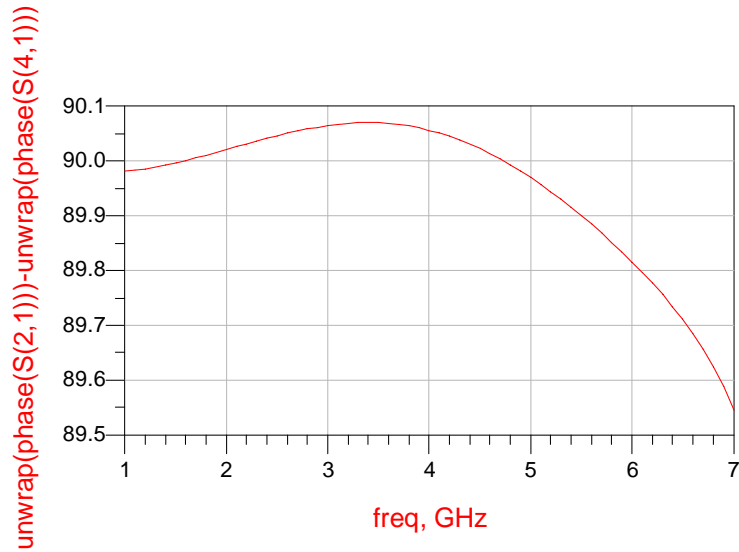
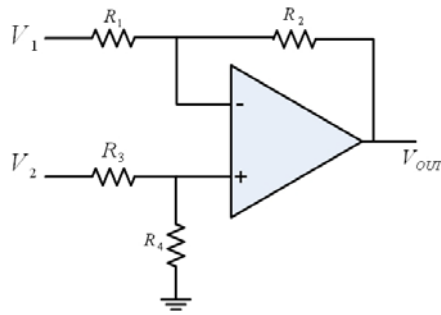


Figure 4.102 Phase difference between through and coupled ports.

After designing the required components, 2-6 GHz I/Q discriminator is constructed as shown in Figure 4.104. Here, green arrows show the delayed and undelayed input signals. Red encircled areas show the bias points of each diode. The diodes (X16, X17, X18, X19) are matched to the circuit by using parallel thin film resistors. Orange spots with numbers show the measurement points. Voltage values obtained from these points are used in calculations as defined in equation (4.18). Additionally they can be also used in ambiguity solving process.

In Figure 4.107, the outputs of medium 3 and 2-6 GHz I/Q discriminator are given. Figure 4.108 shows another nested form. Here, the differences between the outputs (i.e. $V_3 - V_1$ and $V_4 - V_2$) and the outputs of medium tier 3 is given. This difference can be made in digital card after sampling or by a difference amplifier like the one given in Figure 4.103 [39].



$$V_{OUT} = \left(\frac{R_1 + R_2}{R_3 + R_4} \right) \frac{R_4}{R_1} V_2 - \frac{R_2}{R_1} V_1$$

For $R_1 = R_3$ and $R_2 = R_4$

$$V_{OUT} = \frac{R_2}{R_1} (V_2 - V_1)$$

$$R_1 // R_2 = R_3 // R_4$$

Figure 4.103 Difference amplifier.

An important discussion must be made about Figure 4.107 and Figure 4.108. In Figure 4.107, every voltage cycle intersection point of medium tier 3 there is a voltage peaking of the fine tier. On the other hand, as can be seen in Figure 4.108, the outputs of difference between detector pairs fit the voltage peaks of the medium tier 3. The delay line is especially adjusted to obtain such outputs from each of the fine tiers in order to ease the ambiguity resolving process.

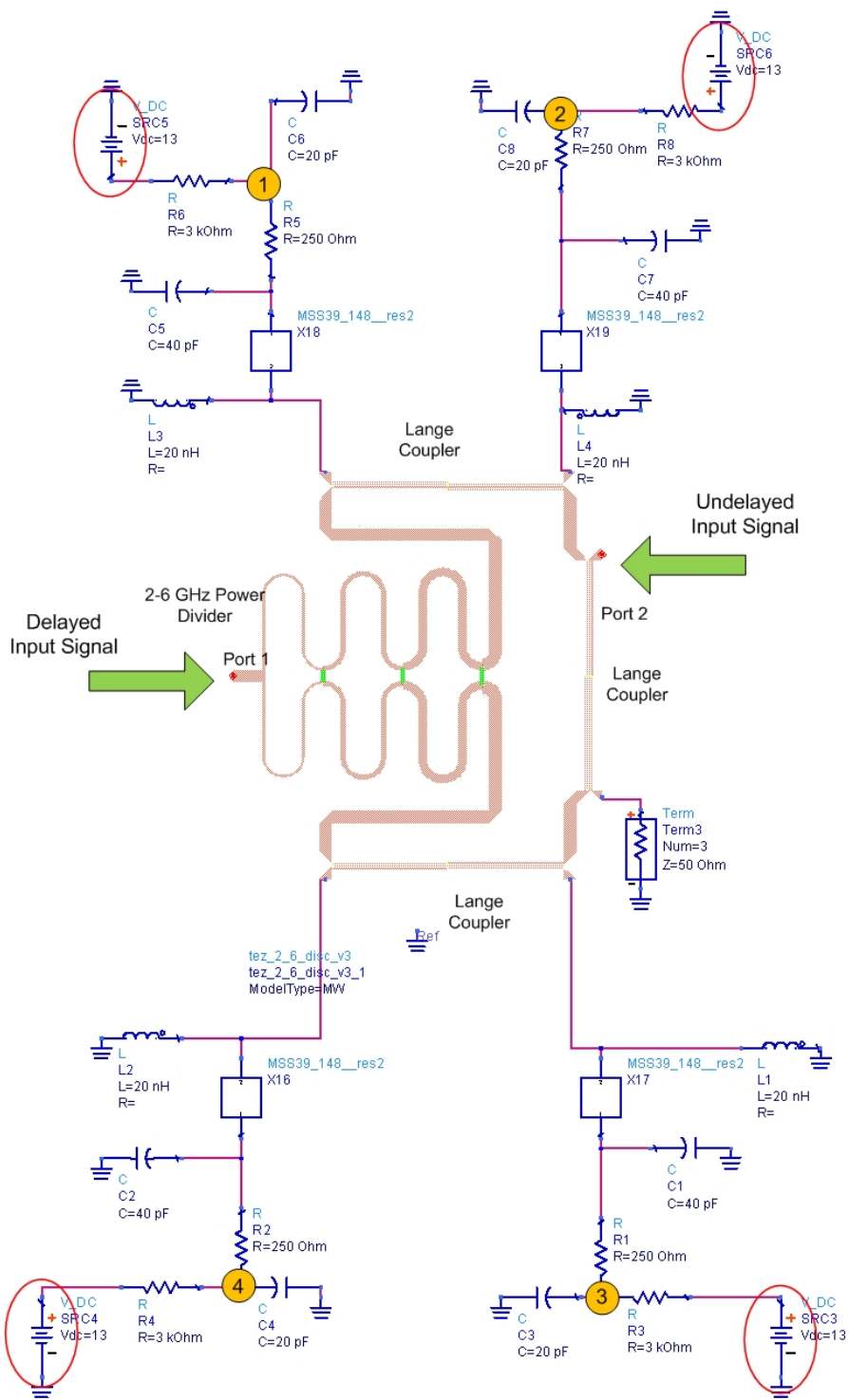


Figure 4.104 2-6 GHz I/Q discriminator.

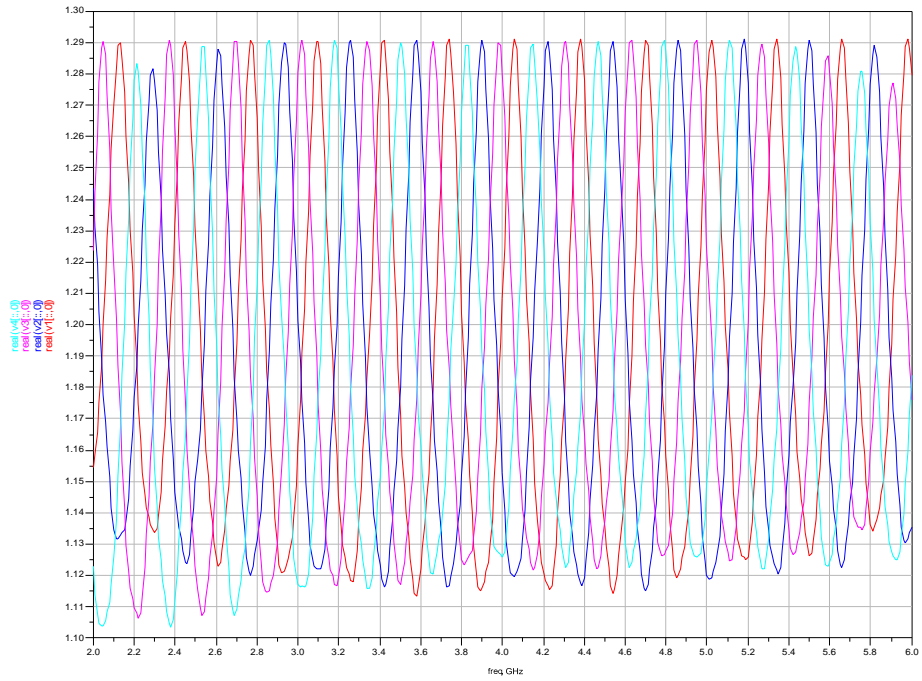


Figure 4.105 Output of 2-6 GHz I/Q Discriminator.

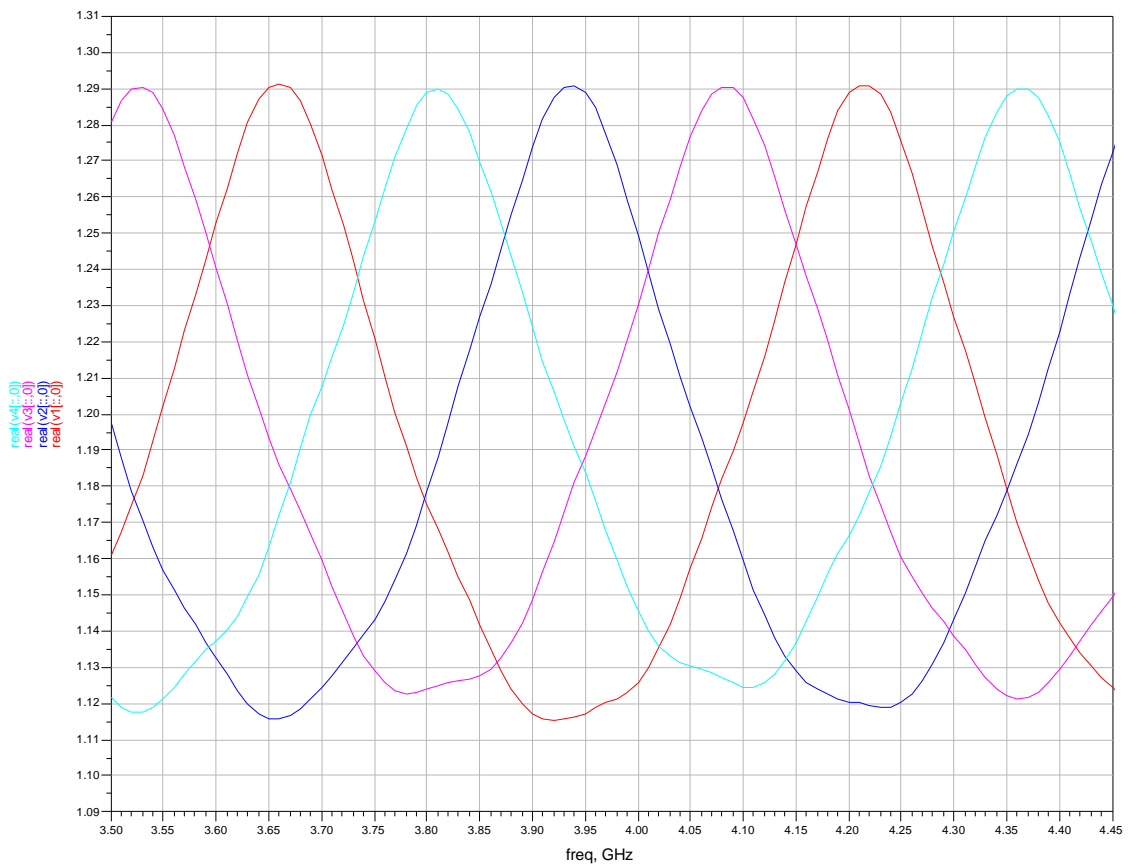


Figure 4.106 Output of 2-6 GHz I/Q Discriminator (zoomed around 4 GHz).

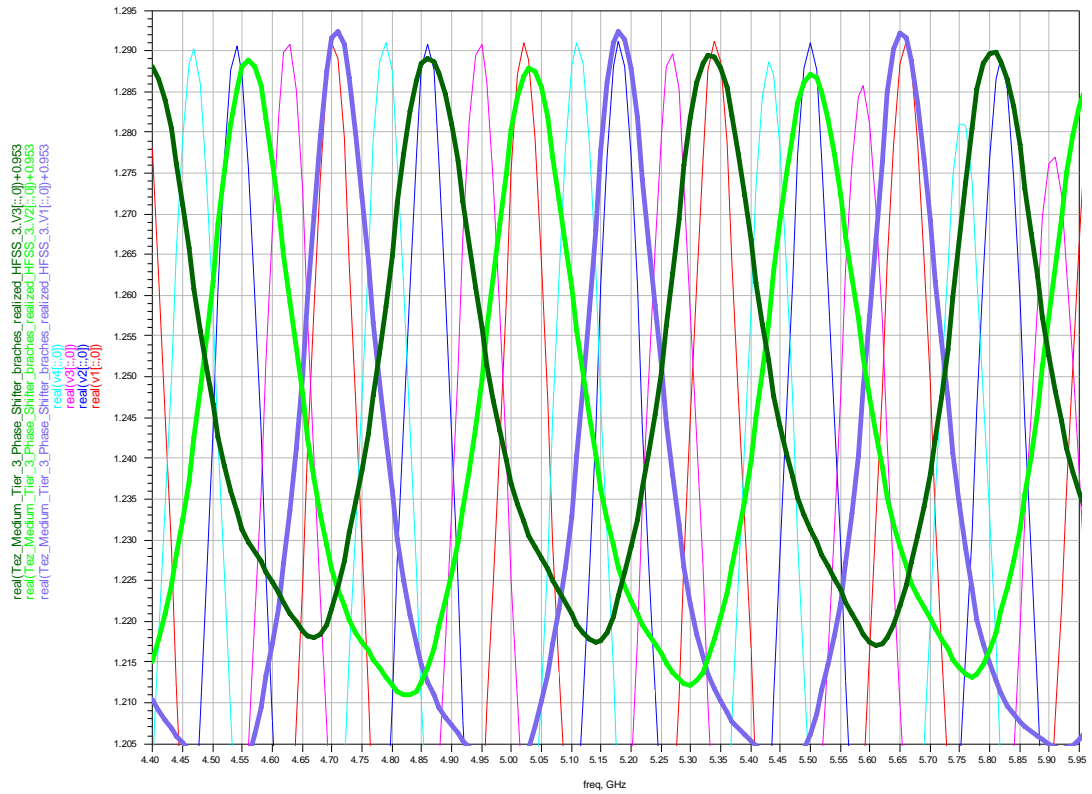


Figure 4.107 Outputs of medium tier 3 and 2-6 GHz I/Q discriminator zoomed around 5 GHz in nested form.

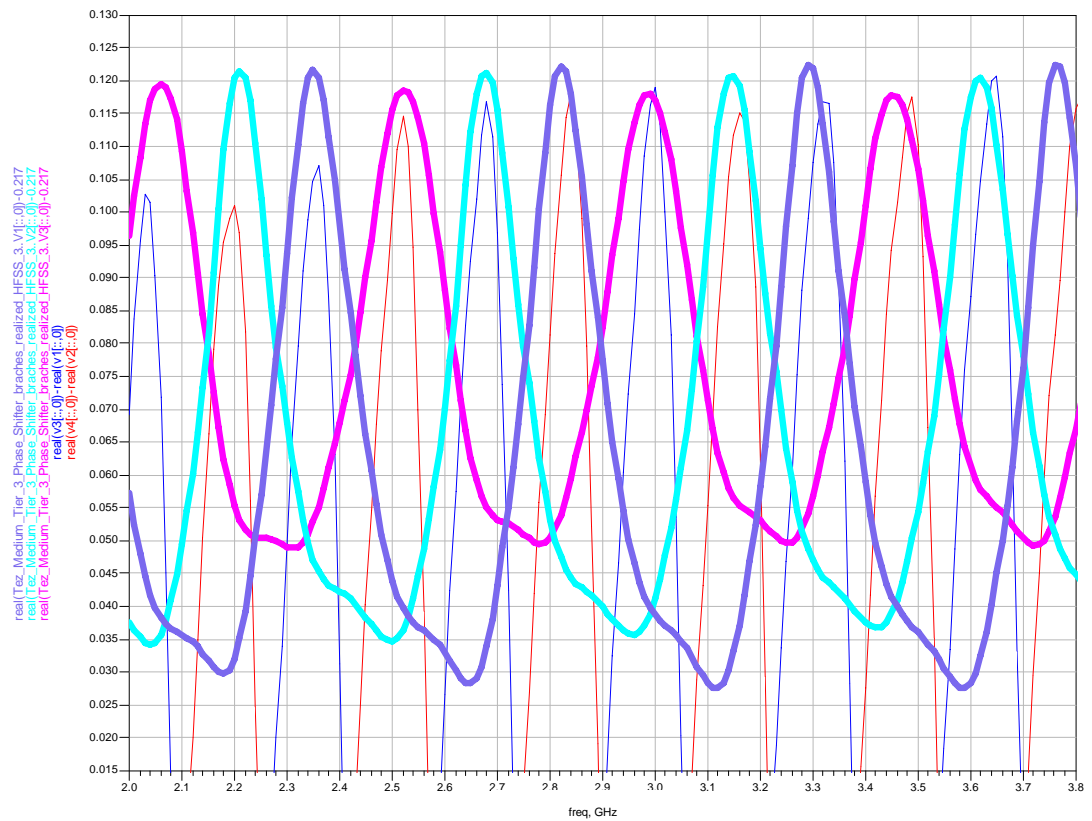


Figure 4.108 Differences of output pairs in 2-6 I/Q discriminator in nested form with medium tier 3.

4.7.3.3.2 6-18 GHz I/Q Discriminator

A 3 section Wilkinson type power divider is designed for this discriminator (Figure 4.109). The momentum simulation results of this discriminator are given in Figure 4.110, Figure 4.111 and Figure 4.112.

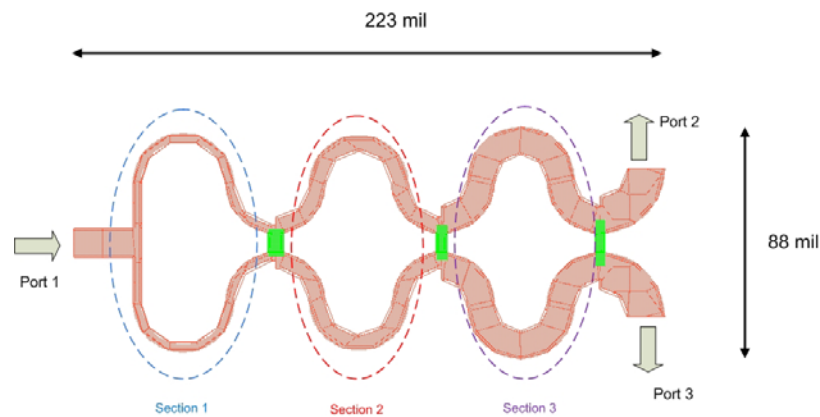


Figure 4.109 Layout of 6-18 GHz power divider.

The approximate line lengths/widths of sections are 100 mil / 3.2 mil, 95 mil / 6.2 mil, and 94 mil / 10.6 mil respectively. The values of resistive elements are 81 ohm, 158 ohm and 249 ohm from left to right. The length and width of the line at port 1 are 11 mil and 22 mil. The lines at port 2 and port 3 are same in length/width and they are 26 mil and 14 mil respectively.

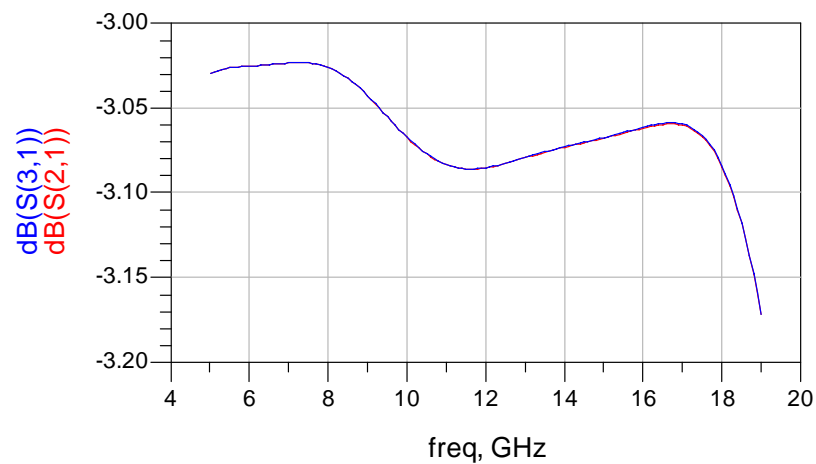


Figure 4.110 S21 and S31 of 6-18 GHz power divider.



Figure 4.111 S11 of 6-18 GHz power divider.

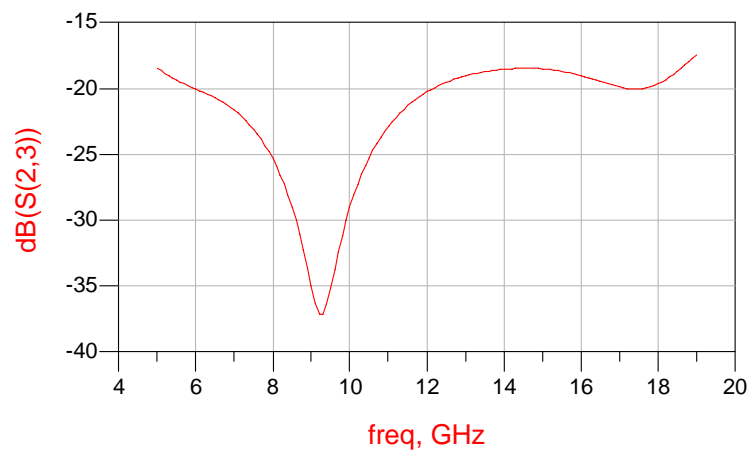


Figure 4.112 Isolation between output ports of 6-18 GHz power divider.

Like the one given for 2-6 GHz I/Q discriminator, four finger Lange coupler is designed. Line widths and lengths are nearly 1.27 mil and 95 mil respectively. The spacing between lines is approximately 1 mil. The momentum layout of this coupler and simulation solutions are given below. As can be seen from Figure 4.113, like the other coupler, the response is over-coupled.

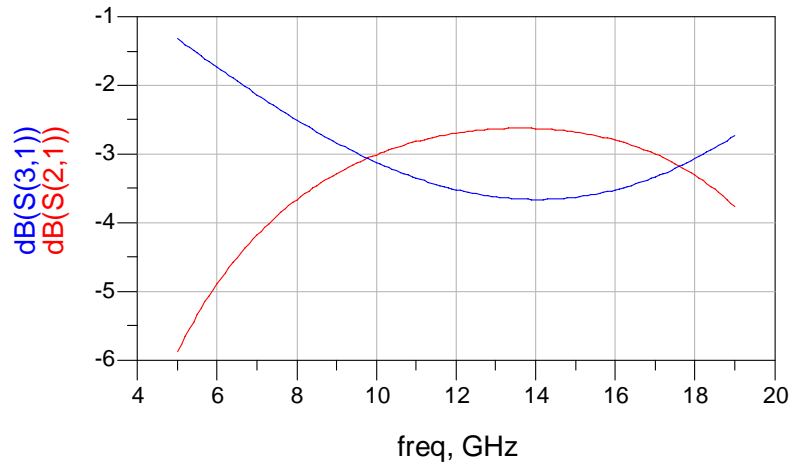


Figure 4.113 S21 and S31 of 6-18 GHz Lange coupler.

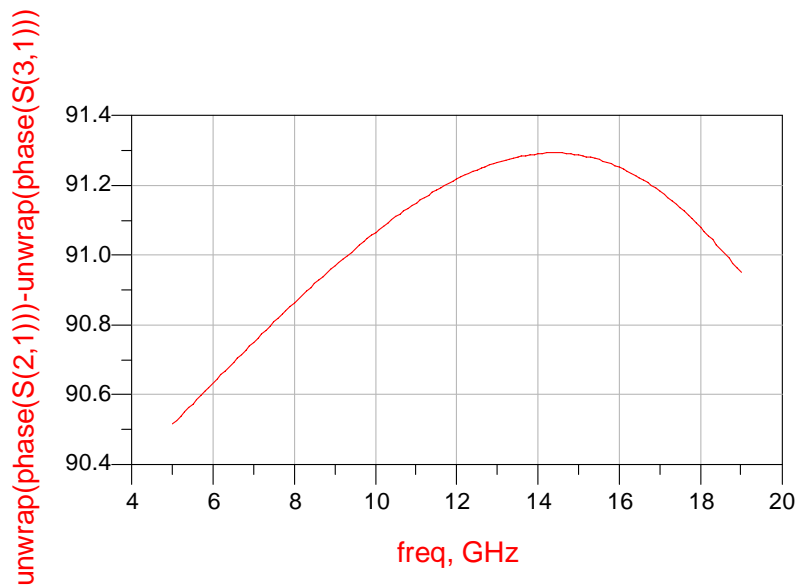


Figure 4.114 Phase difference between coupled and isolated ports.

In Figure 4.115, 6-18 GHz I/Q discriminator design is presented. Here, green arrows show the delayed and undelayed input signals. Red encircled areas show the bias points of each diode. The diodes (X16, X17, X18, X19) are matched to the circuit by using parallel thin film resistors. Orange spots with numbers show the measurement points. As mentioned for the previous discriminator the voltages measured from these points are used in calculations as defined in equation (4.18).

In Figure 4.117, nested form of the outputs of medium 3 and 2-6 GHz I/Q discriminator are given. Figure 4.118 shows the differences between the outputs (i.e. $V_3 - V_1$ and $V_4 - V_2$) and the outputs of medium tier 3.

The discussions made for ambiguity resolving process in 2-6 GHz I/Q discriminator section is also valid for this one.

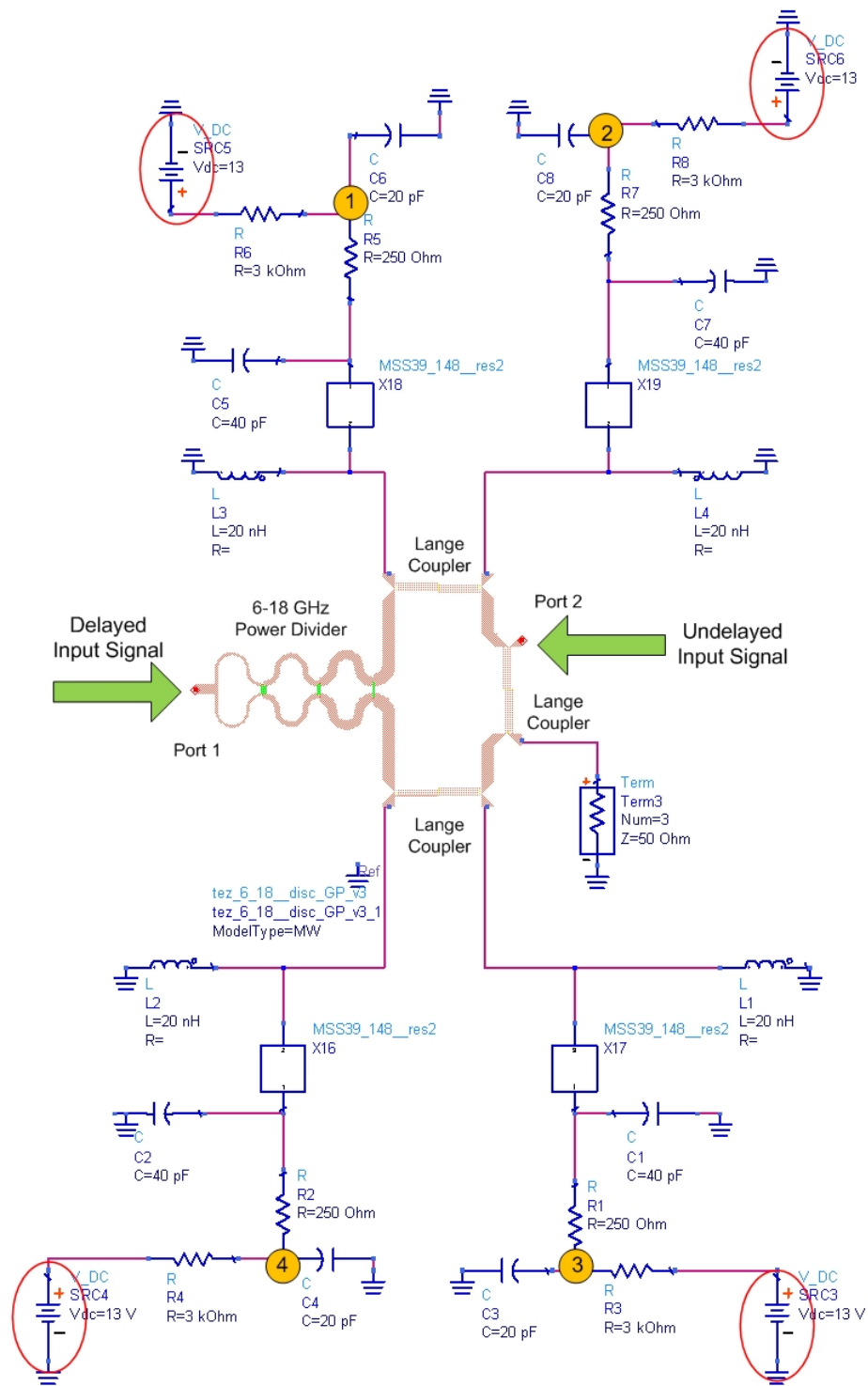


Figure 4.115 6-18 GHz I/Q discriminator.

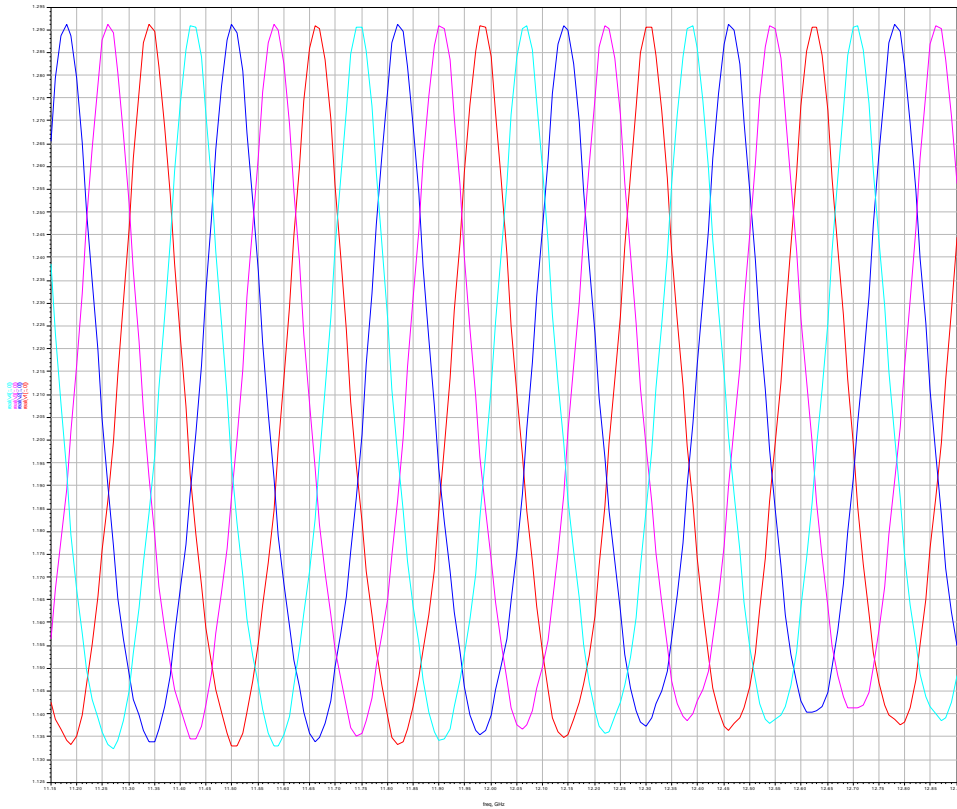


Figure 4.116 Output of 6-18 GHz I/Q Discriminator (zoomed around 12 GHz).

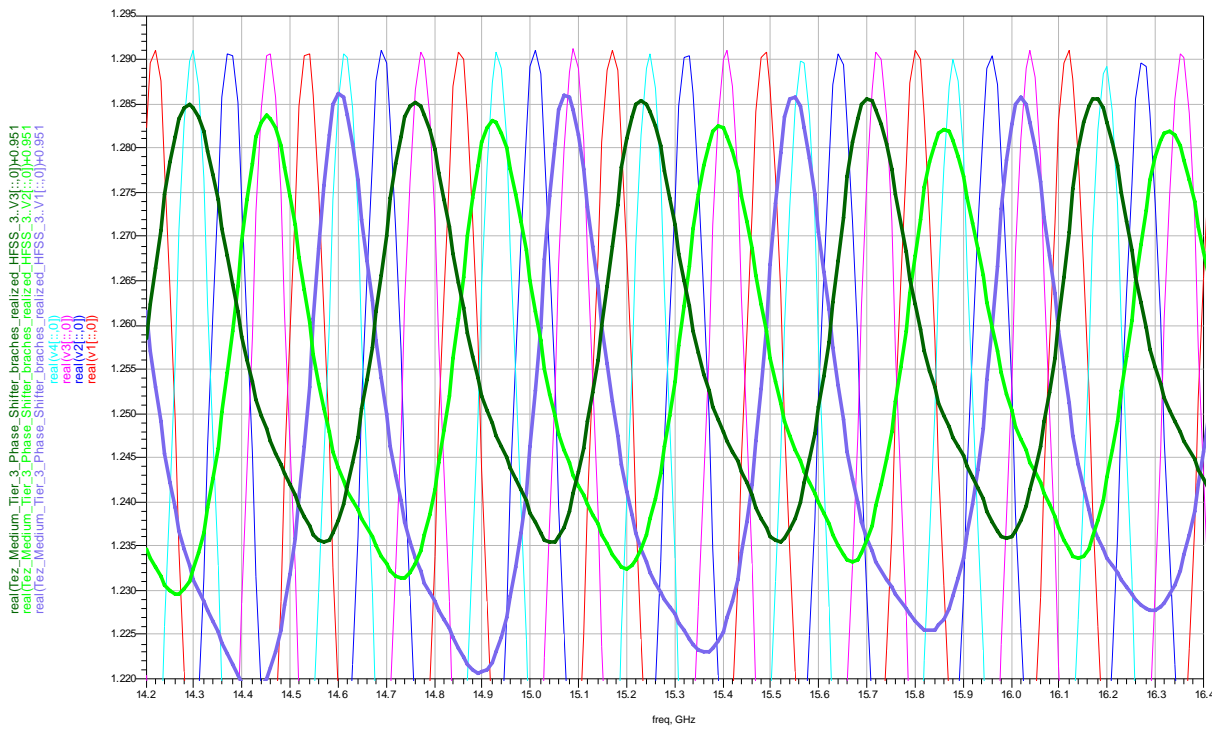


Figure 4.117 Outputs of medium tier 3 and 6-18 GHz I/Q discriminator around 15 GHz in nested form.

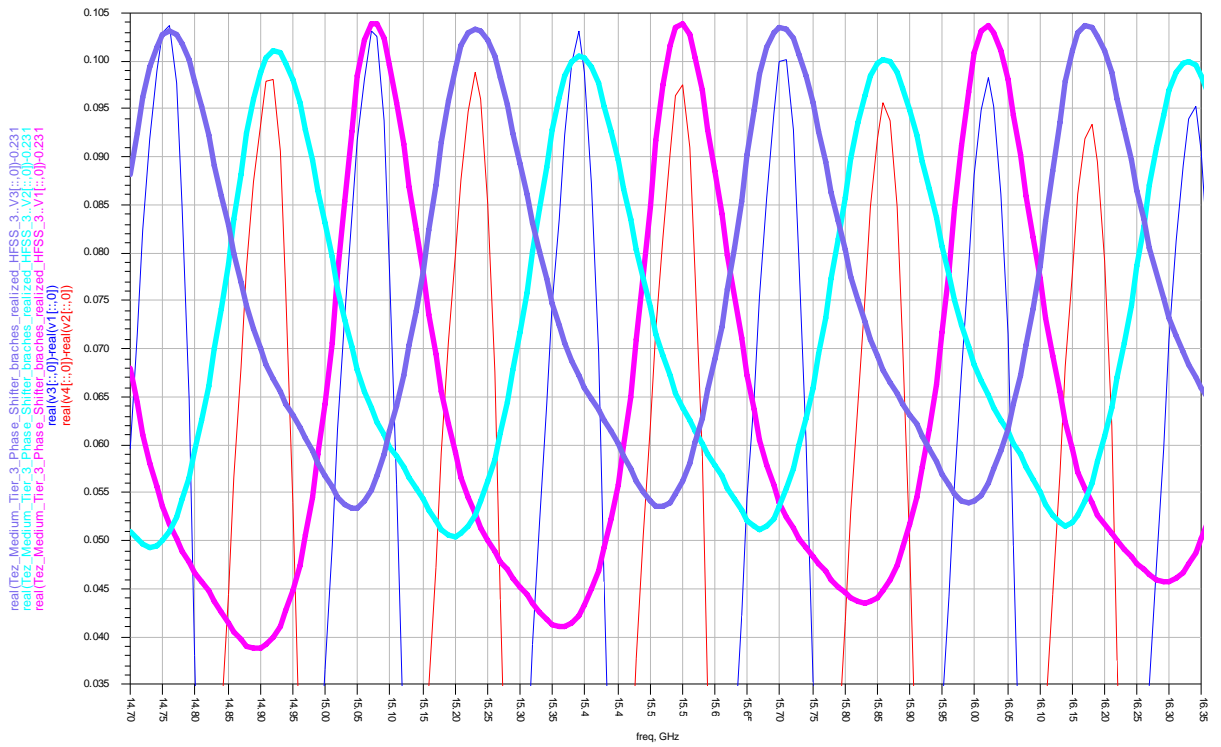


Figure 4.118 Differences of output pairs in 6-18 I/Q discriminator in nested form with medium tier 3.

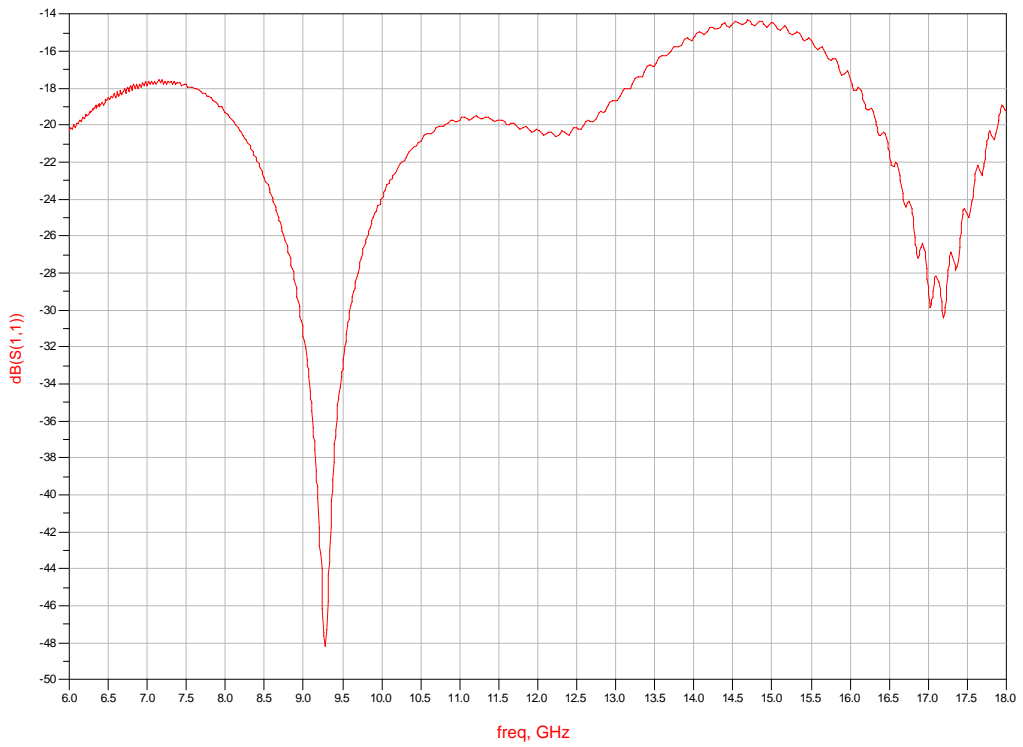


Figure 4.119 Return loss of port 1 in 6-18 GHz I/Q discriminator.

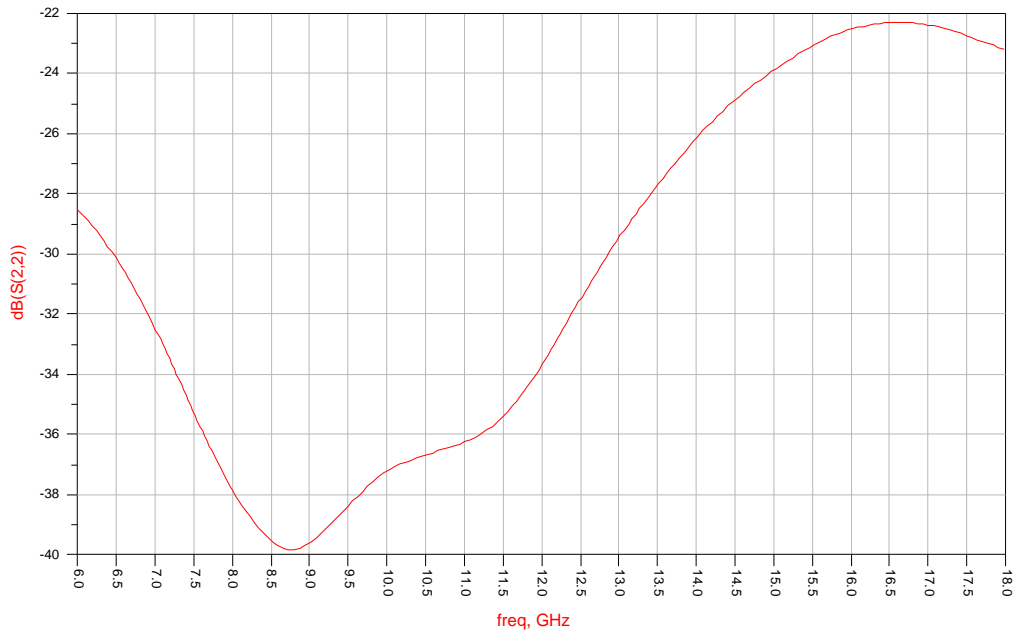


Figure 4.120 Return loss of port 2 in 6-18 GHz I/Q discriminator.

4.7.3.4 Measurement Results

Both I/Q discriminators are fabricated on alumina. Figure 4.121 and Figure 4.122 show fabricated 2-6 GHz and 6-18 GHz I/Q discriminators respectively.

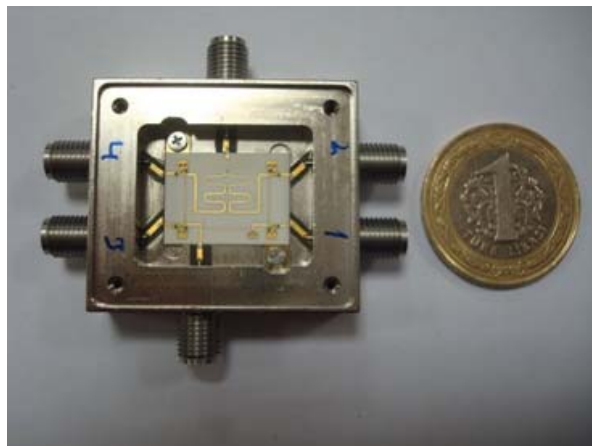


Figure 4.121 Fabricated 2-6 GHz I/Q Discriminator.

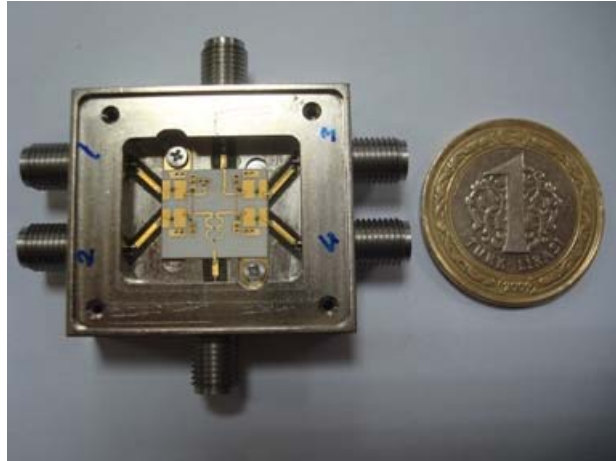


Figure 4.122 Fabricated 2-6 GHz I/Q Discriminator.

For 6-18 GHz I/Q discriminator, detector outputs are measured. The overall result is given in Figure 4.123. Here, a 6 inch coaxial cable is used as delay line and the input power is 10 dBm.

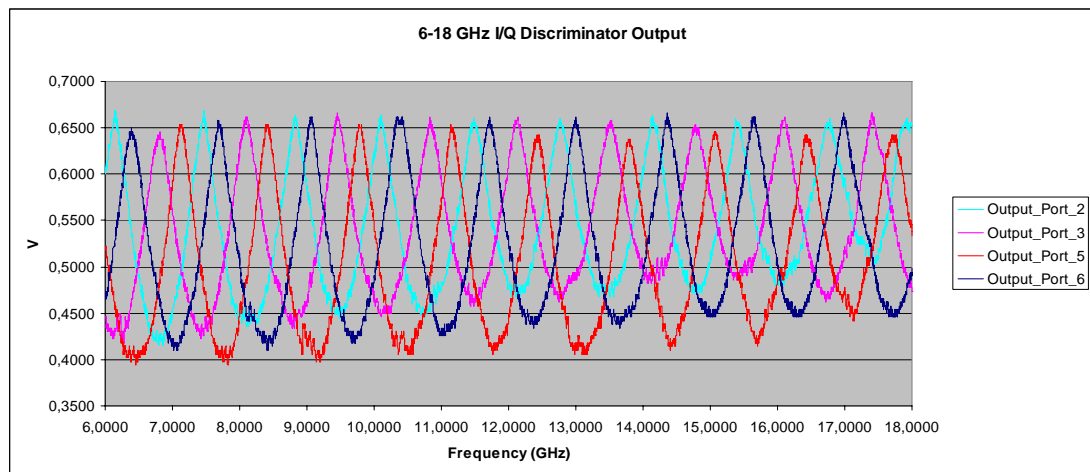


Figure 4.123 Fabricated 6-18 GHz I/Q discriminator detector outputs.

If a 6 inch cable is used as a delay line in ADS, the response given in Figure 4.124 is obtained. As can be seen the zoomed version of the response of fabricated discriminator (Figure 4.125), these two results are similar.

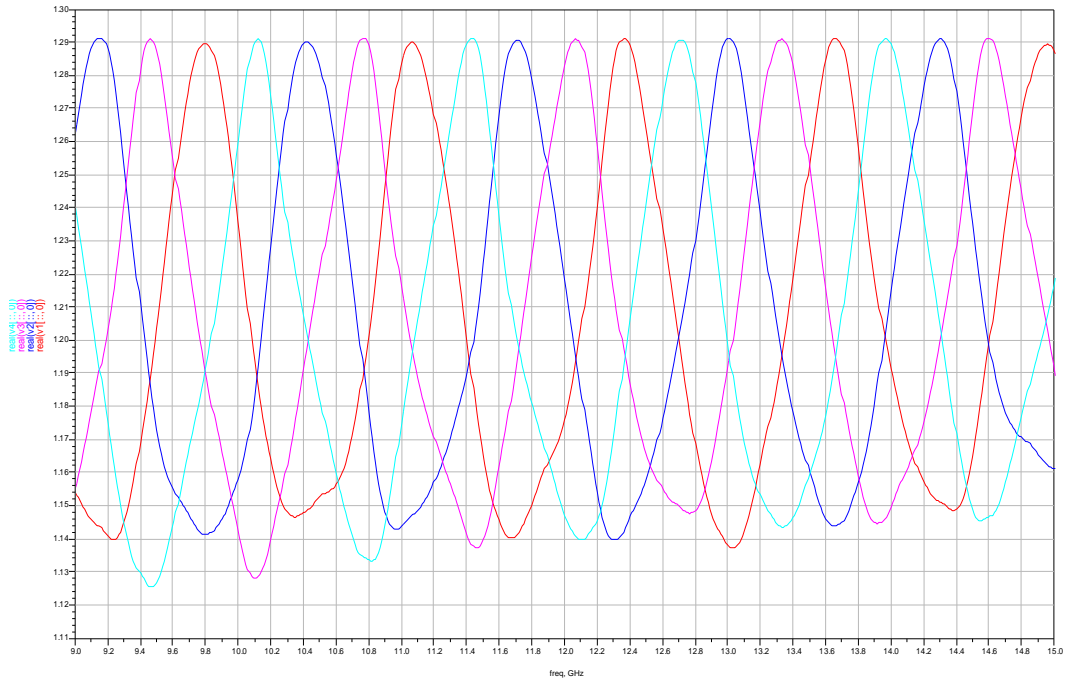


Figure 4.124 Detector outputs of 6-18 GHz I/Q discriminator when a 6 inch cable is used (zoomed around 12 GHz).

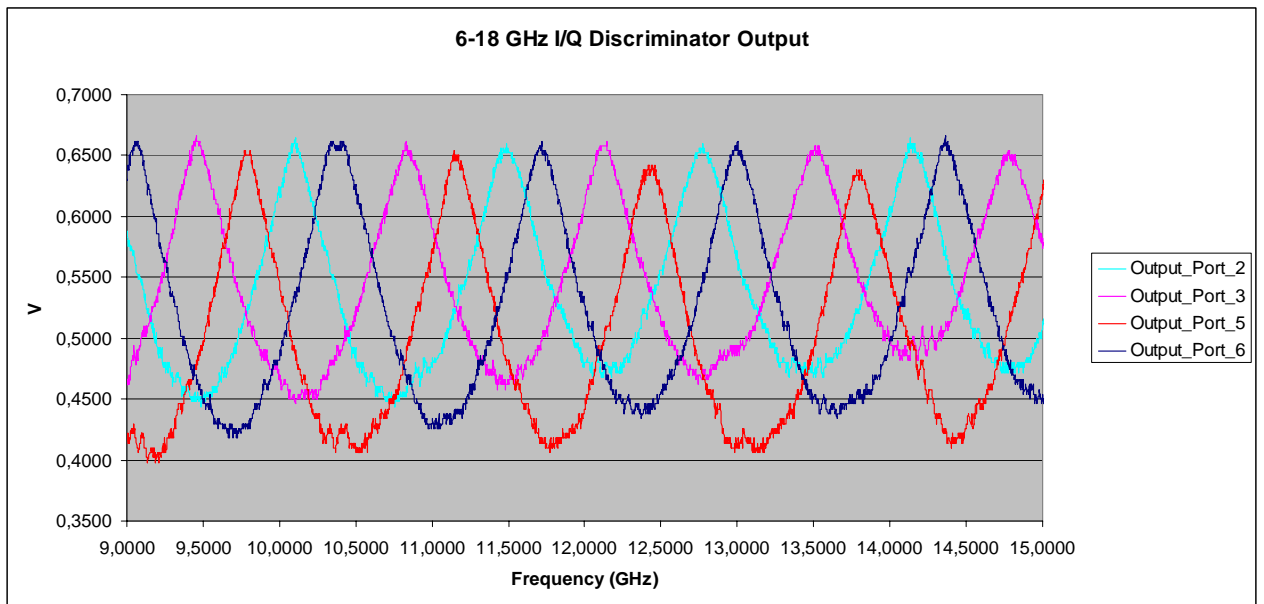


Figure 4.125 Detector outputs of fabricated 6-18 GHz I/Q discriminator (zoomed around 12 GHz).

For 2-6 GHz I/Q discriminator additional circuit components (i.e. detector diodes, inductive/capacitive elements, resistors) are not placed yet. Because of that, only s-parameters could be measured for this component. Simulation results in ADS and measured s-parameters are given in below figures. Figure 4.126 and Figure 4.128 are the simulation results. It can be seen that these two results are so similar with their corresponding measured ones which are give in Figure 4.127 and Figure 4.129 respectively. However for differential phase responses, simulated and measured results do not exactly match to each other. But still the measured differential phase responses look promising as can be seen from Figure 4.131 and Figure 4.133. This phase difference may come from the additional layout and measurement effects that are not included in simulations and/or imperfections of Lange couplers.

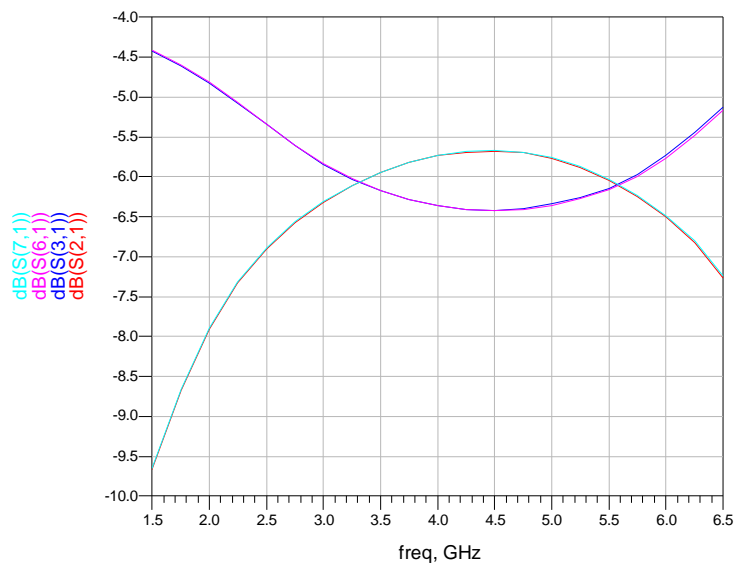


Figure 4.126 Insertion losses with respect to the port 1 (ADS version).

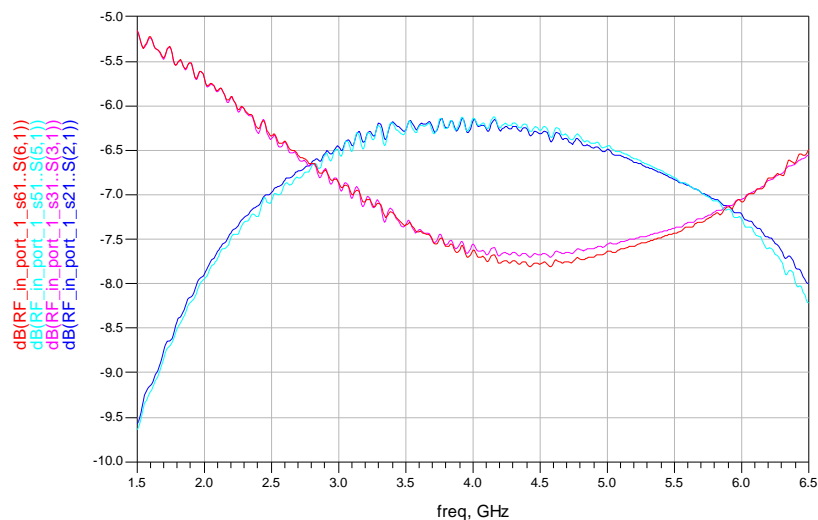


Figure 4.127 Insertion losses with respect to the port 1 (fabricated discriminator).

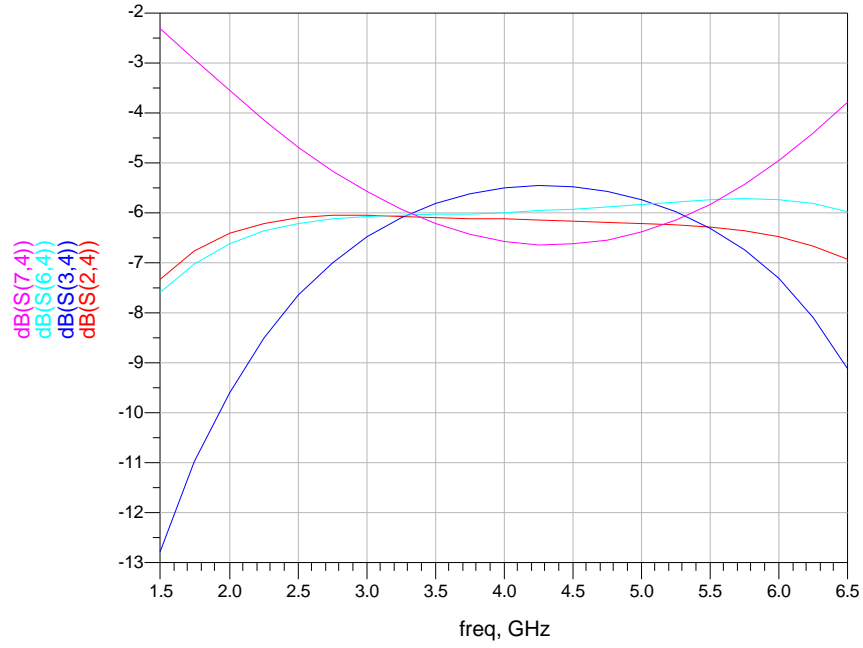


Figure 4.128 Insertion losses with respect to the port 2 (ADS version).

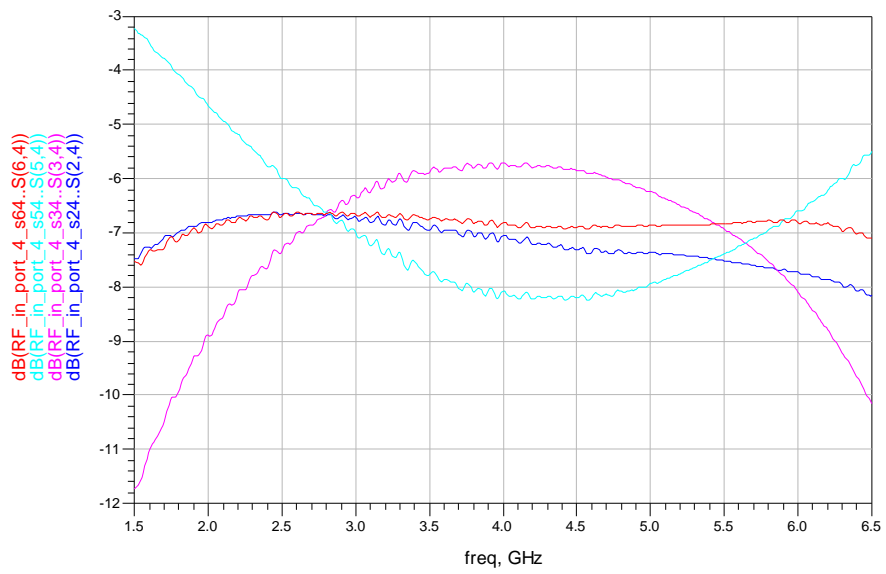


Figure 4.129 Insertion losses with respect to the port 2 (fabricated discriminator).

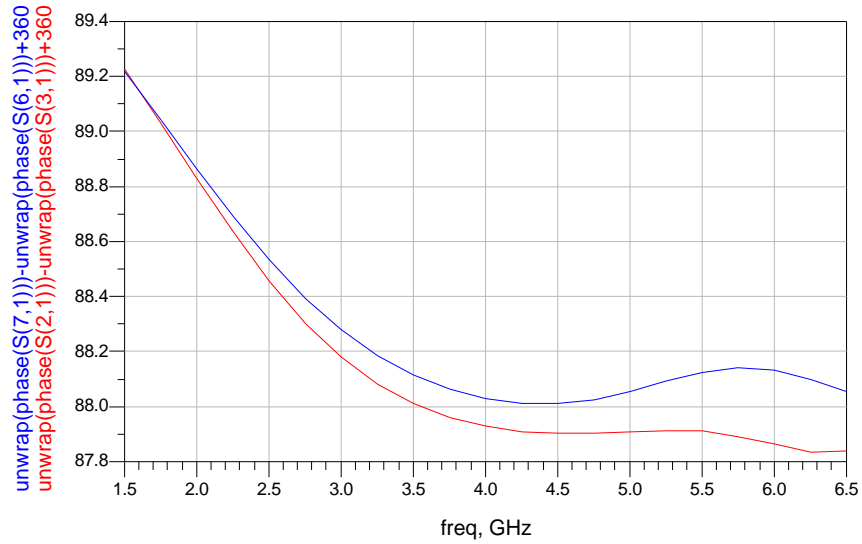


Figure 4.130 Differential phase response between output arms when the input is given from port 1 (ADS version).

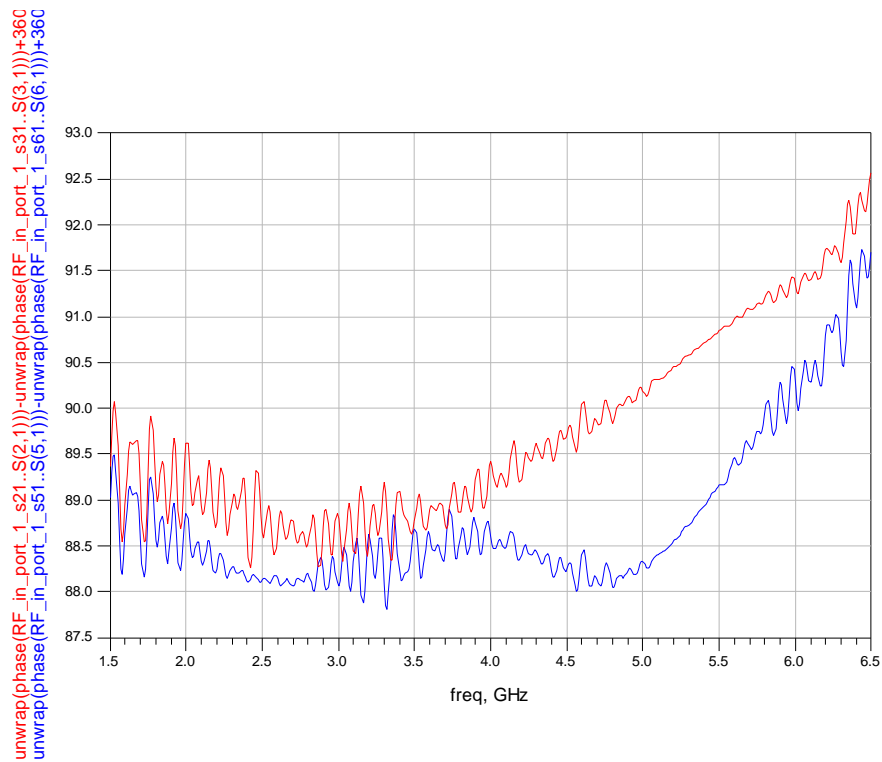


Figure 4.131 Differential phase response between output arms when the input is given from port 1 (fabricated discriminator).

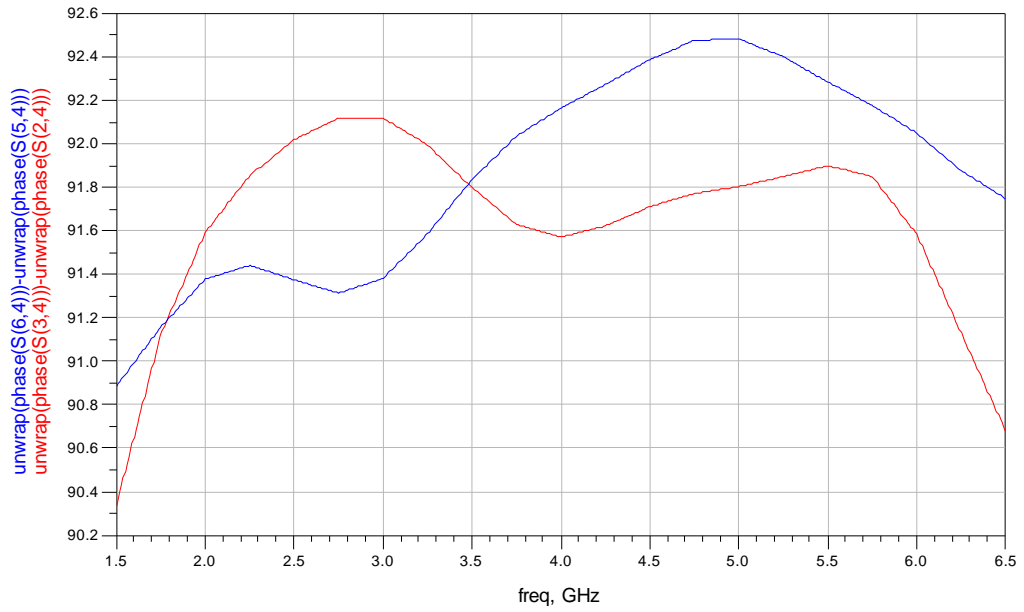


Figure 4.132 Differential phase response between output arms when the input is given from port 2 (ADS version).

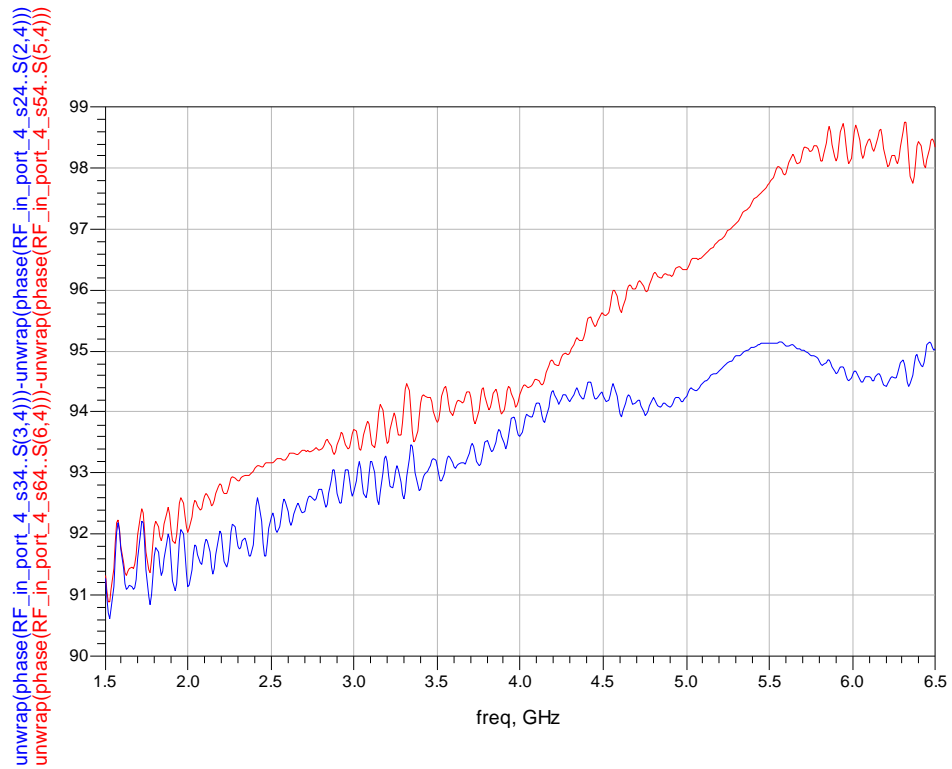


Figure 4.133 Differential phase response between output arms when the input is given from port 2 (fabricated discriminator).

4.8 Final Structure

Figure 4.134 shows the ADS version of final frequency discriminator. In a sense, this figure represents a summary of the designed/fabricated parts of the frequency discriminator. Outputs of this design are given in the figures below. Here, measured s-parameters of the components are used for fabricated parts. Other parts are the momentum components already presented previous sections. Attenuators are used to adjust the input power for every block and to hold the return loss below -15 dBm. The delay line length used in fine tier is 850 mm. The input signal power is 6 dBm.

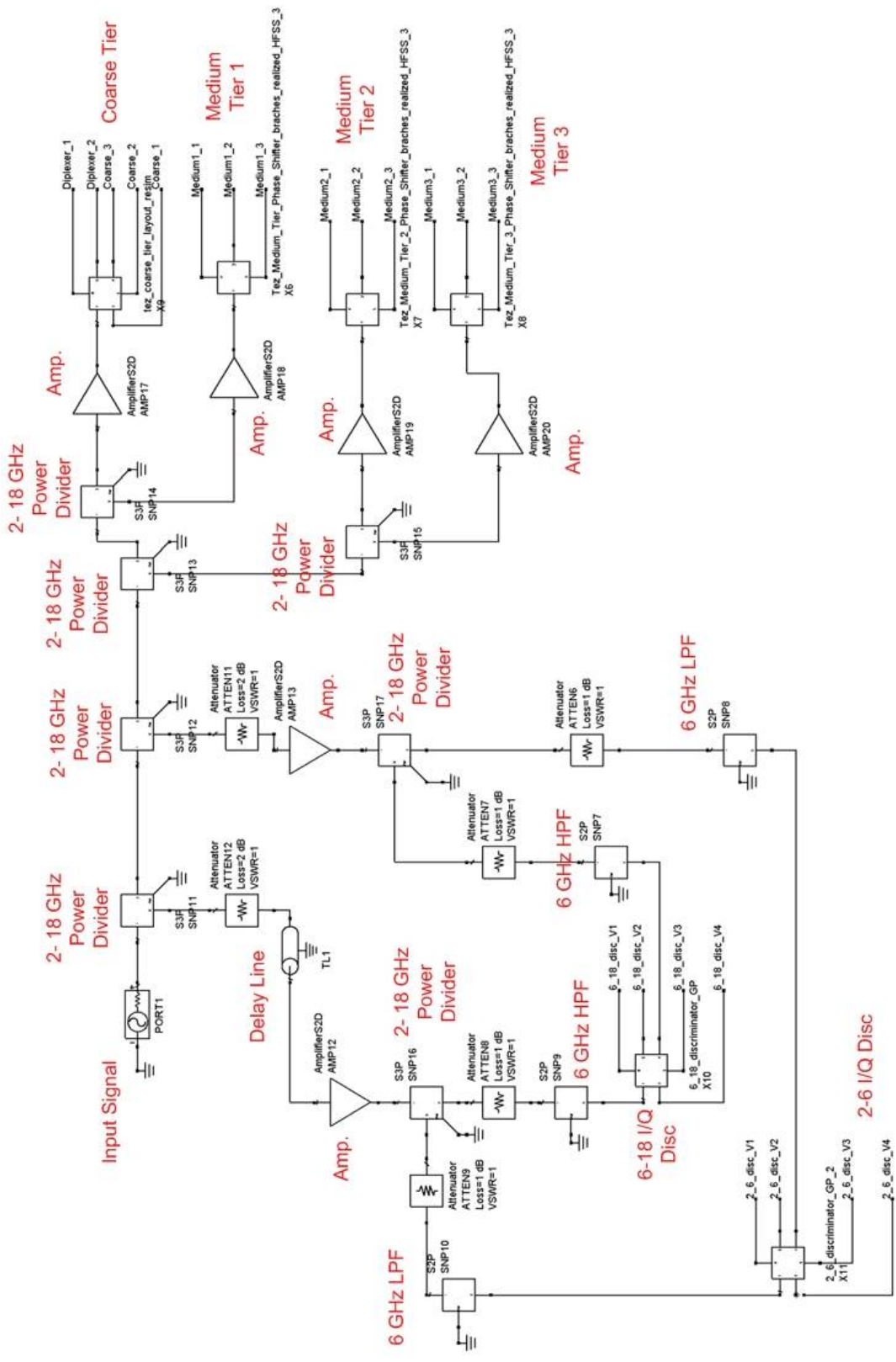


Figure 4.134 Final frequency discriminator in ADS.

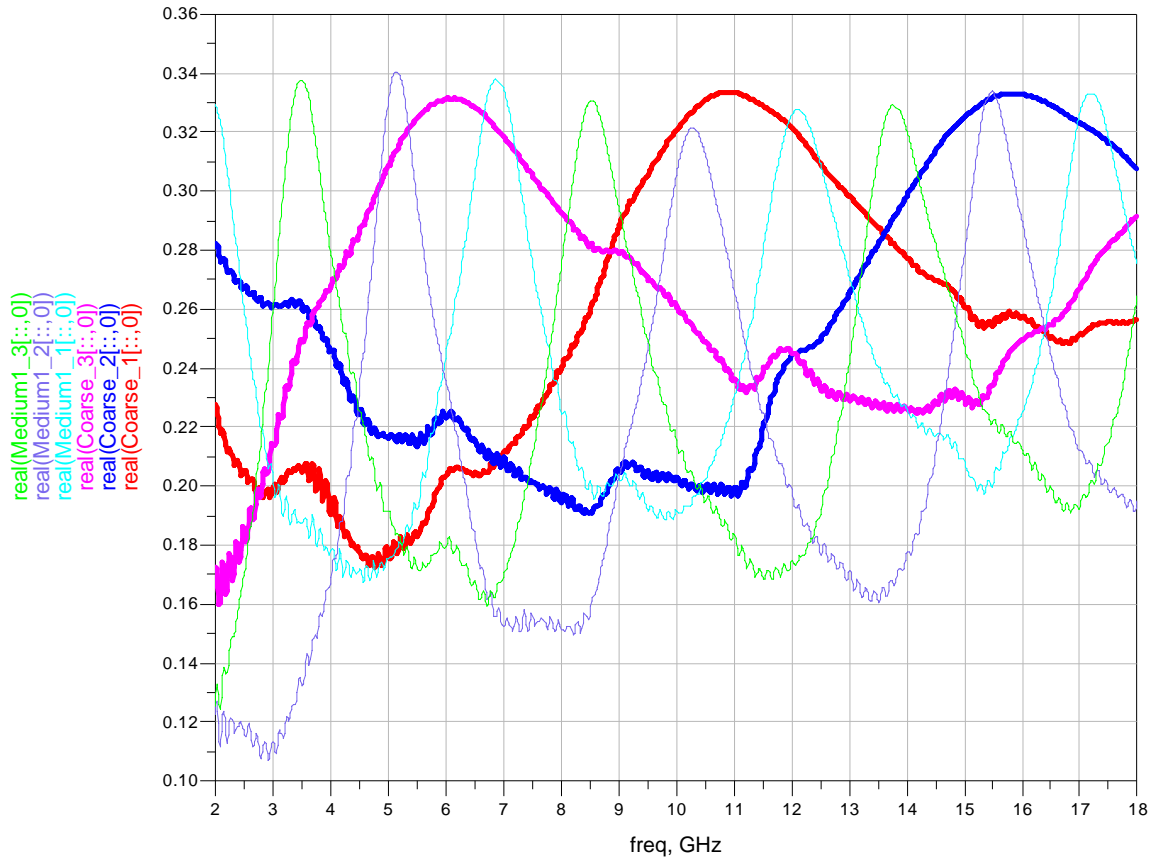


Figure 4.135 Coarse tier and medium tier 1 outputs in nested form.

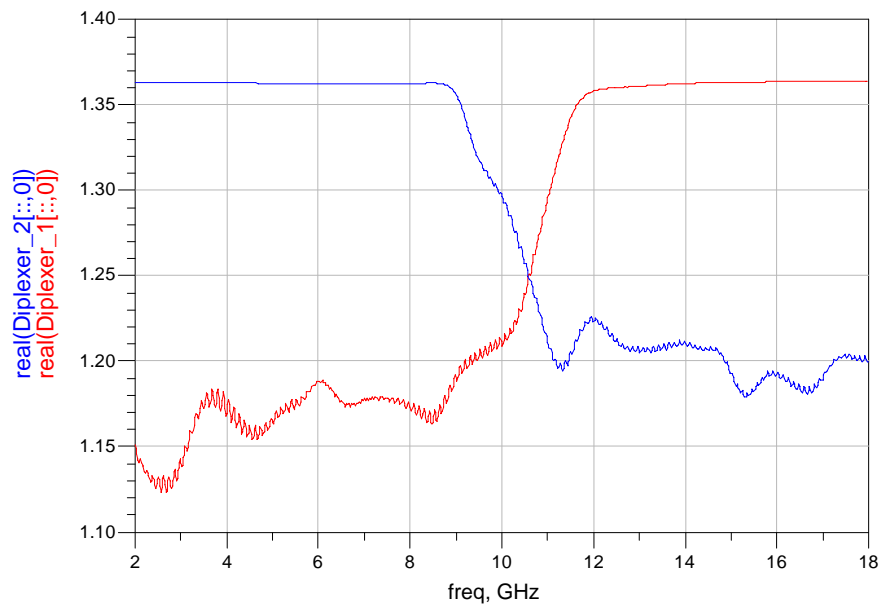


Figure 4.136 Diplexer output of coarse tier.

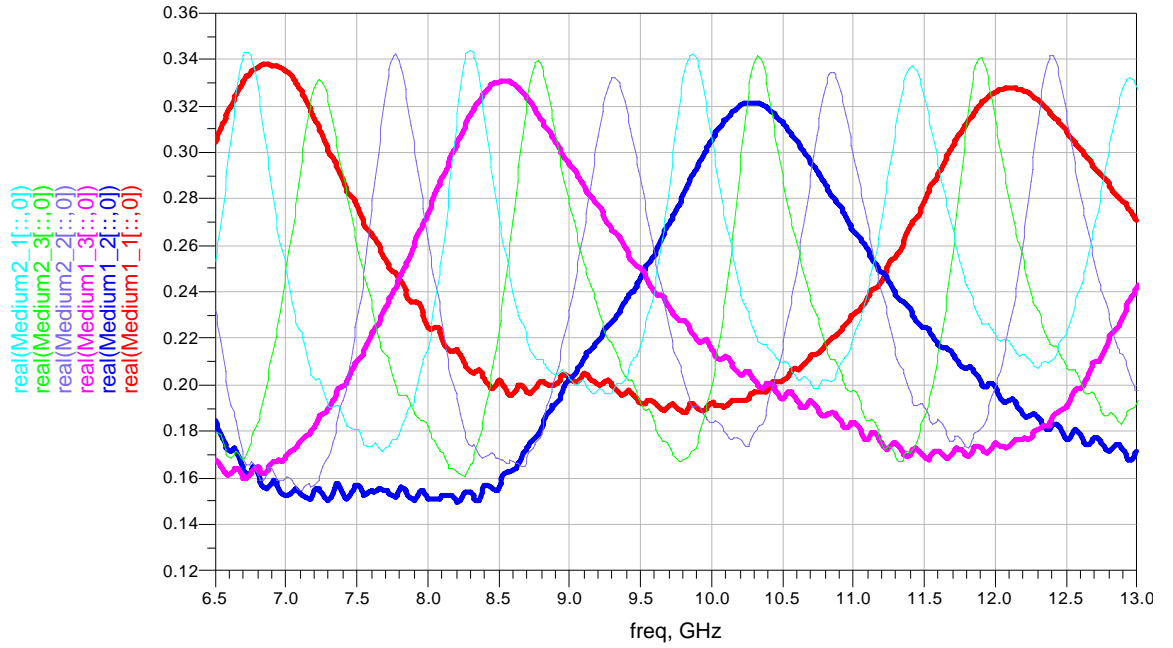


Figure 4.137 Medium tier 1 and medium tier 2 outputs in nested form (zoomed around 10 GHz).

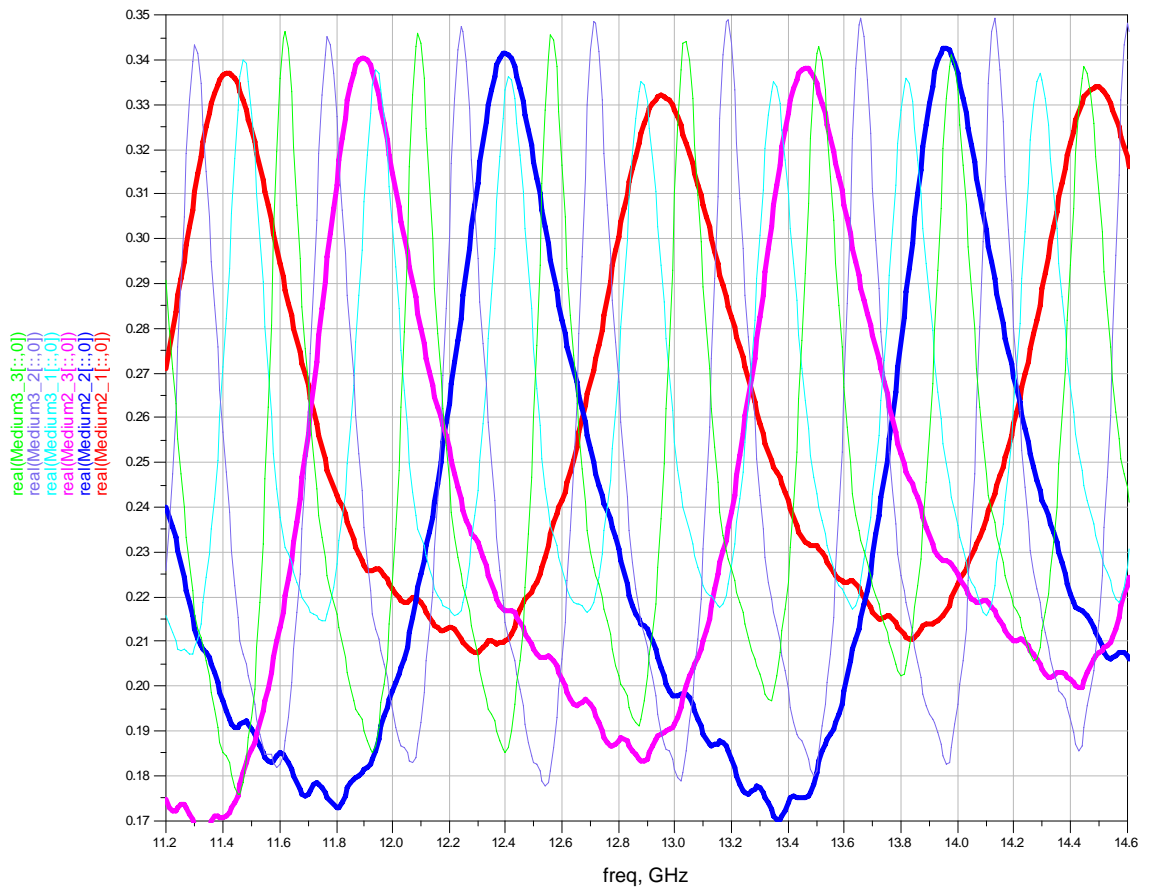


Figure 4.138 Medium tier 2 and medium tier 3 outputs in nested form (zoomed around 12 GHz).

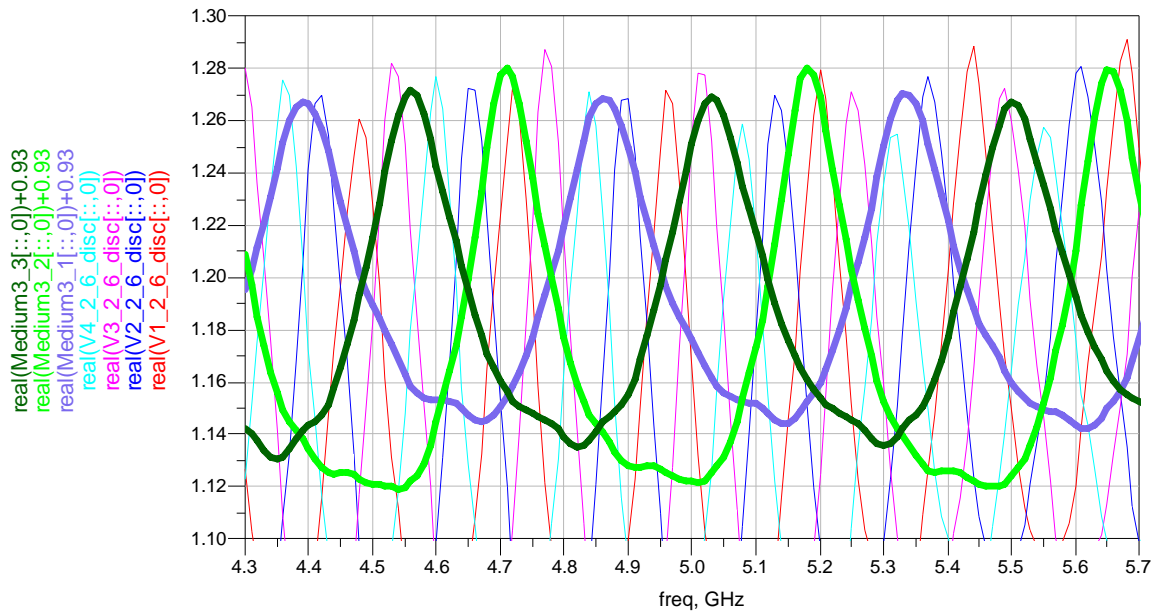


Figure 4.139 Medium tier 3 and 2-6 GHz I/Q discriminator outputs in nested form (zoomed around 5 GHz).

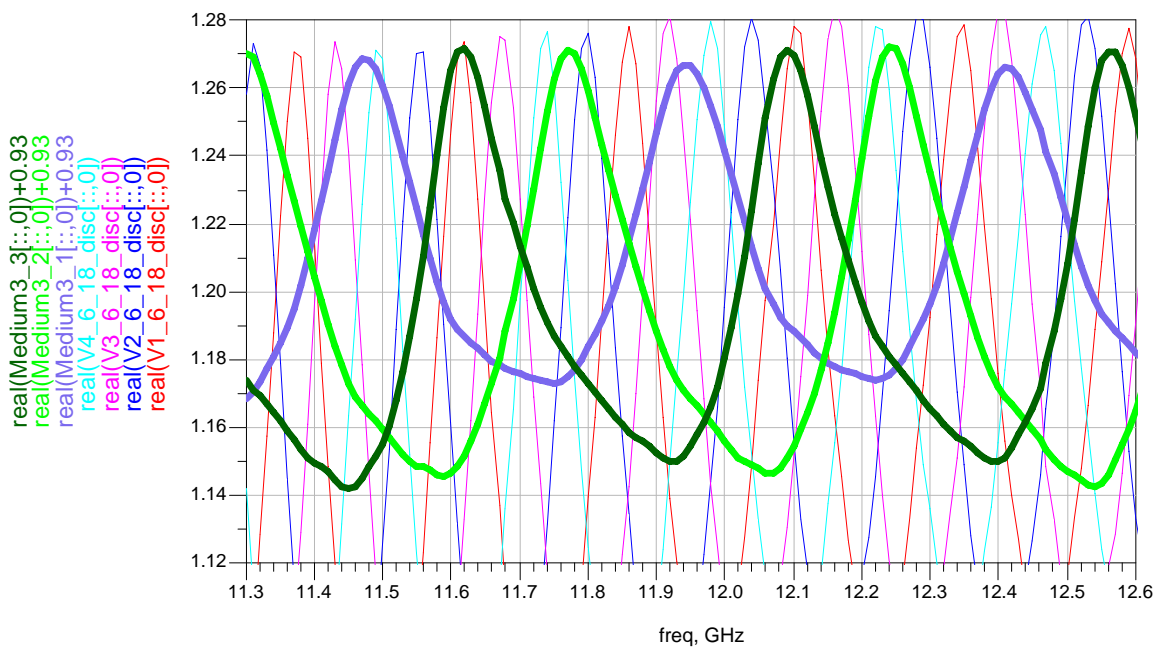


Figure 4.140 Medium tier 3 and 6-18 GHz I/Q discriminator outputs in nested form (zoomed around 12 GHz).

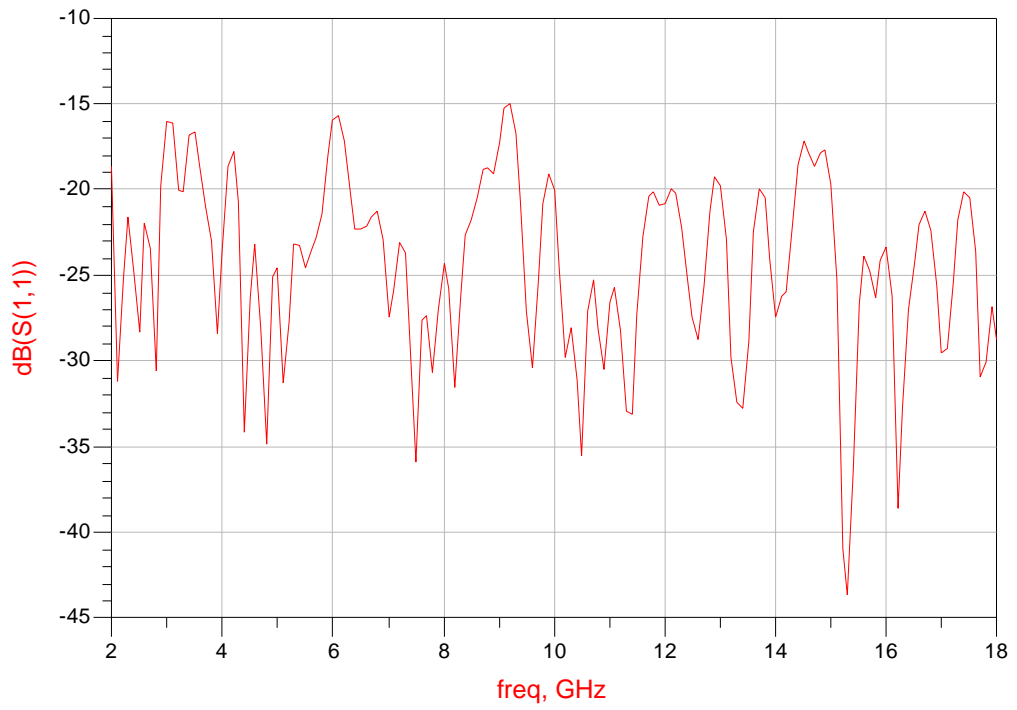


Figure 4.141 Return loss of the final structure.

CHAPTER 5

SUMMARY AND DISCUSSIONS

This chapter summarizes the achievements in this thesis by mentioning the important steps of the design and fabrication.

5.1 Deciding the Phase Shifter Network

Phase shifting process in phase discriminators is the key concept for frequency discriminator structures. Therefore much of the work is devoted to the design and realization of these phase shifters. Typical phase discriminators use 90 degree hybrid couplers in different arrangements to create phase shift for the incoming signal and generally they generate four video outputs which have different phases. However, only three video outputs are sufficient to convey unambiguous 360 degree phase information. In order to do that, phase shifting structures which provide ± 120 degree differential phase shifts must be designed. The research and design efforts about phase shifting techniques are explained as follows.

First, classic Schiffman phase shifter structures are evaluated. In these structures coupled lines are placed sequentially and each coupled line refers to a “section”. Designs and simulations are made for various phase shifting networks with different number of sections. In all these designs extra transmission lines are used to tune the differential phase shift to 120 degrees or -120 degrees. When the simulation results are examined, it is observed that increasing the number of sections improves the phase shift performance. The number of sections is increased up to 6 for the case presented in this thesis. Using more than 6 sections does not improve the

performance. On the other hand, no matter how many sections are used, at least one tightly coupled transmission line must be present in phase shifting arms in order to obtain desired differential phase shift. This situation conflicts the “designing a highly reproducible structure” goal. So this phase shifting alternative is discarded and new techniques are investigated.

As an alternative to the phase shifting technique discussed above, Schiffman “Class II” phase shifters are evaluated. The difference between these shifters and classical Schiffman type phase shifters is the use of un-coupled lines between the couplers. By this way, the desired phase shift can be obtained easily. However, in this design, as the previous one, tight coupled lines must be used in order to achieve ± 120 degree phase shift. Due to this reason, this alternative is also discarded.

As a third alternative, tandem coupled phase shifter technique is investigated. In this design like the previous ones, both un-coupled and coupled transmission lines are used. In this phase shifting technique, the same differential phase shift can be obtained by using different tandem arrangements. The presented arrangement in this thesis satisfies sufficient differential phase responses, which are not as good as the 6 section classic Schiffman type. Also, for this arrangement still one tight coupled line is required. So this alternative is also discarded. But it should be noted that, this technique can be suitable in narrow band applications.

The previously stated three designs include parallel coupled lines, which are difficult to fabricate for wide band operations. Due to this reason, an entirely different phase shifting technique is searched and it is observed that stepped impedance reflective phase shifter structures are suitable for the purpose. The only fabrication limitation for these structures is the width of the narrowest transmission line, which in fact is not a major obstacle.

The origin of the stepped impedance reflective phase shifter technique is decomposing the even and odd branches of a classic Schiffman type phase shifter. Like the case presented in classic Schiffman phase shifting techniques, increasing the number of sections improves the phase shift performance. This design is very

flexible, which gives same differential phase shift by various ways such as terminating the phase shifting branches with a SC or an OC while using increasing or decreasing impedance steps, or using random impedance steps. As a design decision, in order to decrease the discontinuity between sections increasing/decreasing impedance step forms are used. Moreover, to simplify the fabrication processes, mostly open ended phase shifting branches are used. The presented reflective phase shifting network in this thesis not only provides one of the best differential phase response among the other alternatives but also provides simple fabrication. Due to these reasons, this alternative is selected to be used in frequency discriminator tiers.

5.2 Deciding the Parameters

There are three important performance parameters for the design presented in this thesis: Frequency measurement resolution, frequency measurement accuracy and phase margin. The discussions about these parameters are given as follows:

- Frequency measurement resolution changes related to the maximum length of the delay line and sampling bit of the A/D converter. If the sampling bit number is assumed to be 8 bit which indicates a moderate A/D converter is used in the system, in order to obtain approximately 1 MHz frequency measurement resolution, the maximum delay line length should be approximately 78cm long. From this result, the other parameters can be evaluated.
- Frequency accuracy depends on the maximum delay line length, the input SNR, video bandwidth. Video bandwidth is related to the minimum pulse width handling capability of the system. If it is too large then identifying the input signals frequency becomes harder under interference. If it is too narrow, then detecting the desired signal may be problematic. So according to the operational requirements the video bandwidth must be decided by the designer. The presented frequency discriminator design can provide 0.28 MHz (rms) frequency measurement accuracy with 20 MHz video bandwidth if 0 dB input SNR is assumed.

- Phase margin depends on the number of tiers and the ratio between coarse and fine tier unambiguous bandwidths. So it also affects the choice of the number of tiers to be used. For the presented design, approximate phase margin values are calculated with respect to the number of tiers. Table 1 shows the results of this calculation. From this table, considering the phase margin change rate, the number of tiers is decided to be 5. By deciding the number of tiers, the phase margin is found to be approximately 48.26 degrees.

5.3 Designing the Frequency Discriminator Structure

IFM receivers typically contain a series of discriminator tiers operating in parallel to give the required resolution unambiguously over the operating band. Each tier resolves the ambiguity of the adjacent tier and at the end of this process the input frequency is found. Basically, resolving the ambiguities and specifying the input frequency processes depends on nesting the outputs of adjacent phase discriminators into each other. According to decided number of tiers, 3 medium, 1 coarse and 1 fine tier are designed. Selected stepped impedance reflective phase shifting technique is used in coarse and medium tiers. Coarse tier has less section than medium tiers in order to obtain the widest unambiguous bandwidth as much as possible. Medium tiers have the same phase shifting network. The only difference between medium tiers is the length of the delay lines. Nesting the outputs of adjacent tiers into each other becomes problematic as tier numbers increases. Due to that reason, fine tier is designed in a more typical way by using Lange couplers.

Designing the entire layout considering the fabrication process is an entirely different and crucial subject. At this point, the designer should decide the fabrication capability limits, type of substrates for each tier and additional components such as diode and amplifier. On the other hand, the designer should also think the circuit sizes. In this thesis, in order to reduce the size coarse and fine tiers are designed and fabricated on microstrip. But medium tiers are designed on suspended substrate to reduce the loss slope. This choice is especially made to reduce the loss of delay lines used in medium tiers as much as possible.

Encountered problems and corresponding solutions to these problems while designing the final structure are listed below:

- Coarse Tier

- Coarse tier must not create any ambiguity, while it is nearly impossible for even in schematic simulations. It is observed that coarse tier response ambiguous regions are near to the edges of the frequency band. So, in order to overcome this problem, a 10 GHz diplexer is added to coarse tier to obtain a hint about whether the input signal's frequency is below 10 GHz or not.
- According to the first optimization results in ADS, the discontinuity between phase shifter section widths was too much. But, despite the satisfying results in simulations, this situation may be problematic in practical world. On the other hand, the widths of the lines should be consistent with manufacturer's fabrication limit. It is especially important for short circuited phase shifting branches. The simulations are repeated until to reach an optimum solution for differential phase response within the limits of manufacturing capabilities and without creating a major discontinuity between section widths.

- Medium Tiers

- Similar discontinuity problem in coarse tier design is also encountered in one of the phase shifting branches in medium tiers. This problem is overcome by discarding the air spacing at the lower part of the suspended substrate beneath the last section of the phase shifter branch. In other words, a microstrip behavior is created for that section which reduces the width of the last section.

- Fine Tier

- Lange couplers are used to obtain phase shifts. However these couplers are usable only up to around 1.5 octaves. So it is impossible to cover 2 – 18 GHz frequency band with a single discriminator. According to this reason, two individual I/Q discriminator structures which operate in 2 – 6 GHz and 6 – 18 GHz frequency bands are designed for fine tier. Here, in design process, Lange coupler line

widths and spacing between lines are adjusted according to the manufacturer limit.

CHAPTER 6

CONCLUSIONS AND FUTURE WORK

In this thesis, RF sections of a multi tier instantaneous frequency measurement (IFM) receiver which can operate in 2 – 18 GHz frequency band is designed, simulated and partially realized. The designed structure has 5 phase discriminator structures which can measure the input signal's frequency at different resolutions. These discriminator tiers are separated as one coarse tier, three medium tiers and one fine tier.

Phase shifting process in phase discriminators is the key concept for frequency discriminator structures. A novel reflective phase shifter design approach is developed which enables the design of very wideband phase shifters using stepped cascaded transmission lines. Compared to the classical phase shifters using coupled transmission lines, the new approach came out to be much easier to design and fabricate with much better responses. This phase shifting technique is used in coarse and medium tiers. In fine frequency measurement tier, instead of using the developed reflective phase shifting technique, I/Q discriminator approach is used. Otherwise reflective phase shifters would necessitate unacceptably long delay lines. Two I/Q discriminators are designed and fabricated using Lange directional couplers that operate in 2-6 GHz and 6-18 GHz, resulting in satisfactory response. Additionally, 6 GHz HP and 6 GHz LP distributed filters are designed and fabricated to be used for these I/Q discriminators in fine tier.

Additionally, in order to eliminate possible ambiguities in coarse tier, a distributed element LP-HP diplexer with 10 GHz cross-over frequency is designed and fabricated successfully to be used for splitting the frequency spectrum into 2-10 GHz and 10-18 GHz to ease the design and realization problems. Three power dividers

operating in the ranges 2-18 GHz, 2-6 GHz and 6-18 GHz are designed for splitting incoming signals into different branches. All of these dividers are also fabricated with satisfactory response. The fabricated components are all compact and highly reproducible.

The designed IFM can tolerate 48 degrees phase margin for resolving ambiguity in the tiers while special precautions are taken in fine tier to help ambiguity resolving process also. It provides a frequency resolution below 1 MHz in case of using an 8-bit sampler with a frequency accuracy of 0.28 MHz rms for 0 dB input SNR and 20 MHz video bandwidth. By using more bits in sampling process, frequency measurement resolution can be easily improved or the length of the longest delay line can be reduced which may also reduce the volume of the system. The presented system is capable of offering a good performance for many applications even in extreme conditions. On the other hand, it is simple, compact, highly reproducible and suitable for IFM's used in airborne applications.

As a future work, lay-out of the whole system can be designed and the remaining circuit components can be fabricated and measured. According to the outputs of RF part, digital part of the system can be designed.

REFERENCES

- [1] D. M. Pozar, Microwave Engineering, Third Edition, John Wiley & Sons, 2005
- [2] J.B. Y Tsui, Microwave Receivers with Electronic Warfare Applications, John Wiley & Sons, 1986
- [3] P. W. East, "Design techniques and performance of digital IFM," IEE Proceedings-F on Communications, Radar and Signal Processing, vol. 129, pp. 154-163, June 1982
- [4] N.E. Goddard, "Instantaneous frequency measuring receivers," , IEEE Trans. on Microwave Theory and Techniques, vol. 20, pp 292-293, April 1972
- [5] B. El-Asir and E. H. Said, "A Low-Frequency Counter Using Time-Discriminant Connectionist Systems," IEEE trans. On Instrumentation and Measurement, vol. 53, pp 493 – 497, April 2004
- [6] M. de Souza, F. Silva; M.T. de Melo, "A Novel LSB Discriminator for a 5 bit IFM Subsystem Based on Microstrip Band-Stop Filter," 38th Microwave Conference, pp 36-39, October 2008
- [7] D. Auffray and J.L. Lacombe, "A wide band filter IFM," 20th European Microwave Conference, March 2007
- [8] Y Bar-Ness and H. Messer, "Wideband Instantaneous Frequency Measurements (IFM) Using SAW Devices," 1980 Ultrasonics Symposium, 1980
- [9] R. Mulagada and T. P. Weldon, "A Delay Line Discriminator for IFM Using a Left-Handed Delay Line," Proceedings of the IEEE SoutheastCon 2010, pp 185-188, April 2010
- [10] M.J. Thornton, "Ultra-Broadband Frequency Discriminator Designs for IFM Receivers," IEE Colloquium on Multi-Octave Active and Passive Components and Antennas, pp.13/1-13/4, May 1989
- [11] James B. Tsui, Microwave Receivers and Related Components, Wexford College Press, 2008
- [12] N. M. Blachman, Noise and its effects on communications, McGraw-Hill, 1966

- [13] B.M. Schiffman, "A new class of broad-band microwave 90-degree phase shifters," *IEEE Trans. on Microwave Theory and Techniques*, vol. MTT-6, pp.232-237, April 1958
- [14] B.M. Schiffman, "Multisection Microwave Phase-Shift Network," *IEEE Trans. on Microwave Theory and Techniques*, vol.14, pp 209-209, April 1966
- [15] J. L. R. Quirarte and J. P. Starski, "Synthesis of Schiffman phase shifters," *IEEE Trans. on Microwave Theory and Techniques*, vol. 39, no.11, pp 1885-1889, November 1991
- [16] B. Scheik and J. Kohler, "A method for broad-band matching of microstrip differential phase shifters," *IEEE Trans. on Microwave Theory and Techniques*, vol. MTT-25, no.8, pp 666-671, August 1977
- [17] J. L. R. Quirarte and J. P. Starski, "Novel Schiffman phase shifters," *IEEE Trans. on Microwave Theory and Techniques*, vol.41, no.1, pp. 9-14, January 1993
- [18] Yong-Xin Guo, Zhen-Yu Zhang, and Ling Chuen Ong, "Improved Wide-Band Schiffman Phase Shifter," *IEEE Trans. on Microwave Theory and Techniques*, vol.54, no.3, March 2006
- [19] V.P. Meschanov, I.V Metelnikova, V.D. Tupikin, and G.G. Chumaevskaya, "A New Structure of Microwave Ultrawide-Band Differential Phase Shifter," *IEEE Trans. on Microwave Theory and Techniques*, vol.42, no.5, May 1994
- [20] Burkhard Schiek And Jurgen Kohler, "Broadband Matching of Differential Phase Shifters," 6th European Microwave Conference, Italy, pp. 647-651, September 1976
- [21] Burkhard Schiek And Jurgen Kohler, "A Method for Broad-Band Matching of Microstrip Differential Phase Shifters," *IEEE Trans. on Microwave Theory and Techniques*, vol.25, pp. 666-671, August 1977
- [22] J. P. Shelton, and J. A. Mosko, "Synthesis and Design of Wide-Band Equal-Ripple TEM Directional Couplers and Fixed Phase Shifters", *IEEE Trans. on Microwave Theory and Techniques*, vol.14, no.10, October 1966
- [23] G. I. Zysman and A. Matsumo, "Properties of microwave C-sections," *IEEE Trans. on Microwave Theory and Techniques*, col. CT-12, pp. 74-82, March 1965

- [24] E. M. T. Jones and J. T. Bolljahn, "Coupled-strip-transmission-line filters and directional couplers," *IEEE Trans. on Microwave Theory and Techniques*, vol. 4, pp. 75-81, April 1956
- [25] S.J. Foti and T. Macnamara, "Design of wideband Buttler matrices using Schiffman Lines," *IEE Colloquium on Multibeam Antennas and Beamformers*, pp. 5/1 - 5/8, November 1989
- [26] L. Faltin, "Stepped-Impedance Phase Shifters," *Electronics Letters*, pp. 524-525, September 1977
- [27] Peter W. East, *Microwave System Design Tools and EW Applications*, 2nd ed., Artech House, 2008
- [28] Jia-Sheng Hong and M. J. Lancaster, *Microstrip Filters for RF/Microwave Applications*, Wiley, 2001
- [29] James B. Tsui, *Microwave Receivers and Related Components*, Wexford College Press, 2008
- [30] H. Gruchalla and A. Slowik, "The complex signals instantaneous frequency measurement using multichannel IFM systems," *15th International Conference on Microwaves, Radar and Wireless Communications*, vol.1, pp 210-213, November 2004
- [31] H. Gruchalla, A. Slowik and M. Czyzewski, "Intrapulse Analysis of Complex Signals using IFM Receiver," *International Conference on Microwaves, Radar and Wireless Communications*, pp 402-405, October 2007
- [32] H. Gruchalla, A. Slowik and M. Czyzewski, "The Analysis Of Frequency Modulated Signals Based On The IFM Receiver," *17th International Conference on Microwaves, Radar and Wireless Communications*, pp 1-4, September 2008
- [33] H. Gruchalla and M. Czyzewski, "The instantaneous frequency measurement receiver in the complex electromagnetic environment," *15th International Conference on Microwaves, Radar and Wireless Communications*, vol.1, pp 155-158, May 2004
- [34] H. Gruchalla, A. Slowik, A. K. Rutkowski, C. Recko and J.P. Coupez, "High resolution IFMs," *14th International Conference on Microwaves, Radar and Wireless Communications*, vol.2, pp 484-487, August 2002

- [35] A. K. Rutkowski, "Small Passive Direction Finding and IFM Device," 15th International Conference on Microwaves, Radar and Wireless Communications, vol. 3, November 2004
- [36] A. K. Rutkowski, "Small Passive Direction Finding and IFM Device," 15th International Conference on Microwaves, Radar and Wireless Communications, vol. 3, November 2004
- [37] N. B. Nazim, M. F. Ain, and I. S. Hassan, "ADS Simulation of 2 to 5 GHz IFM Correlator," Asia-Pacific Conference on Applied Electromagnetics, March 2006
- [38] G. M. Barbosa and J. C. A. Santos, "2 - 4 GHz Digital Frequency Discriminator (DFD) Design for Microwave Receivers," International Conference on Microwave and Optoelectronics, pp 381-385, July 2005
- [39] R. L. Boylestad and L. Nashelsky, Electronic Devices and Circuit Theory, Prentice Hall, 2002
- [40] Zlatoljub D. Milosavljevic and Miodrag V. Gmitrovic, "Designing of Microwave Diplexers Based on New Kuroda's Identities," 9th Mediterranean Electrotechnical Conference, vol. 1, pp. 513 – 517, May 1998
- [41] Electronic Warfare and Radar Systems Engineering Handbook, Avionics Department, Washington DC, April 1999